



UNIVERSITY OF
BIRMINGHAM

Evaluation of the Thermal and Mixing Performance of an Agitated Vessel for Processing of Complex Liquid Foodstuffs

by

KARIN MEHAUDEN

A thesis submitted to
The University of Birmingham
for the degree of
DOCTOR OF PHILOSOPHY

Department of Chemical Engineering
School of Engineering
The University of Birmingham
May 2008

UNIVERSITY OF
BIRMINGHAM

University of Birmingham Research Archive

e-theses repository

This unpublished thesis/dissertation is copyright of the author and/or third parties. The intellectual property rights of the author or third parties in respect of this work are as defined by The Copyright Designs and Patents Act 1988 or as modified by any successor legislation.

Any use made of information contained in this thesis/dissertation must be in accordance with that legislation and must be properly acknowledged. Further distribution or reproduction in any format is prohibited without the permission of the copyright holder.

Abstract

Thermal treatment is the most common method used by industry to ensure food is safe for consumption and to increase its storage life. To ensure safety, food is often overprocessed which can significantly affect its nutritional value as well as taste and flavour attributes. In this study, the heating and mixing efficiency of a bespoke vessel used for heat treatment of complex foodstuffs (250 litre 'Vesuvio' vessel manufactured by Giusti Ltd) was investigated.

Enzymatic Time Temperature Integrators (TTIs) were used to determine the heat treatment efficiency. TTIs are small unattached measurement devices which contain a thermally labile enzyme: determination of the degree of degradation of the enzyme at the end of the thermal process enables the integrated temperature history to be obtained. TTIs can be used for process validation, particularly when the processing environment is inaccessible for fixed devices such as thermocouples. The reliability and accuracy of the TTIs was determined by exposure to various non isothermal industrially relevant temperature profiles using a Peltier stage and Polymerase Chain Reaction (PCR) device. The integrated temperature histories obtained by the TTIs correlated generally well with data obtained from thermocouples installed in parallel, although the error increases with holding time of the heat treatment. The work showed that the TTIs can be used reliably over a range (e.g. Enzymatic TTI made from the α -amylase from the *Bacillus Licheniformis* can reliably used from 5 to 30 minutes at 85°C) which is relevant for conditions of thermal pasteurisation of interest to this study. The range of time temperature profiles that enzymatic TTIs can monitor depends on the thermal resistance of the enzyme.

The heat treatment efficacy of the 'Vesuvio' vessel was evaluated using TTIs and two thermocouples fixed onto the vessel wall and impeller shaft at the centre of the vessel. In addition to the plain or 'free' TTIs, a new TTI was developed where it was placed at the centre of an open structure to prevent intimate contact between the surface of the TTI and the vessel wall ('Golf Ball' and 'Tie Clip' TTIs). The food fluid could, however, penetrate the structure. The parameters examined in the study were fluid rheology, fill level (100% and 120% filling level) and the heating options (steam heating via wall jacket or direct injection). The study showed that the thermal process efficiency is lowered as the fluid viscosity increases when the wall jacket was used alone; this was observed by greater differences between the temperatures recorded by the thermocouples between the centre and the vessel wall. This was overcome by using direct steam injection into the vessel contents. Overfilling the vessel was also found to affect performance. The 'free' TTIs were found to have a higher thermal treatment than the TTIs which could not directly contact the wall. Under perfect mixing conditions, the 'free' TTIs and the TTIs placed inside the open structure should both give close results. However, this is not the case and it can be seen that the discrepancy increases when the mixing conditions worsen (increase of the fluid viscosity, no use of steam injection).

The reliability of the TTIs as a validation tool is dependent upon their following the same path as the food fluid, i.e. they should be isokinetic and follow the fluid streamlines. To investigate this issue, the flow of both fluid and TTIs was examined on a reduced scale version of the 'Vesuvio' vessel using Particle Image Velocimetry (PIV) and Positron Emission Particle Tracking (PEPT). The effect of changing fluid rheology, agitation speed and filling level were investigated on the basis of a scaling at constant power per unit mass.

The PIV experiments showed that the flow was laminar/transitional through bulk of vessel, with significant flow instabilities at the free surface and at the trailing edge of the impeller. Bulk mixing can therefore be expected to occur by laminar mechanisms with some mixing by eddy diffusion present at the free surface. The mixing pattern was not affected by rheology or agitation speed, however, overfilling of the vessel appeared to move the centre of the fluid rotation to above the impeller shaft, as verified using PEPT. PEPT was also applied by inserting either the free tracer into the fluid or placing it within a TTI. Significant differences in the path taken by the TTI and the fluid were observed when the TTI had a significant settling velocity in the fluid. Hence TTIs cannot be assumed to give reliable results in low viscosity fluids (e.g. water).

Acknowledgements

I would like to express my gratitude to my supervisors, Prof. Peter Fryer, Dr Mark Simmons and Dr Phillip Cox, for their invaluable guidance and advice throughout my project. I would like to thank them for their patience and kindness which helped me to achieve this work. A special thank you goes to Dr Serafim Bakalis, whose help and guidance helped me to achieve so much in my research project.

The financial support of Giusti Ltd (owned part of Briggs Plc) is acknowledged. Particular thanks are due to Mr Gareth Cure and Mr Paul Whittle from Briggs for their kind help and guidance throughout this work.

I would also like to thank the persons who helped me with computer programming and use of equipment: Dr Fabio Chiti, Mr Kenneth Chung, Dr Xianfeng Fan, Dr Andrew Ingram, Mr Benjamin Le Reverend, Dr Phillip Robbins and Dr Andreas Tsofigkas.

I am also grateful to the workshop of the Chemical Engineering Department for their kindness and help to design the mixing equipment.

My thanks also go to all my friends from the University for their support and help throughout my project and more particularly to Mr Mauricio Angeles, Mrs Shih Chi Chu, Mr Roman Pichot and Mrs Asja Portschi who were always there for me.

I am also grateful to Mr Olgun Ural for his help, support, kindness and patience throughout my project and to whom I dedicate this thesis.

Table of Contents

Abstract	i
Acknowledgements.....	iii
Table of Contents	iv
List of Figures	vii
List of Tables.....	x
Nomenclature.....	xi
Chapter 1 Introduction.....	1
1.1. Aims and Objectives	5
1.2. Thesis Plan.....	5
Chapter 2 Literature review	8
2.1 Heat treatment efficiency	8
2.1.1. Making safe food	8
2.1.2. Heat treatment	11
2.1.3. Traditional monitoring technique.....	17
2.1.4. Time Temperature Integrators (TTI).....	18
2.1.4.1. <i>Types of the TTI</i>	19
2.1.4.2. <i>Enzymatic TTI</i>	22
2.1.4.3. <i>Application of enzymatic TTIs</i>	23
2.1.4.4. <i>Types of TTI responses</i>	26
2.1.4.5. <i>Other TTI applications: monitoring the cold chain</i>	27
2.1.4.6. <i>Advantages and disadvantages of TTIs</i>	28
2.1.4.7. <i>Recent researches on TTIs</i>	28
2.1.4.8. <i>Reliability of TTIs as indicators of the efficiency of a thermal process</i> ...	30
2.2. Flow hydrodynamics and mixing	31
2.2.1. Mixing Challenges in Food industries	32
2.2.2. Mixing fundamentals	33
<i>Laminar flow</i>	34
<i>Turbulent flow</i>	35
<i>Statistical analysis of fully developed turbulence</i>	36
<i>Turbulence intensity</i>	37
2.2.3. Flow visualisation	38
2.2.3.1. <i>Optical techniques</i>	39
Laser Doppler Velocimetry (LDV).....	39
Particle imaging techniques	40
Particle Image Velocimetry	42
Tracer particles	44
The laser: Nd:YAG	45
PIV recording technique: Digital PIV	46
The synchroniser.....	47
Image analysis.....	47
Limitations of optical techniques.....	51

2.2.3.2. <i>PEPT (Positron Emission Particle Tracking)</i>	51
The tracer	51
The tracer detection.....	54
Processing of the data	55
Applications.....	56
Latest development in PEPT.....	57
2.3. Conclusion	58
Chapter 3 TTI validation study	59
3.1. Introduction.....	59
3.2. TTI validation study.....	59
3.2.1. TTI preparation	60
3.2.2. Measurement of TTI activity	60
3.2.3. Determination of the Pasteurisation value	62
3.2.4. Evaluations of D_T and z values under isothermal conditions.....	62
3.2.5. Isothermal experiment: Maximal heat treatment duration.....	63
3.2.6. Non isothermal heat treatment experiments using the Peltier stage	64
3.2.7. Non isothermal heat treatment experiments using PCR	68
3.3. Results.....	70
3.3.1. Kinetic parameters under isothermal conditions.....	70
3.3.2. Isothermal experiment: Maximal heat treatment duration.....	72
3.3.3. Estimation of the TTIs variability under non isothermal heat treatments.....	74
3.3.3.1. <i>Simple heat-hold-cool profiles</i>	74
3.3.3.2. <i>Complex heating and cooling cycles</i>	78
3.3.3.3. <i>Time temperature profiles with equal P values</i>	81
3.3.4. Non isothermal heat treatment experiments using PCR	87
3.4. Conclusion	91
Chapter 4 Industrial application: Use of TTIs on the ‘Vesuvio’vessel....	92
4.1. Introduction.....	92
4.2. Material and method	92
4.2.1. Fluids.....	93
4.2.2. The ‘Vesuvio’ vessel.....	95
4.2.3. Industrial application: Use of the TTI on the ‘Vesuvio’ vessel	100
4.2.3.1. <i>Experimental set up</i>	100
4.2.3.2. <i>Statistical tests used</i>	104
4.3. Results.....	105
4.3.1. Thermocouples time temperature profiles	105
4.3.2. Information obtained from TTIs	109
4.3.3. Process analysis using TTIs	117
4.4. Conclusion	118
Chapter 5 Use of PIV technique to investigate the fluid flow inside the vessel	120
5.1. Introduction.....	120
5.2. Scale down ‘Vesuvio’ vessel	121

5.2.1. Fluids.....	121
5.2.2. Model vessel	122
5.2.3. Scaling down at constant power per unit mass	125
5.3. Flow visualisation studies.....	128
5.3.1 PIV	128
5.3.2. Data processing	132
5.3.3. Experimental design.....	132
5.4. Results.....	136
5.4.1. Effect of the agitation speed, the fluid viscosity and filling level.....	142
5.4.2. Velocity profiles.....	149
5.5. Conclusions.....	153
Chapter 6 Investigations of the flow behaviour of TTIs and the fluid in a model ‘Vesuvio’ vessel using Positron Emission Particle Tracking (PEPT)	155
6.1. Introduction.....	155
6.2. Model vessel and fluids used for the PEPT experiments.....	155
6.3. Positron Emission Particle Tracking (PEPT).....	156
6.3.1. Positron camera	156
6.3.2. Radioactive tracer preparation	157
6.3.3. Experimental design.....	159
6.4. Results.....	163
6.4.1. Error in PEPT measurements	163
6.4.2. Comparison between PIV and PEPT	164
6.4.3. Comparison of flow behaviour of free and TTI tracers	169
6.4.4. Transverse movement inside the vessel	183
6.5. Conclusion	189
Chapter 7 Conclusions and Future Work.....	191
7.1. Validation of the statistical reliability of TTIs.....	191
7.2. Application of the TTI technique to an industrial-scale ‘Vesuvio’ vessel	192
7.3. Use of PIV technique to investigate the fluid flow inside the vessel	193
7.4. Investigations of the flow behaviour of TTIs and the fluid in a model ‘Vesuvio’ vessel using Positron Emission Particle Tracking (PEPT).....	193
7.5. Future work.....	194
References	197
Appendix A	209
Appendix B.....	210
Appendix C	212
Appendix D	217

List of Figures

Figure 2-1. The survivor curve	14
Figure 2-2. Thermal resistance curve	16
Figure 2-3. Photos of <i>Pyrococcus furiosus</i> cells.....	25
Figure 2-4. Spectrum of eddy sizes nad their energy in turbulent flow.....	36
Figure 2-5. Digital Particle Imaging Velocimetry (TSI ltd)	43
Figure 2-6. Light Sheet optics	45
Figure 2 -7. Cross correlation.....	49
Figure 2-8. Schematic diagram of PEPT for a single-particle.....	54
Figure 3-1. Diagram of the experiment with the thermoelectric module.....	65
Figure 3-2. The time temperature profile used to check the repeatability of the TTIs results that are obtained from the Linkam thermoelectric module.....	66
Figure 3-3. PCR equipment.....	68
Figure 3-4. (a) The BAA D_T value calculation curve, (b) The BLA D_T value calculation curve (c) The BAA z value curve (d) The BLA z value curve.....	71
Figure 3-5. Scatter of the process time (in waterbath at 85°C) versus the TTIs P values	73
Figure 3-6. Scatter of the thermocouples P values versus the TTIs P values for non isothermal time temperature profile	75
Figure 3-7. Scatter of the P values of the thermocouples versus the P values of the TTIs for industrial time temperature profiles.....	80
Figure 3-8. Equivalent P value results (a) TTIs P values at 85°C (b) Thermocouple P values at 85°C.....	82
Figure 3-9. Illustration of the simulation.....	85
Figure 3-10. Temperature vs time at positions A and B	86
Figure 3-11. Correlation TTI and PCR thermocouple.....	88
Figure 3-12. PCR experiments: Histograms of the results for BAA. Thermal treatment duration at 85°: (a) 2 min (b) 4 min (c) 6 min and (d) 8 min.....	89
Figure 3-13. PCR experiments: Histograms of the results for BLA. Thermal treatment duration at 85°C: (a) 5 min (b) 15 min and (c) 25 min.....	89
Figure 4-1. Viscosity curve of Starch 4% and 5% and Tomato soup	94
Figure 4-2. The 'Vesuvio' vessel (a) and impeller (b).....	96
Figure 4-3. Impeller movement.....	97
Figure 4-4. Details of vessel and TTIs used: (a) vessel schematic, showing the top and side view, (b) and (c) show the two systems which ensured that the TTIs could not get into close thermal contact with the wall. TTIs are shown.....	103
Figure 4-5. The time temperature profiles obtained with the thermocouples positioned in the wall and in the centre for the experiments performed at 83°C.....	106
Figure 4-6. Experiments performed with water.....	110
Figure 4-7. Experiments performed with 4% starch and with a holding temperature of 83°C.....	112

Figure 4-8. Experiments performed with tomato soup and with a holding temperature of 83°C and Experiments performed with 5% gelatinised starch and with a holding temperature of 85°C	115
Figure 5-1. Viscosity curve of CMC 0.25% and 0.5%].....	122
Figure 5-2. Comparison of the dimensions of the 'Vesuvio' vessel and the model vessel.....	124
Figure 5-3. Photographs of the model vessel.....	124
Figure 5-4. Lenses used to produce the light sheet.....	128
Figure 5-5. Digital camera.....	129
Figure 5-6. Diagram of the timing of the camera with the laser pulse	131
Figure 5-7. Experimental set up	133
Figure 5-8. Photo of the experimental design.....	134
Figure 5-9. Impeller positions	135
Figure 5-10. Coordinates of the vessel	137
Figure 5-11. Global mean velocities (\overline{U}_G) calculated for two experiments (a) Experiment performed with water with an agitation speed of 33 rpm (b) Experiment performed with 0.5% CMC with an agitation speed of 11 rpm	139
Figure 5-12. Turbulence intensity recorded for the experiment performed with water and an agitation speed of 33 rpm with (a) impeller position 1 (b) impeller position 2 (c) impeller position 2 (d) impeller position 4.	140
Figure 5-13. Turbulence intensity recorded for the experiment performed with a solution at 0.5% CMC and an agitation speed of 11 rpm with (a) impeller position 1 (b) impeller position 2 (c) impeller position 3 (d) impeller position 4.....	141
Figure 5-14. Normalised velocity for the experiment performed with an agitation speed of 11 rpm with water (a) impeller position 1 (b) impeller position 2 (c) impeller position 3 (d) impeller position 4.	144
Figure 5-15. Normalised velocity for the experiment performed with an agitation speed of 22 rpm with water (a) impeller position 1 (b) impeller position 2 (c) impeller position 3 (d) impeller position 4	145
Figure 5-16. Normalised velocity for the experiment performed with an agitation speed of 11 rpm with 0.5% CMC (a) impeller position 1 (b) impeller position 2 (c) impeller position 3 (d) impeller position 4	146
Figure 5-17. Normalised velocity for the experiment performed with an agitation speed of 22 rpm with 0.5% CMC(a) impeller position 1 (b) impeller position 2 (c) impeller position 3 (d) impeller position 4	147
Figure 5-18. Normalised velocity for the overfilled experiment performed with an agitation speed of 22 rpm with water(a) impeller position 1 (b) impeller position 2 (c) impeller position 3 (d) impeller position 4	148
Figure 5-19. Measurement positions: (a) Velocity measurement positions (b) Impeller position.....	149
Figure 5-20. Impeller position 1, velocity measurement position (A): (a) Low speed (b) Medium speed (c) High speed (d) Overfilled medium speed.....	150
Figure 5-21. Impeller position 3, velocity measurement position (B): (a) Low speed (b) Medium speed (c) High speed (d) Overfilled medium speed.....	152
Figure 5-22. Impeller position 4, velocity measure position (C); Water — , CMC 0.25% — , CMC 0.5% — ; (a) Low speed (b) Medium speed (c) High speed (d) Overfilled medium speed	153
Figure 6-1. Radioactive tracer composition.....	158
Figure 6-2. Addition of the radioactive tracer to the TTI	159
Figure 6-3. The reduced scale vessel used with the PEPT camera	160
Figure 6-4. The model vessel zones	162
Figure 6-5. Identification of the tracer location.....	164
Figure 6-6. (a) Area of measurement for PIV and PEPT (b) Velocity measurement position	166

Figure 6-7. Experiment performed with water (normal filling level) PEPT and PIV velocity profile (a) Position A, (b) Position B and (c) Position C	167
Figure 6-8. Experiment performed with water (overfilled level) PEPT and PIV velocity profile (a) Position A, (b) Position B and (c) Position C	168
Figure 6-9. Experiment performed with a solution of 0.5% CMC (normal filling level), PEPT and PIV velocity profile (a) Position A, (b) Position B and (c) Position C	168
Figure 6-10. Experiments performed with water and at 22 rpm (a) Occupancy plot for the free tracer (b) Occupancy plot for the TTI tracer (c) Normalised speed plot for the free tracer (d) Normalised speed plot for the TTI tracer (e)Free tracer path (f) TTI tracer path	171
Figure 6-11. Comparison of the velocity fields of the free tracer and the TTI tracer for the experiment performed with water at 22 rpm. Each subfigure show the various positions of the velocity measurement (a) Position A, (b) Position B, (c) Position (C) and (d) Position D	172
Figure 6-12. Experiments performed with 0.5% CMC and at 22 rpm (a) Occupancy plot for the free tracer (b) Occupancy plot for the TTI tracer (c) Normalised speed plot for the free tracer (d) Normalised speed plot for the TTI tracer (e)Free tracer path (f) TTI tracer path.	174
Figure 6-13. Comparison of the velocity fields of the free tracer and the TTI tracer for the experiment performed with 0.5% CMC at 22 rpm. Each subfigure show the various positions of the velocity measurement (a) Position A, (b) Position B, (c) Position (C) and (d) Position D	175
Figure 6-14. Experiments performed with 4% starch and at 33 rpm (a) Occupancy plot for the free tracer (b) Occupancy plot for the TTI tracer (c) Normalised speed plot for the free tracer (d) Normalised speed plot for the TTI tracer (e)Free tracer path (f) TTI tracer path	177
Figure 6-15. Comparison of the velocity fields of the free tracer and the TTI tracer for the experiment performed with 4% starch at 33 rpm. Each subfigure shows the various positions of the velocity measurement (a) Position A, (b) Position B, (c) Position (C) and (d) Position D	178
Figure 6-16. Experiments performed with 5% starch and at 11 rpm (a) Occupancy plot for the free tracer (b) Occupancy plot for the TTI tracer (c) Normalised speed plot for the free tracer (d) Normalised speed plot for the TTI tracer (e) Free tracer path (f) TTI tracer path.	179
Figure 6-17. Comparison of the velocity fields of the free tracer and the TTI tracer for the experiment performed with 5% starch at 11 rpm. Each subfigure show the various positions of the velocity measurement (a) Position A, (b) Position B, (c) Position (C) and (d) Position D	180
Figure 6-18. Experiments performed with an overfilled vessel, 4% starch and at 22 rpm (a) Occupancy plot for the free tracer (b) Occupancy plot for the TTI tracer (c) Normalised speed plot for the free tracer (d) Normalised speed plot for the TTI tracer (e)Free tracer path (f) TTI tracer path	181
Figure 6-19. Comparison of the velocity fields of the free tracer and the TTI tracer for the experiment performed with and overfilled vessel and 4% starch at 22 rpm. Each subfigure show the various positions of the velocity measurement (a) Position A, (b) Position B, (c) Position (C) and (d) Position D	182
Figure 6-20. Experiments performed with 4% starch at 22 rpm with the free tracer (a) Velocity on the x axis zone 1 (b) Velocity on the x axis zone 2 (c) Velocity on the x axis zone 3	184
Figure 6-21. The velocity direction on the X axis seen from the top of the vessel.....	184
Figure 6-22. Experiments performed with an overfilled vessel, with water at 22 rpm (a) Velocity on the x axis zone 1 (m/s) (b) Velocity on the x axis zone 2 (m/s) (c) Velocity on the x axis zone 3 (m/s).....	185

List of Tables

Table 1-1. Heat processes applied to foods	2
Table 2-1. Classification of the TTIs	21
Table 2-2. Example of application	31
Table 2-3. The three different particle imaging techniques	41
Table 2-4. Examples of application	50
Table 3-1. Heat treatment duration (min) at 85°C	64
Table 3-2. Summary of the experiments performed where heating and cooling ramp were both set at 30°C/min	66
Table 3-3. Equivalent <i>P</i> values: 3 tables give the equivalent time temperature profiles for 3 different <i>P</i> values at 85°C. For each time temperature profile the heating and cooling rate are 30°C/min	67
Table 3-4. PCR time temperature profiles	69
Table 3-5. PCR time temperature profile: large samples	69
Table 3-6. Coefficient fitting curve of the correlation TTIs and thermocouples results	75
Table 3-7. ANOVA test on the correlation TTIs and thermocouples results	76
Table 3-8. The evolution of the standard deviation of the TTIs and the thermocouples	77
Table 3-9. ANOVA test on the correlation TTIs and thermocouples results for the industrial time temperature profiles	81
Table 3-10. % variation of the TTI/thermocouple response with the theoretical <i>P</i> values	83
Table 3-11. Parameters used in the simulation	84
Table 3-12. Boundary conditions	86
Table 3-13. PCR results: Mean, standard deviation and % variation of the BAA and BLA <i>P</i> values	90
Table 4-1. Values of the Carreau model parameters	94
Table 4-2. Reynolds number for the 'Vesuvio' vessel	99
Table 4-3. Sedimentation times of the TTIs	100
Table 4-4. Summary of the experiments	102
Table 4-5. Heating rates (°C/min) of the experiments described in Figure 4-5	108
Table 4-6. Mean <i>P</i> value and Standard deviation of the TTIs for the 11 experiments	117
Table 5-1. Values of the Carreau model parameters	122
Table 5-2. Scaling down methods	125
Table 5-3. The speed scaling down at constant power per unit mass	127
Table 5-4. Reynolds numbers for the model vessel	127
Table 5-5. Summary of the experiments performed with the PIV camera	136
Table 6-1. Reynolds numbers for the model vessel	156
Table 6-2. Summary of the experiments performed with the PEPT camera	161
Table 6-3. Investigation of zone 2	187

Nomenclature

$A_{initial} / A_{final}$	Ratio of the enzyme activities before and after heat treatment
a_w	Water activity
C	Wall clearance (m)
C_{BAA}	Concentration of BAA or BLA (mol l ⁻¹)
Ci	Unit Curie
C_p	Heat capacity (J kg ⁻¹ K ⁻¹)
D	Diameter of the impeller (m)
d_p	Diameter of the particle (m)
D_T	Decimal Reduction Time (min)
f	Fraction of detected gamma ray used to determine the location of the tracer
F	Sterilisation value (min)
g	Acceleration of gravity (m s ⁻²)
H	Fill height (m)
I and J	First and second images respectively
k	Thermal conductivity (W m K ⁻¹).
K and m	constants with dimensions of time
k_f	First order rate constant
k_s	Constant of proportionality,
L	Length-scale which characterise the flow (m)
N	Rotation rate (rev s ⁻¹)
$N_{initial}$ and N_{final}	Initial and final number of micro organism
n	Number of events
N_d	Number of discrete data point
N_e	Number of events detected for the same location
P	Pasteurisation value (min)
P_0	Power number (dimensionless)
P_i	Impeller power requirement (W)
Q	Impeller pumping flow rate (m ³ s ⁻¹)
R	Spatial auto-correlation function of the intensity of the transmitted light I
R^2	Coefficient of determination
r_A	Reaction rate (mol s ⁻¹)
Re	Reynolds number (dimensionless)
t	duration of the heat treatment (min)
T	Vessel diameter (m)
$T(t)$	Product temperature (°C)
T_{ref}	Reference temperature (°C)
u	Instantaneous velocity
U^*	normalised velocity
u'	Instantaneous fluctuation away from the mean
U_{tip}	Agitation speed of the impeller (m s ⁻¹)
\bar{U}	Mean velocity (m s ⁻¹)

\tilde{u} and \tilde{v}	rms velocities in the X and Y directions respectively (m s^{-1})
w	Intrinsic spatial resolution of the camera
z	z value (number of degrees Celsius to bring about a ten-fold change in Decimal reduction time) ($^{\circ}\text{C}$)
Δx	Displacement of the marker over a short time interval (m)

Greek symbols

μ	Dynamic viscosity (Pa s)
ρ	Density (kg m^{-3}).
τ_s	Relaxation time (s)
σ	Surface tension (N m^{-1})
ε_T	Local energy dissipation rate / Unit mass (W kg^{-1})
λ_K	Kolmogoroff length scale (m)
σ_d	Standard deviation of the perpendicular distances (m)
ε_x and ε_y	Displacement vector between the members of an image pair
μ_{app}	Apparent viscosity (Pa s)
$\dot{\gamma}$	Shear rate (s^{-1})
μ_0 and μ_{∞}	Viscosities at shear rate $\dot{\gamma} = 0$ and $\dot{\gamma} = \infty$ respectively

Abbreviations

2-D	Two dimensional
3-D	Three dimensional
ANOVA	Analysis of Variance
BAA	<i>Bacillus amyloliquefaciens</i>
BLA	<i>Bacillus licheniformis</i>
CCD	Charged Coupled Device
CCP	Critical Control Point
CCRFA	Campden and Chorleywood Food Research Association
CMC	Carboxymethyl Cellulose
DNA	Deoxyribonucleic acid
DPIV	Digital Particle Imaging Velocimetry
F TTI	Free TTI
GB TTI	Golf Ball TTI
HACCP	Hazard Analysis Critical Control Point
HT TTIs	Heat up Time TTIs
LDV	Laser Doppler Velocimetry
Nd:YAG	Neodym-Yttrium-Aluminium-Garnet laser
PCR	Polymerase Chain Reaction
PEPT	Positron Emission Particle Tracking
PET	Positron Emission Tomography
PI	Proportional Integral

PIT	Particle Imaging Techniques
PIV	Particle Imaging Velocimetry
PME	Pectinmethylesterase
PTFE	Polytetrafluoroethylene
PTV	Particle Tracking Velocimetry
TC TTI	Tie clip ball TTI
TTI	Time Temperature Integrators
UHT	Ultra High Temperature
UV	Ultra Violet

Chapter 1

Introduction

The thermal treatment of foods is ubiquitous, both in terms of cooking the food to achieve the required sensory characteristics and in making it safe for consumption by the destruction of micro organisms. The effect of the thermal treatment on the microbial population was discovered in 1810 by a French chef, Nicolas Appert (Moss, 2000) who developed a new method of preserving food. This new technique involved the packing of food in glass containers which were previously sealed and then heated in boiling water. However, Appert believed that food spoilage was caused by the contact with the air and therefore by removing the air, spoilage would not occur. Fifty years later, Pasteur established that the food product putrefaction was caused by the growth of micro organisms in the food product. Both Pasteur and Appert gave their names to two types of heat process which are commonly applied to destroy micro organisms from the food: pasteurisation and appertisation (Moss, 2000). Pasteurisation refers to thermal treatments that eliminate a specific pathogenic micro organism (e.g. *Salmonella*) of the product and to reduce the population of spoilage micro organisms. Appertisation or sterilisation refers to thermal treatment where the only micro organisms capable of surviving are non pathogenic and not able to develop in the product during normal conditions of storage. The main difference between pasteurisation and appertisation is the temperature of the thermal treatment.

According to the temperature of the thermal treatment, the effect on the destruction of the micro organism will be different. Table 1-1 shows the impact of the various temperatures on the food product.

Table 1-1. Heat processes applied to foods (Moss, 2000)

Heat process	Temperature	Objective
Cooking Baking Boiling Frying Grilling	$\leq 100^{\circ}\text{C}$	Improvement of digestibility Improvement of flavour Destruction of pathogenic micro-organisms
Blanching	$<100^{\circ}\text{C}$	Expulsion of oxygen from tissues Inactivation of enzymes
Drying/Concentration	$<100^{\circ}\text{C}$	Removal of water to enhance keeping quality
Pasteurisation	$60\text{-}80^{\circ}\text{C}$	Elimination of key pathogens and spoilage organisms
Appertisation	$>100^{\circ}\text{C}$	Elimination of micro-organisms to achieve 'commercial sterility'

Nowadays, thermal treatment of food is common practice by manufacturers to eliminate micro organisms. From a legal point of view, food manufacturers are responsible for the quality of their products and therefore, have to supply safe food to the consumer. Thermal treatments can be applied in different ways to the food:

- the thermal treatment can be applied directly to the food;
- the thermal treatment can be applied to the packaging of the food product.

Thermal treatments directly applied to the food are often used for the thermal treatment of products such as soup. In this case, the product will be cooked and thermally treated at the same time. To ensure homogeneous thermal treatment, the food product has to be mixed at the same time as it is heated.

In the food industry, it is very common for the heating and mixing of food products to occur simultaneously. Since these operations are critical for the production of safe food, accurate monitoring and assessment is essential.

Food processes initially would seem very easy to evaluate, however, food fluids are often rheologically complex, with very high apparent viscosity and can also contain a high volume fraction of particulates. In addition, the products are often delicate in nature and can be broken down by high shear rates. When this is the case, it is very difficult to evaluate the heat treatment and the mixing efficiency. Large numbers of food manufacturers are concerned about this problem and therefore, they seek help from equipment manufacturers in order to prove the efficacy of their process.

Giusti Ltd (see Appendix A for details) is a company that specialises in process engineering equipment for the food, health and beauty, pharmaceutical and beverage industries. They manufacture large agitated vessels such as the ‘Vesuvio’ (see Appendix B) which performs the heating and mixing of food products simultaneously. The vessel is designed as a low shear apparatus to prevent mechanical breakdown of the food product during treatment. It contains a single, horizontal axis, scraped wall impeller which rotates at a relatively slow speed.

This work presented in this thesis has been sponsored by Giusti Ltd to investigate the heating and mixing efficiency of their ‘Vesuvio’ vessel. Primarily, Giusti Ltd is concerned about the effects of the filling levels within the vessel on the efficiency of the heat treatment and mixing process. The outputs from this project will lead to a better understanding of the design of Giusti’s equipment and improvement of manufacturing efficiency.

In this study, a novel method of assessing the time-temperature history using Time Temperature Integrators, (TTIs), has been applied. TTIs are particles that contain a thermal labile species (enzyme) which can be assayed after passing through a process, and which provide evidence of the thermal processing that they have received (Van Loey *et al.*, 1996a). An assessment of the TTIs is presented from two fundamental viewpoints, firstly on the reliability of the TTIs to follow a thermal process with sufficient accuracy to be applied to the ‘Vesuvio’ vessel and secondly, to determine if the TTI particles record a time-temperature history which is truly representative of the flow and mixing conditions to which the food fluid has been subjected.

The reliability of the TTIs is assessed by application of a number of time-temperature profiles to fixed samples using a Peltier stage and Polymerase Chain Reaction Device. The results are compared to thermocouples fixed in parallel; thermocouples are widely used to monitor thermal treatment.

The TTIs are then applied to an industrial scale ‘Vesuvio’ vessel and the results are again compared with fixed thermocouples. During these experiments, the effect of variable parameters such as fluid viscosity, fill level and heating and cooling methods were investigated.

Within a process, ideally the TTIs should follow the fluid streamlines and be isokinetic with the fluid. Flow visualisation techniques (Particle Image Velocimetry (PIV) and Positron Emission Particle Tracking (PEPT)) have been applied within a scaled-down version of the vessel to determine the flow regime and the motion of the fluid and TTIs respectively. The aim is to identify parameter ranges where results from the TTIs can be used with confidence.

1.1. Aims and Objectives

The aims and objectives of this investigation can be summarised as

- Evaluation of the statistical reliability of TTIs over a range of time-temperature profiles of relevance to pasteurisation (Chapter 3);
- Application of the TTI technique to an industrial-scale ‘Vesuvio’ vessel and comparison of results to those obtained via traditional monitoring techniques, i.e. thermocouples (Chapter 4);
- Construction of a scale-down vessel for determination of flow regime for fluids of different rheology and at different fill heights and rotational speeds using PIV (Chapter 5);
- Use of PEPT to determine the trajectories of the fluid and the TTIs separately to enable justification of the TTI technique when the TTIs follow the fluid streamlines and are isokinetic with the fluid (Chapter 6).

1.2. Thesis Plan

Chapter 2 gives a review of published literature. The first part gives an overview of the theory behind thermal treatment. In addition, the background to the use of TTIs to monitor thermal process efficiency will be presented. The second part of this Chapter focuses on the theory of mixing operations. First the mixing process will be described and then the two techniques (PIV and PEPT) will be described in more detail.

Chapter 3 details the validation work performed on TTIs in order to investigate their reliability in evaluating thermal treatment efficiency. Their reliability is assessed in terms of the likely ranges of operation for pasteurisation processes applied to the ‘Vesuvio’ vessel.

Chapter 4 describes the industrial scale study on the use of TTIs inside the ‘Vesuvio’ vessel. The aim of this work is to enable the use of TTIs to improve the knowledge of thermal processing inside mixing vessels with consequent influences upon future vessel design.

Chapter 5 describes the experiments performed with PIV to investigate the fluid flow inside a reduced scale version of the ‘Vesuvio’ vessel. Changes in parameters such as viscosity, agitation speed and filling level were investigated.

In Chapter 6, PEPT was used to determine the velocities of both the fluid (using a free tracer particle) and the TTIs (using a tracer encapsulated within a TTI tube) using the scaled down ‘Vesuvio’ vessel. The effect of overfilling of the vessel, which can occur within industry, was also investigated.

The main findings and recommendations for future work are summarised in the Chapter 7.

1.3. Publications - (Papers and Posters are given in the CD included with this work at the back of the thesis)

Journal (Peer-Reviewed)

- Fryer, P.J., Simmons, M.J.H., Mehauden, K., Bakalis, S., 2008. Validation of thermal processing using time temperature indicators as process probes. *Japan J. Food Eng.*, 9 (1), 33-42.
- Mehauden, K., Bakalis, S., Cox, P.W., Fryer, P.J., Simmons, M.J.H., 2008. Use of time temperature integrators for determining thermal processing efficiency in agitated vessels. *Innov. Food Sci. Emerg. Tech.* 9 (3), 385-395, doi:10.1016/j.ifset.2007.10.006

- Mehauden, K., Cox, P.W., Bakalis, S., Simmons, M.J.H., Tucker, G.S., Fryer, P.J., 2007. A novel method to evaluate the applicability of Time Temperature Integrators to different temperature profiles. *Innov. Food Sci. Emerg. Tech.* 8 (4), 507-514, doi:10.1016/j.ifset.2007.03.001.

Conference

- Mehauden, K., Cox, P.W., Bakalis, S., Simmons, M.J.H., Fryer, P.J., Verification of the reliability of Time Temperature Integrators made from the α -amylase of the *Bacillus amyloliquefaciens* for assuring the safety of various thermal processes, *IAFP (International Association for Food Association)* - Calgary (Canada) -August 2006
- Mehauden, K., Cox, P.W., Bakalis, S., Cure, G., Tucker, G.S., Simmons, M.J.H., Fryer, P.J. Validation of thermal processing of foods in large agitated vessels *IUFoST (International Union of Food Science and Technology)* - Nantes (France) - September 2006
- Mehauden, K., Cox, P.W., Bakalis, S., Simmons, M.J.H., Fryer, P.J., Time Temperature Integrators: An alternative technique to determine the heat treatment efficiency of large agitated vessels *IFT (Institute of Food Technology)* - Chicago (US) - July 2007

Chapter 2

Literature review

In the food industry, heating and mixing of food products is often performed simultaneously. Ostensibly, these processes seem very easy to evaluate, however, the fluids commonly encountered in food processing routinely possess complex rheology, with very high apparent viscosity and they often contain a high volume fraction of particulates. When this is the case, it is very difficult to evaluate the efficacy of the process, since it is essential that each phase receives the minimum heat treatment to ensure the food is safe to eat. The food industry utilises the expertise of equipment manufacturers to ensure proven heat treatment and safe products which do not harm the consumer. The determination of heating and mixing efficiency is essential in order to have a better understanding and to improve the design of processes. The following section will detail the current state of work on determination of mixing and heating efficiency

2.1. Heat treatment efficiency

The following section will describe the existing techniques available to determine the heating efficiency of processes.

2.1.1. Making safe food

Correct levels of moisture, nutrients, oxygen and favourable pH are the necessary conditions for the growth of micro organisms and food is a most favourable substrate. When micro organisms grow, they consume the nutrients and produce enzymes which can contribute to the

production of off flavour or to the synthesis of compounds which can make food unfit for consumption. When the micro organism is pathogenic (e.g. *Listeria monocytogenes*, *Staphylococcus aureus*, *Clostridium botulinum*), its presence in the food is a public health concern (Frazier and Westhoff, 1978) since it can cause foodborne diseases. However, not all micro organisms are pathogenic and sometimes their pathogenicity depends on their concentration in the food.

Foodborne diseases are often responsible for morbidity and mortality in the general population, more particularly among infants, the elderly and the immunocompromised.

Facing constant consumer pressure, regulations concerning the food safety and quality are becoming stricter. Food producers are responsible for the safety of the products they manufacture. To guarantee the safety of their products, food manufacturers use different techniques to reduce the amount of micro organisms and/or to eliminate the pathogenic micro organisms present in the food. These techniques are called 'food preservation techniques'.

There are various food preservations techniques, some of which will be detailed in the following paragraphs.

Hygiene. The micro organism growth can be delayed or prevented by observing basic hygiene rules during the production of the food (Frazier and Westhoff, 1978). Hazard Analysis and Critical Control Points (HACCP) is an example of a food safety methodology which can be applied in order to reduce food contamination. It relies on the identification of Critical Control Points (CCP's) in food production and preparation processes, which are then closely monitored in order to ensure that food is safe for consumption (Mortimer and Wallace, 1998).

Chemical preservation. Chemicals such as salt or acid can be added to the food in order to decrease the pH of the food or to reduce the water activity, limiting the growth of the micro organisms (Goff, 1999).

Biological fermentation. The aim of food fermentation is to increase the number of desired micro organisms. Desirable micro organisms are added to the food and cause the competitive disappearance of the non desirable micro organisms. This is one of the oldest methods of food preservation (Goff, 1999).

Active packaging. Smart or active packaging are used to extend the shelf life of the food product by acting as oxygen scavengers, carbon dioxide scavengers, moisture control agents, or anti microbial agents (Sacharow, 2006; Kerry *et al.*, 2006). Recent studies were performed on the use of the active packaging to extend the shelf life of meat and fish products. Natural antioxidants were added to the polypropylene film used as a packaging material of beef meat. The results of this study showed that by using active packaging the oxidation of both the myoglobin and the fresh meat was stabilised, and therefore, the shelf life of the meat could be extended (Nerin *et al.*, 2006). In another study, an absorber of volatile amines and liquids was added to the plastic tray of fish products packed under modified atmosphere enabling to increase the shelf life of the fish product by 10 days (Franzetti *et al.*, 2001). An edible antimicrobial film based on yam starch and chitosan was studied by Durango *et al.* (2006) where the potential of active packaging in the production of anti microbial active packaging was shown.

Removal of micro organism by micro filtration. This technique is considered as a cold pasteurisation and it is only used for liquid products such as milk or beer (Goff, 1999).

Thermal treatment. Unlike heat treatment, cold preservations typically does not kill the micro organisms present, it only retards their growth. Low temperature methods include refrigeration and freezing. Applying high temperature ($>60^{\circ}\text{C}$) to food to reduce the quantity of micro organisms and spores present is a commonly used thermal treatment (Fryer *et al.*, 1997) and will be described more in detail in § 2.1.2

Irradiation. In this technique, electro magnetic waves or electrons are applied to the food. Ionizing and UV radiations damage the microbial DNA and cause potentially lethal DNA lesions. However, the application of this technique is limited due to current public concern.

High pressure. Pressures ranging from 100 to 1000 MPa are applied to the food causing damage to the micro organism cell membrane and denaturation of its proteins. This novel technique is already being used by some industries and is starting to attract new industries (Manas and Pagan, 2005; Stewart, 2004; Devlieghere *et al.*, 2004; Lado and Yousef, 2002; Fonberg-Broczek *et al.*, 2005; O'Reilly *et al.*, 2001; Deliza *et al.*, 2005).

Pulsed electric field. Short duration (1-100 μs) high electric field pulses (10-50kV cm^{-1}) are applied to food between two electrodes. The structure of the membrane of the micro organism is generally damaged during the exposure at high voltage field. This technique can only be applied to liquid foods such as orange juice and liquid eggs (Manas and Pagan, 2005; Stewart, 2004; Devlieghere *et al.*, 2004; De Haan *et al.*, 2002; Lado and Yousef, 2002).

2.1.2. Heat treatment

Quality requirements in food manufacturing are stricter than 20 years ago. Fundamentally, food products must not harm the consumers. In order to ensure the safety of their products,

food manufacturers are using different food preservation techniques. One of the techniques commonly used is heat treatment.

Heat treatment is a unit operation aiming at the same time to cook the product and to reduce the quantity of micro organisms and spores responsible for food poisoning or food deterioration, by applying high temperatures to the food (Fellows, 2000; Fryer *et al.*, 1997). The impact of these preservation techniques on the safety and quality of the food product has to be quantified in order to determine their effectiveness (Hendrickx *et al.*, 1995). Listed below are the two main heat treatments classified by their applied temperatures:

Pasteurisation is the process of heating food for the purpose of killing the harmful organisms (bacteria, viruses, protozoa, moulds, and yeasts). However, pasteurisation does not kill all micro-organisms in the food, it only reduces the number of heat sensitive micro organisms to a safer level and inactivates most of the enzymes (Lloyd *et al.*, 1999). It is considered to be a mild treatment and the applied temperature generally does not exceed 100°C. The pasteurised product is typically refrigerated and consumed before its expiration date.

Sterilisation is a high level of treatment and the commonly used temperature range is 115°C – 125°C. The aim of this treatment is to ensure the destruction of all the pathogenic micro organisms, their toxins and their spores. Sterilisation treatment is based on the destruction of *Clostridium botulinum*, which can prove fatal if ingested. Laboratories use this micro organism as a reference to ensure the safety of the products. This micro organism produces spores and a highly temperature resistant exotoxin (botulin). In addition, *C. botulinum* grows in anaerobic and low acid (pH > 4.5) conditions enabling growth in packaged and canned products (Valentas *et al.*, 1997). The US Food and Drug Administration define the ‘minimal

thermal process’ as ‘the application of heat to food, either before or after sealing in a hermetically sealed container, for a period of time and at a temperature scientifically determined to be adequate to ensure the destruction of micro organisms of public health concern’ (Lopez, 1987). Sterilised products can be stored at ambient temperature for many years.

Theoretically, the duration of the thermal treatment chosen depends on several parameters (Fellows, 2000):

- the thermal resistance of the micro organisms and spore potentially present into the food
- the heating characteristics
- the pH of the food and other nutrient characteristics
- the shape and size of the container
- the physical conditions of the food (liquid, solid, mixture).

Thermal processes used to ensure the safety of the food products can be determined by mathematical modelling. Mathematical models depend on the time temperature profile of the product and the kinetics of the destruction of the targeted micro organism and its spores. (Holdsworth, 1985). The calculation of the thermal process will be based on the destruction of the heat resistant spore of *Clostridium botulinum* (Fellows, 2000).

At constant temperature T , the death of micro organisms (with hypothesis that the death of the micro organisms follows a first order kinetic) is given by: (Ball and Olson, 1957)

$$\frac{N_{final}}{N_{initial}} = 10^{-t/D_T} \quad (2.1)$$

where $N_{initial}$ and N_{final} are the initial and final number of micro organisms, t is the duration of the heat treatment and D_T is the Decimal reduction time (Figure 2-1) necessary to reduce the number of micro organisms by 90% at temperature T , and which varies with the type of organism (Valentas *et al.*, 1997).

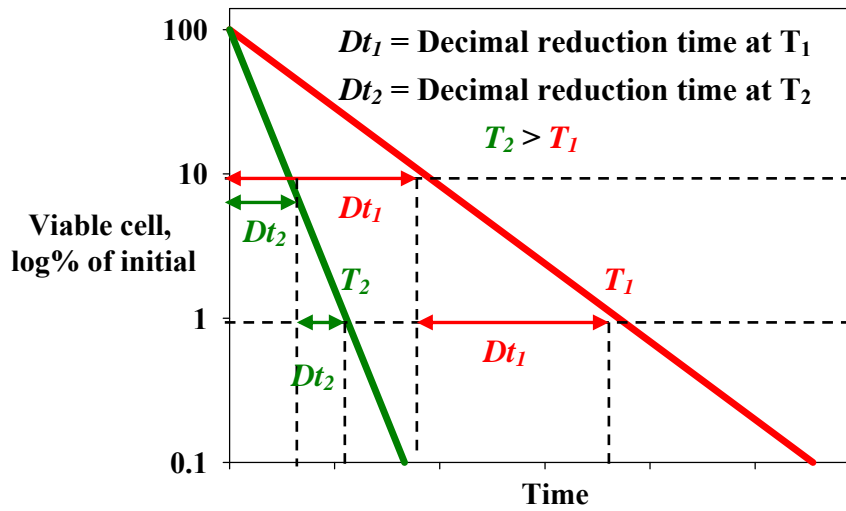


Figure 2-1. The survivor curve

In order to have a safe product, the final number of micro organisms must be reduced to a safe level. Traditionally, in canning industry, the concept of 12 D_T cook (botulinum cook) is used. It refers to a 12 log reduction in the micro organism population (Richardson, 2004).

Equation 2.1 can be rearranged to give the relationship in a form that can be used for the determination of the thermal processing time, t :

$$t = D_T \cdot \log \left(\frac{N_{initial}}{N_{final}} \right) \quad (2.2)$$

Any thermal process considers quality and safety of the product. Excessive heat treatment, while ensuring safety, reduces product quality attributes such as flavour and texture (Lewis and Heppell, 2000). The kinetic behaviours of the micro organisms and the quality attributes are different (Holdsworth, 1985). Until recently, the level of destruction of nutrients has attracted little attention, and thermal treatments were not optimised. However, the duration of the heat treatment should be chosen by considering both the safety and the quality of the product. Thermal processes are commonly compared using equations such as:

$$F \text{ (or } P) = D_{T(ref)} \cdot \log \left(\frac{N_{initial}}{N_{final}} \right) \quad (2.3)$$

Where F or P are the process values (F for sterilisation and P for pasteurisation). In order to calculate the process value, the organism should follow the thermal death time model described by Bigelow (Figure 2-1) (Bigelow, 1921; Guivarç'h *et al.*, 2005b). The F or P value can also be calculated from the time temperature history of the product upon which the heat treatment is applied. The product time temperature history from a particular thermal process will be translated into an equivalent time at a chosen reference temperature (Ball and Olson, 1957; Hendrickx *et al.*, 1995; Bhowmik and Tandon, 1987; Holdsworth, 1985; Ohlsson, 1980). This allows the comparison between different thermal processes.

$$P \text{ or } F = \int_0^t 10^{\frac{T(t) - T_{ref}}{z}} \cdot dt \quad (2.4)$$

where $T(t)$ is the product temperature at the coldest point (°C), T_{ref} is the reference temperature for the D_T value (°C), t is the process time (min) and z (Figure 2-2) is the number of degrees Celsius needed to bring about a ten-fold change in decimal reduction time. The z

value represents the temperature sensitivity of the system and should ideally be the same as that for the targeted micro organism.

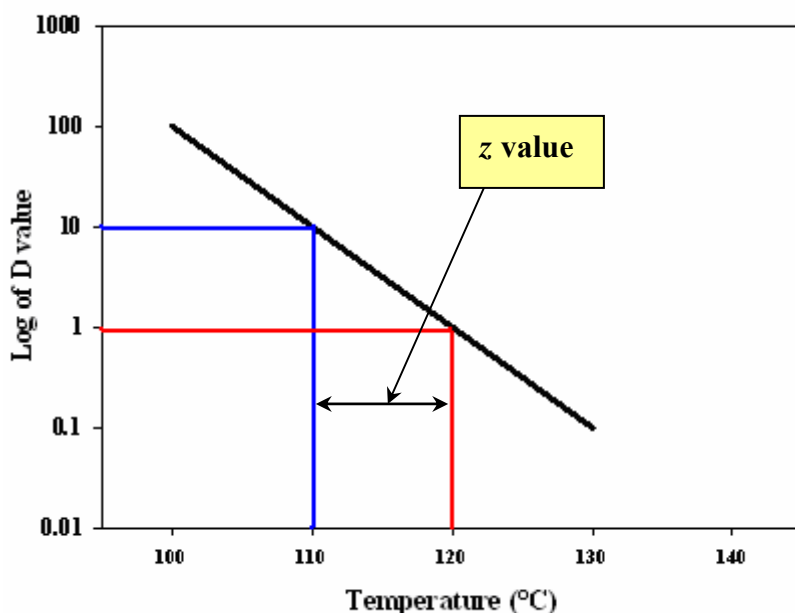


Figure 2-2. Thermal resistance curve

Clostridium botulinum has a z value of 10°C (Hendrickx *et al.*, 1995; Richardson, 2001). Most of the micro organisms vegetative cells and spores have a z value ranging from 5°C to 12°C while the z value for the destruction of thermal labile chemical substances start from 25°C to 30°C . Thus the destruction of nutrients is less temperature sensitive than the destruction of micro organisms.

The P or F value represents the thermal treatment received by the food. These values have to be evaluated from the product at the coldest location inside a food container or food mixing vessel for the ‘worst case scenario’. However, it is not straightforward to locate the coldest point inside a food container / food mixing vessel. The coldest point has to be determined before starting process validation and thermocouples can be used to find this location. The coldest location depends on the physical properties of the container / vessel and of the food

product (e.g. viscosity, density) (Richardson, 2001). Depending on the physical properties of the food, the heating of the coldest point can be done by conduction or convection. When the container is large and the product is viscous, the convection phenomena will be slow and the centre of the container will be colder than the edges. When the product is solid, the heat transfer will occur only by conduction and thus, the centre of the container will take longer to reach the microbial lethal temperature. When the food is heated inside a mixing vessel, the heating of the coldest point will depend on the efficacy of the impeller to agitate the product. Therefore, the time temperature profile used in the process validation must be recorded at the coldest location of the container (Fellows, 2000; Holdsworth, 1985).

2.1.3. Traditional monitoring technique (thermocouple, number of micro organism)

The effectiveness of the thermal treatment has to be validated in order to ensure that the food product is safe for consumption. Listed below are two techniques commonly used to validate thermal treatment efficiency.

Thermocouples and data loggers can be used as a validation technique; they can measure temperature as a function of time and can be placed inside the food container to record the thermal treatment undergone by the food. This time temperature history can therefore be translated into an equivalent time at a reference temperature (P or F value, equation 2.4). This validation technique is straightforward to apply and the data analysis is relatively fast and easy. However, thermocouples and data logger are not convenient for every type of thermal processes. In some cases, they can interfere on the movement of the fluid and lead to incorrect time temperature history and sometimes it is impossible to put them at the coldest location of the container. Moreover, the size of the wireless data logger is an issue (caused by

the battery), since it has been not possible so far to miniaturize them sufficiently (Hendrickx *et al.*, 1995; Marra and Romano, 2003).

The efficiency of the thermal treatment can be determined by measuring the change of a quality or safety attribute (e.g. micro organism counts) before and after thermal treatment. A sample of the food is taken before and after thermal treatment and the micro organisms are counted. The F or P value is calculated using Equation 2.3 (Richardson, 2001). However this technique is laborious, lengthy (incubation takes days), expensive (the media used to grow the micro organism can be expensive) and sometimes the analysis is problematic due to detection limits (Van Loey *et al.*, 1996a). The disadvantages encountered by these two techniques have led to the development of a new monitoring technique, the Time Temperature Integrators (TTIs).

2.1.4. Time Temperature Integrators (TTI)

As described previously, various techniques are available to determine the efficiency of thermal processes. Nonetheless, these techniques present various limitations. The evaluation of the level of a food attribute before and after heat treatment is an efficient and widely used technique. However, when the parameter of interest is the determination of the presence of some micro organisms, the analysis can take several days while the shelf life of a product can be limited (Hendrickx *et al.*, 1995).

The analysis of thermocouple data is relatively fast and easy. However, the development of new technologies makes the access for probes sometimes impossible. This is the case for agitated vessels where surface scraped heat exchangers are used (Hendrickx *et al.*, 1995; Weng *et al.*, 1991). Another problem emerges when industry needs to know the thermal

process that a food particulate floating in liquid (e.g. soup with pieces of meat) receives. If a thermocouple is attached to a food particulate in liquid, the thermocouple will interact with the fluid motion and will modify the process. Therefore, it will not be possible to know what the food particulate undergoes during the process.

Time Temperature Integrators (TTIs) are alternatives to conventional temperature probe systems. It is a relatively new technology which allows determination of the impact of a process on a product attribute (Van Loey *et al.*, 1996a). TTIs are devices which contain a thermally labile substance, which under a heat treatment undergoes irreversible changes which can be quantified as a *F* or *P* value (Guiavarc'h *et al.*, 2005b; Hendrickx *et al.*, 1992; Hendrickx *et al.*, 1995; Taoukis and Labuza, 1989; Tucker and Holdsworth, 1991; Van Loey *et al.*, 1996a).

TTIs are small (Hendrickx *et al.*, 1992), shock resistant monitoring devices which can be made neutrally buoyant from materials with the same thermal conductivity as the food. Their shape can be modified to simulate food particles and they can be put inside a particle without interfering with the fluid motion. Their analysis is fast and relatively simple (Guiavarc'h *et al.*, 2005b; Van Loey *et al.*, 1996b). Conversely to the thermocouples, the time temperature history of the product is not needed to determine the impact of thermal treatments (Guiavarc'h *et al.*, 2005b; Hendrickx *et al.*, 1995; Van Loey *et al.*, 1996a).

2.1.4.1. Types of the TTI

TTIs can be classified according to the substance that they contain, which can be microbiological, enzymatic, chemical or more rarely physical. Alternatively, TTIs can be classified according to their origin and application within the food.

Intrinsic TTI. They are naturally present in the food and, the efficiency of the thermal treatment can be evaluated by quantifying it before and after treatment. Intrinsic TTI presents some advantages such as being homogeneously dispersed inside the food. Researches have been undertaken to assess the heat treatment received by the milk (Claeys *et al.*, 2002). In this study, some components naturally present in the milk are used as TTIs.

Extrinsic TTI. Extrinsic TTIs are artificially added to the food (Claeys *et al.*, 2002). Extrinsic TTIs can be subdivided into 3 groups (Hendrickx *et al.*, 1995; Van Loey *et al.*, 1996a):

- dispersed TTIs are added and mixed to the food and are in direct contact with the food;
- permeable TTIs are located in separate units with a permeable barrier allowing exchange between the food and the TTIs;
- isolated TTIs are located in separate units and their barrier is not permeable and therefore does not allow exchange with the food material.

A summary of different TTIs is given in Table 2-1

Table 2-1. Classification of the TTIs

	Microbiological TTI	Enzymatic TTI	Chemical TTI	Physical TTI
Principle	Microbiological TTIs can be divided into 2 types of techniques. In the first one, the impact of the process is quantified from the number of micro organisms that survives. The second one, just show if there is growth or no growth of micro organisms	Quantification of the activity of a thermally labile enzyme that remains after the heat treatment. The amount of remaining activity reveals the impact of the temperature history	Detection of concentration change of a chemical substance voluntarily added to the food.	Diffusion of a coloured chemical compound in a paper wick
Popularity	Most commonly used type of TTIs	Relatively new technique. Food companies starting to use them	Rare because Chemical TTIs still cannot be used for food monitoring since no chemical reactions have been identified so far with an applicable z value	Development limited - it is not currently used in food safety determination
Application	Monitoring of the sterilisation of food or pharmaceutical products	Their high thermostability allows them to be used at very wide range of temperatures (pasteurisation, sterilisation) for food and pharmaceutical products	Used for the monitoring of the deterioration of other quality attributes	Limited application
Advantage	Widely spread	See § 2.1.4.6	Fast and analytically accurate	Easy to prepare to calibrate, user-friendly, fast to obtain the results and easy to recover
Inconvenient	Long and analytically not precise enough	See § 2.1.4.6	Can not be used for food safety monitoring	This system is activated by steam therefore no other heating media can be monitored
Reference	(Hendrickx et al., 1995; Van Loey et al., 1996a))	(Hendrickx et al., 1995; Van Loey et al., 1996a)	(Adams and Langley, 1998)	(Hendrickx et al., 1995; Van Loey et al., 1996a)
Origin	Intrinsic or extrinsic	Intrinsic or extrinsic	Extrinsic	Extrinsic

2.1.4.2. Enzymatic TTI

The usage of enzymatic TTIs is currently increasing in the determination of heat treatment effectiveness since they do not cause any food safety issues, unlike microbiological TTIs (Guiavarc'h *et al.*, 2002a; Guiavarc'h *et al.*, 2004a; Guiavarc'h *et al.*, 2004b; Maesmans *et al.*, 1994b; Tucker, 1999; Van Loey *et al.*, 1997). However, the selection of the enzyme can be difficult since it has to fulfil several requirements:

- the enzyme isothermal inactivation must follow a known order of kinetics (Welt *et al.*, 2003);
- the enzyme must be thermally resistant;
- the enzyme must have a z value that matches organisms of interest typically $z = 8 - 10^{\circ}\text{C}$ in order to be used as a food safety tool. (Van Loey *et al.*, 1996a);

Studies have been undertaken on various enzymes in order to determine the most suitable to use for heat treatment effectiveness. Tomato and cucumber Pectinmethylesterase (PME) has been studied as a potential TTI by Guiavarc'h *et al.* (2003), who showed that the purified tomato PME could follow a first order kinetics. D_{Tref} and z could be changed by modifying stabilizer agent (buffer pH, presence of glycerol). However, the cucumber PME exhibits a biphasic inactivation curve which made it not useable as a TTI. Peroxidase enzyme has been used to determine the efficiency of pasteurisation and gave excellent correlation with the measured time-temperature values (Hendrickx *et al.*, 1992). However, most studies have focused on use of α -amylase from *Bacillus spp.*, which possesses good thermal resistance, has a z value more or less equal to that of the targeted micro organism (*Clostridium botulinum*)

and its denaturation follows first order kinetics (Tucker *et al.*, 2002). Amylases which are amylolytic enzymes catalyse the breakdown of starch, glycogen and some polysaccharides. The α -amylase hydrolyses the alpha 1,4 glycosidic bonds in the inner region of the starch polymer (Hewitt, 1993). This enzyme has important industrial applications in starch liquefaction, brewing, sizing in textile industries, and paper and detergent manufacturing processes (Roychoudhury *et al.*, 1988). α -amylase is produced on the industrial scale using *Bacillus spp.*

The α -amylase directly extracted from the *Bacillus spp* is stable for pH values ranging from 5.5 to 8. By adding calcium this stability can be changed. With the optimum amount of calcium, the α -amylase from *Bacillus spp* can resist high temperatures for relevant times (90°C) (Hewitt, 1993). Several studies have been undertaken to determine the temperature ranges in which amylases from various micro organisms could be used (Guiavarc'h *et al.*, 2004a; Guiavarc'h *et al.*, 2004b; Haentjens *et al.*, 1998; Van Loey *et al.*, 1996a). However, when the enzyme does not fulfil these requirements, it is still possible to change the thermal sensitivity of the enzyme by changing the conditions of the enzyme (immobilised or not) and its environment (e.g. pH, concentration in Calcium, NaCl).

2.1.4.3. Application of enzymatic TTIs

Pasteurisation: It is relatively easy to find enzymes which are thermostable at pasteurisation temperatures. No specific system is needed to protect the enzyme thus, these experiments are easily undertaken. As an example, some TTIs have been added to batches of fruit preparations in order to evaluate the pasteurisation achieved by two different ways of heating, namely by using an ohmic column or a tubular heat exchanger (Tucker *et al.*, 2002). The successful results gave a *P* value in various cases where the thermocouples could not be used.

The use of α -amylase to evaluate a pack pasteurisation process has also given promising results. In the pasteurisation domain, the comparison of the results from the read out of the TTI and the results from the integration of the processing value shows that the TTI could be used as an alternative process evaluation tool when others more accurate methods can not be applied (Van Loey et al., 1996a). TTIs were used to measure the pasteurisation in baked mushroom quiches. Usually the temperature measurements of product which undergo a change of phase during processing are not easy. The use of temperature probes to measure the temperature in the centre of the quiches was not possible since during the process the quiches travel along a belt of a continuous oven. However, TTI could be used since they would stay at the correct location during processing. TTI were made from the α -amylase from *Bacillus amyloliquefaciens*, their D_{70} value was 8.4 min with a z value of 8.9°C. For 10 quiches, one TTI was put in the centre and one on the edge. The quiches were then put on the conveyor belt of a continuous oven set at a 210°C for 25 minutes. In food safety point of view, the target thermal treatment was 70°C for 2 minutes in order to kill the strains of *Salmonella* and *Listeria monocytogenes* and all 10 quiches received the targeted thermal treatment. However, the centre of the quiches received a lower thermal treatment than the edge. The average P value at 70°C of the 10 quiches for the centre was 12.3 min and for the edge was 14.7 min. This result was not surprising since the centre was the expected cold spot (Tucker et al., 2005a). This study shows a successful application of the Enzymatic TTI to monitor thermal processes undergone at pasteurisation temperature.

Sterilisation: Finding an enzyme with the adequate thermostability in these ranges of temperatures (around 121°C) is difficult. Some studies have been undertaken with some enzymes under reduced water content (Guiavarc'h et al., 2004b; Guiavarc'h et al., 2004a; Haentjens et al., 1998). This is easily realised in laboratories; however this is not the case in

factories. The hyperthermophile *Pyrococcus furiosus* presents some good characteristics in terms of heat resistance. Indeed, this micro organism has been isolated from a shallow marine solfatara at Vulcano Island off southern Italy where the temperature, pH and oxygen availability are not favourable for common micro organism development (Figure 2-3).

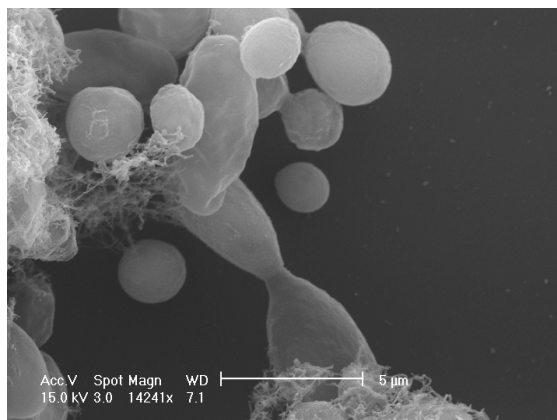


Figure 2-3. Photos of *Pyrococcus furiosus* cells (Source: Photo taken by SEM (Scanning Electron Microscopy) - Ian Brown, PhD student of the University of Birmingham)

The maximal temperature at which the organism will grow is 103°C with an optimum growth rate at 100°C (Robb *et al.*, 2001). The enzyme of these micro organisms is potentially interesting to use, however, it is difficult to culture or to obtain as it is produced only by few laboratories. Recently, the CCRFA (Campden and Chorleywood Food Research Association) published some results obtained with the amylase of the *Pyrococcus furiosus* during industrial applications. This research shows that the *z* value of the amylase of the *Pyrococcus* is 10°C and the industrial trials show promising results. However, this enzyme is difficult to obtain and more tests are necessary to validate its effectiveness for sterilisation processes (Tucker *et al.*, 2007; Tucker *et al.*, 2005b).

2.1.4.4. Types of TTI responses

The impact of the process on the TTI is determined by the quantification of a modification within the TTI. In the case of enzymatic TTIs, the enzyme is denatured by heat treatment and the enzyme activity decreases. The quantification of the change of activity before and after heat treatment shows its impact on the TTI. However, there are two cases to be considered:

- When the z value of the TTIs is equal to the z value of the targeted micro organism (*Clostridium botulinum* for food safety), the modification in enzyme activity will correlate well with the decrease of the number of targeted micro organisms. In this case, the time temperature history of the product is not needed in order to determine the impact of the thermal treatment on the micro organism population present in the food and can be directly determined from the reading of the TTI.
- However, when the z value of the TTIs is not equal the targeted micro organism z value, the correlation between the change of enzyme activity and the reduction of micro organism number can not be done. In this case, the time temperature history of the product is needed. However, it is possible to use multi component TTIs (composed of several units containing enzymes with different z values) in order to determine the impact of the thermal treatment when the z values are different and the time temperature history of the product is not available (Van Loey et al., 1995; Van Loey et al., 1996a).

Until recently, the use of multi components TTIs as a tool to evaluate the impact of thermal treatment on the targeted micro organism was limited since no reliable extrapolation technique was available. The multi component TTIs could not be used without information about the time temperature history (Maesmans *et al.*, 1993; Maesmans *et al.*, 1994a;

Maesmans *et al.*, 1995). However, a recent study showed that multi component TTIs having a z value relatively close to the targeted z value can now be used instead of the single component TTIs when these are not available. It was shown that two components TTIs with z values respectively below and above the targeted z value could be potentially used to evaluate thermal efficiency of food for sterilisation processes (Guiavarc'h *et al.*, 2005a; Hendrickx *et al.*, 1995).

2.1.4.5. Other TTI applications: monitoring the cold chain

TTIs are already commercially available as tools for quality monitoring and control of frozen products. Several studies were undertaken on the reliability of these commercially available TTIs. The A12 Fresh Check TTIs label (Lifetimes Technologies, NJ, USA) were used to monitor the distribution chain in real world applications. These TTIs have the shape of a label and can be stuck on the food packaging. A chromatic variation appears on the label depending on the time temperature that they have been exposed to, which can be related to a quality loss. This study showed that the temperature effects recorded by the TTIs were well correlated to the decreasing quality of the food. In this study, it was found out that the TTIs could be used as an alternative technique to the direct temperature recording (Riva *et al.*, 2001). Other TTIs are available for commercial uses such as: the MonitoMark TTI (3M, St Paul, USA) which was used in research on the reliability of TTIs when temperature abuse occurs during the distribution and the storage of frozen food. (Shimoni *et al.*, 2001).

Other studies showed that TTIs can be used to monitor changes in quality attributes of perishable and semi perishable foods (e.g. tomatoes, naked and wrapped lettuce, canned fruitcake and UHT sterilized milk) and that they can be used as effective tools to monitor the cold chain (Wells and Singh, 1988; Giannakourou *et al.*, 2005).

2.1.4.6. *Advantages and disadvantages of TTIs*

TTIs are small, wireless and shock resistant which made them suitable for processes where the thermocouples and data loggers can not be used. TTIs are relatively fast to analyse compared with the microbiological method where incubation times are long (3 days), inexpensive and minimal training is needed for their analysis. The major advantage of the TTIs is that there is no need to know the time temperature history of the product in order to determine the impact of the thermal treatment on the food. TTIs can be used as a measuring tool in process validation or optimisation when the use of thermocouples or other methods is not possible. However, TTIs are not suitable for on-line monitoring of the thermal treatment efficiency since their analysis is not immediate. In addition, since they are very small, their retrieval from the food product can be an issue. TTIs can be used for determining the efficiency of thermal treatments in order to improve the design of processes or to improve the quality of a product by validating processes routinely used. Another limitation of the TTIs is the need to know their D_T and z values in order to process the data. Preliminary experiments are needed before being able to use them and each batch of enzyme has to be calibrated (Maesmans *et al.*, 2005; Van Loey *et al.*, 1996a; Van Loey *et al.*, 1996b).

2.1.4.7. *Recent researches on TTIs*

Recently, some studies have been undertaken on the applicability of intrinsic TTIs from thermally processed milk to assess high pressure process. The study found out that the heat markers for high pressure are different from the criteria used for the thermal treatment of milk and therefore can not be used to evaluate the efficiency of high pressure processes (Claeys *et al.*, 2002).

New types of TTIs are still being developed having faster analysis techniques. This is the case of a TTI based on an amperimetric glucose oxidase biosensor. The TTI consists of enzymes trapped within an electronically generated poly o-phenylenediamine film. This film is coated on the interior wall of a capsule made of platinum or platinized stainless steel. After the thermal treatment, the TTIs were rapidly analysed (10 min) by an amperometer. Some isothermal treatments were performed at low pasteurisation temperature (70°C - 80°C). The enzyme followed a first order reaction and z values of 6°C -7°C were found. These TTIs showed a potential for fast assessments of pasteurisation processes where *E.Coli* and *Listeria monocytogenes* are the targeted micro organisms (Reyes-De-Corcuera *et al.*, 2005).

As stated previously, several studies have been undertaken on the production of sterilisation TTIs. Industrialists who produce various kinds of sterilised products are keen on the future development of a TTI for sterilisation temperatures. Several studies have been published on sterilisation TTIs that are made from the α -amylase from the *Bacillus subtilis* and the *Bacillus licheniformis*. This α -amylase was used at reduced water content and was immobilised on glass beads. These TTIs (z value of 9.4°C) that were equilibrated at $a_w = 4.8$ could monitor process values at 121.1°C in the range of 0-30 min under non isothermal conditions with an absolute error of 14%. The results showed that this TTI can be used for the determination of heat treatment efficiency of sterilisation processes (Guiavarc'h *et al.*, 2004a). The same type of enzyme was used by the same group of researchers for an industrial application of sterilisation processes (Guiavarc'h *et al.*, 2005b). The continuous rotary processing of canned ravioli was investigated by using both temperature probes and TTIs together. The *Bacillus licheniformis* α – amylase and the *Bacillus subtilis* α – amylase were used to make the TTIs which have z values of 13.9 and 16.4°C respectively. These 2 enzymes have different z values above 10°C; therefore they were used together as multi component TTIs (§ 2.1.4.4).

For the same thermal process, the multi component TTI inserted inside ravioli gave a F value at 121.1°C of 23.6 min with a standard deviation of 1.5 min while the temperature probe measuring the sauce temperature gave a F value at 121.1°C of 33.6 min. This study showed that by measuring the temperature in the sauce, the impact of the thermal process is overestimated, causing food safety issues. The drawback of the use of these TTIs was the complicated preparation and the need for technical skills to produce and analyse the TTIs.

The sterilisation TTI made from the α -amylase of the *Pyrococcus furiosus* seems to be a better alternative since its preparation and use is similar to the pasteurisation TTIs. However, the culture of this micro organism is difficult and α -amylase production is difficult to control (Tucker *et al.*, 2007 ; Tucker *et al.*, 2005b).

2.1.4.8. Reliability of the TTIs as indicators of the efficiency of a thermal process

Investigations have been undertaken on the reliability of TTIs under non isothermal conditions (Taoukis and Labuza, 1989). Non isothermal experiments of 2 types were performed: the first experiment was performed using high temperature for a long time followed by storage at low temperature to investigate the ‘history effect’ and the second experiment was done by storage at controlled sinusoidally varying temperatures. The result of this research shows that there is a direct correlation between the TTIs’ responses and the quality of the food under variable time temperature profiles. Guiavarc'h *et al.* (2002b) used TTIs to monitor thermal impact inside a solid/liquid model food and showed that incorrect conclusions could be drawn using F values for solid pieces obtained just by using temperatures recorded at the centre of the solid at the tip of a thermocouple. Nevertheless, these results show the potential of TTIs in the evaluation of the thermal process efficiency. Yet, currently published literature on their use is limited. In general, there is a lack of

knowledge on their accuracy and efficiency. Errors in the measurement arise from a number of factors, including variability in the manufacture of the TTIs, errors in determining the final and initial value of activity, as well as non-linearities and variations in the kinetics of the enzyme. Some understanding of the inherent accuracy of the devices is needed in order to develop TTIs as effective process probes. TTIs have been used for various industrial applications and are described in Table 2-2, which shows that it is not clear if the variability of the TTIs is due to the process variability or due to the TTI itself.

Table 2-2. Example of application

	Study 1	Study 2	Study 3
Application	<i>P</i> -values for fruits processed in a tubular heat exchanger	<i>F</i> values for Raviolis inside cans processed in a spiral retort (Sterilmatic, Belgium)	<i>P</i> values in a stirred vessel (250l) – 200l batch of 5% Colflo 67 starch
Number of TTIs used	70	7 cans with 10 TTIs in each	50
Mean <i>P</i> value or <i>F</i> value	$P_{85^{\circ}\text{C}} \sim 60$ min	$F_{121.1^{\circ}\text{C}} \sim 18.8$ min	$P_{85^{\circ}\text{C}} \sim 3.9$ min
Variability	$P_{85^{\circ}\text{C}}$ vary from 33 min to 109 min	$F_{121.1^{\circ}\text{C}}$ vary from 10 min to 29.1 min	$P_{85^{\circ}\text{C}}$ vary from 1.2 min to 11.3 min
Reference	Tucker <i>et al.</i> , 2002	Guiavarc'h <i>et al.</i> , 2005	Lambourne et Tucker, 2001

Hence there is a need to investigate the variability and accuracy of TTIs by removing any process variability. This objective is key to this thesis since it will enable results obtained from thermal processing using TTIs to be analysed with improved understanding.

2.2. Flow hydrodynamics and mixing

The first part of this literature review focused on the measurement of the heating efficiency inside large agitated heated vessels. However, this investigation is not complete without understanding how the fluid flows inside the vessel which is key to determine the thermal processing received by the food. In addition, since the flow may be turbulent, it is even more

difficult to characterise (Harnby *et al.*, 1992). Moreover, when TTIs are used to determine the thermal treatment efficiency, it is essential to ensure that they are representative of the fluid flow and the fluid behaviour has to be studied to ensure this is the case. This is necessary to ensure that the P values determined by the TTIs are representative of the vessel.

Recently, a large number of studies focused on the determination of the fluid pattern inside vessels and several techniques are available for visualisation. The present study will show the use of some of the techniques available to determine the flow path inside a vessel. This type of information is essential for companies that aim to improve the design and performance of the vessels that they manufacture.

2.2.1. Mixing Challenges in Food industries

Mixing is a common feature of any food production process. From the point of view of thermal processing, the aim of the mixing operation is to ensure homogenous treatment. If this operation is not well performed, the product quality will get lowered with possible safety implications.

Mixing operations can be classified according to the type of phase that they intend to mix:

- Single-phase liquid mixing: This operation is used to mix miscible liquids together (e.g. Tomato soup made from concentrate).
- Solid-liquid mixing: This operation is used to suspend solid particles into a liquid fluid (e.g. mushroom soup).
- Gas-liquid mixing: It is used to disperse the gas into a continuous liquid phase. This operation can be performed to create structure such as foams (e.g. chocolate mousse).

- Liquid-Liquid mixing: This operation takes place between 2 immiscible liquids (oil and aqueous phase). The droplets of one liquid are dispersed into the other one. Emulsification is a very common process of liquid-liquid mixing (e.g. Mayonnaise) (Harnby *et al.*, 1992).

2.2.2. Mixing fundamentals

Liquid-mixing devices can be composed of two different components: (i) the first element is a convective flow to prevent any stagnant regions within the vessel. (ii) The second element is a high shear mixing region. These two parts are energy consuming and the amount of energy needed is determined by the application. Some food products are highly viscous and therefore require high energy inputs to be homogeneously mixed (Harnby *et al.*, 1992). The Reynolds number, Re , can be calculated in order to determine if the fluid is laminar or turbulent:

(i) For flows in a circular pipe or tube:
$$Re = \frac{\rho \bar{U} L}{\mu} \quad (2.5) \text{ (a)}$$

Where \bar{U} is the mean velocity of the flow (m s^{-1}), L is the length-scale which characterises the flow (m), μ is the dynamic viscosity (Pa.s) and ρ is the density (kg m^{-3}).

(ii) For flows in a mechanically stirred vessel:
$$Re = \frac{\rho N D^2}{\mu} \quad (2.5) \text{ (b)}$$

Where N is the Rotation rate (rev s^{-1}) and D is the impeller diameter (m)

Once the Reynolds number is determined, the fluid flow can be classified in one of the three different categories. For example, for flows in a circular pipe or tube:

- $2000 < Re$: laminar flow
- $2000 < Re < 3000$: transitional flow
- $3000 < Re$: turbulent fluid

And for stirred vessels:

- $10 < Re$: laminar flow
- $10 < Re < 10000$: transitional flow
- $10000 < Re$: turbulent fluid

These values will change for different geometries.

Laminar flow

The mixing of highly viscous fluids such as pastes, doughs and melts often lead to laminar flow conditions and therefore long processing times are necessary. To achieve a turbulent flow for these types of fluids, unfeasibly high energy inputs would be necessary.

Blending and incorporation of fine particulates are usually the types of duties that need to be achieved to highly viscous fluids. For blending operations, two or more fluids of different viscosities have to be mixed. The resulting product must have a uniform texture and the desired quality. For the dispersion of fine particulates into high viscous fluid, the distribution of the fine solids must be homogenous within the fluid.

In the case of laminar flow, the basic mixing mechanisms are as follows:

- *Laminar shear*: Mixing is due to the motion between the streamlines which causes deformation of the fluid element. The velocity gradient is normal to motion and causes an increase of the interfacial areas between the liquid to be mixed.

- *Elongation flow*: Mixing due to a change in flow channel geometry or the acceleration of the fluid. In that case the velocity gradient will be parallel to the motion, as a result of this the interfacial areas liquid to be mixed will increase.
- *Chaotic mixing*: Mixing due to folding of the flow. Usually accomplished by changes of flow direction (e.g. Static mixer) (Harnby et al., 1992).

Turbulent flow

When the *Re* number is sufficiently high, the regime becomes turbulent. It is no longer possible to predict the instantaneous velocity of the fluid at any point, but it is possible to use statistical approaches to calculate as mean and rms (root mean square) velocities provided the flow is steady on average (constant flow rate).

During turbulent mixing in vessels, the energy provided by the rotating impeller is transmitted to the fluid which starts circulating throughout the vessel and back to the impeller. This fluid circulation causes diffusion by turbulent eddies which will reach a maximum in the impeller region where most of the energy is dissipated (Harnby et al., 1992). An eddy can be defined as any event in a flow with a length scale assigned to it (Paul et al., 2003). The eddy diffusion will lead to a more rapid mixing when compared to the rate of mixing that occurs for laminar flow.

The process of mixing occurs at different length scales within a flow field. The macromixing relates to the fluid mixing for the largest length scale. In this case, the large eddies whose sizes are comparable to the impeller diameter, have large velocity fluctuations of low frequency. At this length scale, the motion of the fluid is anisotropic and this type of mixing

is essential for gross circulation of the fluid and the dispersion of reactants within the vessel. These large eddies break down to form smaller eddies which continue to break down further. The energy is passed from the impeller to the larger eddies which is then passed down to smaller eddies. Kolmogoroff established that for small eddies, the energy dissipation is isotropic and the smaller eddies are independent of the bulk motion. The properties of the eddies are dependent mainly on the local energy dissipation rate/unit mass, ϵ_T . Eddies are anisotropic above a cut off length scale and are isotropic below it. When the size of the eddy becomes of the order of λ_K (Kolmogoroff length scale), they decay and dissipate their energy as heat. It was established that for an eddy with a size between D (diameter of the impeller) and λ_K , the energy will not be dissipated and will transfer from bigger to smaller eddies (Figure 2-4) (Harnby *et al.*, 1992; Hall *et al.*, 2005; Paul *et al.*, 2003).

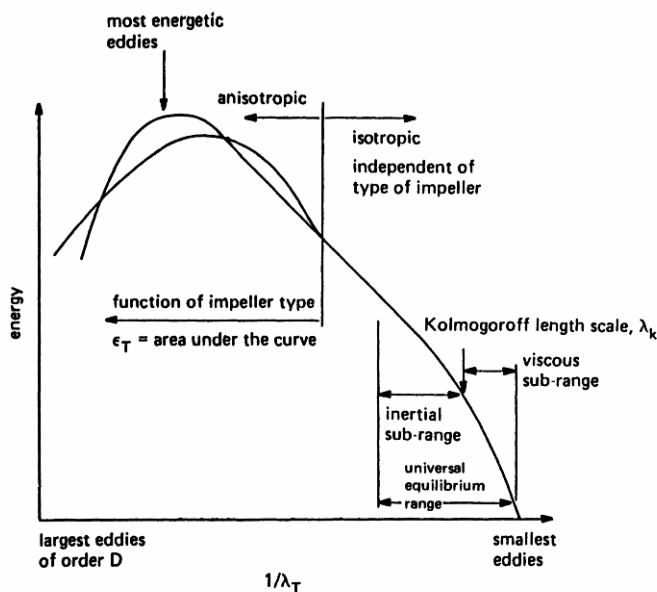


Figure 2-4. Spectrum of eddy sizes and their energy in turbulent flow. Source: Harnby *et al.*, (1992)

Statistical analysis of fully developed turbulence

Turbulent flow is complex and cannot be described easily. It is not possible to know the exact properties of the turbulence at any point. However, statistical properties such as averages can

be used to describe the turbulence (Paul *et al.*, 2003; Frisch, 1995). The velocity signal is commonly decomposed into a mean and a fluctuating component using the Reynolds decomposition:

$$u = \bar{U} + u' \quad (2.6)$$

Where u the instantaneous velocity at any point, \bar{U} is the time averaged mean velocity and u' is the instantaneous fluctuation away from the mean. For a discrete velocity signal of N_d data points, the mean, \bar{U} can be calculated as:

$$\bar{U} = \frac{\sum_{i=1}^N u}{N_d}, \quad (2.7)$$

Where N_d is the number of discrete data points.

The fluctuating component is characterised over the whole velocity signal using the rms, \tilde{u}

$$\tilde{u} = \sqrt{u'^2} = \sqrt{(\bar{U} - u)^2} \quad (2.8)$$

Turbulence intensity

For a 2-D investigation, the turbulence level can be determined by measuring the turbulence intensity:

$$\text{Turbulence intensity} = \frac{\sqrt{(\tilde{u}^2 + \tilde{v}^2)}}{\bar{U}} \quad (2.9)$$

Where \tilde{u} and \tilde{v} are the rms velocities in the X and Y directions respectively.

Typically, for turbulent flow the turbulent intensity is a significant proportion of \bar{U} , typically values ranges from 0.2-0.6

2.2.3. Flow visualisation

Various techniques are available for flow visualisation (Mavros and Baudou, 1997)

- Optical techniques: The properties of the flow are determined via analysis of the trajectories of small particles added to the flow. These can be obtained via point wise measurements by Laser Doppler Velocimetry (LDV) (Lauterborn and Vogel, 1984) or by whole field imaging using Particle Imaging Techniques (PIT). These techniques are Eulerian in nature since they record flow behaviour at a fixed point or field of view.
- Tomographic techniques: The modifications of the properties of a flow within a volume are recorded and a 2-D or 3-D image is constructed (e.g. radioactive tracer -Positron Emission Tomography PET) (Lauterborn and Vogel, 1984)
- Lagrangian tracking techniques: One tracer is added to the fluid and the view follows the particle that is tracked (e.g. Positron Emission Particle Tracking).

2.2.3.1. Optical techniques

Laser Doppler Velocimetry (LDV)

Laser Doppler Velocimetry is an optical technique which allows the measurement of the local instantaneous velocity of seeded particles (~0.5 - 5 microns (in air) or 1~20 microns (in water)) conveyed by a fluid flow (Mavros *et al.*, 1997; Mavros and Baudou, 1997). This method is not intrusive (since apart the seeded particles) no probe is added to the fluid (Mavros *et al.*, 2005).

This technique uses a laser as a source which produces an oscillating light with a known frequency and wavelength directed toward the seeded particles. The light scattered by the particles is emitted at a certain frequency which is related to the velocity of the particles.

The principles of the measurement of the particles velocity is based on an optical principle called Doppler effect. A moving observer can record the change of wavelength and frequency of a stationary source emitting wave. This assumption can be applied when the source is moving and the observer is stationary. Therefore, the scattered laser light oscillates with a specific frequency that is related to the velocity of the particles (Durst *et al.*, 1981).

This technique has been widely used for flow investigation. It has been used for specific applications such as high speed flow measurement or measurement in flames (Durst *et al.*, 1981). This technique was used by Yu *et al.* (2003) to measure 3-D laminar flow in helical pipes. The experimental observations were compared to the numerical calculation and a good agreement was found between the data. Wu and Paterson (1989) used the LDV technique to measure turbulent flow parameters in a baffled Rushton turbine agitated vessel. This study

show that 60% of the energy transmitted from the impeller to the vessel was dissipated around the impeller and impeller stream, and 40% was dissipated in the bulk of the vessel. LDV technique has been widely used to examine flow in stirred vessels.

Particle imaging techniques

Particle imaging techniques measure the motion of a fluid on a small pre determined region. Depending on the nature of the fluid, markers are added in various densities. Two or more successive images are taken one after each other and from the positions of the markers on the successive images; the flow field can be reconstituted.

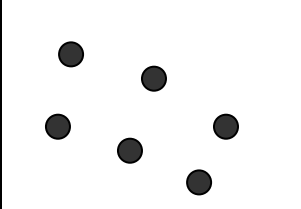
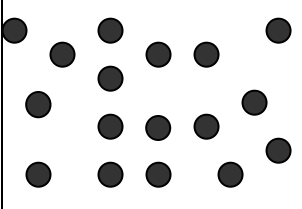
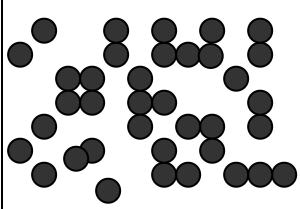
The fluid velocity can be measured from the position of the markers on the two successive images by the fundamental equation

$$u(x,t) = \frac{\Delta x(x,t)}{\Delta t} \quad (2.10)$$

Where Δx is the displacement of the marker over a short time interval Δt . Initially the marker is located at the position x at the time t (Adrian, 1991).

Different types of particle imaging techniques exist and depend on the concentration of the tracer added to the fluid. The different types of techniques are described in Table 2-3:

Table 2-3. The three different particle imaging techniques

Name of the technique	a: Particle Tracking Velocimetry	b: Particle Image Velocimetry	c: Laser Speckle Velocimetry
Density of the tracers	Low	Medium	High
Tracers inside an image			

Particle Tracking Velocimetry (PTV): Since there are no overlapping particles between the images, the density of the tracer is low and therefore the image analysis is fast (Lagrangian) (Adamczyk and Rimai, 1988).

Particle Image Velocimetry (PIV): The density of the tracers is medium and still no overlapping particles can be observed. This technique is most popular and will be described in detail in the next section (Adrian, 1991; Khan, 2005).

Laser Speckle Velocimetry (LSV): The seeding density is high. It is difficult to follow the displacement of a single particle. Therefore, this technique does not consider a single particle but consider the image of the particles as a whole (Barker and Fourney, 1977; Meynart, 1983).

PTV and LSV will not be described in more detail here since the technique used in this work is PIV. The PIV is a suitable technique for this study and the department of Chemical Engineering of the University of Birmingham has the expertise of using it.

Particle Image Velocimetry

Particle Image Velocimetry (PIV) is a flow visualisation technique which allows quantification of the fluid velocity and the flow structure (La Fontaine and Shepherd, 1996). According to Adrian (2005), PIV enables ‘the accurate, quantitative measurement of fluid vectors at a very large number of points simultaneously’.

Particles within the flow are illuminated by a sheet of pulsed laser light. The pulse frequency should be high enough to ensure that the displacement of particle is small between the images. Photographic recording is made of the light scattered by the particles and the displacement of the particles between the images is analysed. The data recording has been improved by the increased use of digital cameras, called Digital PIV (DPIV) and will be used in this study (Grant and Smith, 1988; La Fontaine and Shepherd, 1996; Law and Wang, 2000; Raffel *et al.*, 1998; Willert *et al.*, 1996).

PIV technique is a useful flow measurement technique with some important advantages compared to other techniques. It is non intrusive and unlike LDV, PIV can obtain whole fields data rapidly in a wide range of applications (Raffel *et al.*, 1998).

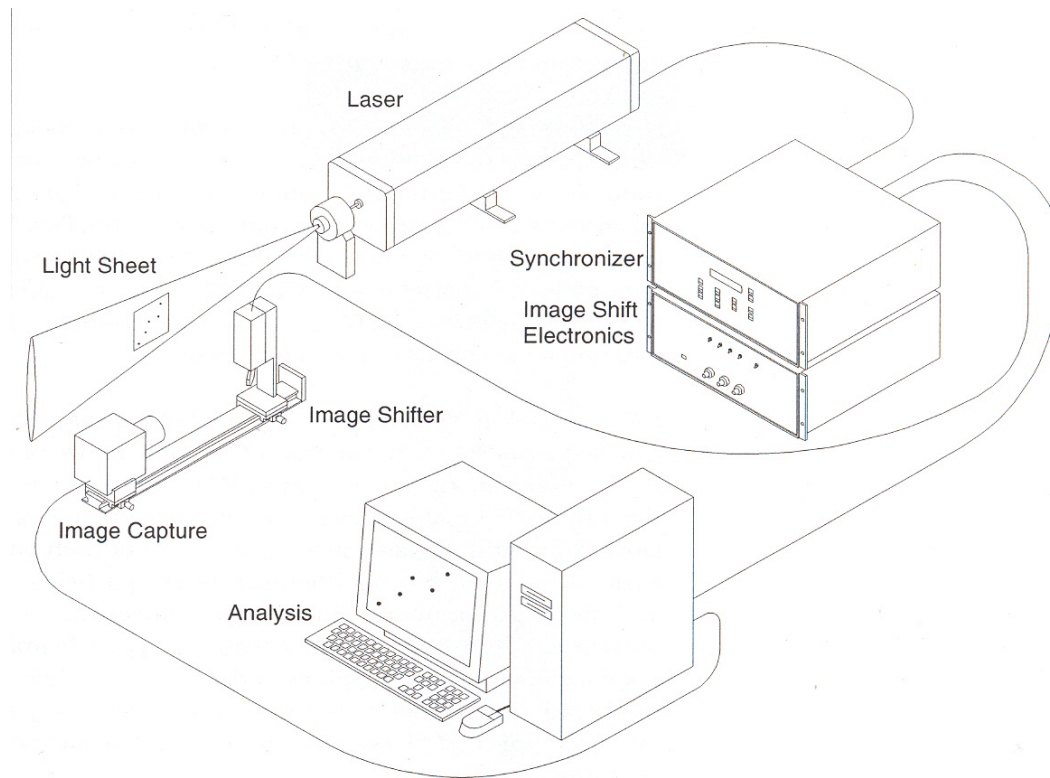


Figure 2-5. Digital Particle Imaging Velocimetry (TSI ltd)

Figure 2-5 shows the main components of the DPIV system. The particles added to the fluid are illuminated by the pulsed light from the laser beam. The displacement of the particles is recorded with the camera. The image acquisition and timing of the laser pulse are controlled by the synchroniser. Finally, the data are collected and the displacement of the particles is calculated. Each component of the DPIV system will be described in more detail in the following sections.

Tracer particles

The measurement of the velocity is indirect since particles are added to the flow and the velocity of the fluid is measured through the displacement of these particles. The size of the particles must be chosen by considering the following parameters (Law and Wang, 2000):

- The particle must be small and neutrally buoyant to exactly follow the fluid path. It is usually not too difficult to find particles which have similar densities (Raffel *et al.*, 1998). The relaxation time must be as small as possible in order for the particle to be able to follow the fluid path. The relaxation time defines the tendency for the particle velocity to reach equilibrium with the fluid velocity. The equation is obtained from the Stokes drag law and is as given below.

$$\tau_s = d_p^2 \frac{\rho_p}{18\mu} \quad (2.11)$$

Where τ_s is the relaxation time (s), d_p is the diameter of the particle (m), μ is the dynamic viscosity (Pa.s) and ρ is the density (kg m^{-3}). The relaxation time needs to be < 0.1 s.

- The light scattered by the particles must be intense enough to be detected by the camera. The size, shape, polarisation and observation angle influence the intensity of the light scattered by the particles. According to Khan (2005), the size of the particles for liquid flow in the field of view should be 1-2 pixels.

The laser: Nd:YAG

Lasers are commonly used in PIV since they emit high intensity monochromatic light which can be manipulated to form a thin sheet for the illumination of the tracers.

Nd:YAG (Neodym-Yttrium-Aluminium-Garnet) lasers are used most commonly. They have a wavelength of 532 nm (green light) with pulses of energy varying from 10 mJ to 400 mJ per pulse. The 2 pulses are separated by a time interval, Δt . The time separation Δt is an important adjustable parameter in PIV experimentation since it defines the maximum and minimum velocities which can be measured. The Nd:YAG laser can have a wide range of Δt and can measure slow flow speed to supersonic speeds. Pulse duration for the Nd:YAG laser can vary from 4 ns to 20 ns (Adrian, 1991; Adrian, 2005; Raffel *et al.*, 1998).

The production of a light sheet at the required dimensions is essential for the PIV experimentation and cylindrical lenses are used to generate it. Additional focussing lenses are used to produce a sheet with thickness < 1 mm (Figure 2-6).

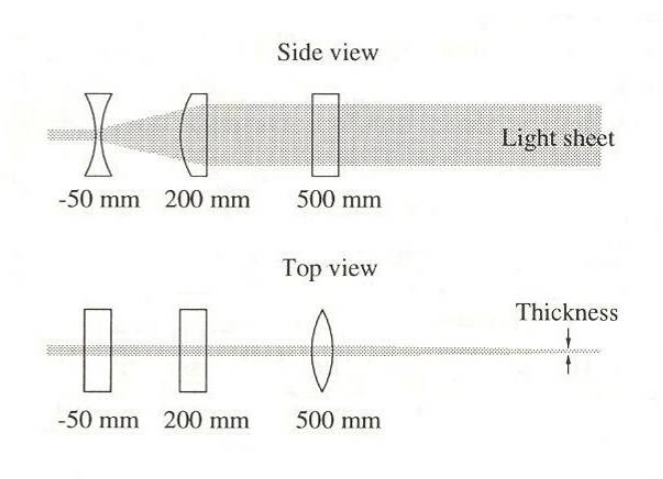


Figure 2-6. Light Sheet optics (Raffel *et al.*, 1998)

PIV recording technique: Digital PIV

In the early 1990s, the use of digital camera increased dramatically compared to the use of photographic recording and now it is used almost exclusively. The digital camera used for PIV experiments are called Charged Coupled Device (CCD). The CCD camera which is an electronic sensor, transforms photons (light) into electric charge (electrons). The CCD sensor is composed by many individual CCD which are arranged as a line or as a rectangle. Each individual CCD is called a pixel and its size is usually $10 \times 10 \mu\text{m}^2$. The electric image recorded by the camera is then sent to the computer. There are different types of CCD sensors used in PIV (Full frame CCD, Frame transfer CCD, Interline transfer CCD and Full-frame interline transfer CCD). Their working principles vary and the type of application determines which one should be used.

There are two PIV recording modes:

- Single frame/multi-exposure: This technique is historically the oldest one. Two or more exposures are recorded on a single frame. In this case, the sign of the direction of the particle displacement can not be determined and further analyses are required to resolve this issue.
- Multi frame/single exposure: Each image contains one exposure and multiple images are taken. This technique preserves the time order of the image of the particle. Therefore, the data analysis is easier than for the single frame/multi exposure (Raffel *et al.*, 1998). This technique was used for this study.

The synchroniser

The camera has to be synchronised with the laser in order to allow recording of the two or more full frames for short time intervals. The camera sends the timing to the pulsed laser by a special frequency divider/multiplexer device (the synchroniser). The pulse separation time can be very short since for some studies such as aerodynamics where the flow velocity is high (Stanislas *et al.*, 2000; TSI Inc., 2002).

Image analysis

The recordings are transferred from the CCD camera to the Computer memory in order to be processed. The images are divided into interrogation windows or interrogation cells. The size of the interrogation windows can be 8×8 pixels, 16×16 pixels, 32×32 pixels or 64×64 pixels. The interrogation methods are basically statistical approaches. In each interrogation cells, the displacement of the particle is measured by statistically pairing the particles. The most commonly used methods are:

- The auto-correlation method: This technique is applied for single frame/ multi exposure recording (one image I , contains two sets of points). The equation is given below:

$$R(x, y) = \iint I(x, y) I(x + \varepsilon_x, y + \varepsilon_y) dx dy \quad (2.12)$$

Where R is the spatial auto-correlation function of the intensity of the transmitted light I , x and y are the positions of the particles in the image and ε_x and ε_y are the displacement vector between the members of an image pair. For each interrogation windows, the auto-correlation

function is used in order to calculate the displacement of the particles. However, this technique does not give the flow direction (+/-).

- The cross-correlation method (Figure 2-7): This technique is used for multiple frames/single exposures. Two images are taken with a short delay between them. Ideally, particles found on an interrogation cell from the first image can still be seen within the same interrogation cell from the second image. The displacement of the particle can be therefore calculated. However, errors arise from the loss of particles between interrogation cells. Hence, the second interrogation window can be displaced by up to 50% of the first one to compensate. Compared to the auto-correlation technique, the ‘in plane’ loss of correlation is lowered. The cross-correlation function represents the statistical distribution of all possible direction which could be taken by the particles (two image $I + J$ separated by Δt).

$$R(x, y) = \iint I(x, y) J(x + \varepsilon_x + y + \varepsilon_y) dx dy \quad (2.13)$$

where R is the spatial cross-correlation function of the intensity of the transmitted light and I and J are the first and second images respectively. The cross-correlation method was used in this study, see Figure 2-7 (Adrian, 1991; Adrian, 2005; Khan, 2005; Raffel *et al.*, 1998; Stanislas *et al.*, 2000). Some recent applications of PIV are given in Table 2-4.

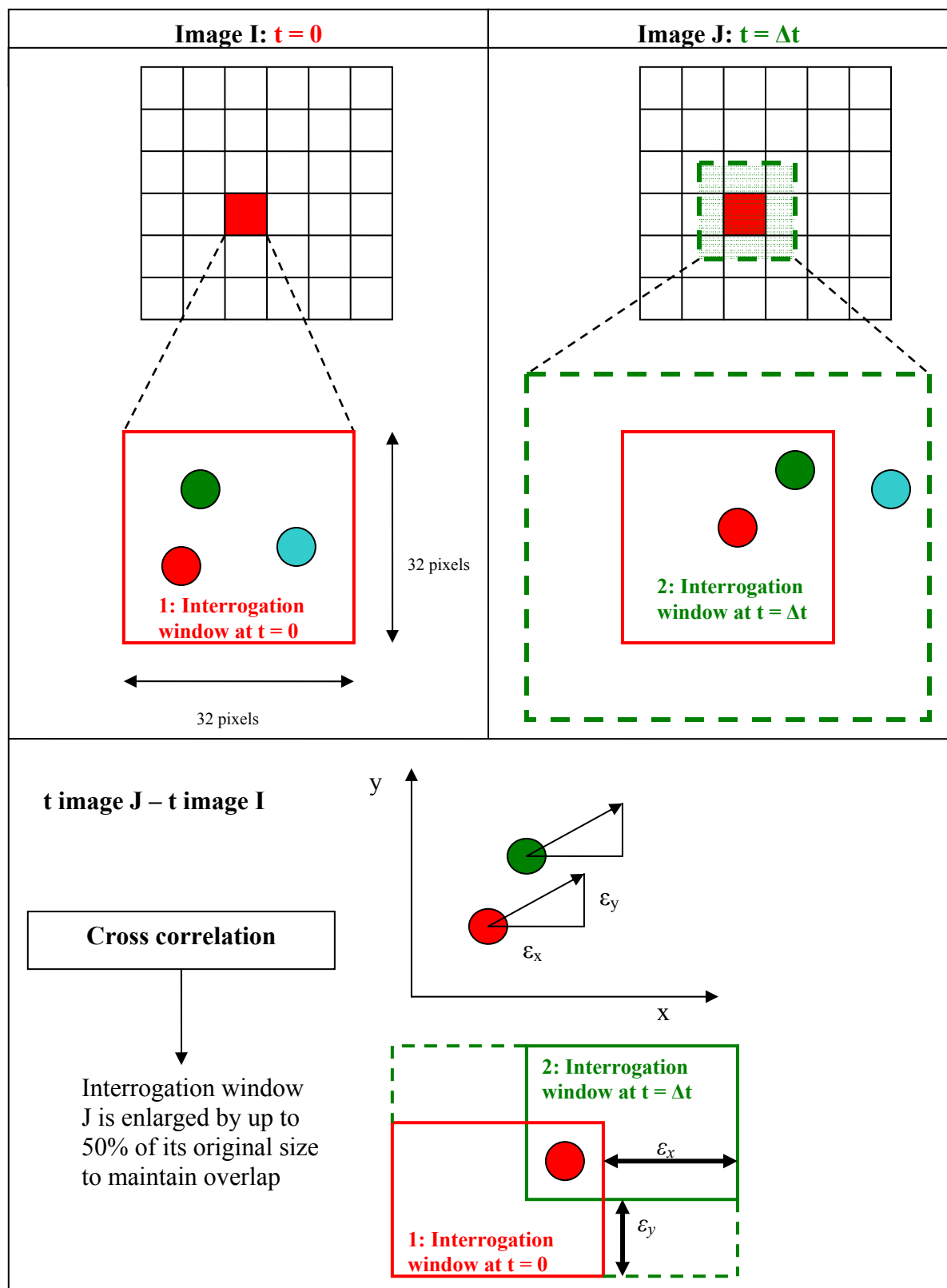


Figure 2 -7. Cross correlation

Table 2-4. Examples of application

Reference	La Fontaine and Shepherd (1996)	Aubin et al. (2004)	Hall et al. (2005)	Simmons et al. (2007)	Chung et al. (2007)
Study	A scanning PIV system was used in order to study the pattern of the flow. This automated scanning PIV system was moved at different location of the vessel and the flow was interrogated at these different locations.	Investigation of the effect of the agitator configuration and the gas phase on the mean velocity fields and turbulent quantities	Effect of eccentric agitation in order to improve the mixing performance. The performance of the mixing was compared for three different configurations: unbaffled with centreline agitation, baffled with centreline agitation and unbaffled with eccentric agitation	PIV to study the mixing behaviour of 3 different up-pumping agitators in a model bioreactor of 15 cm diameter	2-D PIV technique to reconstruct a 3-D flow field inside miniature stirred vessels was used. This study was performed for 3 different types of configuration of agitators: unbaffled with centreline agitation, baffled with centreline agitation and unbaffled with eccentric agitation
Applied to	Stirred vessel	Aerated stirred tank	Small high throughput experimentation reactors	Bioreactor	Miniature stirred vessel
Impeller type	Not given but impeller offset from the vessel axis	6 blade 45° Pitched Blade Turbine (PBT)	Up pumping 6 bladed PBT	six-blade PBT, Hayward Tyler hydrofoil and Applikon 'elephant ear' impeller	Up pumping 6 bladed PBT
Presence baffles	2 of dissimilar shape	4 placed at 90° of each other	Removable baffle: 4 equally spaced	4 placed at 90° of each other	3 different configuration
$D =$ Diameter of the Impeller	Not given	95 mm	3 reactors: 35, 24 and 19 mm	67.5 mm	24.5
$T =$ Diameter of the vessel	250 mm	190 mm	3 reactors: 60, 45 and 35 mm	150 mm	45 mm
Fluid	Water	Water	Water	Water	Water

Limitations of optical techniques

Optical techniques have some limitations. The fluid used can not be opaque since the laser light has to go through the vessel. Many real-life fluid are not translucent and therefore the applicability of the technique is limited (Mavros *et al.*, 2005). Additionally, the vessel needs to be made of glass in order to have the laser light being able to pass through the vessel to illuminate the particles. In food industries, vessels are usually made of stainless steel.

2.2.3.2. PEPT (Positron Emission Particle Tracking)

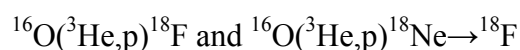
Positron Emission Particle Tracking (PEPT) is a technique used to monitor motion inside opaque systems. It is a non invasive method which allows the study of complex fluid flow in three dimensions where other visualisation technique can not be used (e.g. PIV). PEPT is a development of Positron Emission Tomography (PET) which is commonly used in medicine to study the functioning of the human body via measurement of the distribution of a radioactive tracer. However, PEPT uses a small particle as a tracer to track fast moving fluids. The University of Birmingham started successfully to use this technique for the study of fluid flow inside engineering equipment (Fan *et al.*, 2006b; Fitzpatrick *et al.*, 2003).

The tracer

The particle used as a tracer for PEPT must be chosen according to the fluid used for the experiments. The tracer has to be isokinetic with the fluid, since otherwise it will not be possible to relate the particle velocity to the fluid velocity. The tracer size, density, shape and surface property considerably affects its motion relative to the fluid so, the material used to

produce these tracers must be the same from experiment to experiment. The most frequently used radioisotope for PEPT study in the University of Birmingham is ^{18}F , the half life of this radioisotope is short enough to avoid persistent radioactivity in the equipment and long enough to be detected during the whole experiment (109 min). This is a reasonable time scale for most experiments. Other radioisotopes such as ^{66}Ga , ^{22}Na , ^{61}Cu and ^{64}Cu could be used for PEPT study. However, compared to the others, ^{18}F presents a key advantage. It does not emit γ -rays other than the 511 keV annihilation photons which means that it can be detected with a high accuracy (Bakalis *et al.*, 2006; Fan *et al.*, 2006a; Fan *et al.*, 2006b; Parker *et al.*, 2005b; Barigou, 2004).

The ^{18}F radioisotope is produced in the cyclotron of the University of Birmingham (the SCANDITRONIX MC40) where either purified water or solid materials are bombarded using a 33MeV ^3He beam. The ^{18}F is produced via the following reactions:



Purified water is bombarded with a 33MeV ^3He beam inside the cyclotron for 30 min at a current of 10 μA . After 20 minutes, the water has a specific radioactivity of 15-18mCi/ml. During this bombardment, ^{18}F produced is in ionic state and can be added to a particle via ion-exchange or surface adsorption. Ion exchange technique was used here and can produce a tracer with a minimum size of 60 μm . The ^{18}F can be adsorbed into organic or inorganic materials. Two kinds of anion exchange resins can be potentially used for the production of radioactive tracers:

- Weak- base anion exchange resins

Water interacts with the free amine and form $\text{RCH}_2\text{NH}(\text{CH}_3)_2^+\text{OH}^-$. The OH^- can be exchanged by the ^{18}F . However, this reaction is weak and is dependent on the concentration of hydroxide ions in water. Therefore, in order to keep the capacity of the anion exchange resin, the pH must be kept low.

- Strong-base anion exchange resins

The resins used for strong-base anion exchange resins are quaternary ammonium derivative and are provided in chloride form. However, the affinity of the ^{18}F to the functional group ($-\text{CH}_2\text{N}(\text{CH}_3)_3^+$ or $-\text{CH}_2\text{N}(\text{CH}_3)_2(\text{CH}_2\text{CH}_2\text{OH})^+$) is lower than the affinity with the chloride. Therefore the resin must be converted into a fluoride or hydroxide form before being able to label the tracer. This resin is less affected by the pH of the water or the concentration in hydroxide ions.

In this study, the tracer was labelled with the strong-base anion exchange resins. The amount of radioactivity measured in a single resin bead is greater than 300 μCi for a tracer with a minimum size of 60 μm (Fan *et al.*, 2006b).

Once the tracer is produced, it has to be coated with a fine layer of lacquer in order to use it for liquid mixing application. If the tracer is not coated, the radioactivity will leak into the fluid inside the mixing tank. In addition, the tracer can be made neutrally buoyant by painting it.

The tracer detection

The labelled ^{18}F tracer particle decays (in the form of beta-decay) to produce a positron. The positron annihilates by combining with an electron, generating energy which is released in the form of two 511 ke V γ -rays emitted back to back (180°). The γ -rays are detected by two cameras positioned facing each other (Figure 2-8). The location of the tracer can be determined several times per second by triangulation of multiple successful annihilation vectors (Schutyser *et al.*, 2003; Stellema *et al.*, 1998).

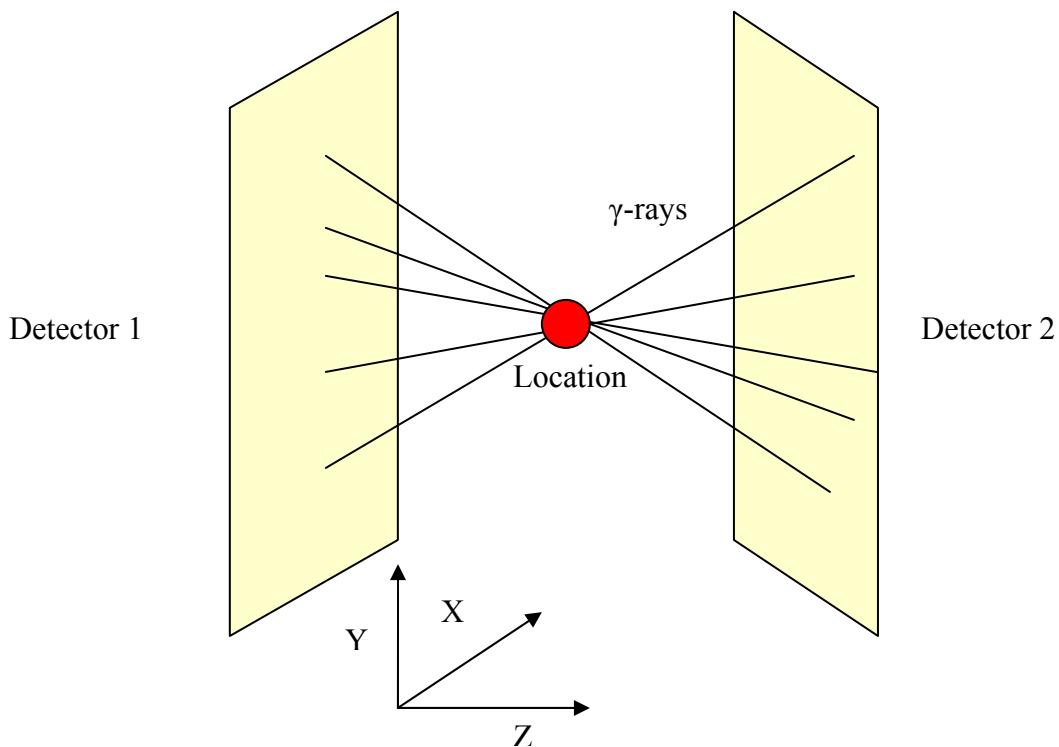


Figure 2-8. Schematic diagram of PEPT for a single-particle

Each detector is composed by a single sheet of 16 mm thick sodium iodide scintillator backed by an array of 55 multiplier tubes. The light intensity detected by several tubes is compared

and the location of the gamma ray event can be determined within few mm. Unfortunately, a significant number of these gamma rays detected are invalid since they can have been scattered prior to detection. These invalid events are discarded by using an iterative procedure in which the centroid of the gamma rays detected is calculated and the gamma rays passing the furthest from the centroid are removed. This procedure is repeated until a fixed fraction ' f ' of the initial events remains. The optimum value of ' f ' depends on the geometry and the mass of the material studied. The number of scattered events will increase with the increase of the mass of the material. The precision of the PEPT camera is given by the following equation:

$$\text{Precision of the PEPT camera} = \frac{w}{\sqrt{fN_e}} \quad (2.14)$$

Where w is the intrinsic spatial resolution of the camera, N_e is the number of events detected for the same location and f is the fraction of detected gamma ray used to determine the location of the tracer (Bridgwater *et al.*, 2004; Parker *et al.*, 2002; Parker *et al.*, 2005b).

Processing of the data

Various software packages are available to process the data obtained with PEPT. Dr David Parker from the University of Birmingham developed a software package called TRACK dedicated to the visualisation of PEPT data. This software determines velocity vectors and occupancy (Stellema *et al.*, 1998).

Other packages such as Matlab and Tec Plot can also be used to process the data. However, in this case, the codes to process the data need to be developed specifically for each different application.

Applications

Parker *et al.* (2005a) used PEPT to study the particulate motion inside rotating drums. Sand grains, glass beads and TiO₂ with a size going down to a diameter of 0.5 mm were labelled. The transition between rolling and slumping modes were identified with the PEPT and the velocity of the active layer was calculated for various drum diameters.

PEPT was used for various applications in food industries. The velocity distributions were measured for a viscous fluid inside an aluminium pipe using two different tracers in the study of Bakalis *et al.* (2003). The study showed that the velocity profiles for the two different tracers were significantly different. In addition, it was noticed that the smaller tracer was passing closer to the flow boundaries than the larger one.

Bakalis *et al.* (2004) demonstrated that the accuracy of the PEPT method decreased when the tracer velocity increased. This was shown by following isokinetic tracers in viscous fluid under isothermal and non isothermal conditions.

Three dimensional flows were visualised in axially rotating cans using PEPT in the study of Cox *et al.* (2003). Fluid viscosity and the amount of headspace were varied. The study showed the headspace caused the flow within the two-phase system to become three-dimensional. It was proven that it was the shape of the headspace which gives rise to the three-dimensional mixing rather than the rheological properties of the fluid.

PEPT was used by Bakalis *et al.* (2006) to measure the velocity of a viscous fluid inside a pilot scale heat exchanger. Velocity distributions were calculated from the location of the tracer for a range of barrel speed. At the same, the flow field was simulated using a simple 2-D approach and a full 3-D simulation. The comparison of the results from the PEPT with the results from the simulation showed a good correlation.

Flow patterns in non-Newtonian CMC (Carboxymethyl cellulose) solutions inside a vessel agitated by an axial flow impeller were studied by Fangary *et al.* (1999). The study shows that the agitator behaved as a radial flow impeller as the viscosity of the fluid increased. It was found out that the use of PEPT helps to characterise the mixing efficiency by identifying the stagnant zones and the zones of low mixing. A similar study was done by Fangary *et al.* (2000), on the mixing effectiveness of two axial flow impellers (A410 and A320). The trajectories of the tracer were determined by a statistical analysis and results showed that an increase in agitation speed give a wider trajectory distribution in the tank.

PEPT is a relatively new technology and limited number of studies are available on the use of PEPT on stirred tanks. The few studies of PEPT on mixing tanks are usually not relevant for food industries since the impellers used are never used for food processing (i.e. Rushton turbine). This study will use PEPT for measuring the mixing efficiency in a food mixing vessel.

Latest development in PEPT

PEPT was successfully applied for the tracking of a single tracer. New studies focus now on using multiple particles. Yang *et al.* (2006) used multiple tracers with different radioactivity concentration. The use of multiple tracers allows obtaining comparative information on the

physical processes. Examples showed that the use of multiple tracers still gives valuable and accurate results for stationary or for moving particles. Unfortunately, this technique will not be used in this study because it is beyond the scope of this study.

2.3. Conclusion

TTIs are used almost exclusively without consideration of their location in fluid systems (which is not a problem in solid products such as quiches). In industry, vessels used to process food are heated from the bottom and in some cases steam is injected towards the centre of the vessel. Therefore, according to the path that TTIs take inside the vessel, the measured thermal efficiency will be different. If the TTIs remain at the bottom of the vessel during the whole process, the P values of the TTIs will be high and therefore, the process would be underestimated. It is therefore essential to have an understanding of the fluid flow and the location of the TTIs during the process. Fryer and Robbins (2005) stated that the trajectories of the TTI particles through the equipment (due to the heating surfaces) need to be known in order to be able to use TTIs as tools to determine thermal treatment efficiency. This analysis could be carried out by using flow visualisation techniques such as PIV and PEPT. Understanding the fluid flow inside vessels is essential in order to validate the use of TTIs to determine thermal process efficiency. This work will start by examining the variability of TTIs alone. Then, the fluid flow inside the vessel will be studied and the TTI path within the vessel will be investigated. To complete this work, the TTI will be used to measure the thermal treatment efficiency of the vessel

Chapter 3

TTI validation study^{*}

3.1. Introduction

The TTI is a relatively new technique which could potentially be used as an alternative to thermocouples for the monitoring of thermal processing of food stuffs. However, an extensive validation process is required before they can be used in industries since it is essential to know their accuracy and reliability before determination of the heat treatment efficiency. This chapter will first describe the validation tests performed in § 3.2 and will then present the results in § 3.3. First the kinetic parameters were studied, and then the maximum process duration that the TTI could monitor was determined. In addition, several TTIs were tested on a Peltier stage where various time temperature profiles were reproduced. Finally, repeatability tests were performed using a PCR (Polymerase Chain Reaction) equipment.

3.2. TTI validation study

This section describes the methods used to determine the efficiency of TTIs. α -amylase of *Bacillus amyloliquefaciens* and α -amylase of *Bacillus licheniformis* were used as test systems.

^{*} Part of this work was published in the journal *Innovative Food Science & Emerging Technologies* : Mehauden, K., Cox, P.W., Bakalis, S., Simmons, M.J.H., Tucker, G.S., Fryer, P.J., 2007. A novel method to evaluate the applicability of Time Temperature Integrators to different temperature profiles. *Innov. Food Sci. Emerg. Tech.* 8 (4), 507-514, doi:10.1016/j.ifset.2007.03.001.

3.2.1. TTI preparation

The enzymes used in the TTI preparation were α -amylase (EC 3.2.1.1. A6380 Type II-A supplied by Sigma, UK) isolated from *Bacillus amyloliquefaciens* (called BAA hereafter) and α -amylase (EC 3.2.1.1. A4551, Sigma, UK) isolated from *Bacillus licheniformis* (called BLA hereafter). BAA has a pH activity range from 5.5 to 6.5 with an optimum at 5.9 and its optimum rate of activity is at 65°C. BLA has a pH activity range from 5 to 9 with an optimum at 7-9. The supplier specifies that the maximal activity is observed at 90°C.

The BAA and BLA solutions were prepared by dissolving 200 milligrams of BAA / BLA powder into 20 ml of 0.05 M tris buffer at pH 8.6 (prepared from Trizma base C₄H₁₁NO₃) giving a final enzyme concentration of 10 mg/ml. These solutions were stored in a freezer at -18°C and exhibited excellent storage stability over several months (Lloyds *et al.*, 2003).

The BAA and BLA solutions (20 μ l) were encapsulated into Altesil (Altec, Cornwall, UK) high strength silicone tubing with a 2 mm internal bore and 0.5 mm wall thickness cut into lengths of 15 mm. The extremities of the tubes were closed by silicone elastomer (Sylgard 170, Dow Corning, USA) and they were stored in a freezer at -18°C.

3.2.2. Measurement of TTI activity

The Randox amylase test method (Randox, 2006) was used to measure the remaining activity of BAA and BLA. This method uses ethylidene-blocked p-nitrophenyl-maltoheptaoside as substrate, which is cleaved by BAA or BLA into various fragments. These are further hydrolysed in a second step by α -glucosidase producing glucose and p-nitrophenol. The

presence of the p-nitrophenol can be detected by absorbance using a spectrophotometer due to its yellow colour.

The BAA or BLA were removed from the TTIs using a syringe and diluted with the tris buffer to a concentration of 10 µl of enzyme solution per 300 µl of buffer. 1 ml of the enzyme assay reagent from Randox (Crumlin, UK) was added to the diluted enzyme solution, put into the measurement cell of a spectrophotometer (CECIL, Cambridge, UK) and the absorbance at a wavelength of 405 nm was recorded at 30°C for 200 seconds online.

From this data, the rate of the reaction can be determined. The initial rate of reaction is linear with respect to the concentration of BAA or BLA, i.e.

$$r_A = k_f C_{BAA}, \quad (3.1)$$

where r_A is the reaction rate, k_f is the first order rate constant and C_{BAA} is the concentration of BAA or BLA (Cornish-Bowden and Wharton, 1988). The rate of reaction can be found from the slope of the absorbance, versus time data obtained from the spectrophotometer. This rate can be compared with that, r_{A0} from a sample at a known initial concentration, C_{BAA0} .

Hence the ratio of initial to the final activity of the enzyme can be calculated as

$$\frac{A_{initial}}{A_{final}} = \frac{C_{BAA0}}{C_{BAA}} = \frac{r_{A0}}{r_A}, \quad (3.2)$$

The same calculation also applies to the BLA.

3.2.3. Determination of the Pasteurisation value

When the inactivation is a first order reaction, the P value measured by the TTIs can be calculated using equation (3.3),

$$P = D_T \cdot \log \left(\frac{A_{initial}}{A_{final}} \right) \quad (3.3)$$

where $A_{initial} / A_{final}$ is the ratio of the enzyme activities before and after heat treatment as measured by the Randox test. Combining equations (2.4) and (3.3) gives:

$$P = \int_0^t 10^{\frac{T(t)-T_{ref}}{z}} \cdot dt = D_T \cdot \log \left(\frac{A_{initial}}{A_{final}} \right) \quad (3.4)$$

In this case, T_{ref} was chosen to be 85°C (Pasteurisation reference temperature). Integration of measured time-temperature profiles was carried out using Microsoft Excel.

3.2.4. Evaluations of D_T and z values under isothermal conditions

Calculation of the enzyme kinetic parameters is important as it determines the D_T value used in subsequent P value calculations. The experimental design and the time temperature profiles used for the determination of the z and the D_T value were chosen according to previous studies (Tucker and al, 2002). For BAA, D_T was calculated at 80°C, 85°C, and 90°C and for BLA, it was calculated at 85°C, 90°C and 95°C. The z values were calculated from the variation in D_T . The TTIs were put into a water-bath (Grant, UK) at the 3 different temperatures for different lengths of time and were then cooled rapidly in cold water. It took

approximately 20 seconds for the TTI to reach the temperature of the water bath so D_T was determined under essentially isothermal conditions. This was validated by doing a simulation using the finite element analysis and solver software package Comsol Multiphysics 3.2 (COMSOL, Inc, Sweden). The logarithm of the reaction rate for each profile was calculated and plotted against time in the water-bath allowing D_T to be calculated. The z value was then determined using the identified D_T values using:

$$z = \frac{\log\left(\frac{D_{T_2}}{D_{T_1}}\right)}{T_1 - T_2} \quad (3.5)$$

Where D_{T_2} and D_{T_1} are the decimal reduction times at T_2 and T_1 .

3.2.5. Isothermal experiment: Maximal heat treatment duration

Tucker *et al.* (2002) showed that amylase activity could be measured accurately for 2 log reductions of activity. Thus, the α -amylase could be used for 2 times the D_T value at 85°C. This assumption was tested for the BAA and the BLA. Thermal treatments were chosen according to the limits given by the study of Tucker *et al.* (2002). Isothermal treatments were applied using the water bath described in the previous section at 85°C. Table 3-1 shows the heat treatment duration at 85°C for the 2 enzymes. P values were calculated for these various thermal treatments.

Table 3-1. Heat treatment duration (min) at 85°C

	BAA	BLA
Heat treatment duration in minutes at 85°C	1	5
	2	10
	3	15
	4	20
	6	25
	8	30
	10	35
	12	40
	14	45
	16	50
	18	55
	20	60

3.2.6. Non isothermal heat treatment experiments using the Peltier stage

The non isothermal heat treatments were applied using a Peltier stage (Linkam, Tadworth, UK). The Peltier is a semiconductor based system which functions as a small heat pump: heat can be transferred across the thermoelectric module by applying a voltage. Using this method any time temperature profile can be obtained (Noll, 1999) and the heating and cooling rates can be controlled.

Figure 3-1 shows the configuration of the Peltier unit. During the experiments, TTIs were attached to the thermoelectric module using heat sink compound (RS, Corby, UK) (thermal conductivity = 0.9 W/m.K) to ensure good thermal contact between the TTIs and the surface of the Peltier. Two calibrated thermocouple (type K) data loggers (TC-08) from PICO instruments (St Neots, UK) having a temperature accuracy of $\pm 0.5^\circ\text{C}$ were also put inside the heat sink compound as shown in Figure 3-1. To insulate the system a piece of polystyrene

foam was placed on the top of the thermoelectric module. The time temperature profiles were set using a computer which controlled the thermoelectric module.

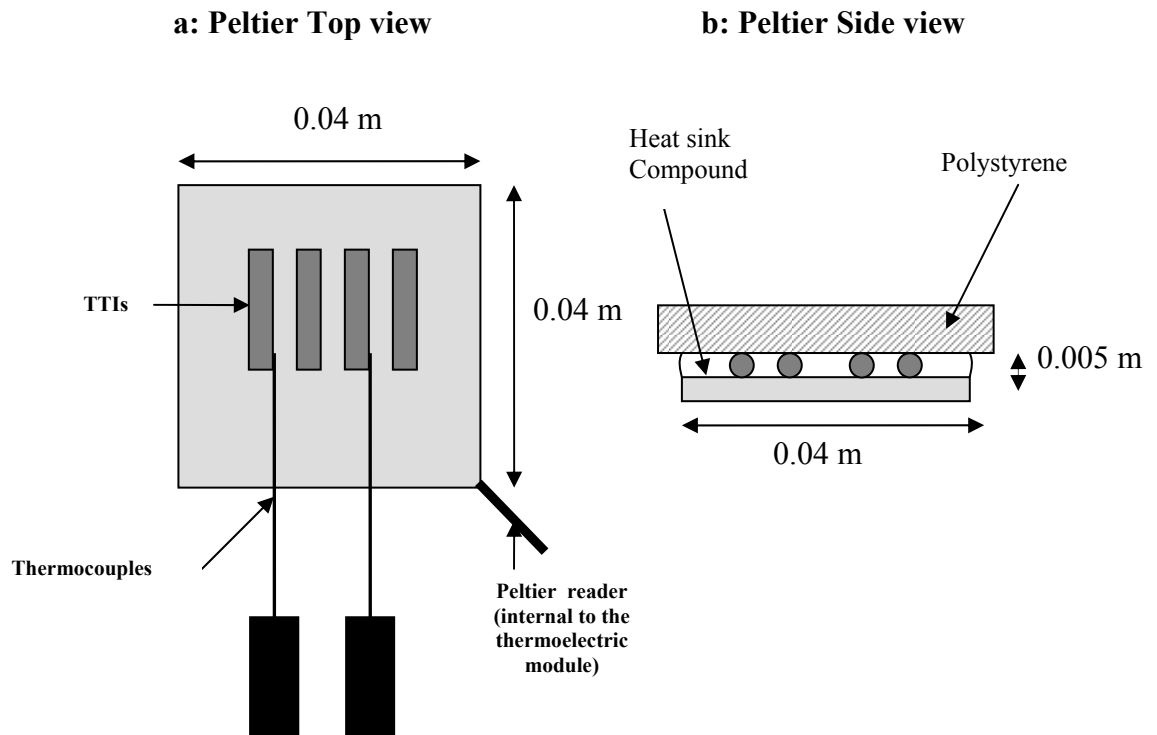


Figure 3-1. Diagram of the experiment with the thermoelectric module

Three different types of non isothermal experiments were performed:

(i) The first was characterised by a constant heating/cooling rate and a fixed holding temperature. The Peltier stage was used to heat the TTIs at $30^{\circ}\text{C}/\text{min}$ until the target temperature of 85°C was reached. The TTIs were then held at this temperature for various lengths of time (BAA: 2, 4 and 8 minutes and BLA: 5, 10, 15 and 20 minutes), and were then cooled at $30^{\circ}\text{C}/\text{min}$ until 20°C was reached. Figure 3-2 compares temperatures measured within the Peltier stage and from the thermocouples on the surface of the stage. The

temperatures on the stage closely follow those delivered by the Peltier, but there is a very small difference when the gradient of temperature alters. The profiles were repeated several times to obtain large number of P values (see Table 3-2). P values were obtained by integration of the temperatures from the thermocouple data values to compare with TTIs. All results were analysed statistically using SPSS software.

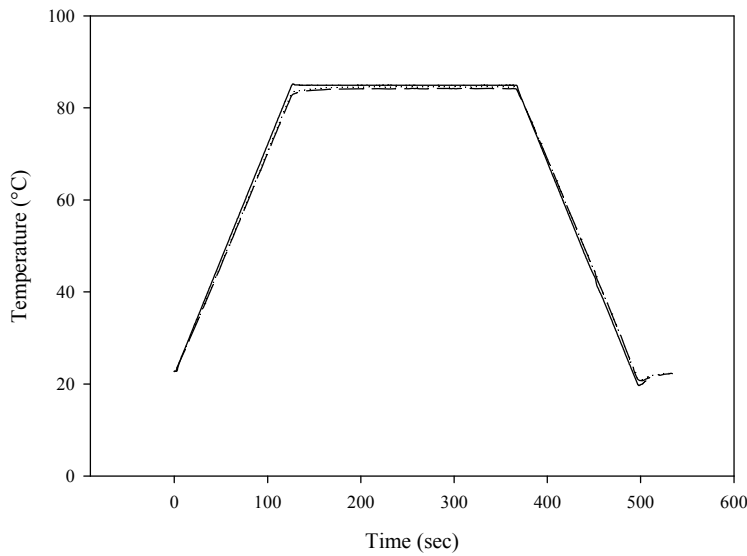


Figure 3-2. The time temperature profile used to check the repeatability of the TTIs results that are obtained from the Linkam thermoelectric module. Peltier thermocouples [—], PICO Thermocouple 1 [...], PICO Thermocouple 2 [---].

Table 3-2. Summary of the experiments performed where heating and cooling ramp were both set at 30°C/min

	Holding time at 85°C (min)	Number of repetition of experiments	Number of TTIs P values obtained	Number of the thermocouples P values
BAA	2	5	18	10
	4	10	32	20
	8	5	18	10
BLA	5	3	5	5
	10	3	6	6
	15	36	36	18
	20	4	8	8

(ii) The second type of experiment was based on more industrially relevant time temperature profiles in which heating and cooling rates were not constant. These experiments were carried out to compare P values obtained from the BAA with those obtained from the thermocouples. Different time temperature profiles (Stoforos and Taoukis, 1998) and defined in detail later in § 3.3.3.2. were generated to examine whether the TTIs were accurate over these different conditions.

(iii) The third type of experiment involved the production on the Peltier of various time temperature profiles, all of them having equal P values (at 85°C). The aim of these experiments was to investigate the sensitivity of the TTIs as a measurement technique. These experiments were only performed with the BAA. The heating and cooling rates used were 30°C/ min. Table 3-3 shows the equivalent time temperature profiles for the same P value. The P values were calculated using the z value of the BAA.

Table 3-3. Equivalent P values: 3 tables give the equivalent time temperature profiles for 3 different P values at 85°C. For each time temperature profile the heating and cooling rate are 30°C/min

P value (min) at 85°C	Equivalent time temperature	P value (min) at 85°C	Equivalent time temperature	P value (min) at 85°C	Equivalent time temperature
2.4	305 s at 80°C	4.35	580 s at 80°C	8.3	1128 s at 80°C
	120 s at 85°C		344 s at 83°C		678 s at 83°C
	39 s at 90°C		240 s at 85°C		480 s at 85°C
			91 s at 90°C		196 s at 90°C

3.2.7. Non isothermal heat treatment experiments using PCR (Polymerase Chain Reaction)

A PCR (Polymerase Chain Reaction) device (figure 3-3) was used as an alternative to the Peltier plate. PCR equipment, traditionally used for DNA amplification can produce perfectly controlled time temperature profiles.



Figure 3-3. PCR equipment

The use of PCR presents some advantages over the Peltier plate, indeed it can hold a large number of samples (40 Eppendorff tubes could fit) and the lid is heated preventing heat losses. The PCR device used was the 'Eppendorf Mastercycler gradient' (Eppendorf UK Limited, Cambridge, UK) which offered fast temperature control and homogenous temperature inside the device. The heating/cooling rates were fixed to 100°C/ min for the heating rate and 55°C /min for the cooling rate. In this study, the BAA and BLA solutions

were directly put inside Eppendorff tubes as TTI tubes could not be used. The tubes were then put in the PCR machine. 10 μ l of enzyme solutions were put in the Eppendorff tube per experiment. Two types of experiments were performed:

(i) Various time temperature profiles were produced with the PCR and are described in Table 3-4. The PCR device was used to heat the BAA solution at 100°C/min until the target temperature was reached. The TTIs were then held at this temperature for various length of time, and were then cooled at 55°C/min until 20°C was reached. *P* values were obtained by integration of the temperatures from the thermocouple data values to compare with TTIs.

Table 3-4. PCR time temperature profiles

Experiment number	Holding temperature	Time at the holding temperature	Cycle repetition
1	80°C	10 min	No
2	85°C	4 min	No
3	90°C	1.5 min	No
4	85°C	2 min	Yes: 2 Peaks of 2 min

(ii) Large number of *P* values was obtained by using a large sampling. 40 Eppendorff tubes of BAA and BLA were used per time temperature profile. The experiments were performed at 85°C for different lengths of time. All results were analysed statistically using SPSS software. The time temperature profiles used are described in Table 3-5 below.

Table 3-5. PCR time temperature profile: large samples

Experiment number	Time at 85°C	
	BAA	BLA
1	2 min	5 min
2	4 min	15 min
3	6 min	25 min
4	8 min	

3.3. Results

3.3.1. Kinetic parameters under isothermal conditions

The kinetic parameters ($D_{85^{\circ}\text{C}}$ and z values) were calculated for the BAA and BLA. The determination of enzyme kinetic parameters is important as these are used in subsequent P value calculations. The $D_{85^{\circ}\text{C}}$ value (95% of confidence) obtained from the batch of BAA used in this study was $6.1 \text{ min} \pm 0.4 \text{ min}$ (Figure 3-4 (a)). This value was close to the $D_{85^{\circ}\text{C}}$ of 6.8 min found by Lambourne and Tucker, (2001) at CCFRA. Data for D_T at different temperatures is plotted in Figure 3-4 (c). The z value for the BAA (95% of confidence) was found to be $12^{\circ}\text{C} \pm 1.3^{\circ}\text{C}$ (Figure 3-4 (c)). In the literature, a range of z values has been reported from 7.6°C (Van Loey *et al.*, 1997) to 9.4°C (Lambourne and Tucker, 2001). These are all within the target range for viable cell destruction in pasteurisation processes (Tucker, 1999). According to Van Loey *et al.*, (1997), the z value should lie between 5°C to 12°C for the evaluation of pasteurisation processes. Hendrickx *et al.*, (1992 and 1995) have shown that it is relevant to use the α -amylase from *Bacillus amyloliquefaciens* as a tool to monitor the food safety during pasteurisation processes because its z value is close to 10°C . The values found by Van Loey *et al.* (1997) and Lambourne & Tucker (2001) are lower than that found here. This was investigated, and it was found that the supplier had changed the composition of the amylase extract within the last two years and some variations in the z value could appear when compared with early studies. This demonstrates that in practice measurements should be carried out on each batch of enzyme, rather than relying on published values. The Decimal reduction time at 85°C of the batch of BLA (95% of confidence) used in this study was found to be $29.15 \pm 4.7 \text{ min}$ (Figure 3-4 (b)) and its z value was $10^{\circ}\text{C} \pm 0.8^{\circ}\text{C}$ (Figure 3-4

(d)). This result matches the z value of 9.1°C obtained by Lambourne & Tucker (2001). Again, the z value calculated here is in the range of the z values required for the monitoring of pasteurisation processes.

The determination of the z value is essential to compare the P value from the TTIs and from the thermocouples. A conditioning procedure could be used to standardize the z value of the amylase. However, this study does not focus on the z value variability as z is only required to process the data and the thermocouple time temperature history was thus integrated using the experimentally determined z value. The D_T value and z values obtained here were used in the calculation of P values in the following study.

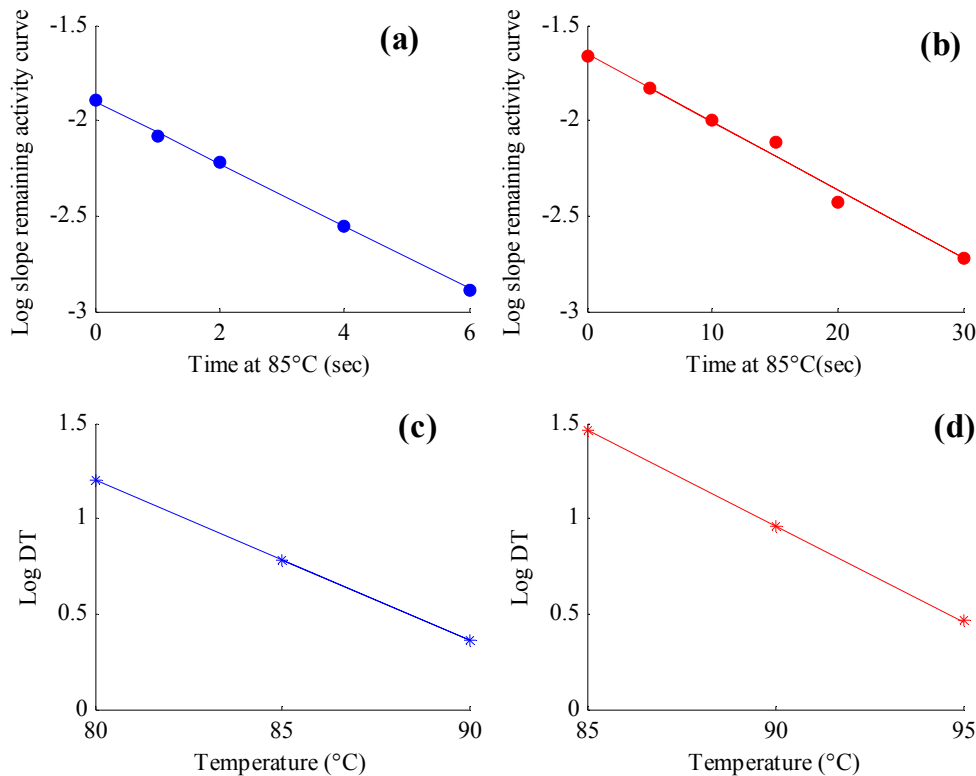


Figure 3-4. (a) The BAA D_T value calculation curve. Fitting curve equation $Y = -0.1639X - 1.9011$ [—], (b) The BLA D_T value calculation curve. Fitting curve equation $Y = -0.03599X - 1.647$ [—], (c) The BAA z value curve. Fitting curve equation: $Y = -0.0833X + 7.8643$ [—] (d) The BLA z value curve. Fitting curve equation: $Y = -0.09985X + 9.95$ [—] Confidence interval of 95%

3.3.2. Isothermal experiment: Maximal heat treatment duration

One of the drawbacks of the TTIs is that they have a maximum life within the process. According to the type of α -amylase chosen, the length of time in which the enzyme can work will vary. The following experiment checked the maximum time that the TTIs made from BAA and BLA could be used.

In addition, Tucker et al., (2002) showed that amylase activity could be measured accurately for 2 log reductions of activity using the same absorbance technique previously used and therefore, TTIs could be used for durations equal to $2 \times D_T$ values at 85°C.

BAA and BLA were subjected to long thermal treatments. Figure 3-5 (a) and (b) show the P values measured from the TTIs for the isothermal experiments plotted against the process time (time that the TTIs stayed in the water bath at 85°C). The $Y = X$ curve plotted on the Figures represents the ideal relationship between TTIs and process time at 85°C. Fitting the data gives R^2 values of 0.9703 and 0.933 for the BAA and BLA respectively, hence showing reasonable agreement.

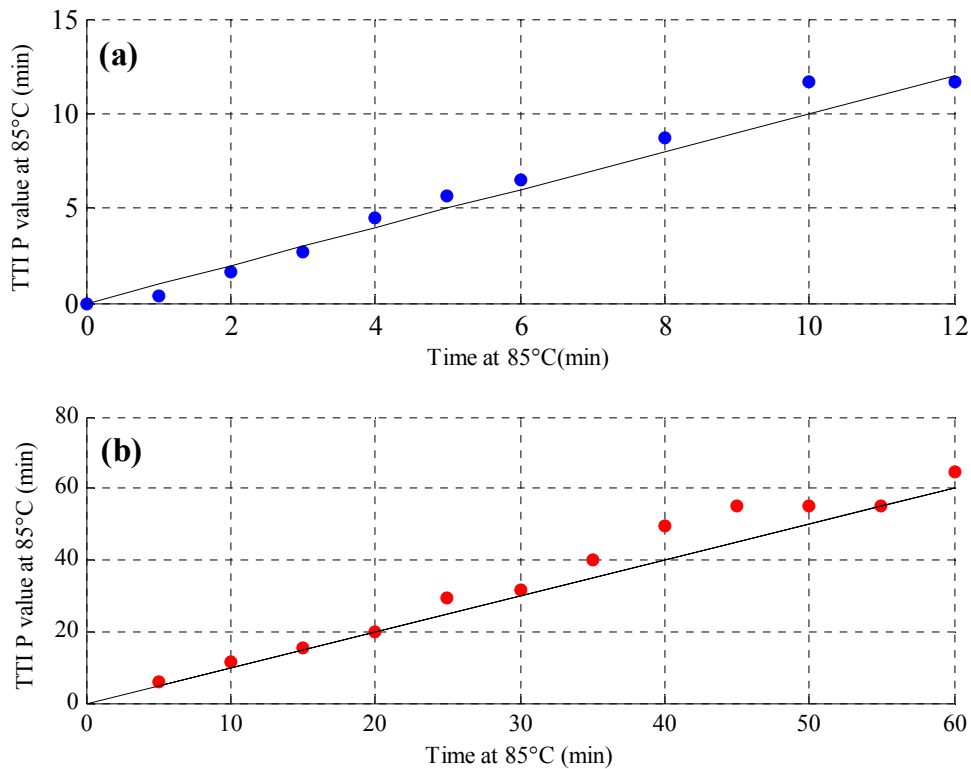


Figure 3-5. Scatter of the process time (in water bath at 85°C) versus the TTIs P values. (a) BAA: Thermocouples Y values versus TTIs P values [\bullet], $Y = X$ [—], (b) BLA: Thermocouples Y values versus TTIs P values [\bullet], $Y = X$ [—]; one specific run was repeated several time and similar results were achieved

However, it can be seen on the plots (a) and (b) in Figure 3-5 that after some time (8 minutes for BAA and 30 minutes for BLA), TTIs overestimate the thermal process. Therefore, the P values obtained with the TTIs are higher than the process time at 85°C.

As described previously, the study of Tucker et al., (2002) shows that the length of time that TTIs can be accurately used in thermal processes is $2 D_T$ at 85°C which corresponds to 12 (BAA) and 60 (BLA) minutes. In the present study, it was determined that the BAA and BLA will not be used for thermal treatments that last longer than 8 minutes and 30 minutes at 85°C since the TTIs do not accurately predict the thermal process above these lengths of times due to errors in absorbance analysis.

3.3.3. Estimation of the TTIs variability under non isothermal heat treatments

3.3.3.1. Simple heat-hold-cool profiles

TTIs were placed on the heating stage and subjected to temperature profiles such as those shown in Table 3-2. Before the experiments were carried out, it was ensured that the temperature across the surface of the Peltier stage was uniform. P values from calibrated thermocouple data were estimated using equation (2.4) where z was equal to 12°C and 10°C for BAA and BLA respectively. The P values were compared with those calculated from equation (5), using D_T and z from the water bath experiments; i.e. 6.1 minutes (BAA), 29.15 minutes (BLA) and 12°C (BAA), 10°C (BLA). In Figure 3-6, P values calculated from thermocouple data are plotted versus P values measured from the TTIs for non isothermal conditions (for BAA (a) and BLA (b)). The relationship between the P values obtained for the TTIs and for the thermocouples is illustrated by the fitting curve drawn on Figure 3-6. In addition, a $Y = X$ curve which represents the ideal relationship between TTIs and thermocouples has been plotted on the same graph.

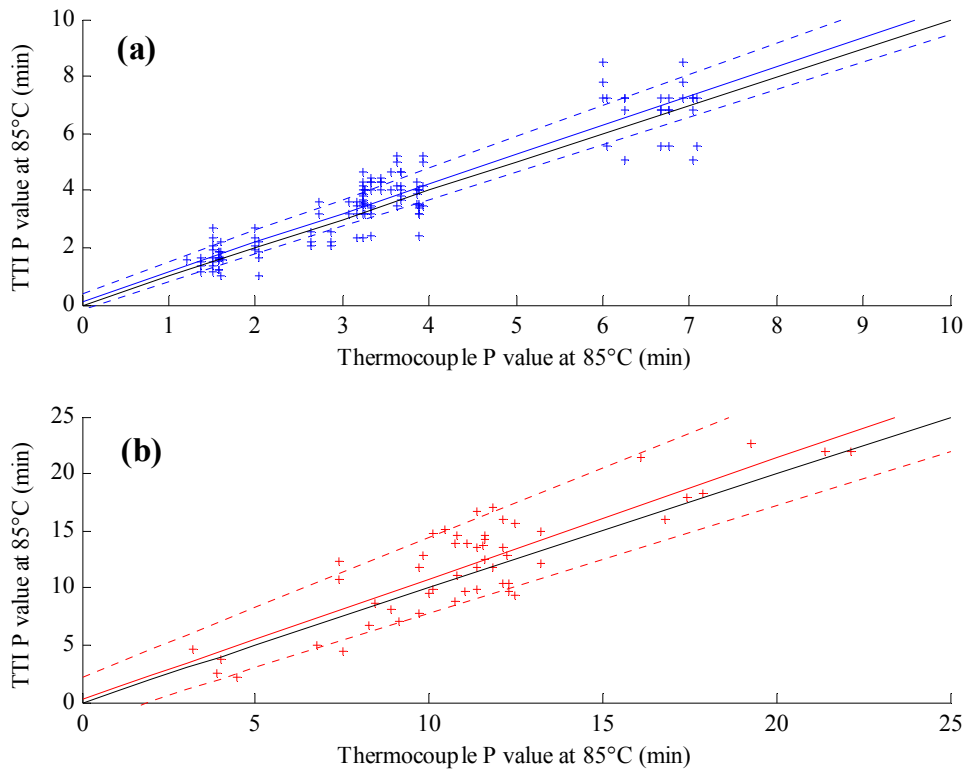


Figure 3-6. Scatter of the thermocouples P values versus the TTIs P values for non isothermal time temperature profile. (a) BAA: Thermocouples P values versus TTIs P values [$+$], fitting curve [—], $Y = X$ [—] and confidence intervals (95%) [---] (b) BLA: Thermocouples P values versus TTIs P values [$+$], fitting curve [—], $Y = X$ [—] and confidence intervals (95%) [---]. No data was removed.

The regression analysis shows that the TTIs and the thermocouples results correlated well (Table 3-6). For BAA, the equation that fits the set of data is $Y = 1.0303 X + 0.121$ and the R^2 for this equation is 0.866. For BLA, the equation that fits the set of data is $Y = 1.058 X + 0.212$ with a R^2 of 0.765.

Table 3-6. Coefficient fitting curve of the correlation TTIs and thermocouples results

Model	$Y = aX + b$	Coefficients (confidence interval = 95%)	
		B	Std. Error
BAA	a	1.030	0.035
	b	0.121	0.139
BLA	a	1.058	0.081
	b	0.212	0.989

These plots and the fitting curves showed that for high P values, TTIs tend to overestimate the thermal process. From a food safety point of view, this can be an issue since overestimation of the thermal process means that the product will be undercooked.

ANOVA tests (Table 3-7) were used to test the acceptability of the models (fitting curve) and confirmed that the variation explained by the models was not random. Therefore the model described well the correlation between the P values obtained with the TTIs and the thermocouples.

Table 3-7. ANOVA test on the correlation TTIs and thermocouples results

Model		Sum of Squares	Degree of freedom	Mean Square	F	Significance
BAA	Regression	437.668	1	437.668	867.690	0.000
	Residual	67.590	134	0.504		
	Total	505.259	135			
BLA	Regression	982.752	1	982.752	169.238	0.000
	Residual	301.961	52	5.807		
	Total	1284.713	53			

In addition, when the data sets are fitted into the equation $Y = X$, the R^2 values obtained are 0.85 for BAA and 0.73 for BLA, which confirm reasonable agreement between thermocouple and TTI P values.

The scatter in measured P value increases with the holding time at 85°C for both TTIs and thermocouple P values. However, the variation of the P value obtained from the calibrated thermocouples is lower than that for the TTIs. Uncertainty (error) from the TTIs might be due to a variety of reasons such as (i) manipulation errors in the experiments (measurement error), (ii) different temperature-time behaviour on the Peltier plate or (iii) inherent variation in the behaviour of the enzyme also reflected in the scatter in D_T and z since they are obtained from

material of biological origin. Here, the uncertainty observed with the thermocouples (type K) is most likely due to the variation of their location on the Peltier stage since the thermocouples were calibrated and therefore can not have inherent variation as observed for the TTIs. Location errors are common sources of thermocouple response variation in all practical situations.

Table 3-8 shows the standard deviation obtained from the thermocouples and TTIs data for similar time temperature profiles. Table 3-8 shows that the error obtained from the TTIs increases more rapidly than that from the thermocouples as the holding time increases. The variability of the TTIs is almost twice that of the thermocouples. This would be expected given the nature of the experimental procedure required to determine the enzyme z value. It should be noted that the percentage accuracy of both methods increases with holding time, for the BAA TTI from $\pm 20\%$ error at 2 min hold to $\pm 15\%$ at 8 min hold. This data suggests that the inherent accuracy of the TTI is on the order of $\pm 20\%$ or less. Although, this would be acceptable for a real food process where thermocouples can not be used, the data should be used with caution, being aware of the accuracy of the method.

Table 3-8. The evolution of the standard deviation of the TTIs and the thermocouples

	BAA		BLA	
	Standard deviation (min)		Standard deviation (min)	
Holding time at 85°C	TTIs	Thermocouples	TTIs	Thermocouples
2 min	0.44	0.25	n/a	n/a
4 min	0.81	0.39	n/a	n/a
8 min	0.96	0.44	n/a	n/a
5 min	n/a	n/a	1.15	0.58
10 min	n/a	n/a	1.67	0.88
15 min	n/a	n/a	2.37	1.3
20 min	n/a	n/a	2.58	2.33

The experiments overall demonstrate that P values measured using TTIs can be correlated very well with the responses of the thermocouples. For the two enzymes (BAA and BLA), it can be noticed that for high P values the TTIs slightly overestimate the thermal process which is a concern for food safety. The uncertainty of the TTIs was successfully determined using a Peltier stage where various time temperature profiles were reproduced.

3.3.3.2. Complex heating and cooling cycles

TTIs were placed on the heating stage and subjected to complex temperature profiles. Only TTI made from BAA were used in this experiment since BLA works in the same way and the only difference between the enzymes is thermostability which is higher for BLA. A wide range of temperature-time profiles could be run on the Peltier stage are shown in Figure 3-7.

Theses profiles are of several types:

(i) Single heating and cooling conditions (Plots 1-4 in Figure 3-7), in which the shape of the curves is closer to those seen in industrial practice (for examples, see Stoforos and Taoukis, 1998). The time temperature profile of Plot 3 is similar to those of Plots 1 and 2 except that it includes a holding time stage. The time temperature profiles of Plot 4 were used to investigate the behaviour of TTIs under rapid change of temperature without holding time.

(1) Slow heating to 85°C over 753 s followed by cooling; and slow heating to 80°C over 726 s followed by cooling

(2) Heating to 89°C over 691 s followed by cooling

- (3) Heating to 85°C over 324 s followed by 240 s holding and cooling
- (4) Heating to 91°C over 360 s followed by cooling; and heating to 90°C over 414 s followed by cooling
- (ii) Multiple heating and holding conditions, in which the responses of the TTI for several repetitions of time temperature profiles (Plot 5 and 6 Figure 3-7).
- (5) Heating to 85°C over 360 s followed by cooling: repeated twice
- (6) Heating to 85°C over 360 s followed by cooling: repeated 3 times

Figure 3-7 (Plot 1-6) shows that the Peltier stage is highly flexible and can generate a wide range of temperature-time profiles.

The graph in the middle of Figure 3-7 plots the P values obtained from the integrated time temperature history of the thermocouples against the TTIs P values at 85°C for all of the experiments of plots (1-6) (using the same legend). The data shows a good correlation between the responses of the TTIs and the thermocouples. The fitting curve equation of the TTIs/thermocouples data is $f(X) = 0.995 X - 0.119$ with confidence level of (0.82 - 1.18) and (-0.95 - 0.71) for an interval of confidence equal to 99% ($R^2 = 0.8479$). An ANOVA test (Table 3-9) confirmed that the variation explained by the model was not due to chance. The significance value of the 'F statistic' is less than 0.05. When the data set is fitted into the equation $Y = X$, the R^2 obtained is 0.8376. Therefore, the data fits the equation $Y = X$ and the

responses of the TTIs correlate well with the responses of the thermocouples, even over a wide range of time-temperature profiles.

The results obtained from the different time temperature profiles show that TTIs are sensitive devices that can measure small differences; for example the slight difference (5°C) between the two data sets in plot (1). The effect of multiple temperature peaks does not seem to affect the TTIs responses which still correlate well with the thermocouples. Despite the several temperature cycles, the TTIs still gave an accurate reading. These experiments show clearly that the Peltier stage is a useful tool which provides the ability to reproduce complex time temperature profile, and allows testing of the TTIs under relevant industrial conditions which would be otherwise difficult to reproduce. Using this type of approach will allow the practical accuracy of TTIs to be confirmed and thus give confidence in their industrial use.

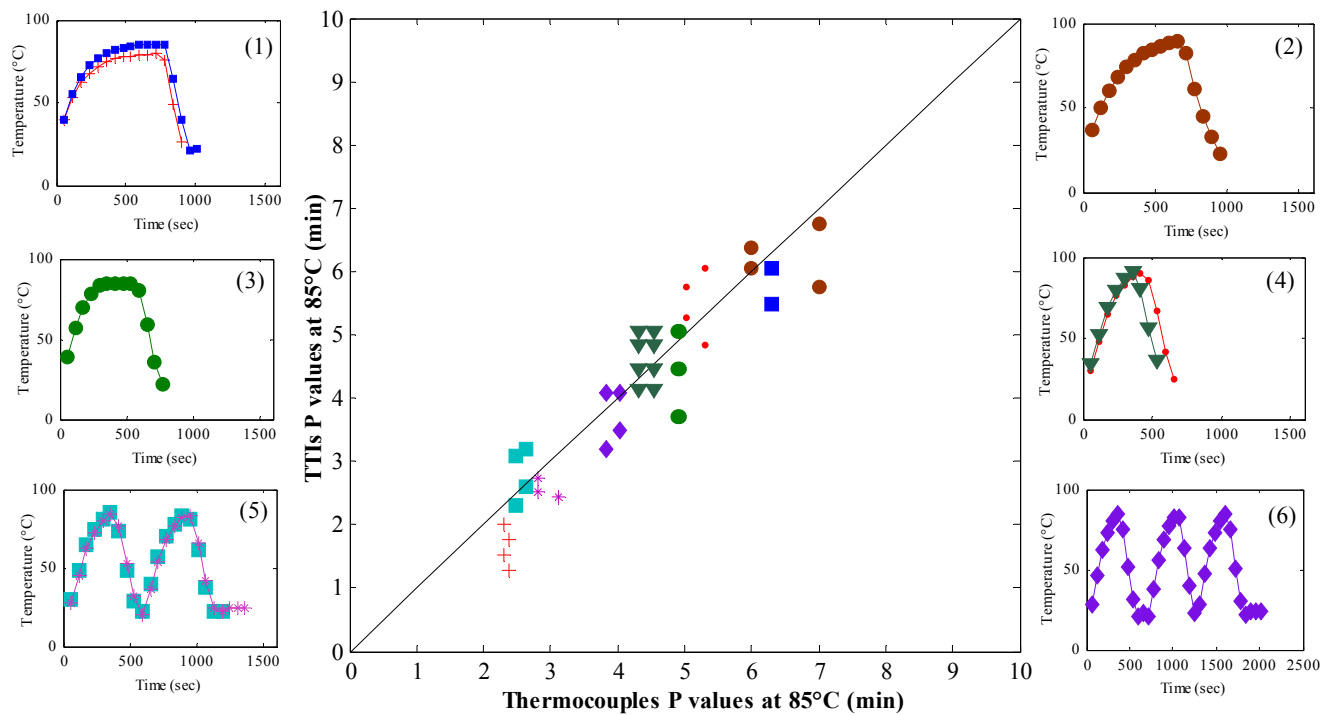


Figure 3-7. Scatter of the P values of the thermocouples versus the P values of the TTIs for industrial time temperature profiles. [—] equation $Y = X$

Table 3-9. ANOVA test on the correlation TTIs and thermocouples results for the industrial time temperature profiles

Model		Sum of Squares	df	Mean Square	F	Sig.
BAA	Regression	67.972	1	67.972	217.362	0.000
	Residual	12.196	39	0.313		
	Total	80.168	40			

3.3.3.3. Time temperature profiles with equal P values

A set of experiments was performed to validate the applicability of TTIs under processing conditions having the same thermal effect (P value) but using different process times and temperatures.

Several different time temperature profiles with equal P values were produced on the Peltier plate. Experiments were performed for three different P values i.e. 2.37 min, 4.36 min and 8.29 min. For each P value, several profiles with different holding time and temperature (80°C, 83°C, 85°C and 90°C) were generated.

Figure 3-8 shows the results obtained from these experiments. P values obtained by TTI (Figure 3-8 (a)) and thermocouple (Figure 3-8 (b)) are plotted against the holding temperature. The P values obtained are consistently below the values expected (2.37, 4.36 and 8.26 min) for both TTIs and thermocouples, with the values from the TTIs being generally lower. The causes of the TTI and thermocouples uncertainty were described in §3.3.3.1. As stated previously, thermocouples should be accurate since they have been calibrated, however, depending on their location on the Peltier stage a variation of the temperature recorded can be observed, and therefore P values can also vary.

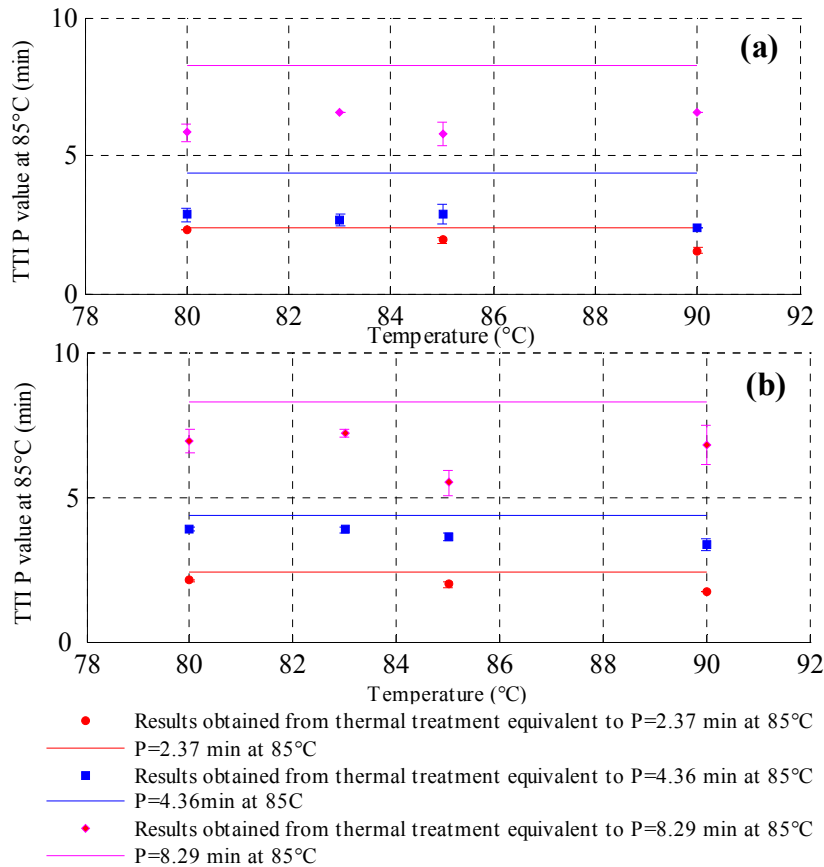


Figure 3-8. Equivalent P value results (a) TTIs P values at 85°C (b) Thermocouple P values at 85°C

Table 3-10 shows the percentage variation between the P values obtained from the TTI/thermocouple with the theoretical P value. For example, for a thermal treatment of 39 s at 90°C with a heating and cooling rate of 30°C/s (equivalent to a P value of 2.37 min at 85°C), the TTI and thermocouple variations are 35.2% and 27.8% respectively. Whilst for a thermal treatment of 35 minutes at 80°C , the variations are 4.2% and 11.2% respectively. This illustrates the thermal lag that the TTI/thermocouple experienced. When the theoretical P value increases, the time spent at the holding temperature increases therefore minimising the effect of the thermal lag. The thermal lag experienced by the thermocouple is shorter than the TTI. This is related to the uncertainty experienced by the TTIs and the thermocouples. The thermocouple has less potential causes of variation than the TTI (see § 3.3.3.1).

Table 3-10. % variation of the TTI/thermocouple response with the theoretical P values

P value equivalent at 85°C	Temperature	% variation with the theoretical P value: TTI	% variation with the theoretical P value: Thermocouple
2.37 min	80	4.2	11.2
	85	19.2	17.1
	90	35.2	27.8
4.36 min	80	34.6	11.0
	83	39.0	11.0
	85	34.4	16.8
	90	46.0	23.1
8.29 min	80	29.6	16.7
	83	21.2	13.2
	85	30.0	33.8
	90	21.2	18.3

A computer simulation was run to study the thermal lag experienced by the TTIs. The finite element analysis and solver software package Comsol Multiphysics 3.2 was used. The software simulates the heat transferred from the Peltier stage to the TTI. In this simulation, it is assumed that the heat transfer is done by conduction. The equation below describes the heat transfer by conduction and is used in the simulation. In this simulation, the heat transfer is measured on the X and Y directions.

$$\rho C_p \frac{\partial T}{\partial t} = \frac{\partial}{\partial X} \left(k \left(\frac{\partial T}{\partial X} \right) \right) + \frac{\partial}{\partial Y} \left(k \left(\frac{\partial T}{\partial Y} \right) \right) \quad (3.6)$$

Where ρ is the density (kg m^{-3}), C_p is the heat capacity ($\text{J kg}^{-1} \text{K}^{-1}$), T is the temperature ($^{\circ}\text{C}$) and k is the thermal conductivity ($\text{W m}^{-1} \text{K}^{-1}$).

The parameters used in the simulation are given in Table 3-11.

Table 3-11. Parameters used in the simulation

	Water (Enzyme solution)	Tubing	Heat sink compound
Thermal conductivity (W/mK)	0.67	0.24	0.7
Density (kg/m ³)	1000	85	2860
Heat capacity (J/kgK)	4180	2000	1300

The Figure 3-9 shows the simulation design. The simulation was done on a 2-D section of the TTI and the Peltier stage. During this simulation, the bottom of the TTI was considered as being made from silicone tubing.

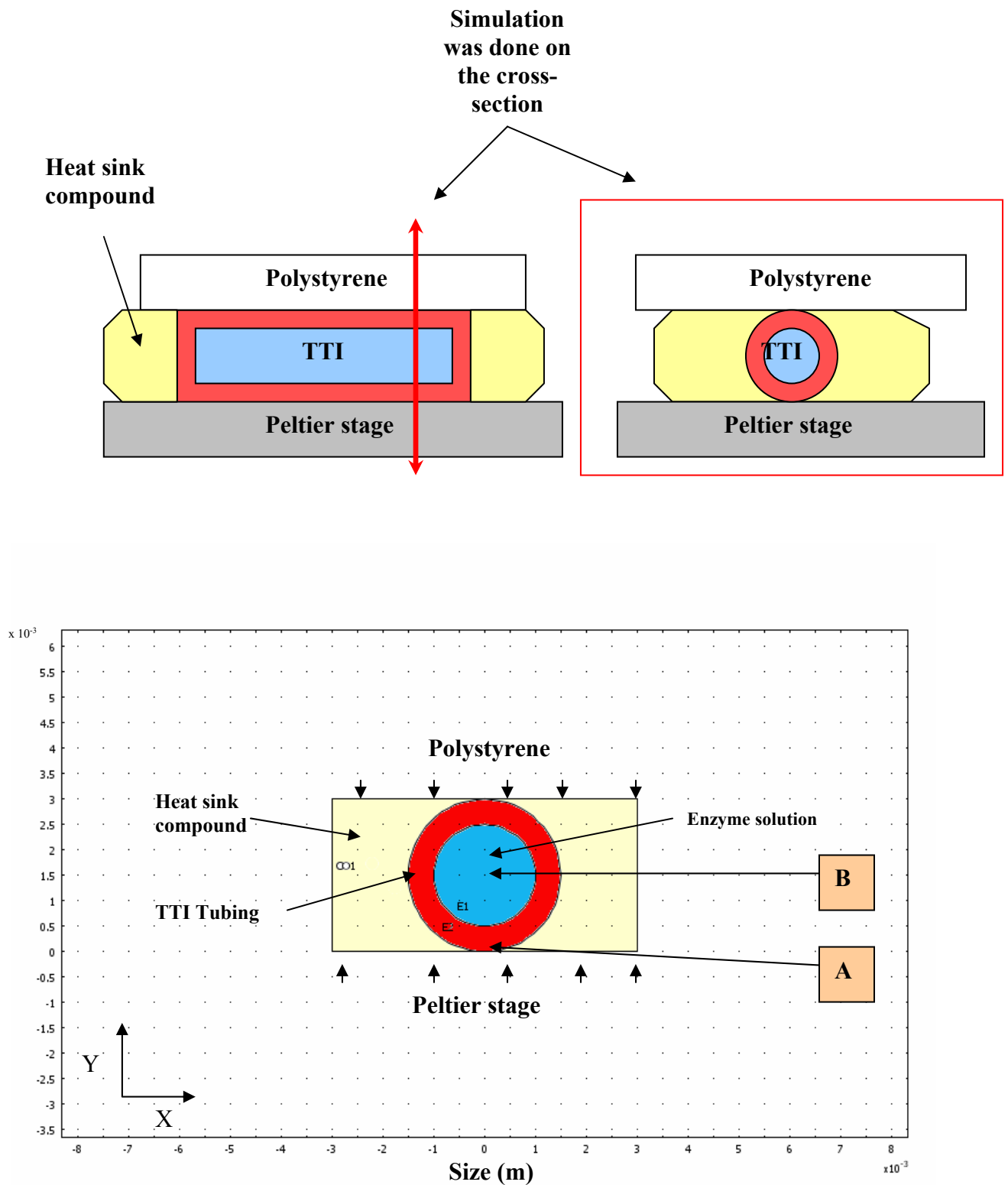


Figure 3-9. Illustration of the simulation (blue: enzyme solution and red: silicone tubing)

During the simulation, the Peltier stage has a constant temperature of 85°C. The boundary conditions are given in Table 3-12.

Table 3-12. Boundary conditions

Coordinates	At $t = 0$
$Y = 0$	Temperature = 85°C
$Y = 3 \times 10^{-3}$	Thermal insulation
$X = -3 \times 10^{-3}$	Temperature = 20°C
$X = 3 \times 10^{-3}$	Temperature = 20°C

Temperatures were simulated for 200 seconds on Position A (coordinates (0, 0.0015)) and B (coordinates (0, 0)) and are shown in Figure 3-10.

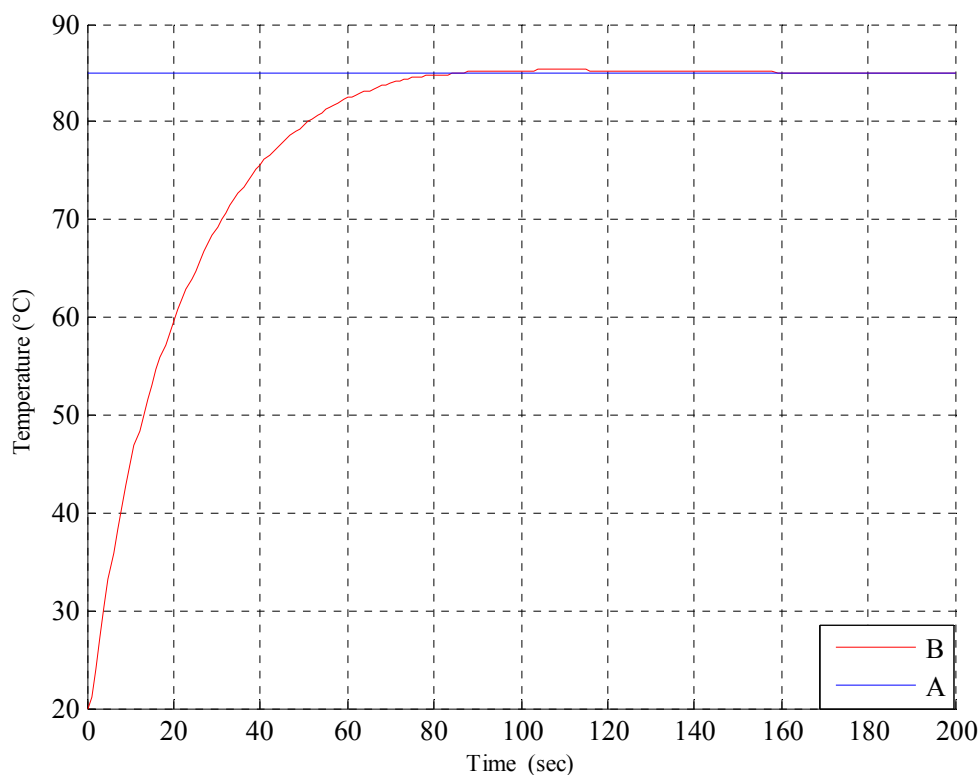


Figure 3-10. Temperature vs time at positions A and B (The slight overshoot of the temperature recorded in the centre of the TTI is a numerical artefact)

Figure 3-10 shows that it takes around 80 seconds for the TTI to reach 85°C. The P value at 85°C of the TTI obtained during this 80 second heating up period is 2.45 minutes. On the other hand the P value at 85°C of the Peltier stage obtained for the same period of time is 3.35 minutes. The difference between the two P values is 54 seconds at 85°C. This explains the thermal lag experienced by the TTI and the systematic underestimation of the thermal process performed on the Peltier. It should be noted that this simulation is only valid for the TTIs on the Peltier stage.

3.3.4. Non isothermal heat treatment experiments using PCR

PCR equipment was used as an alternative to the Peltier plate to produce non isothermal heat treatment. The thermal treatments given in Table 3-4 were reproduced on the PCR device. Figure 3-11 plots the P values obtained from the integrated time temperature history of the PCR internal thermocouples against the TTIs (BAA) P values at 85°C.

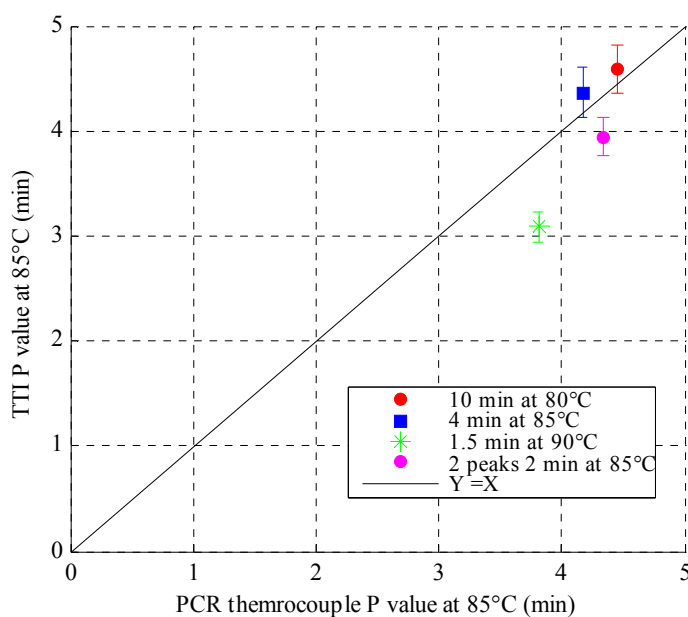


Figure 3-11. Correlation P values obtained by the TTI and PCR thermocouples (error bars represent one standard deviation)

The data shows a good correlation between the responses of the TTIs and the PCR thermocouples. For HTST profiles (90°C for 1.5 min), a thermal lag was observed which was caused by the Eppendorff tubes acting as a heat barrier.

Additional experiments were performed with the PCR device to check the TTI response variability. The PCR machine can hold up to 40 Eppendorff tubes containing enzyme solution (BAA and BLA) at the same time. Therefore, 40 samples could be processed per time temperature profile. By processing the 40 samples together in once, the variation due to the process was reduced.

The time temperature profiles given in Table 3-5 were reproduced on the PCR device. 40 Eppendorff tubes containing enzyme solution were used per experiment. Figure 3-12 and 3-

13 show histograms of the BAA and BLA P values distribution for various thermal treatments.

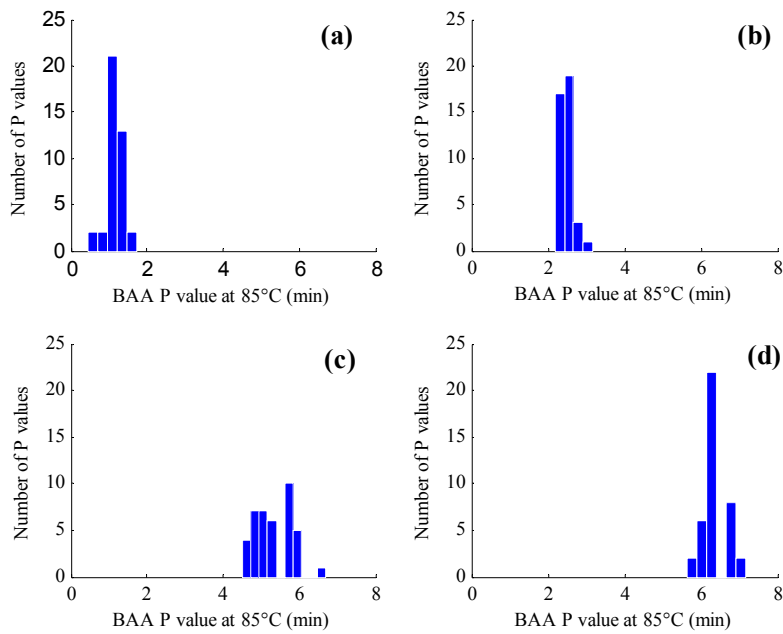


Figure 3-12. PCR experiments: Histograms of the results for BAA. Thermal treatment duration at 85°C: (a) 2 min (b) 4 min (c) 6 min and (d) 8 min

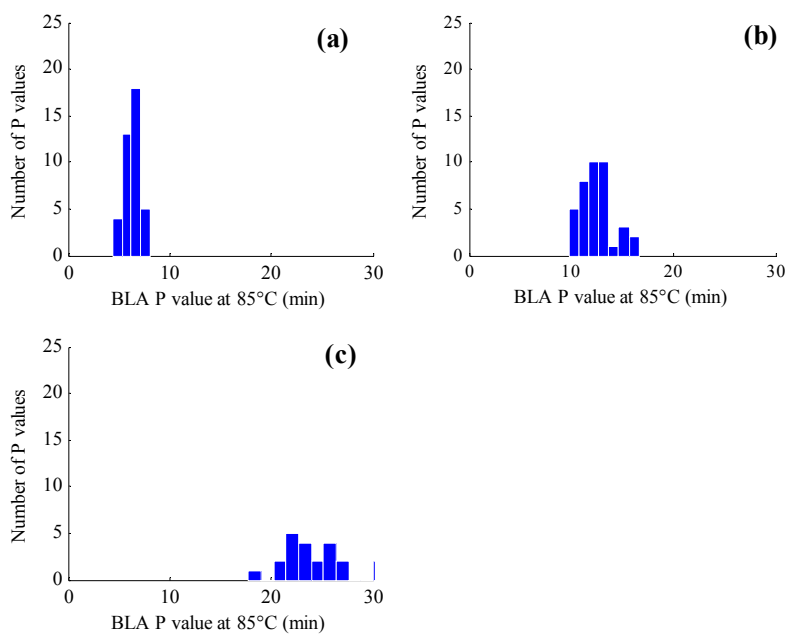


Figure 3-13. PCR experiments: Histograms of the results for BLA. Thermal treatment duration at 85°C: (a) 5 min (b) 15 min and (c) 25 min

Table 3-13 gives the mean, standard deviation and percentage of variation of the TTIs responses for BAA and BLA.

Table 3-13. PCR results: Mean, standard deviation and % variation of the BAA and BLA *P* values

	<i>P</i> value at 85°C of BAA				<i>P</i> value at 85°C of BLA		
	2 minutes at 85°C	4 minutes at 85°C	6 minutes at 85°C	8 minutes at 85°C	5 minutes at 85°C	15 minutes at 85°C	25 minutes at 85°C
Mean (min)	1.1	2.5	5.4	6.3	6.3	12.6	27.0
Standard deviation (min)	0.2	0.2	0.4	0.3	0.8	1.6	5.6
% variation	20%	7%	8%	5%	13%	12.5%	20%

As stated previously, the TTI error reported here might be due to various reasons which are (i) manipulation errors in the experiments, (ii) different temperature-time behaviour inside the PCR device or (iii) inherent variation in the behaviour of the enzyme. When compared with the Peltier plate experiments, the standard deviations observed for the PCR experiment are lower. For the Peltier plate experiment, a significant contribution to the variation in the results was caused by difficulties in the placement of the TTIs and thermocouples onto the flat plate, and in obtaining good contact between them using the heat sink compound. With the PCR device, since the enzyme is placed within the Eppendorf tube which is in good contact with the well within the device, these errors are eliminated. The results from these experiments suggest that the TTI accuracy is on the order of $\pm 20\%$ or less (Table 3-13). This confirms the accuracy calculated with the Peltier experiments.

3.4. Conclusion

A Peltier stage and a PCR device have generated a range of temperature-time profiles which have been used to determine the accuracy of Time Temperature Indicators. TTIs have been made from the α -amylase from *Bacillus amyloliquefaciens* and from *Bacillus licheniformis* and the accuracy of the data studied. The study shows that the TTIs responses correlate well with the thermocouples responses for a range of non isothermal processes. When the holding time increases, variation in P values measured from TTIs and calculated from thermocouple measurement also increase, but the increase of the error from the thermocouples is lower than the increase of TTIs error. Overall error is less than $\pm 20\%$ over a wide range of temperature-profiles.

In practice, the accuracy of the TTIs will be constrained by (i) a lower limit of P , where there is sufficient thermal lag between the TTIs and the process, so that the TTI value is not correct, and (ii) a higher limit of P , where the value of the enzyme activity is so low that it is not sensitive to the change in P . In between, is the operational window in which measurements can be taken with sufficient accuracy which is approximately 2 to 8 minutes at 85°C for BAA and 5 to 30 minutes at 85°C for BLA.

Chapter 4

Industrial application: Use of TTIs on the 'Vesuvio' vessel[†]

4.1. Introduction

In Chapter 3, lab scale experiments were performed on TTIs in order to validate their ability to determine heat treatment efficiency. In this Chapter, an industrial scale study on the use of TTIs inside a specialist mixing vessel for food processing is described. The use of TTIs can lead to optimised thermal processing of food and therefore improvements in food quality and nutritional value. In this study, fluids with rheologies similar to those of foods were used and the vessel fill level and heating and cooling methods were varied. The vessel used in this study is termed 'Vesuvio' by the manufacturer (Giusti Ltd). This vessel is commonly used in food industries and is able to heat and mix the food simultaneously. The aim of this work is to use TTIs to improve the knowledge of thermal processing inside mixing vessels with consequent influences upon future vessel design.

4.2. Material and method

In the following section, the design of the experiment performed to investigate the use of TTI for industrial scale studies will be described. Firstly, the fluids used during the experiments will be characterised. Following this, the vessel used and the experiments performed with the TTIs within the vessel will be described. The effect of parameters such as fluid viscosity,

[†] Part of this work was published in the journal of Innovative Food Science and Emerging Technology: Mehauden, K., Bakalis, S., Cox, P.W., Fryer, P.J., Simmons, M.J.H., 2008. Use of time temperature integrators for determining thermal processing efficiency in agitated vessels. *Innov. Food Sci. Emerg. Tech.* 9 (3), 385-395. doi:10.1016/j.ifset.2007.10.006

vessel filling level and heating and cooling methods on the heating efficiency of the vessel will be investigated.

4.2.1. Fluids

The fluids used for the experiments were water, aqueous solutions of starch (Colflo 67, National Starch & Chemicals, Manchester UK) and Heinz cream of tomato soup (Heinz, Wigan UK). Colflo 67 is a modified food starch derived from waxy maize which is used as a thickening and stabilising agent for water based food systems and therefore directly applicable to this study. Colflo 67 starts to gelatinise at approximately 69°C and its maximum viscosity is reached at 80-85°C. Concentrations of 4% and 5% by mass were used. The soup was condensed and was mixed with an equal amount of water before it was used.

The apparent viscosities of the starch mixtures and the tomato soup were determined using an AR1000 rheometer from TA instruments (Newcastle, Delaware, USA) equipped with a 0.06 m diameter 2° cone and plate geometry. An upward shear stress sweep was performed for applied stresses, τ of $0.01 < \tau < 100$ Pa and each experiment was repeated twice. The apparent viscosity μ_{app} was calculated at each applied shear rate, $\dot{\gamma}$, as $\mu_{app} = \tau / \dot{\gamma}$. The starch mixtures and the soup exhibited shear thinning behaviour (Figure 4-1).

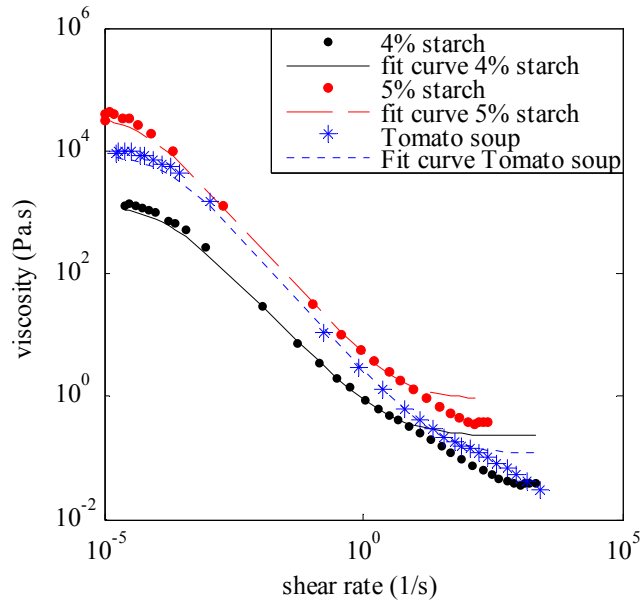


Figure 4-1. Viscosity curve of Starch 4% and 5% and Tomato soup

The Carreau model was selected as the most appropriate model to fit all the data (equation 4.1), (Holdsworth, 1993).

$$\frac{\mu - \mu_{\infty}}{\mu_0 - \mu_{\infty}} = \left[1 + (K \dot{\gamma})^2 \right]^{\frac{m-1}{2}} \quad (4.1)$$

Where K and m are constants with dimensions of time and μ_0 and μ_{∞} are the viscosities at shear rate $\dot{\gamma} = 0$ and $\dot{\gamma} = \infty$ respectively. Values of the model parameters for the fluids are given in Table 4-1.

Table 4-1. Values of the Carreau model parameters

	4% starch	5% starch	Tomato soup
μ_{∞}	0.232	0.906	0.119
μ_0	1220	38240	8360
K	7440	22100	6640
m	1.84	1.91	1.92
R^2	0.877	0.851	0.854
At shear rate 10s^{-1}	400-450 mPa.s	1400-1600 mPa.s	430-550 mPa.s

4.2.2. The 'Vesuvio' vessel

Experiments were performed on a vertical jacketed mixing vessel ('Vesuvio' vessel) manufactured by Giusti Ltd (Burton on Trent, UK) as shown in Figure 4-2. The maximum capacity of the vessel is 250 litres. It is equipped with a horizontal rotating agitator with polytetrafluoroethylene (PTFE) scrapers attached to the steel blades which make contact with the vessel wall, designed to perform an efficient and gentle mix for highly shear-sensitive products (Figure 4-2). Agitation speeds used for experiments range from 3 to 15 rpm.

Various heating and cooling options can be used, with the vessel contents vented to atmosphere. Indirect heating and cooling can be produced by the introduction of either steam at 3 bar gauge or cooling water into the vessel jacket. Direct heating is provided by steam injection into the vessel contents and evaporative cooling by pressure reduction of the vessel contents to below atmospheric pressure. Additional heating or cooling can also be provided by use of the jacket.

When steam was flowing in the vessel jacket for heating, the wall temperature was not less than 130°C. The saturation temperature of steam at the working pressure, 3 bar gauge, is 143.6°C. Steam was introduced into the jacket until the vessel contents were heated to the set temperature, based on a measurement from a calibrated PT 100 thermocouple with an accuracy of $\pm 0.15\%$ at 100°C, situated in a housing at the bottom of the vessel as seen in Figure 4-2 (b). When vessel contents were heated directly, steam was injected through a wall aperture directed towards the centre of the vessel. In both cases, the steam flow rate was controlled automatically using a Proportional Integral (PI) controller with the wall thermocouple providing the temperature input.

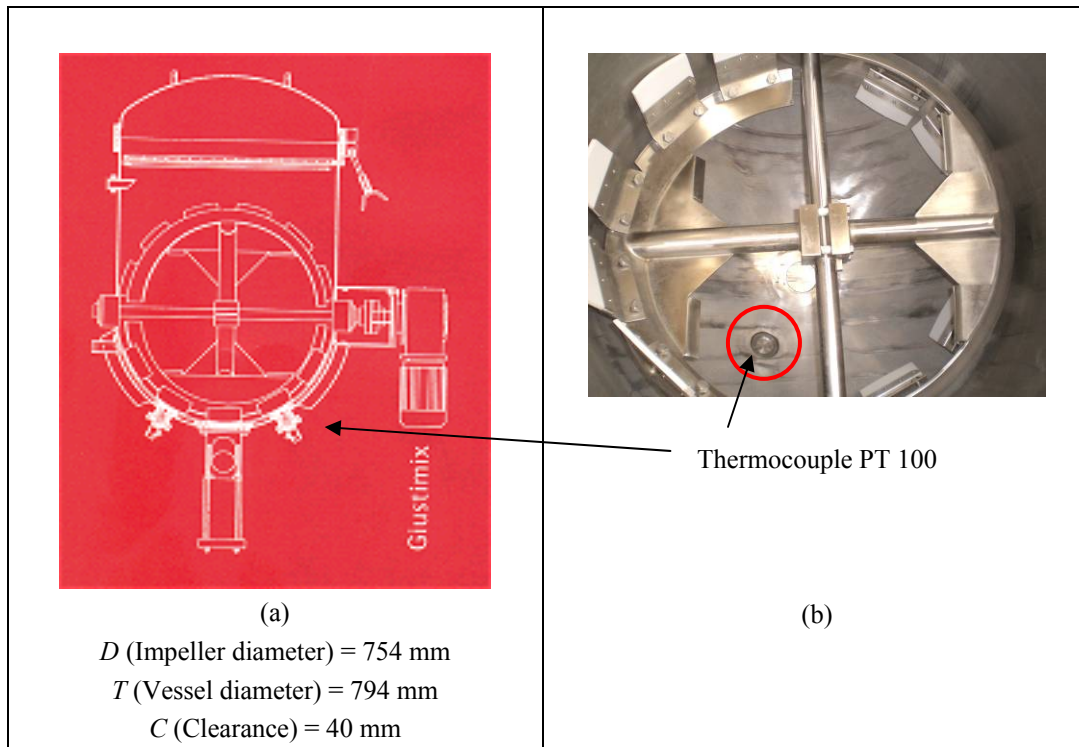


Figure 4-2. The 'Vesuvio' vessel – Source: Giusti Ltd - (a) and impeller (b)

The vessel is controlled with the GiustiMax modular package. This software allows manual and semi automatic command of the vessel. An illustration of the impeller movement is shown in Figure 4-3.

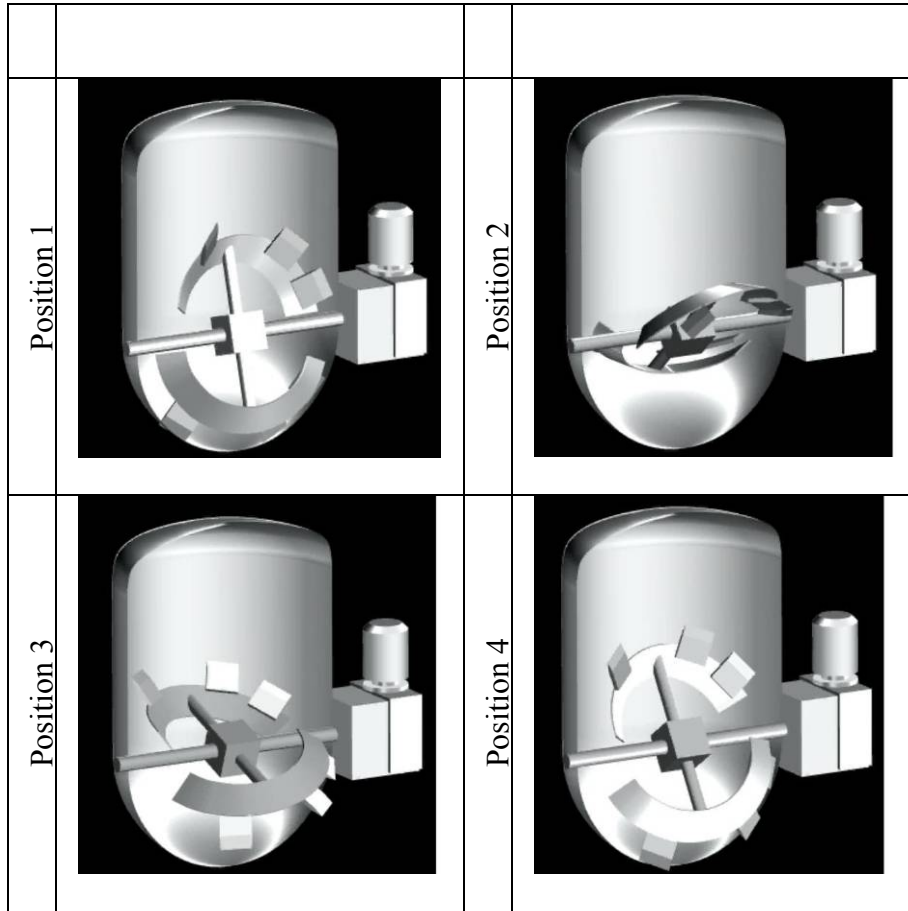


Figure 4-3. Impeller movement (Source: Giusti Ltd)

The Reynolds number was calculated for 3 different agitation speeds (5 rpm, 10 rpm and 15 rpm) using equation 2.5 (Table 4-2). For the experiments performed with water (Newtonian fluid), the dynamic viscosity (μ) was $8.4 \times 10^{-4} \text{ Pa s}^{-1}$ and the density was 1000 kg m^{-3} . For the experiments performed with the starch mixtures and the tomato soup, the apparent viscosity, μ_A , was calculated assuming that the Metzner-Otto approach (Metzner and Otto, 1957) holds, where the average shear rate in the impeller region ($\dot{\gamma}$) can be assumed to be proportional to the impeller speed, N . ie.

$$\dot{\gamma} = k_S N \quad (4.2)$$

In the 1957 paper, the constant of proportionality, k_s , was fitted by use of a modified Reynolds number based upon a power-law fluid. ie

$$\mu_A = K\dot{\gamma}^{n-1} \quad (4.3),$$

Hence,

$$Re = \frac{\rho ND^2}{\mu_A} = \frac{\rho ND^2}{K\dot{\gamma}^{n-1}} = \frac{\rho ND^2}{K(k_s N)^{n-1}} \quad (4.4)$$

Measuring the power draw and hence Power number, Po , as a function of Reynolds number for a Newtonian fluid for a given impeller geometry allows the relationship $Po=f(Re)$ to be obtained. Measurement of Power draw for non-Newtonian fluid allows determination of the modified Reynolds number from the same $Po-Re$ curve, and hence the apparent viscosity and thus, k_s can be determined. In the laminar regime, k_s was found to be generally insensitive to small changes in geometry and is a weak function of impeller type. For small impeller/tank ratio, k_s is approximately equal to 10-12. For ribbon/anchor impellers with a small wall clearance, C , the following concentrations have been proposed (Harnby et al., 1992).

$$k_s = 34 - 114\left(\frac{C}{D}\right) \quad \text{for } 0.026 < \left(\frac{C}{D}\right) < 0.164 \quad (4.5)$$

$$k_s = 33 - 172\left(\frac{C}{T}\right) \quad \text{for } 0.02 < \left(\frac{C}{T}\right) < 0.13 \quad (4.6)$$

Although this approach is only strictly valid for laminar regime, it has been applied here since the high apparent viscosity and slow rotation rate in the 'Vesuvio' vessel makes it unlikely that the conditions within the vessel are fully turbulent. This is discussed further later.

For the 'Vesuvio' vessel, $C = 20$ mm, T (Vessel diameter) = 754 mm and D (Impeller diameter) = 794 mm, using (4.5) and (4.6) the value of k_s would be 31 and 28. Although the type of impeller used in this work is not the same as a ribbon or anchor, the insensitivity of k_s to small geometrical changes allows the assumption of the use of these correlations based upon impellers with small wall clearances.

It can be seen from Figure 4.1 that the Carreau model described previously fits well all the viscosity data for shear rates ranging from 10^{-5} to 10^1 s $^{-1}$. However, the shear rate that is used to calculate the Reynolds number (equation 4.2 with $k_s=29.5$) ranges from 10^2 to 10^3 s $^{-1}$. Therefore for the following Reynolds number calculations, the data were fitted again using another model for shear rates ranging from 10^2 to 10^3 s $^{-1}$.

Table 4-2. Reynolds number for the 'Vesuvio' vessel

		5 rpm	10 rpm	15 rpm
Reynolds number for:	Water	5900	11800	17700
	Starch 4%	715	1940	3430
	Starch 5%	140	295	450
	Tomato Soup	360	960	1750

Transition criteria for flow in stirred vessels usually indicate that the flow is laminar for $Re < 10$ and turbulent for $Re > 10^4$. In this work, allowing for the assumption of $k_s = 29.5$, the flow is laminar/transitional. Hence analysis of the fluid flow will proceed assuming the fluid is turbulent, although it is possible that the turbulence is not fully developed.

4.2.3. Industrial application: Use of the TTI on the 'Vesuvio' vessel

4.2.3.1. Experimental set up

The enzyme used in the TTI preparation was α -amylase isolated from *Bacillus licheniformis*. The TTI preparation and analysis were described in § 3.2.1. During the experiments, a calibrated wireless thermocouple (Tracksense pro, Ellab UK Ltd., King's Lynn, Norfolk UK) with a 50 cm long probe was fixed securely onto the middle of the agitator shaft (Figure 4-4 (a)). This thermocouple tolerates temperatures from -50°C to +150°C at pressures up to 10 bar, with a precision of $\pm 0.05^\circ\text{C}$. In addition, the temperature of the vessel contents were regulated based a measurement from a calibrated PT 100 thermocouple which was located in a housing at the bottom of the vessel, used as the wall thermocouple during this study.

The P value at 85°C was obtained from the time temperature history recorded by both the wall and the wireless thermocouple using equation (2.4) with $T_{ref} = 85^\circ\text{C}$ and $z = 10^\circ\text{C}$ and was used for comparison with the P values given by the TTIs.

The fluids used for the experiments were water, aqueous solutions of starch at different concentrations (4% and 5%) and Heinz cream of tomato soup which were described in § 4.2.1. The sedimentation times of the TTIs were measured for the different fluids used and are given in table 4-3. In order to calculate the sedimentation times a TTI was dropped to the surface of the fluid and the time it took for the TTI to drop 10 cm was recorded for each fluid.

Table 4-3. Sedimentation times of the TTIs

Fluids used	Water	4-5% starch	Tomato soup
Sedimentation time	12 s	Neutrally buoyant	Neutrally buoyant

11 experiments were performed as shown in Table 4-4. Parameters varied were the fluid used, the set temperature, the filling level of the vessel and the heating options. Heating and cooling rates observed were dependent upon the heating options and the fluid used. Controllable parameters were the holding time and the set temperature. The holding time chosen was 15 min (14 minutes + 1 minute used to evacuate condensate from the jacket of the vessel) at the set temperature. Cooling was performed by using both the jacket and the vacuum cooling. During all the experiments, the agitation speed was kept constant at 10 rpm.

The condition of the starch used was varied by using solutions which had either been previously gelatinised (high apparent viscosity) or where the starch was still in its native state (close to aqueous viscosity). Where the starch was not previously gelatinised, the correct mass of starch was put in the vessel together with the water and the vessel brought up to the set temperature to gelatinise the starch in the vessel. For experiments using gelatinised starch, a precook stage was used where starch in water was heated up to 70°C for approximately 1 min and was then cooled down to 40°C. This allowed the starch to be in its viscous gelatinised form from the start of the subsequent experiment.

Table 4-4. Summary of the experiments

Exp. number	Fluid used	Fluid viscosity at shear rate 10s^{-1} (mPa.s)	Set up temperature	Filling level	Heating option
1	Water	1 mPa.s	83°C	Max filling level 250 L	Jacket heating
2	Water	1 mPa.s	83°C	Max filling level 250 L	Jacket heating + steam injection
3	Water	1 mPa.s	85°C	Max filling level 250 L	Jacket heating
4	4% not previously gelatinised	A the start (until temperature reaches 70°C) fluid similar to water and after gelatinisation viscosity = 400-500 mPa.s	83°C	Max filling level 250 L	Jacket heating
5	4% starch previously gelatinised	400-500 mPa.s	83°C	Max filling level 250 L	Jacket heating
6	4% starch previously gelatinised	400-500 mPa.s	83°C	Max filling level 250 L	Jacket heating + steam injection
7	4% starch not previously gelatinised	A the start (until temperature reaches 70°C) fluid similar to water and after gelatinisation viscosity = 400-500 mPa.s	83°C	Overfilled 300 L	Jacket heating
8	Tomato soup	430-550 mPa.s	83°C	Max filling level 250 L	Jacket heating
9	Tomato soup	430-550 mPa.s	83°C	Max filling level 250 L	Jacket heating + steam injection
10	5% starch previously gelatinised	1400-1600 mPa.s	85°C	Max filling level 250 L	Jacket heating
11	5% starch previously gelatinised	1400-1600 mPa.s	85°C	Max filling level 250 L	Jacket heating + Steam injection

The same number of TTIs was used in each experiment. 20 TTIs were placed in the fluid at the start and were able to move freely around the vessel (F TTIs). However, it is possible that collisions between the TTIs and the hot vessel wall (130°C) give extra denaturation of the enzyme leading to an abnormally high P value. To assess the effect of wall collisions, their influence was removed by placing some TTIs inside either 4 cm diameter airflow golf balls with widened holes (called GB hereafter) or inside a system of 2 tie clips (called TC hereafter) stuck together to form a 5 cm diameter ball (both sizes are about 5% of the vessel diameter, so will not greatly affect the overall flow pattern). Photographs of the GB and TC TTIs are shown in Figure 4-4 (b) and (c) respectively. The effective density ranged from 1050 to 1150 kg m^{-3} for the TTIs, was 1480 kg m^{-3} for the GB and was 1430 kg m^{-3} for the TC.

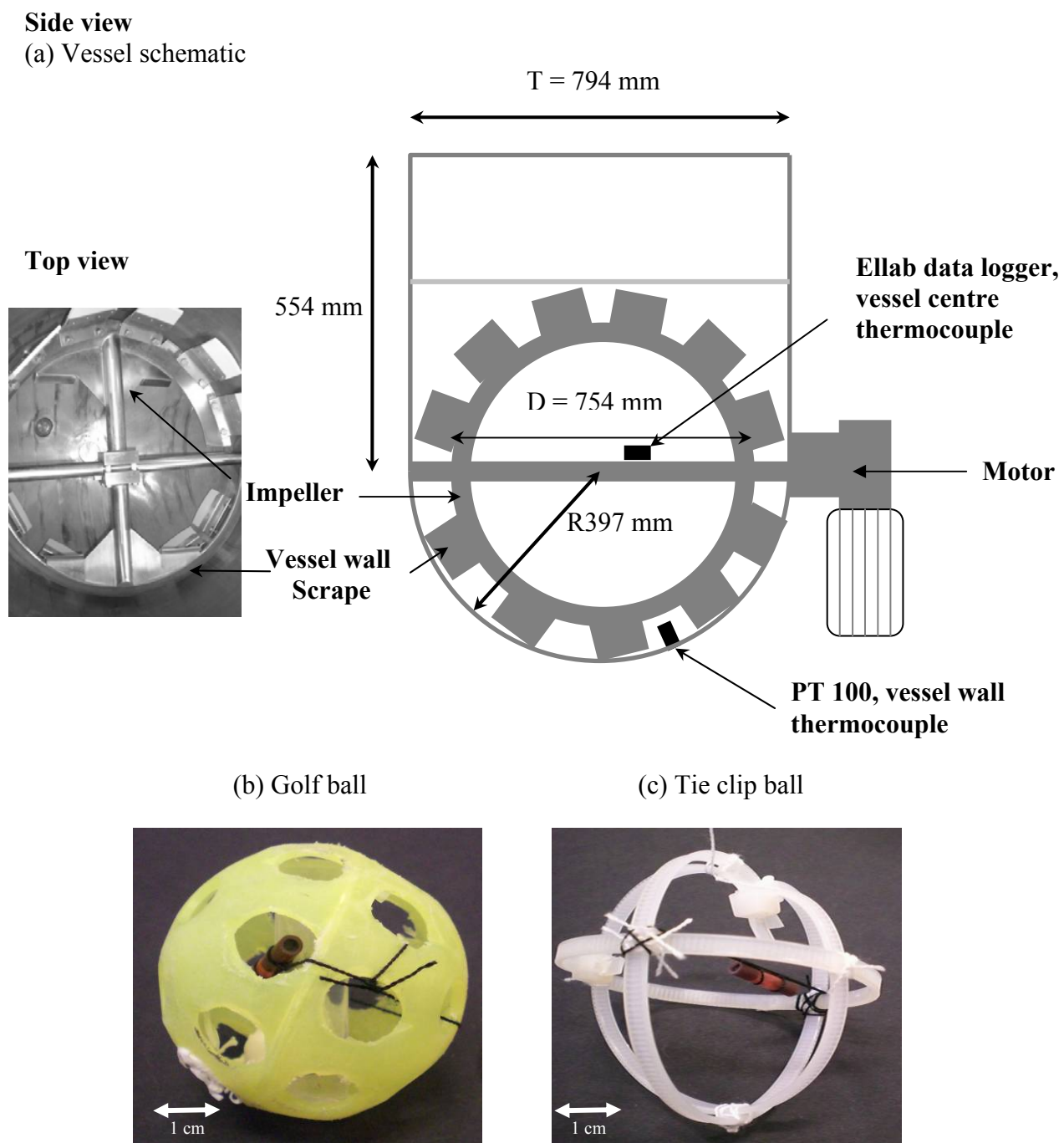


Figure 4-4. Details of vessel and TTIs used: (a) vessel schematic, showing the top and side view, (b) and (c) show the two systems which ensured that the TTIs could not get into close thermal contact with the wall. TTIs are shown

The effective density was calculated as the ratio of the mass of the TTI to its displaced volume calculated by immersion in water. In each experiment, 6 GB and 6 TC TTIs were used.

In addition, 20 free TTIs were added inside the vessel through the aperture of the vessel at the end of the vessel heat up time just before the start of the 'holding time' (when the steam is switched off) to identify the effect of the heat up time (when the steam is constantly on) on the TTIs. These TTIs are referred to as HT TTIs hereafter. Hence, a total of 52 TTIs were used in each experiment.

4.2.3.2. Statistical tests used

The P values obtained by the F, the HT, the GB and the TC TTIs were compared by statistical tests. The Mann-Whitney U and the Kruskal-Wallis H tests were used and implemented using SPSS software (SPSS Inc. Chicago USA). The Mann-Whitney U test was used for measurements between two samples. This non parametric test is used when the t test can not be applied (when normal distribution can not be assumed). The sample values are combined in an array classified from the smallest value to the highest. Each sample value is given a rank. For each sample, the sum of the rank gives a value called R (R_1 and R_2). The size of the sample is given by N (N_1 and N_2), N_1 being the smaller size sample. The equation (4.8) can be applied to test the difference between the samples.

$$U = N_1 N_2 + \frac{N_1(N_1+1)}{2} - R_1 \text{ (For sample 1),} \quad (4.7)$$

The sample distribution is now symmetrical and the mean and variance can be calculated:

$$\text{Mean: } \mu_U = \frac{N_1 N_2}{2} \quad (4.8)$$

$$\text{Variance: } \sigma_U^2 = \frac{N_1 N_2 (N_1 + N_2 + 1)}{12} \quad (4.9)$$

Hence,

$$w = \frac{U - \mu_U}{\sigma_U} \quad (4.10)$$

By consulting tables, it is possible to determine if samples are significantly different.

The Kruskal-Wallis H test was used for measurements between several samples. This is an alternative to the ANOVA test, when the assumption of normality or equality of variance is not met. The equation below is used to calculate H

$$H = \frac{12}{N(N+1)} \sum_{j=1}^k \frac{R_j^2}{N_j} - 3(N+1), \quad (4.11)$$

Where N and N_j are the sizes of the j samples, R_j is the sum of the rank for the k sample and k is the number of samples. The sampling distribution of H is almost a chi-square distribution with a $k-1$ degrees of freedom (N needs to be higher than 5). If H exceeds the critical value at some significance level (usually 0.05) it means that there is evidence to reject the null hypothesis in favour of the alternative hypothesis (Spielger, 1988). Samples may be considered as significantly different if the results from both tests are lower than 0.05.

4.3.Results

4.3.1. Thermocouples time temperature profiles

The time-temperature profiles obtained from the centre and wall thermocouples using Ellab Tracksense and PT100 respectively for the various experiments are shown in Figure 4-5.

Figure 4-5 (a) shows the time temperature histories for the 2 thermocouples for experiments with water at 83°C; the two profiles exactly overlap. Similar overlap was seen where steam injection was used to heat up the vessel, with only a small discrepancy during the cooling down period.

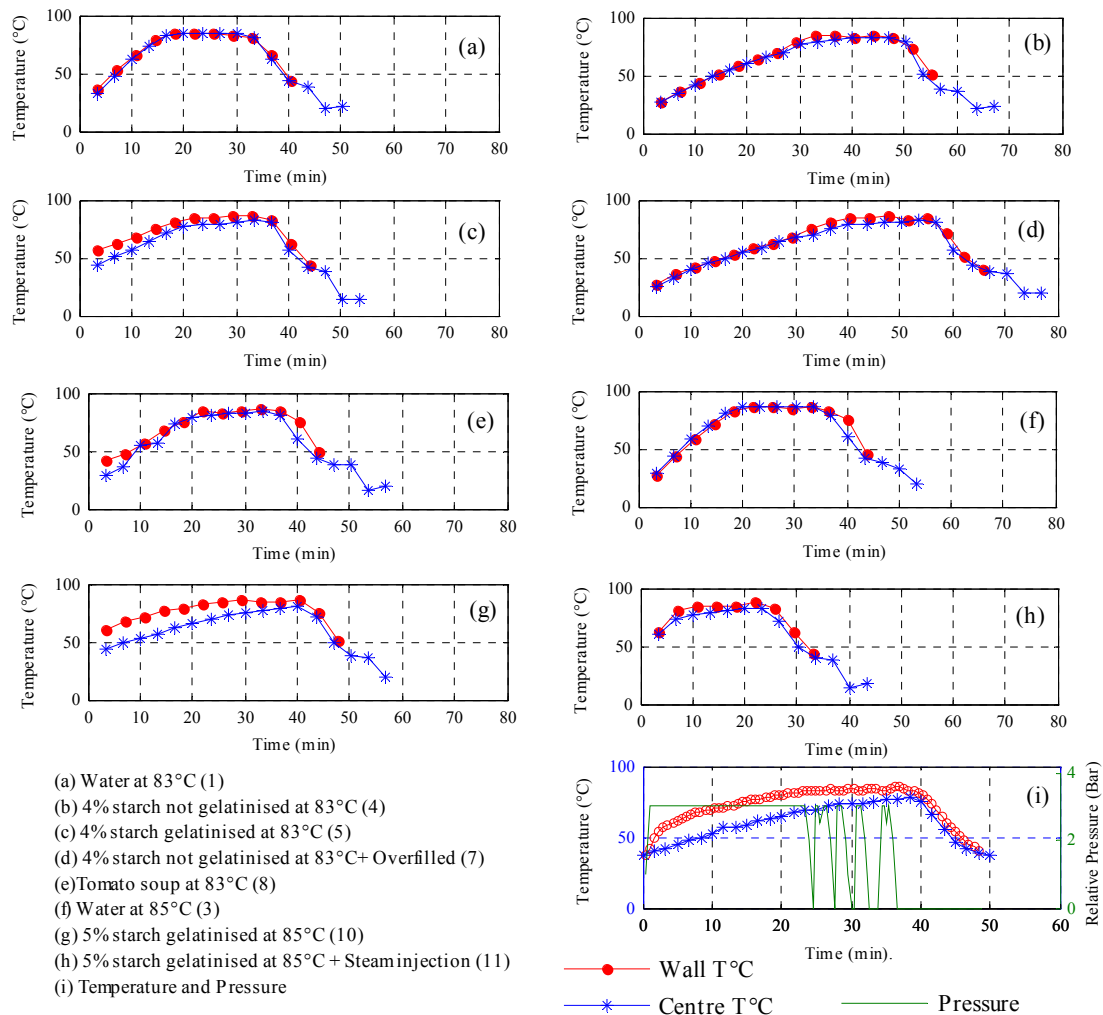


Figure 4-5. The time temperature profiles obtained with the thermocouples positioned in the wall and in the centre for the experiments performed at 83°C – The number in brackets in the legend refer to the experiment number of the Table 4-4

Figure 4-5 (b) shows the time temperature profiles for the experiment with non pre-gelatinised 4% starch, showing a good correlation between the two. However, when the starch starts to gelatinise (70°C) at $t = 25$ min, the centre temperature starts to lag slightly behind the wall temperature (max = 5°C difference). This thermal lag is reduced after 40 min to

approximately 0.7°C and remains this way during cooling. Figure 4-5 (c) shows the time temperature profiles obtained when the starch has already been gelatinised. This graph shows significant thermal lag (9°C) between the centre and the wall temperatures which remains unchanged until the end of the holding time (35 min).

For the experiment with 4% starch previously gelatinised and steam injection as well as jacket heating time temperature profiles again overlap, perhaps due to improvement in mixing efficiency caused by steam injection.

Results for the experiment performed with the overfilled vessel are presented in Figure 4-5 (d) and are similar to Figure 4-5 (b). A similar thermal lag appears due to the starch gelatinisation when the temperature recorded by the two thermocouples reaches 70°C .

Figure 4-5 (e) shows the results for the tomato soup experiments. The starch from the tomato soup was already gelatinised when the experiment started. A small thermal lag (1°C) between the two thermocouples can be observed throughout. This is noticeably reduced when the same experiment was performed using steam injection.

Figure 4-5 (f) shows profiles for experiment performed with water at 85°C and very similar results are observed than on Figure 4-5 (a). Figure 4-5 (g) shows the time temperature histories obtained using highly viscous fluid (pre-gelatinised 5% starch solution) - thermal lag is equal to 16°C . Figure 4-5 (h) shows the same experiment (5 % starch), performed with steam injection - thermal lag is equal to 5.5°C - and again this causes a reduction in the thermal lag. Increased viscosity due to gelatinised starch leads to increased thermal lag between the centre and wall temperatures, although this can be partly mitigated by use of steam injection.

The pressure of the steam injected inside the jacket is plotted on Figure 4-5 (i) together with the temperatures recorded at the centre and the wall of the vessel. During the heating stage pressure is on all the time; the action of the PI controller can be observed after the temperature reaches the set point as the pressure pulses and finally drops to atmospheric pressure between $t = \sim 22 - 37$ min.

To summarize, it can be seen that the size of the thermal lag observed correlates with the viscosity of the fluid processed. When the viscosity of the fluid increases, the thermal lag increases. The use of steam injection allows reducing significantly the thermal lag (see experiment performed with 5% starch).

Table 4-5. Heating rates ($^{\circ}\text{C}/\text{min}$) of the experiments described in Figure 4-5

	Heating rate ($^{\circ}\text{C}/\text{min}$)							
Plot of Figure 4-5	a	b	c	d	e	f	g	h
PT 100 (bottom of the vessel)	3.36	1.85	1.64	1.48	3.3	3.04	1.02	6.3
Ellab (centre thermocouple)	3.52	1.84	1.9	1.53	2.46	2.83	1.25	5.52

Table 4-5 shows the heating rates for the experiments described in Figure 4-5. The letters given in the second row correspond to the plots of Figure 4-5. It can be seen in this table that when the viscosity increases or when the vessel is overfilled, the heating rate decreases and when steam injection is used the heating rates increases. The use of steam injection allows to the content of the vessel to be heated up more quickly. It can be seen that for the experiment performed with high viscous fluid (5% starch), the heating rate is very low (1.02 and $1.25^{\circ}\text{C}/\text{min}$). This heating rate can be increased by using steam injection (6.3 and $5.52^{\circ}\text{C}/\text{min}$) in combination with the jacket heating.

4.3.2. Information obtained from TTIs

Additional information on the thermal behaviour within the vessel can be achieved using TTIs. The bar charts in Figure 4-6 to Figure 4-8 display P values at 85°C obtained for all 11 experiments. Each chart has error bars included which show one standard deviation; clearly if the error is taken into consideration some of the results overlap. For this reason, statistical tests (Mann-Whitney U and the Kruskal-Wallis H tests – see § 4.2.3.2) were used to verify if the differences between the results from each type of TTI within each experiment were significant. The results of the statistical tests are tabulated on the legend of each graph in Figures (4-6) – (4-8) and differences are considered significant only for values below 0.05.

Figure 4-6 presents experiments performed with water (Experiments 1, 2 and 3 of Table 4-4). Figure 4-6 (a) shows P values obtained by the thermocouples and TTIs for the experiment performed at a holding temperature of 83°C. There is reasonable agreement between the P values obtained by both thermocouples ($P = 13$ min at 85°C), and the HT and GB TTIs. The F TTIs added at the start of the experiment, gave higher P values than the thermocouples ($P = 17$ min); probably due to contact with the hot steam jacket. Since the GB and TC TTIs are protected from wall contact, and the HT TTIs are added later, these do not contact the jacket and the P values obtained are lower than those of the F thermocouples. However, in this experiment the scatter in the GB TTIs meant that results were not statistically significantly different from the F TTIs.

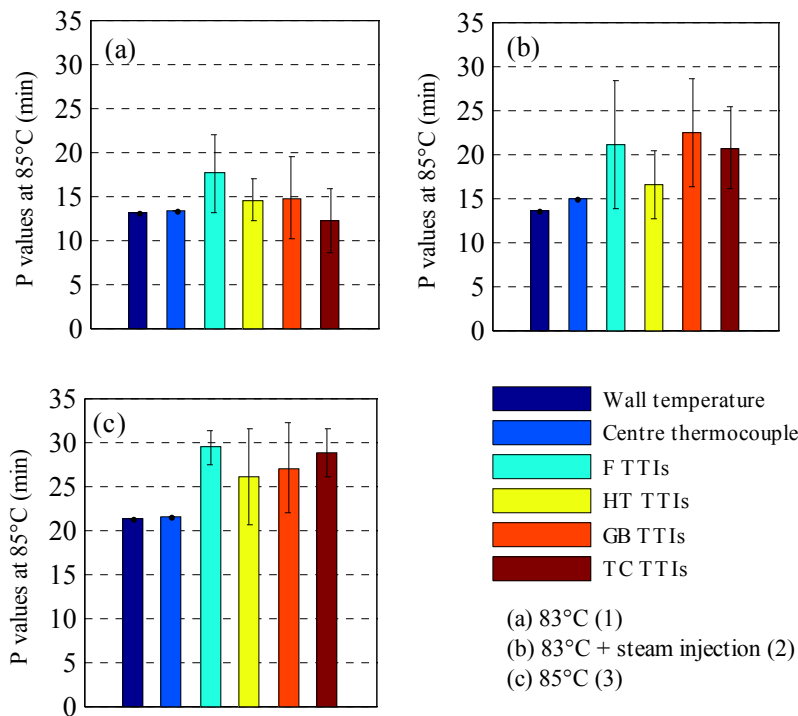


Figure 4-6. Experiments performed with water (a) Experiment 1 of Table 4-4. Statistically significant differences between F and HT, F and TC and all TTIs (b) Experiment 2 of Table 4-4. Statistically significant differences between HT and GB, HT and TC and all TTIs (c) Experiment 3 of Table 4-4. No statistically significant differences between all TTIs. Error bars show one standard deviation

Figure 4-6 (b) shows results from the experiment performed with water at 83°C using steam injection. Notably, the P values of all TTIs are higher than those obtained with the two thermocouples. The P values from the thermocouples are similar to those measured without steam injection, (although the centre value is slightly higher, $P = 15$ min at 85°C). As steam is injected in the centre of the vessel, any TTIs passing through the steam jet will receive localised heating and thus higher P values. It is notable that the standard deviations are much larger than for Figure 4-6 (a) suggesting that some TTIs have passed through the steam jet whilst others have not. Only the results for the HT TTIs compared with the GB and TC TTIs are significantly different, with the values for the HT TTIs being lower. Since the HT TTIs were added at the end of the heat up time, they were not exposed to continuous steam injection, with the steam only used intermittently to maintain the set temperature. Therefore,

the probability for the HT TTIs to pass through the steam was lower than for the GB and TC TTIs which were inside the vessel from the start. In addition, it can be seen that the P value of the thermocouple located in the centre of the vessel is higher than the P value of the thermocouple located at the bottom. The steam is injected towards the centre of the vessel and this causes the centre of the vessel to have higher P values than the bottom. Figure 4-6 (c) shows similar results, although none of the different TTIs produce significantly different answers. This experiment is similar to the experiment performed in Figure 4-6 (a) except that the holding temperature is higher which results in higher P values for both thermocouples and TTIs. In this experiment, it can be seen that the difference between the P values of the TTIs and the thermocouples is higher than the one of the experiment performed at lower temperature (Figure 4-6 (a)). This TTI (made from BLA) can measure thermal treatment ranging from 5 to 30 minutes at 85°C with the accuracy being the best at around 12-20 minutes at 85°C. Beyond 20 minutes the TTIs overestimate the thermal treatment (§ 3.3.2). In this experiment Figure 4-6 (c), the P values recorded were higher than 22 minutes and therefore the accuracy of measurement was lower which resulted in slight overestimation of the thermal process.

Figure 4-7 shows experiments performed with 4% starch at a holding temperature of 83°C (Experiments 4, 5, 6 and 7, Table 4-4). The experiment of Figure 4-7 (a) was performed with non-gelatinised 4% starch solution. The P value obtained from the centre thermocouple is 9 min (at 85°C) and is lower than that obtained by the wall thermocouple. P values for the 4 different kinds of TTIs are very similar to that of the centre thermocouple (9 min at 85°C) and there is no significant difference between results from the TTIs. The starch starts to gelatinise at 75°C and until this temperature, the fluid is of similar viscosity to water. Therefore initial mixing is very efficient and fluid reaches the set temperature relatively quickly. Since the

fluid temperature is uniform, the starch begins to gelatinise throughout the vessel once 75°C is reached, so, all the TTIs receive a similar thermal treatment due to the efficiency of the initial mixing.

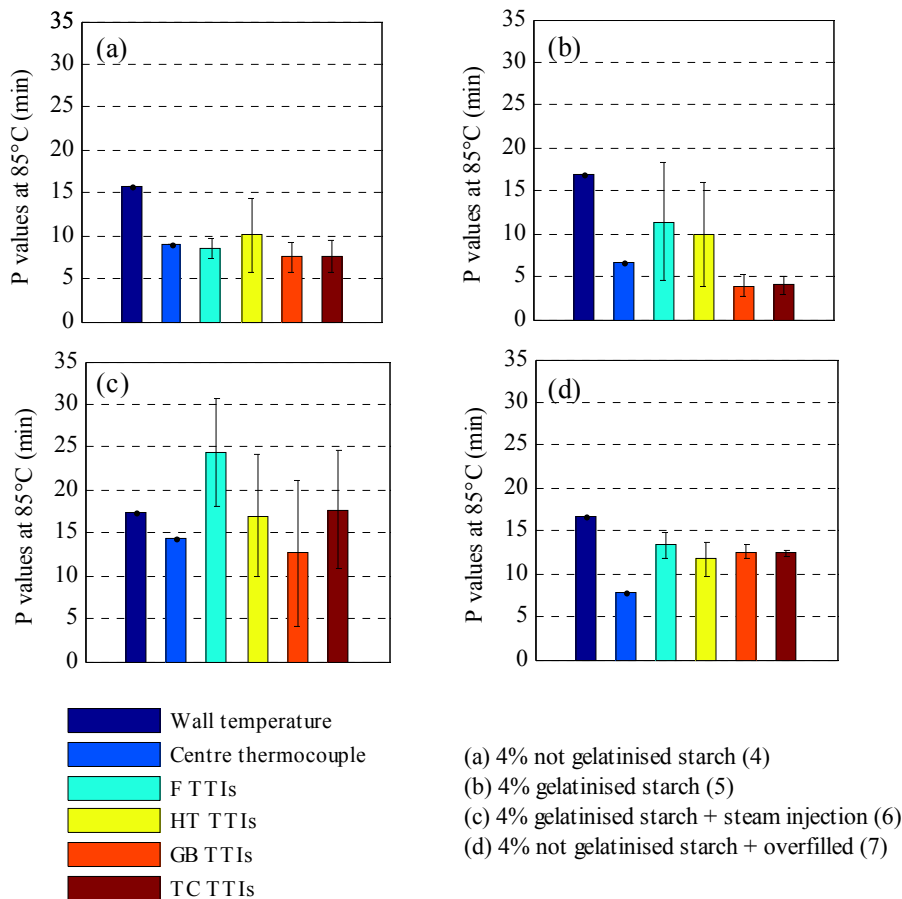


Figure 4-7. Experiments performed with 4% starch and with a holding temperature of 83°C (a) Experiment 4 of Table 4-4. No statistically significant differences between all TTIs (b) Experiment 5 of Table 4-4. Statistically significant differences between F and GB, F and TC, HT and GB, HT and TC and all TTIs (c) Experiment 6 of Table 4-4. Statistically significant differences between F and HT, F and GB, F and TC and all TTIs (d) Experiment 7 of Table 4-4. Statistically significant differences between F and HT and all TTIs. Error bars show one standard deviation

However, when the starch (4%) is already viscous at the start of the experiments as seen in Figure 4-7 (b), the results of the TTIs are significantly different. The difference between the P values of the 2 thermocouples is high (10 min at 85°C). During the heating time, mixing efficiency is lowered due to the fluid being viscous. Therefore the temperature is not

homogenous inside the vessel. The free TTIs have high P values, similar to that of the wall thermocouple, and that of the TTIs fitted in the balls are similar to the P values of the centre thermocouple. The GB TTIs and the TC TTIs have lower P values due to the lack of contact with the vessel wall. The heat up time is energy consuming stage and viscous fluids are difficult to process without hot and cold spots in the vessel. This can lead to local under-processing and over-processing of the fluid with consequent influences upon safety and product quality.

Figure 4-7 (c) displays P values for the TTIs and thermocouples for experiments performed with 4% pre gelatinised starch and with steam injection. Steam injection seems to improve heating efficiency since the difference between the P value of the centre and the wall thermocouples is lower compared with Figure 4-7 (b). The P values of the F TTIs are higher than the P value of the wall thermocouple. During the heat up time F TTIs could easily have passed close to the steam injection nozzle and therefore received further localised heating. After the heating time the steam injection was not in operation most of the time and hence the HT TTIs have lower P values. Values for the GB and TC TTIs are also significantly lower than those of the F TTIs and they appear less affected by steam injection.

Figure 4-7 (d) shows results from experiments performed with 4% starch and overfilled vessel. The P values from the TTIs are all similar and on average equal to 14 min at 85°C. They are surprisingly closer to the P values of the wall thermocouple (16 min at 85°C) than to those of the centre thermocouple (8 min at 85°C). In this experiment, the fluid path is different which may change the thermal treatment the TTIs have received. When this experiment is compared to one performed with a normal filled vessel (Figure 4-7 (a)), it can

be seen that all the TTIs have higher P values suggesting that fluid mixing in the overfilled case is different.

Figure 4-8 (a) and (b) show experiments performed with tomato soup from Heinz (§ 4.2.1) (experiments 8 and 9). These experiments are essential for the characterisation of the heating efficiency of the vessel since it uses a real food product. The experiment performed with tomato soup using only the jacket heating is shown in Figure 4-8 (a). Results are similar to that obtained with 4% gelatinised starch. The TTIs fitted inside 'golf ball' and 'tie clip ball' have significantly lower P values than those that are freely moving. The P value obtained by the wall thermocouple is similar to the P values of the F and HT TTIs. A similar observation can be made between the P value of the centre thermocouple and those of the TTIs fitted inside the balls. This experiment shows that product does not get most thermal treatment during the heating time as the average P value of the HT TTIs added after the heating time is similar to that of the F TTIs added at the start of the experiment.

In the experiment of Figure 4-8 (b), steam injection was used together with jacket heating. The P values obtained from the free TTIs are higher than that of the thermocouple located on the wall. The P values obtained by the TTIs fitted in balls are similar to the P value of the centre thermocouple. The difference between the P values of the thermocouples located on the wall and in the centre is smaller than for the same experiment without steam injection (Figure 4-8 (a)). P values obtained from the experiment without steam injection are lower than those from the experiments performed with steam injection. In both cases, the TTIs positioned inside golf ball and tie clip ball are more protected and record lower P values than the F and HT TTIs which are more exposed and move more freely inside the vessel.

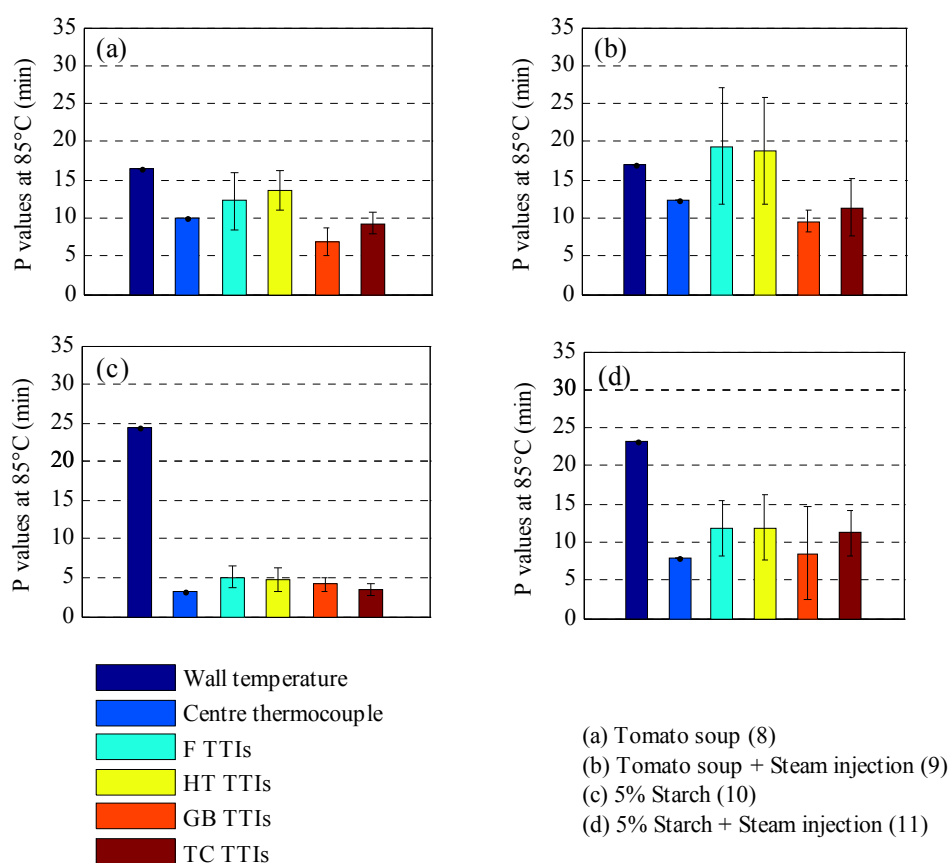


Figure 4-8. Experiments performed with tomato soup and with a holding temperature of 83°C and experiments performed with 5% gelatinised starch and with a holding temperature of 85°C (a) Experiment 8 of Table 4-4. Statistically significant differences between F and HT, F and GB, F and TC, HT and GB, HT and TC and all TTIs (b) Experiment 9 of Table 4-4. Statistically significant differences between F and GB, F and TC, HT and GB, HT and TC and all TTIs (c) Experiment 10 of Table 4-4. Statistically significant differences between F and GB, F and TC, HT and TC and all TTIs (d) Experiment 11 of Table 4-4. Statistically significant differences between F and GB, HT and GB and TC and GB. Error bars show one standard deviation

Figure 4-8 (c) and (d) show two experiments performed at 85°C with a high (5%) concentration pre-gelatinised starch solution with different heating options (experiments 10 and 11). The starch exhibits a high viscosity (at a shear rate of 10 s^{-1} , the apparent viscosity was 1400 mPa.s). Figure 4-8 (c) shows results obtained using the heating jacket only. *P* values of the TTIs are low compared to those obtained by the wall thermocouple and comparable with those obtained from the centre thermocouple. As observed in the experiments using gelatinized 4% starch solution, which also exhibited *P* values from the

TTIs and centre thermocouple lower than those measured by the wall (Figure 4-8 (c) and (d)), increasing fluid viscosity causes greater inhomogeneity in the uniformity of the heating. Steam injection is also used to heat up the solution in Figure 4-8 (d). P values from the TTIs and the centre thermocouple are much higher than those obtained in Figure 4-8 (c); again the use of steam injection improves the heating efficiency of the vessel.

The standard deviation of the P values of the TTIs obtained for the 11 experiments are summarized in Table 4-6 and are in general relatively high. In around 40% of cases the standard deviation of the P values obtained by the GB TTIs is lower than the error from the two types of free F and HT TTIs. The table shows that the standard deviation increases when the steam injection is used, possibly due to localised heating imparted by direct contact with the jet of steam. High standard deviation is also observed for the experiments performed with low viscosity fluids where the mixing efficiency is expected to be high, however this may be due to the TTIs passing close to the vessel wall. This can be caused by sedimentation of the TTIs. The sedimentation time decreases with the decrease of the fluid viscosity. For water, the sedimentation time was 12 s (for 10 cm) while for the starch solutions and tomato soup they are neutrally buoyant. The high standard deviations of the P values of the TTIs mean that the thermal process is not uniform throughout the vessel. The use of steam injection increases the heterogeneity of the process. During the process, when the product (in this case the TTI) touches the hot wall of the vessel, it will instantaneously receive a high thermal treatment (it could even burn the product). In contrast, other parts of the product could avoid contact with the hot wall and therefore receive insufficient thermal treatment. The study of the standard deviation of the TTIs allows investigation of this issue.

Table 4-6. Mean P value and Standard deviation of the TTIs for the 11 experiments

	Exp 1	Exp 2	Exp 3	Exp 4	Exp 5	Exp 6	Exp 7	Exp 8	Exp 9	Exp 10	Exp 11
	Water 83°C	Water 83°C Steam injection	Water 85°C	4% Starch not gelatinis ed 83°C	4% Starch gelatinis ed 83°C	4% Starch gelatinised 83°C Steam injection	4% Starch not gelatinised 83°C Overfilled	Tomato soup 83°C	Tomato soup 83°C Steam injection	5% Starch gelatinised 85°C	5% Starch gelatinised 85°C Steam injection
Mean P values (min at 85°C)											
F TTI	17.6	21.0	29.3	8.4	11.4	24.3	13.3	12.2	19.4	5.1	11.8
HT TTI	14.5	16.5	25.6	10.1	9.9	17.0	11.7	13.6	18.8	4.7	11.8
GB + TC TTIs	13.5	21.5	27.8	7.5	4.0	15.1	12.5	8.1	10.5	3.6	9.9
Standard deviation P values (66% of probability)											
F TTI	4.4	7.3	1.9	1.2	6.9	6.3	1.5	3.7	7.6	1.4	3.8
HT TTI	2.4	3.9	5.4	4.2	6.1	7.1	2.0	2.5	7.0	1.4	4.3
GB + TC TTIs	4.2	5.2	4.0	1.7	1.1	7.8	0.6	2.1	2.8	1.1	4.7

4.3.3. Process analysis using TTIs

The above experiments demonstrate how different types of TTI can be used to study the effects of a process. It was not attempted here to propose a protocol for formal validation of a process; more work is needed before this can be done. However, the results suggest that:

- (i) TTI particles that are free to be close to the steam-heated wall show the highest P value; these are likely to be representative of the processing the fluid has received.
- (ii) TTI particles that have constrained to be away from the wall show lower values, indicating the processing received by fluid that is not heated by the wall.

The process should be designed so that the two sets of results give P values that are as close as possible. The influence of overfilling shows that mixing profiles changes and that greater variation is seen; it is probable that the TTI results seen here show the overprocessed fraction only, and that underprocessing also results.

4.4. Conclusion

TTIs were used together with thermocouples to investigate the thermal efficiency of an industry scale 250 litre agitated vessel used for the thermal processing of viscous food fluids. The parameters varied were the fluid apparent viscosity, direct and indirect heating options and filling level. The study showed that the thermal process efficiency is lowered as the fluid viscosity increases; however this can be overcome by using steam injection. Overfilling the vessel modifies the heating efficiency of the vessel. This is probably due to the different path taken by the fluid during the mixing and the additional amount of fluid to process.

The effect of the heating time on the product was studied by adding some TTIs (HT) once the vessel had reached the set up temperature. During the heating time, steam was constantly injected inside the jacket and therefore the wall temperature was high. By adding other free TTIs at the end of the heating time, it was possible to investigate if the product was getting most of its cooking during the heating time. However, comparison of the *P* values obtained from the F and the HT TTIs showed that for 70% of the cases the product did not get most of its cooking during the heating time.

Novel designs of TTI (GB and TC) were successfully used to monitor the thermal treatment received by the fluid in the central area of the vessel. Close approach to the hot wall was prevented by putting the TTIs inside plastic balls. The free-flowing TTIs showed the effect of the whole process, including the time spent close to the hot wall, whilst those in the balls reported *P* values closer to that calculated from bulk temperatures. The bulk values reported by GB+TC TTIs thus underestimate the processing the fluid has received. For all the experiments, no significant difference between the GB or TC designs was observed; therefore

either GB or TC could be used to monitor the thermal treatment. For 70% of the experiments, the average P values obtained by the TTIs from the GB and TC were close or similar to the P value of the thermocouple located in the centre of the vessel. This observation showed that the use of GB or TC TTIs could help to investigate the thermal treatment efficiency in the centre of the vessel. The results show how TTIs might be applied to determine the process safety (i.e. the minimum value identified) the degree of overcooking due to the wall (i.e. the differences between the different types of TTIs) and the variability or uncertainty induced by the process.

Chapter 5

Use of PIV technique to investigate the fluid flow inside the vessel

5.1. Introduction

In Chapter 3, lab scale experiments were performed on TTIs to evaluate their accuracy for measurement and validation of thermal processes. Following this, a description of the application of TTIs inside a specialist mixing vessel ('Vesuvio' vessel), which represents a real world food processing application, was given in Chapter 4. TTIs were used in parallel with thermocouples within the 'Vesuvio' vessel for further validation as a thermal process monitoring technique.

However, this investigation is not complete without understanding how the fluid flows inside the vessel since this is key to the understanding of the thermal processing received by the food. In addition, it is essential to make sure that the TTIs move through all locations inside the vessel, moving with the fluid, and that the P values obtained are representative of the vessel when TTIs are used to determine the thermal treatment efficiency.

In this Chapter, the fluid flow inside the vessel is investigated using PIV. Of key interest is the determination of the average flow field and the flow regime within the vessel, since this determines the mixing mechanisms which are present. PIV is used to determine the motion of the liquid phase and the flow regime only: an alternative technique, PEPT, is used to determine the relative motion of the TTIs to the fluid, which is described in Chapter 6.

5.2. Scale down ‘Vesuvio’ vessel

Since fluid flow experiments could not be performed on the ‘Vesuvio’ vessel for reasons which will be detailed later in this Chapter, a reduced scale version of the vessel was built. The production of this reduced scale version of the ‘Vesuvio’ vessel will be described in § 5.2.2. Prior to this, the viscosity of the fluids used during the experiments had to be characterised in order to perform the scaling down of the vessel. In the next section, the fluids used are described.

5.2.1. Fluids

The fluids used for the experiments were water and CMC (Carboxymethylcellulose, Sigma-Aldrich, Poole UK) solution at different concentrations. CMC was used at concentrations of 0.25% and 0.5% by mass as a transparent mimic fluid with similar rheology to the starch.

The apparent viscosities of the CMC solutions were determined using the same experimental technique and parameters used for the starch solution (§4.2.1). The CMC mixtures exhibited shear thinning behaviour (Figure 5-1).

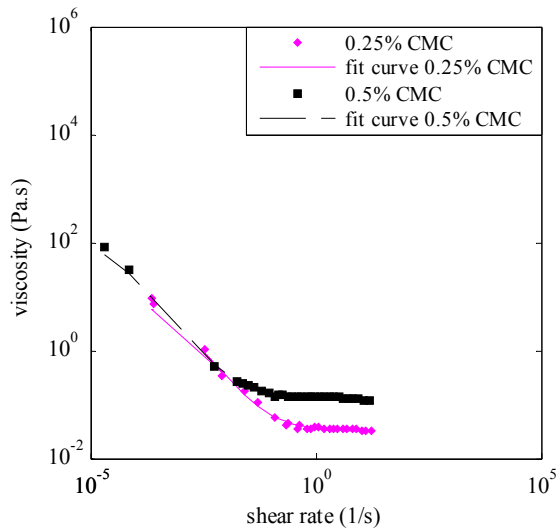


Figure 5-1. Viscosity curve of CMC 0.25% and 0.5%

The Carreau model was selected as the most appropriate model to fit all the data (equation 4.1), (Holdsworth, 1993) and values of the model parameters for the fluids are given in Table 5-1.

Table 5-1. Values of the Carreau model parameters

	0.25% CMC	0.5% CMC
μ_{∞}	0.033	0.132
μ_0	10	146
K	3240	67280
m	2.007	1.988
R^2	0.9242	0.8884
μ_A at shear rate $10s^{-1}$	30-50 mPa.s	120-140 mPa.s

5.2.2. Model vessel

The scale-down vessel was built to enable experiments on the fluid flow using PIV and PEPT (Chapter 6). PIV studies can only be carried out using transparent media and equipment because the laser light has to pass through the vessel to illuminate and visualise the particles.

The vessel was made from borosilicate glass. In addition, the vessel was designed to fit within the cavity of the PEPT camera which was of limited size

The scale-down vessel has a diameter of 244 mm, height of 174 mm and the radius R of the spherical part is equal to 122 mm. This will be called ‘model vessel’ hereafter. The proportions of the ‘Vesuvio’ vessel were kept constant, but the diameter size was reduced by a factor of 3.2 to fit in the PEPT equipment. The vessel was placed inside a square tank made of glass which was filled with water to minimize refraction at the surface of the model vessel (Aubin *et al.*, 2004).

The impeller was a proportional replica of the full scale version. The impeller was made from aluminium to reduce weight and was anodised in order to avoid reflection of the laser light. The paddles were made from plastic to prevent scratching of the glass. Figure 5-2 shows the comparison of the dimensions of the two vessels. The maximum volume of liquid that the ‘Vesuvio’ vessel can process at a time is 250 litres. When this volume is compared to the model vessel, it corresponds to 7.5 litres. In industry, the ‘Vesuvio’ vessel is often overfilled in order to process the maximum amount of product. Unfortunately, the manufacturer does not have information on the effect of overfilling on the thermal efficiency of the vessel. Therefore, some experiments were also carried out on the vessel when it was overfilled. The overfilling volume is approximately 300 litres for the ‘Vesuvio’ vessel and 9 litres for the model vessel. The motor used allowed speeds ranging from 5 to 45 rpm. No heating and cooling options were available on the model vessel since it was necessary to be able to see through easily without paralax, so it could only be used at room temperature. An illustration of the model vessel is given in Figure 5-2 and 5-3.

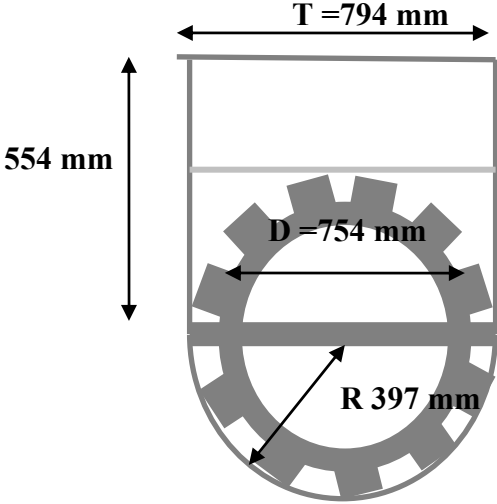
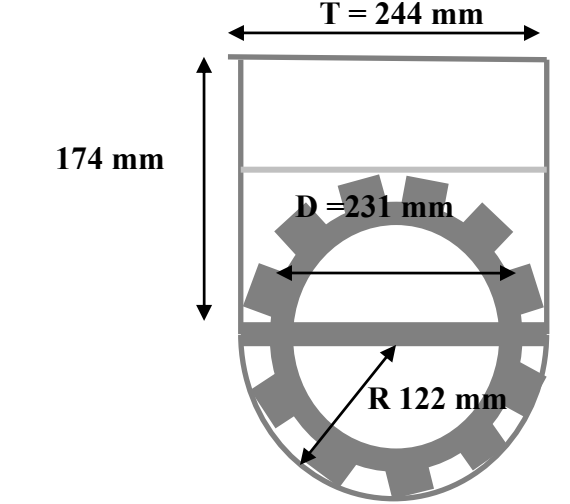
'Vesuvio' vessel	Model vessel
 <p> Required filling volume = 250 litres Overfilling = 300 litres Wall Clearance (C) = 20 mm T vessel diameter D = Impeller diameter </p>	 <p> Required filling volume = 7.5 litres Overfilling = 9 litres Wall clearance = 6 mm </p>

Figure 5-2. Comparison of the dimensions of the 'Vesuvio' vessel and the model vessel

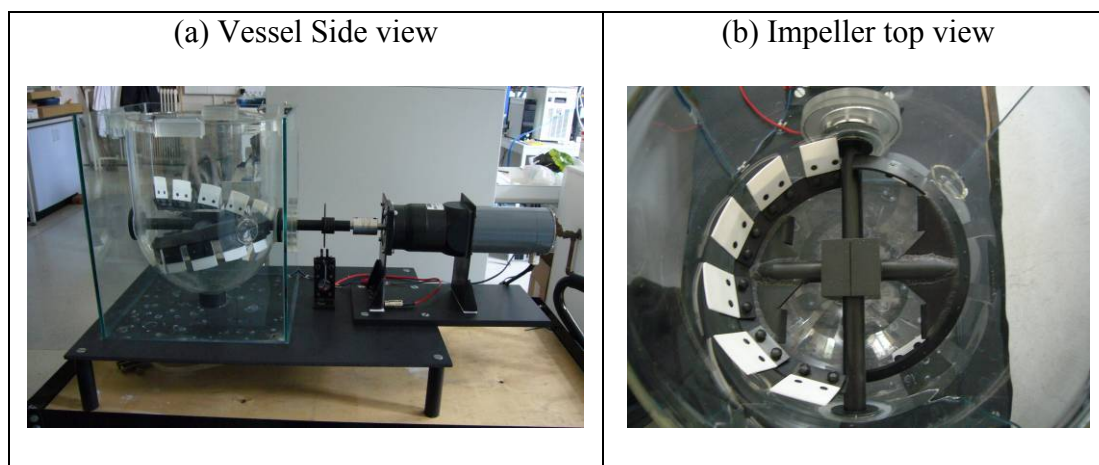


Figure 5-3. Photographs of the model vessel

Movies showing the agitation of a solution of CMC at 0.5% can be seen in the CD included with this work at the back of the thesis (Mushroom_normal filling level.wmv and Visualisation_Normal filling level.wmv).

5.2.3. Scaling down at constant power per unit mass

There are various methods to achieve the scaling down process and, some parameters of the vessel have to be kept constant. These parameters can be seen in Table 5-2 below. Generally, constant power per unit mass (Power/mass) or power per unit volume is considered as the most effective scaling criterion for turbulent flows, since the energy is dissipated at the smallest scales of the flow which only depend on local specific energy dissipation rate (which is related to the total power input) and kinematic viscosity, ν (Harnby *et al.*, 1992).

Table 5-2. Scaling down methods (N = Rotation rate (rev s⁻¹), D = Impeller diameter (m), g = acceleration of gravity (m s⁻²), σ = the surface tension (N m⁻¹), ρ = Density (kg m⁻³), μ = Dynamic viscosity (Pa s) and Q = Impeller pumping flow rate m³ s⁻¹))

Parameter to be kept constant	Function	Scale-up equation
Blend time	$1/N$	$N_2 = N_1$
Froude number	DN^2/g	$N_2 = (D_1/D_2)^{1/2} N_1$
Power/mass	$N^3 D^5 / D^3$	$N_2 = (D_1/D_2)^{2/3} N_1$
Solids suspension	$ND^{3/4}$	$N_2 = (D_1/D_2)^{3/4} N_1$
Tip speed	ND	$N_2 = (D_1/D_2) N_1$
Weber number	$\frac{N^2 D^3 \rho}{\sigma}$	$N_2 = (D_1/D_2)^{3/2} N_1$
Reynolds number	$\frac{\rho ND^2}{\mu}$	$N_2 = (D_1/D_2)^2 N_1$
Pumping number	Q/ND^3	$N_2 = (D_1/D_2)^3 N_1$

For this study, it was first decided to use the Reynolds number as a scaling down criterion. For the same fluid and for an agitation speed of 5 rpm ('Vesuvio' vessel), the speed that should be used for the model vessel should normally be 52 rpm which is far beyond the range in which the model vessel can operate and would lead to ejection of the fluid. However, it was possible to equalise the Reynolds numbers of the two vessels by changing the viscosity

and the agitation speed together. By scaling down using the Reynolds number, the number of experiments that could be done was limited and therefore it was decided to use constant power per unit mass as a scaling down criteria. This scaling down method is the most commonly used for turbulent flow, although as already identified, the flow regime within ‘Vesuvio’ vessel is likely to be transitional due to high viscosity of fluid and low rpm of impeller.

The power requirement is calculated as follows:

$$P_i = P_0 \rho N^3 D^5 \quad (5.1)$$

Where P_i is the impeller power requirement, P_0 is the power number, ρ is the density of the fluid, N is the rotational speed and D is the impeller diameter. When the system is geometrically similar, $D \propto T$ and $H \propto T$ (T = Tank diameter, m and H = Fill height, m).

The Power per unit mass can be obtained by the ratio $\frac{P_i}{\rho V}$ where V is the filled volume vessel

and is equal to $\frac{\pi}{4} T^3$

$$\text{Thus, } \frac{P_i}{\rho V} = \frac{P_0 \rho N^3 D^5}{\rho \frac{\pi}{4} T^3} \quad (5.2)$$

If the flow is assumed as turbulent, P_0 is constant. Due to geometric similarities $D \propto T$.

$$\frac{P_i}{\rho V} \propto \frac{N^3 D^5}{T^3} \propto \frac{N^3 D^5}{D^3} \propto N^3 D^2 = \text{constant}$$

$$\text{Hence, } N_2 = (D_1 / D_2)^{2/3} N_1 \quad (5.3)$$

For laminar flows, since $P_i/\rho V$ is independent of D , the usual procedure is to keep N constant. Clearly the actual flow regime in the vessel lies between these two extremes. It was initially decided to scale on the basis of turbulent (transitional) flow, leading to the agitation speeds in Table 5-3. In examination of the speed ranges for the model (11 – 33 rpm) and ‘Vesuvio’ (5 – 15 rpm) there is some overlap, hence to a certain extent, both laminar and turbulent scaling criteria have been covered in the same set of experiments. Table 5-3 shows the corresponding agitation speeds for the two vessels.

Table 5-3. The speed scaling down at constant power per unit mass

	Low speed (rpm)	Medium speed (rpm)	High speed (rpm)
‘Vesuvio’ vessel	5	10	15
Model vessel	11	22	33

The Reynolds numbers were calculated (the same way as described in §4.2.2.) for 3 different agitation speeds (11 rpm, 22 rpm and 33 rpm) for the model vessel and given in Table 5-4 below. The fluids used for the experiments were described in Chapter 4 and §5.2.1.

Table 5-4. Reynolds numbers for the model vessel

		11 rpm	22 rpm	33 rpm
Reynolds number	Water	1220	2450	3680
	CMC 0.25%	440	1115	1935
	CMC 0.5%	180	495	900

Table 5-4 shows that the fluid flow is transitional for all the experiments. In this study, the analysis of the fluid flow will proceed initially assuming the fluid is turbulent to identify regions of flow instabilities within the vessel. However, it is important to mention that any regions of the flow where the fluid velocity has a significant fluctuating component is not due

to fully developed turbulence, merely transient instabilities most likely due to the passage of the impeller or disturbance of the free surface.

5.3. Flow visualisation studies

This section describes the flow visualisation experiments (PIV) that were performed on the model vessel. The experimental set up will be described in the following part.

5.3.1. PIV

Silver coated hollow glass spheres of 10 μm diameter manufactured by Dantec (Denmark) were used in this work as tracer particles. The small size and neutrally buoyant properties of the particles leads to a very short relaxation time so that they can be assumed to follow reliably the fluid streamlines. The seeding density was about 10 particles per interrogation spot during the cross correlation process.

The illumination system consisted of the pulsed laser and the lightsheet optics. In order to create the desired lightsheet size and thickness, a combination of cylindrical and spherical lenses were used (see § 2.2.3.1 and Figure 5-4).

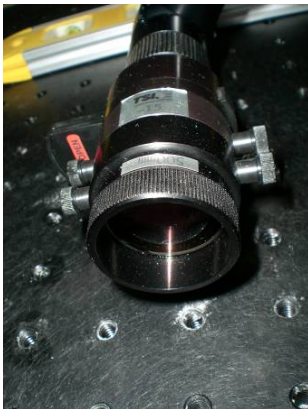


Figure 5-4. Lenses used to produce the light sheet

A double-head Nd:YAG laser was used which had an emission wavelength of 532 nm. The pulse rate of this laser was 15Hz (double pulses). The laser was attached to a light arm allowing the laser sheet to be conveniently adjusted. The time between the two Q pulses was determined to be 1000 μ s and ideally the two energy pulses should be equal. However, in this case, the energy pulse had to be different due to a default of the PIV installation. The laser pulses were set to be 95 μ s and 110 μ s for laser 1 and 2 respectively.

The digital camera used was a PIVCAM 10-30 cross correlation CCD camera (TSI Inc, USA), see Figure 5-5. The digitized resolution of the camera used here was 1008 \times 1018 pixels. The maximum rate of the camera was 15 pairs of frames per second in frame straddling mode. The objective used was a 28 mm 1:2.8 D AF NIKKOR lens (NIKON Inc, JP). The focal length was 28 mm and the maximum aperture was f/2.8D. The focussing range was from 0.25 m to infinity and the magnification ratio was a maximum of 1:5.6 at 0.25 m. The camera was operated from the computer through the TSI Insight® software. By producing a double exposure, the camera could take a pair of images on two separate frames. The camera could be used in other modes (continuous or single) but these modes were not used.

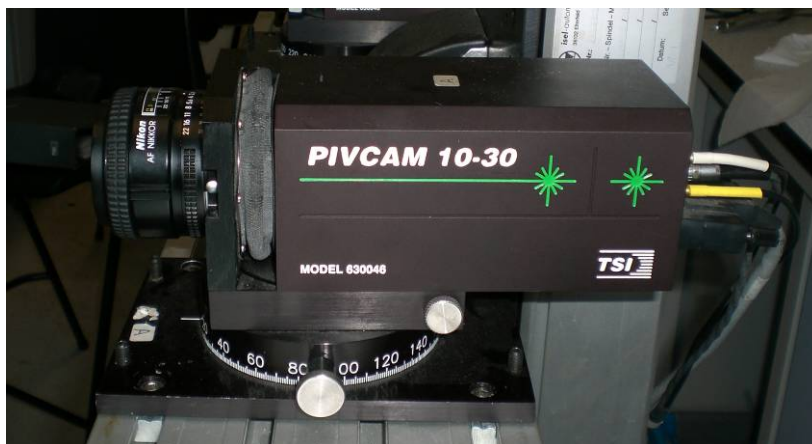


Figure 5-5. Digital camera

The timing between all components of the PIV system was controlled by a TSI 630036 synchroniser (TSI Ltd) which was used with an external trigger. The external trigger was coupled to an encoder fixed to the shaft of the impeller. The use of the external trigger together with an encoder allowed images to be taken at a fixed impeller position. The laser pulse had to be synchronised perfectly in order to coincide with the appropriate frame in the camera. The figure 5-6 below shows the diagram of the timing of the camera with the laser pulse.

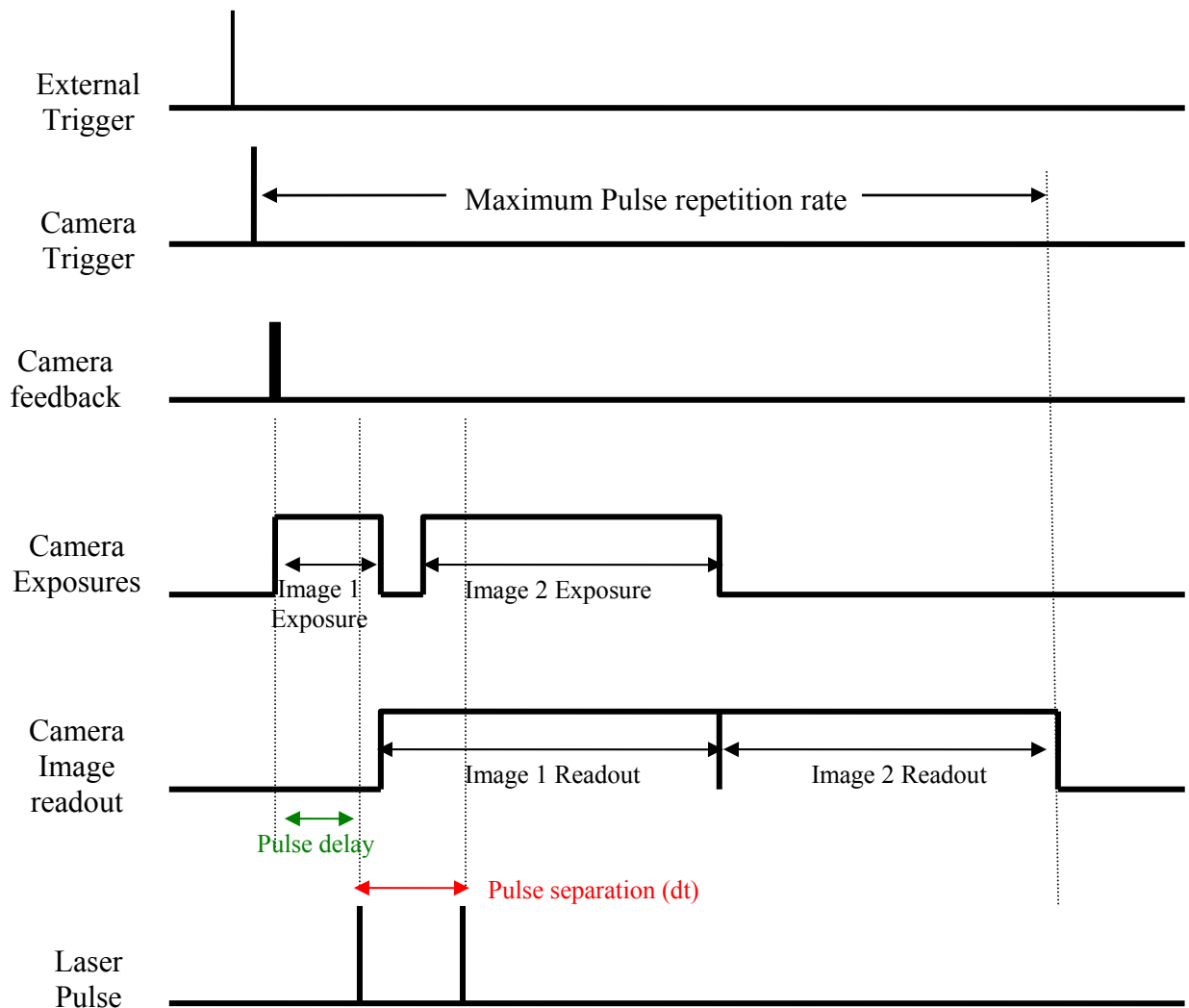


Figure 5-6. Diagram of the timing of the camera with the laser pulse

The straddle mode allowed capture of two successive images. These two images were processed further by cross correlation to obtain the flow field vectors. The external trigger connected to the shaft of the vessel sent a signal to the camera to start capturing the two images. The first image exposure lasts $264 \mu\text{s}$ and the first laser pulse is fired at the end of this first exposure time. The second image exposure starts straight after the first one, however the exposure duration is longer as the first image is read out. This is due to the fact that only one image can be processed at a time, therefore the second exposure lasts until the first image

has been processed. The second laser pulse occurs 1000 μs after the first one. The pulse delay was chosen to be long because of the slow agitation speed of the vessel (11 -33 rpm). Per experiment, 250 image pairs were taken. It was observed by Sharp *et al.* (2001), that for turbulent flow measurements, the difference between the mean and rms calculated for 50 and 100 frames was less than 1%.

5.3.2. Data processing

To process the photos the TSI Insight[®] software was used. Velocity vectors were obtained from the displacements of the particles between the two images. Cross correlation was used with an overlap window of 50% to process the data. Due to the distance of the vessel from the camera, the size of the interrogation window was of 32 \times 32 pixels and the resolution was 261 μm /pixel. With an overlap of 50%, a total of 61 \times 62 vectors were obtained.

When the TSI Insight[®] software calculates the velocity vectors, it automatically removes any vectors that are twice the magnitude of the standard deviation of the magnitude of surrounding vectors in a 9 \times 9 grid around them. The velocity vectors removed were replaced by vectors issued from the interpolation of the 9 \times 9 grid. These vector replacements only affect 1% of the processed vectors.

5.3.3. Experimental design

The model vessel was set up and located inside the PIV equipment with the PIV camera was facing the side of the agitator, see Figures 5-7 and 5-8.

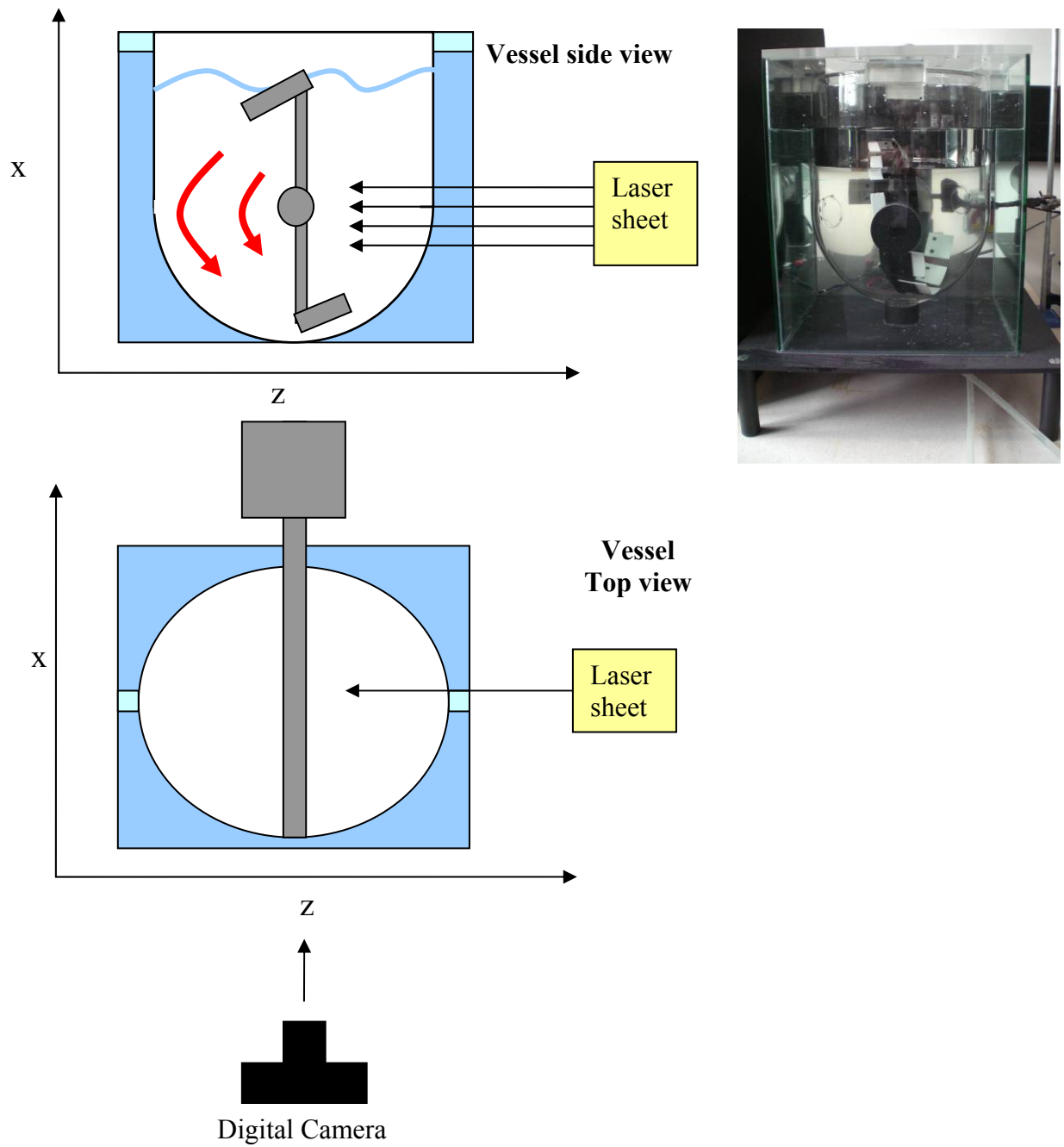


Figure 5-7. Experimental set up



Figure 5-8. Photo of the experimental design

A total of 48 experiments were performed on the model vessel. Factors such as fluid viscosity, filling level and agitation speed on mixing efficiency were studied. The fluids used for the experiments were water and aqueous solution of CMC at concentrations of 0.25% and 0.5% by mass. Three different agitation speeds were used: 11 rpm, 22 rpm and 33 rpm calculated from the scaling down using the power per unit mass. Images were taken at 4 different impeller positions separated from each other by an angle of 45° . Figure 5-9 shows the different positions used. A summary of all experiments that are carried out is given in Table 5-5 below.

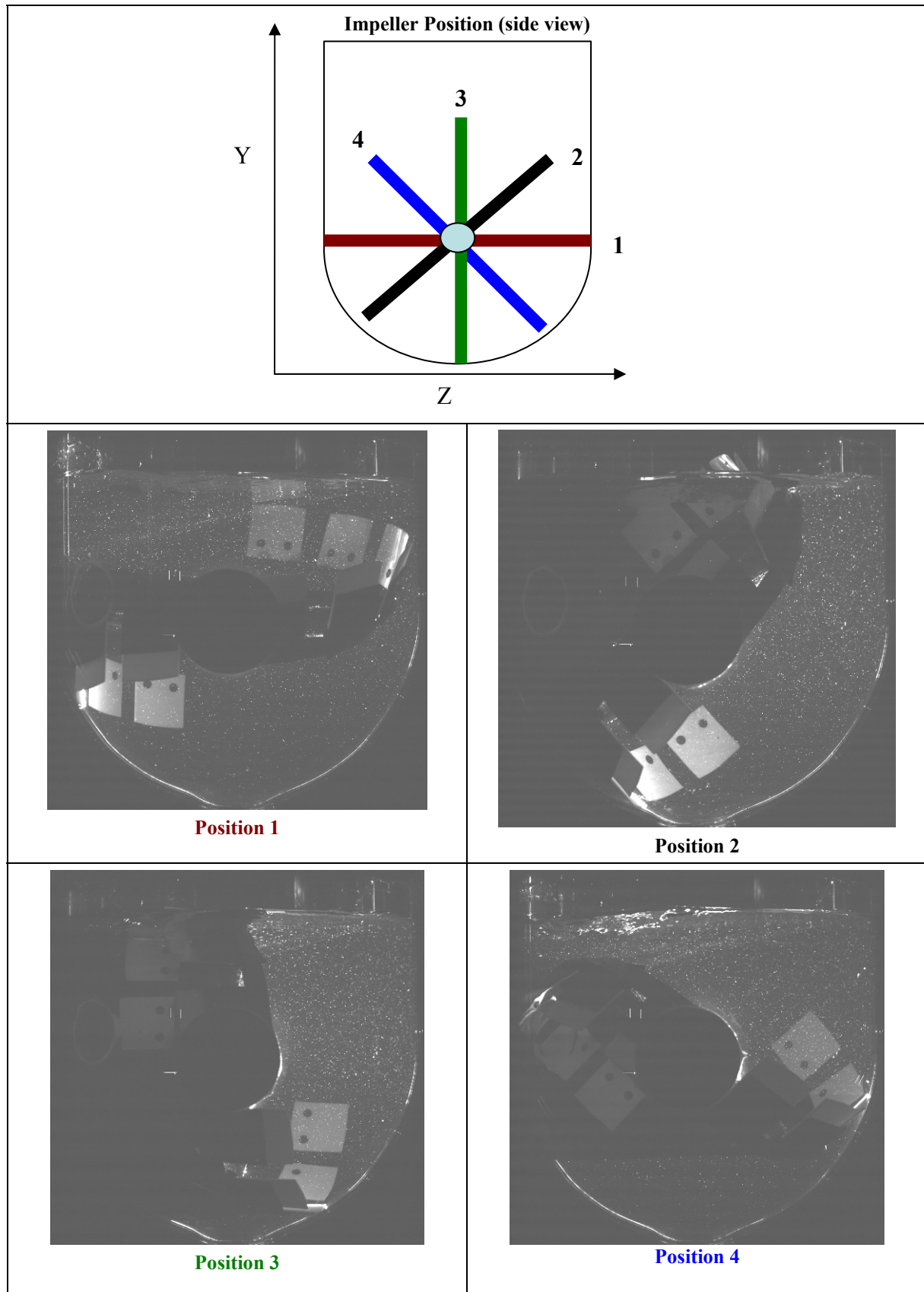


Figure 5-9. Impeller positions

Table 5-5. Summary of the experiments performed with the PIV camera

Experiment number	Fluids	Agitation speed	Filling level
1,2,3,4	Water	11 rpm	Recommended level
5,6,7,8	Water	22 rpm	Recommended level
9,10,11,12	Water	33 rpm	Recommended level
13,14,15,16	Water	22 rpm	Overfilled level
17,18,19,20	CMC 0.25%	11 rpm	Recommended level
21,22,23,24	CMC 0.25%	22 rpm	Recommended level
25,26,27,28	CMC 0.25%	33 rpm	Recommended level
29,30,31,32	CMC 0.25%	22 rpm	Overfilled level
33,34,35,36	CMC 0.5%	11 rpm	Recommended level
37,38,39,40	CMC 0.5%	22 rpm	Recommended level
41,42,43,44	CMC 0.5%	33 rpm	Recommended level
45,46,47,48	CMC 0.5%	22 rpm	Overfilled level

The data obtained from the PIV experiments were processed using Matlab 7 and Tecplot 9. Matlab is a programming software package specialized in numerical computing (MathWorks, Inc, USA). This software allows operations such as matrix processing and plotting of functions and data. Tecplot is a numerical simulation software package which is used for post-processing the results. Using the combination of these software packages, various parameters, namely the average velocity and turbulence intensity, which were described in §2.2.2, were calculated.

5.4. Results

Before starting to analyse the results obtained with the PIV technique, it is essential to validate the statistical reliability of the data obtained during the experiments. The change of the mean velocity with the number of acquisitions was investigated; the value of the mean should converge to a constant value as the number of acquisitions is increased. This ensures

that the number of acquisitions taken and sampling time were sufficient for the mean values to be stable and thus that the data is reliable. For these experiments, the global mean as a function of number of acquisitions is described below.

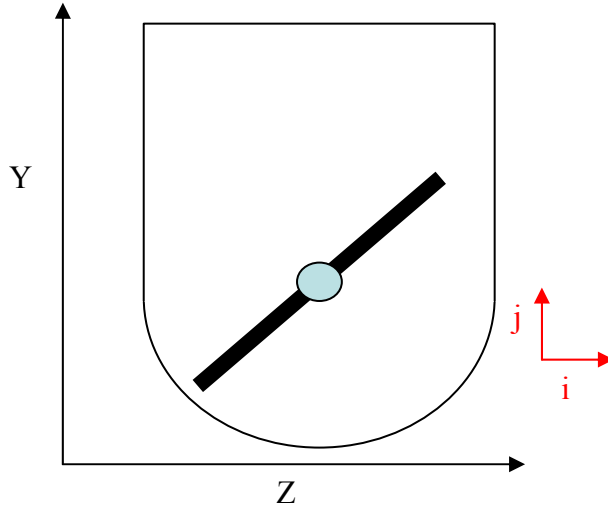


Figure 5-10. Coordinates of the vessel

For any location on the 2-D plane (Figure 5-10), the fluid flow velocity is equal to:

$$U_{x,y} = \sqrt{U_i^2 + U_j^2} \quad (5.4)$$

Where U is the velocity (ms^{-1})

For all the acquisitions, at any point in the image, the mean velocities are calculated as follows:

$$\overline{U}_{x,y} = \frac{\sum_{k=1}^N (U_{x,y})_k}{N} \quad (5.5)$$

Where N is the number of acquisitions and $\overline{U}_{x,y}$ is the mean velocity.

Then, the global mean velocity \overline{U}_G is calculated from equation 5.6.

$$\overline{U}_G = \sum_x \sum_y \overline{U}_{x,y} \quad (5.6)$$

Since a large number of experiments were performed with the PIV, it was decided to calculate the global mean velocity for two experiments which present the best and worst case scenarios in terms of the expected degree of turbulence:

- the best case scenario: experiment performed with high speed agitation and low fluid viscosity (water)
- the worst case scenario: experiment performed with low speed agitation and high fluid viscosity (0.5% CMC)

For the two experiments (and for the four impeller positions), the global velocities are calculated for $N = 50, 100, 150, 200$ and 250 acquisitions and are plotted in Figure 5-11. The figure shows that the mean values do not change with increasing number of acquisitions; indeed 250 images are more than is actually needed.

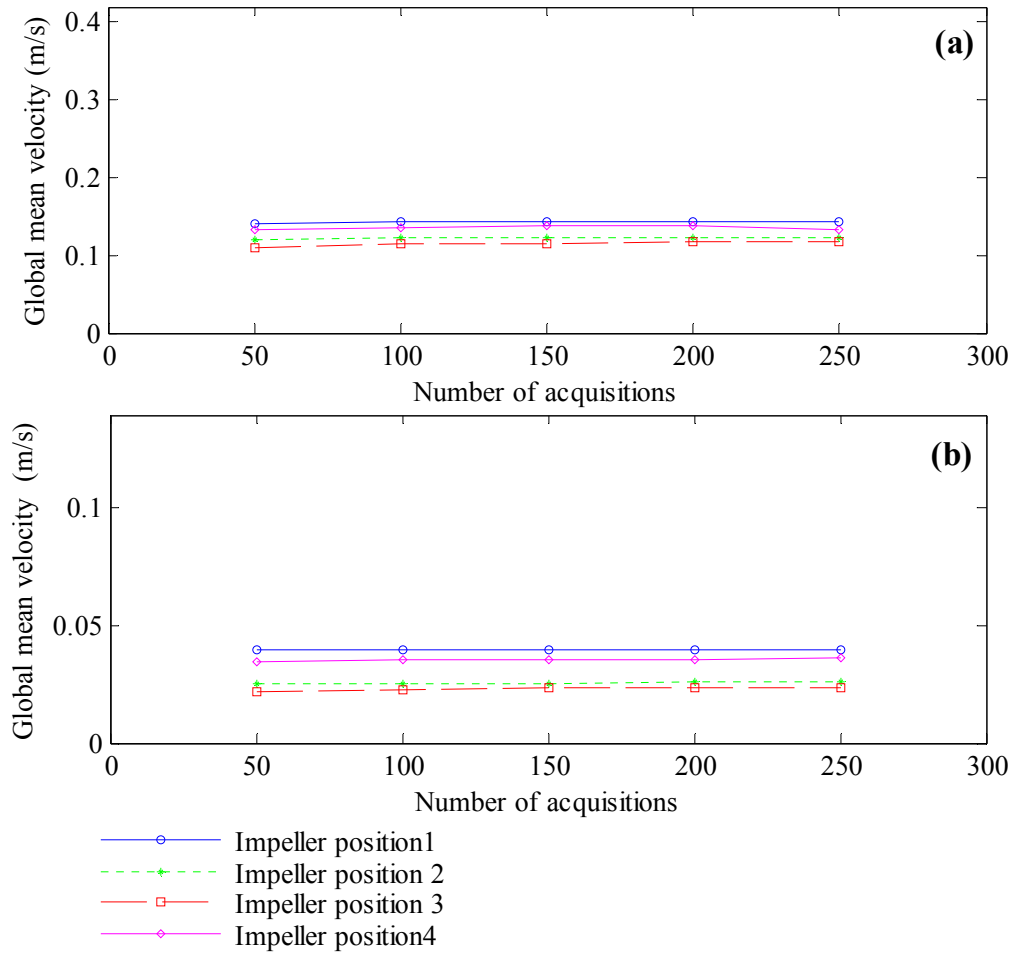


Figure 5-11. Global mean velocities (\overline{U}_G) calculated for two experiments (a) Experiment performed with water with an agitation speed of 33 rpm (b) Experiment performed with 0.5% CMC with an agitation speed of 11 rpm

Turbulence Intensity

As described previously in § 2.2.2, the rms and turbulence intensity are parameters that can be calculated for turbulent flows; the calculated Reynolds number showed that the fluid flow is laminar/transitional. However, for some areas of the vessel, in region of high local velocity, velocity fluctuations may be present. To investigate these phenomena, particularly with respect to the transitional flow regime which is likely to be observed, the turbulence intensity was calculated.

Figure 5-12 and 5-13 shows the turbulence intensity contours at the 4 different impeller positions ((a), (b), (c) and (d)) for the best case and worst case scenario experiments respectively. In general, it can be seen that the turbulence intensity values recorded in the bulk of the vessel are very low ($\ll 0.05 \bar{U}$).

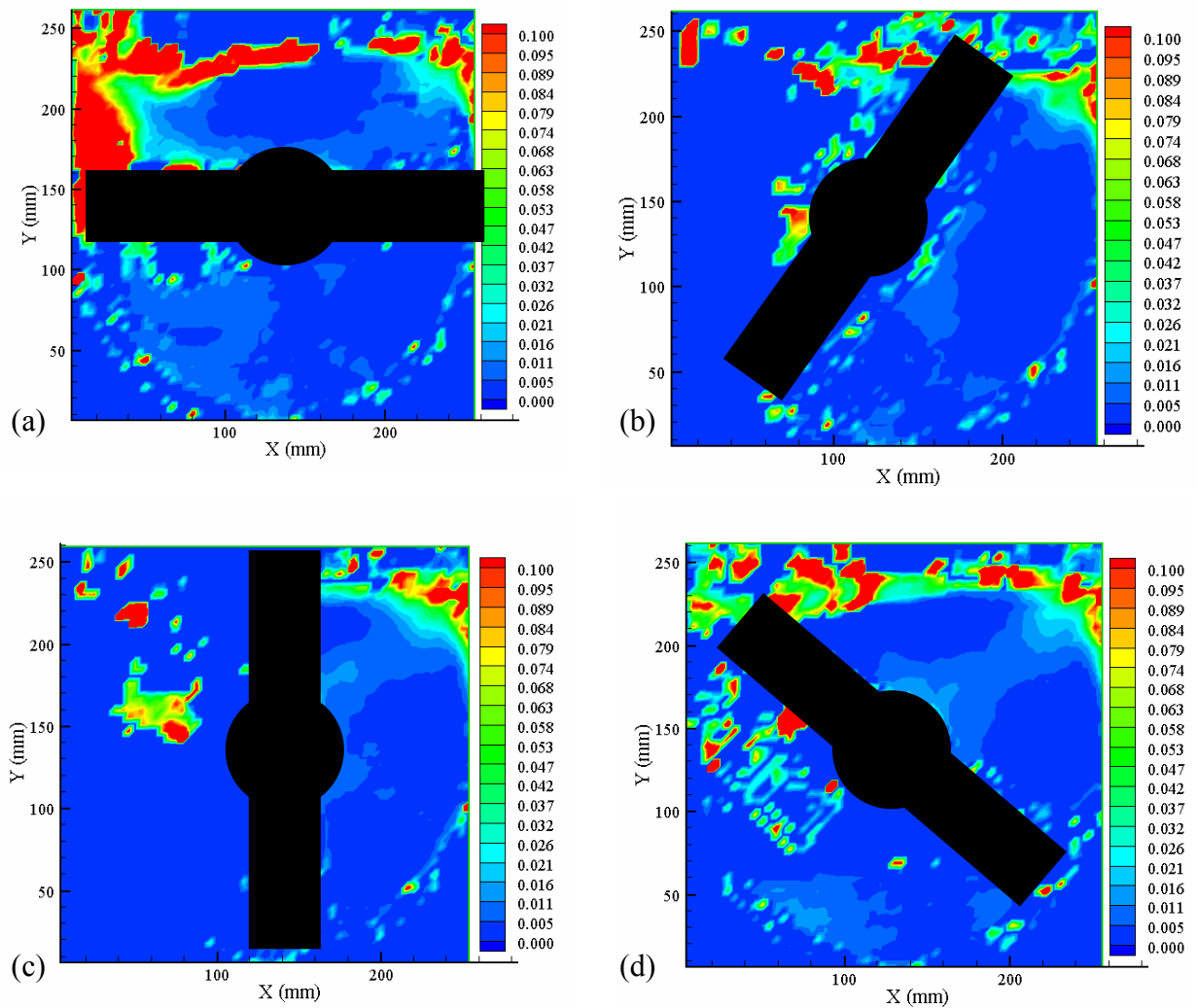


Figure 5-12. Turbulence intensity recorded for the experiment performed with water and an agitation speed of 33 rpm with (a) impeller position 1 (b) impeller position 2 (c) impeller position 2 (d) impeller position 4. The turbulence intensity of the red coloured regions is above 0.1.

In regions close to the free-surface or the impeller blades, Figures 5-12 and 5-13 show respectively that the maximum turbulence intensity recorded is ~ 0.9 . This indicates that some localised instabilities are present in these regions and that some mixing may occur due

to eddy dissipation caused by the passage of the blade through the free surface or by local vortex creation close to the blades. Otherwise, the flow in the bulk of the vessel is dominated by laminar (streamline) flow, i.e. mixing would be expected to occur by shear/elongation or possibly folding due to any periodic change in flow direction. As will be seen later the folding mechanism is not generally observed due to the general solid body rotation of the fluid with the impeller.

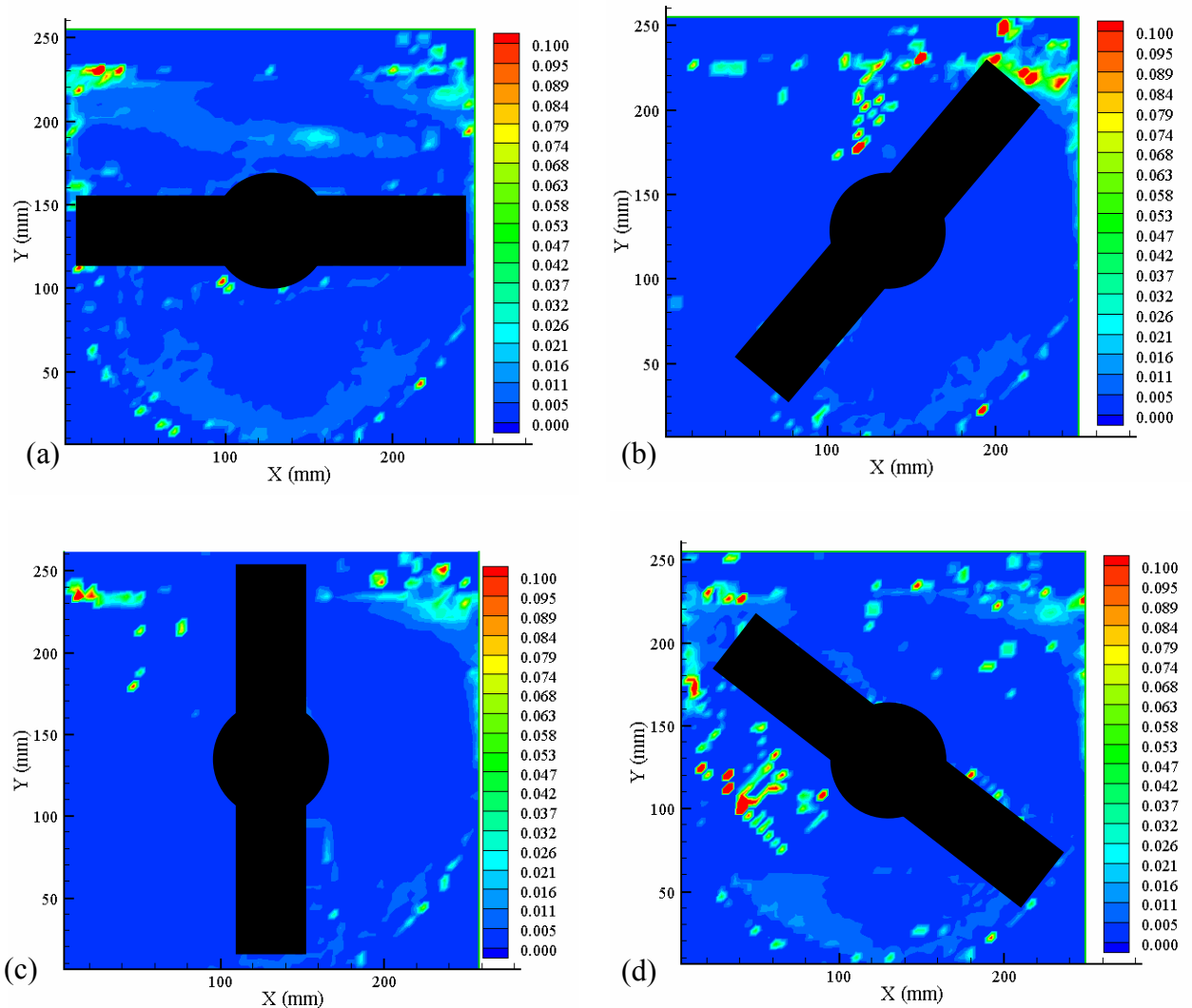


Figure 5-13. Turbulence intensity recorded for the experiment performed with a solution at 0.5% CMC and an agitation speed of 11 rpm with (a) impeller position 1 (b) impeller position 2 (c) impeller position 2 (d) impeller position 4. The turbulence intensity of the red coloured regions is above 0.1.

In conclusion, the flow is predominantly laminar and indicates that the mechanism of mixing is due to bulk motion and turnover at the free-surface. In addition, these results show that the calculation of rms and turbulence intensity are not meaningful here since the fluid cannot be considered as ‘turbulent’. Further analysis will therefore be conducted considering laminar flow and the general flow pattern and average velocities measured, although it must not be forgotten that local disturbances are present at the free-surface.

5.4.1. Effect of the agitation speed, the fluid viscosity and filling level on the flow

In this section, the 2-D velocity fields from a selection of the PIV experiments (given in Table 5-5) are discussed. The focus of this section is to determine the effect on the flow pattern of changing impeller speed, using low (water) and high (0.5%) viscosity fluids, and also the effect of overfilling.

In Figure 5-20 and 5-21, the normalised velocity field for water at 11 and 22 rpm are shown respectively. Each figure comprises four plots, each giving the average velocity field of the vessel at each impeller position. Plot (a) gives the velocity of the fluid when the impeller is at position 1, plot (b) is for position 2, plot (c) is for position 3 and plot (d) is for position 4. In these Figures, the normalised velocity vectors are plotted. The magnitude of the normalised velocity is calculated from equation (5.7).

$$U^* = \frac{\bar{U}}{U_{tip}} \quad (5.7)$$

Where U^* is the normalised velocity, \bar{U} is the mean velocity and U_{tip} is the velocity of the agitator tip. The use of normalised velocities allows the comparison of experiments

performed at different agitation speeds. In Figure 5-20, each of the sub-figures shows that the motion is predominantly rotating with the impeller, i.e. the fluid is close to solid body rotation. At each impeller position, velocities in the bulk of the vessel are $U^* \sim 0.5$. Regions of maximum velocity vary according to impeller position, with local maxima evident at position 1 and 4:

- Position 1: at free-surface, $U^* \sim 0.9$
- Position 4: at free-surface, $U^* \sim 0.8-0.9$

These regions of local maxima are due to dissipation of disturbances at the free-surface caused by the passage of the impeller, which scoops through the free-surface.

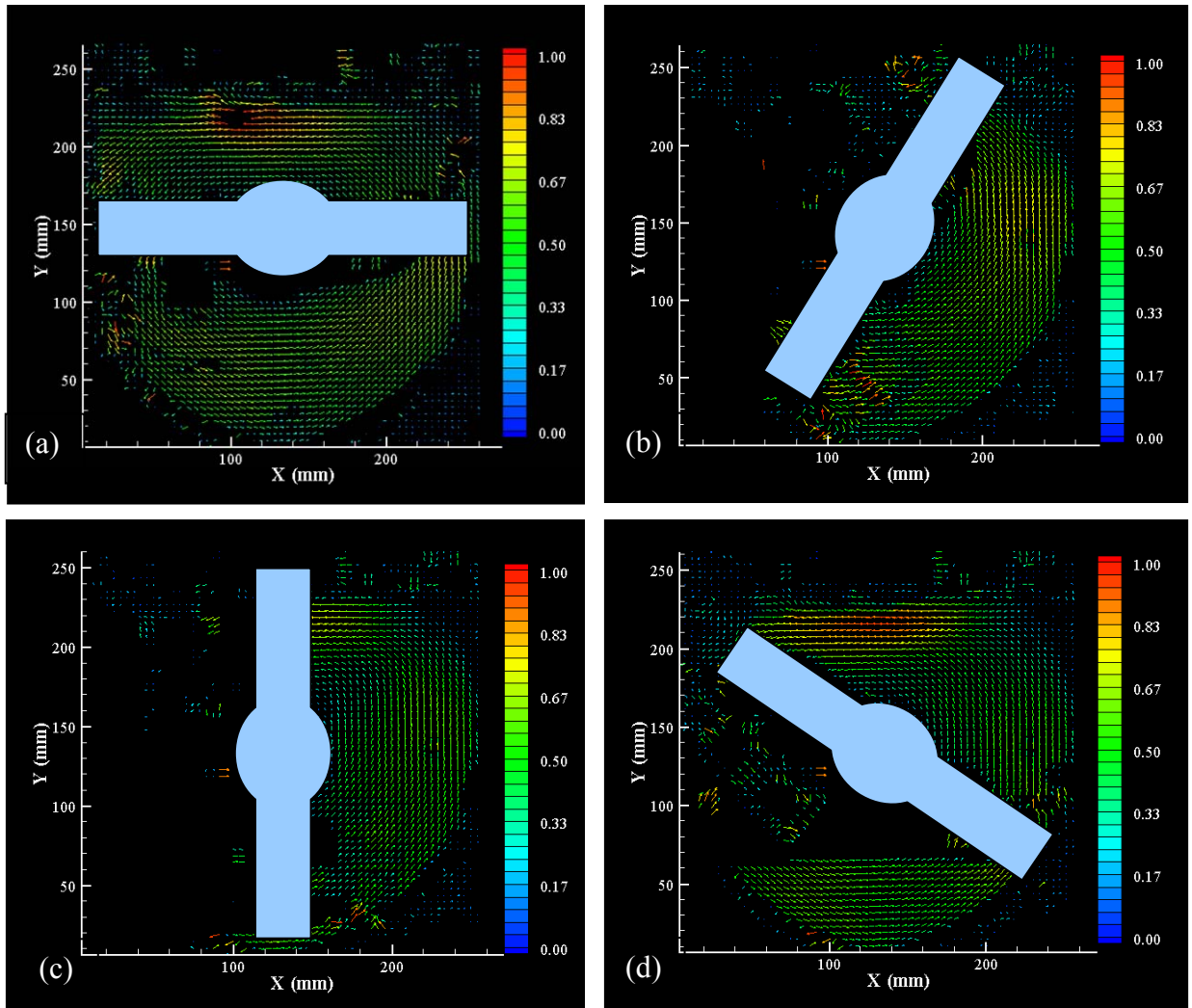


Figure 5-14. Normalised velocity for the experiment performed with an agitation speed of 11 rpm with water (a) impeller position 1 (b) impeller position 2 (c) impeller position 2 (d) impeller position 4. The blue shape in the middle represents the impeller.

Increasing the speed to 22 rpm gives a similar picture, although the overall velocity magnitudes have increased to $U^* \sim 0.6$ in the bulk. Velocity magnitudes in the maximum regions near free-surface are still of order $U^* \sim 0.8$. At position 4, a new local maximum is observed at the trailing edge of the impeller in the bottom corner of the vessel.

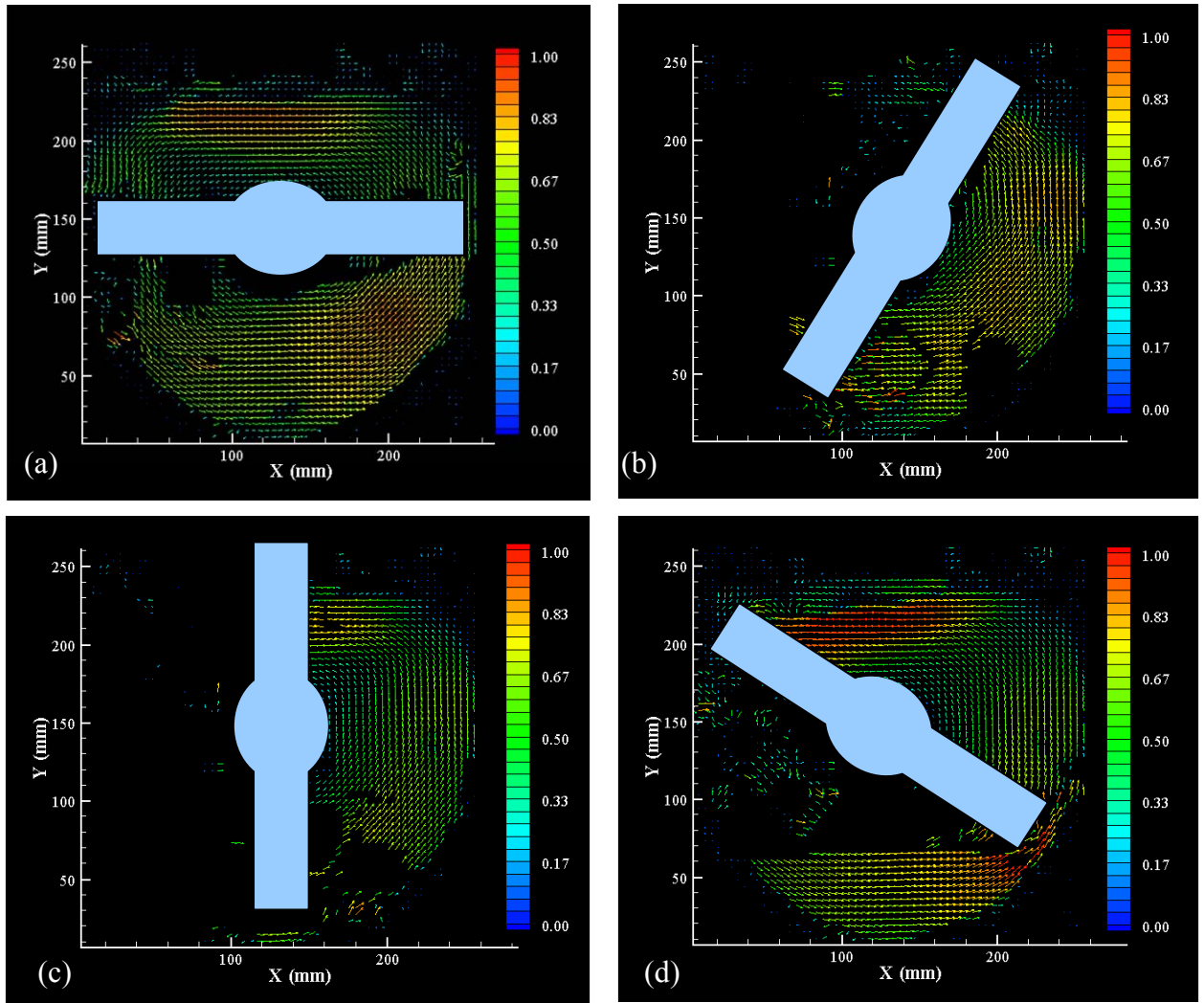


Figure 5-15. Normalised velocity for the experiment performed with an agitation speed of 22 rpm with water (a) impeller position 1 (b) impeller position 2 (c) impeller position 2 (d) impeller position 4. The blue shape in the middle represents the impeller.

The effect of the increased fluid viscosity on the fluid flow is shown using the 0.5% CMC solution in Figures 5-16 and 5-17 at 11 and 22 rpm respectively.

Figure 5-16 shows that for low agitation speed, increasing the speed does not modify the bulk value ($U^* \sim 0.5$). However, the magnitudes of the local maxima recorded at the free-surface are reduced ($U^* \sim 0.5-0.7$). Clearly, with more viscous fluids, less sloshing occurs at the free-surface.

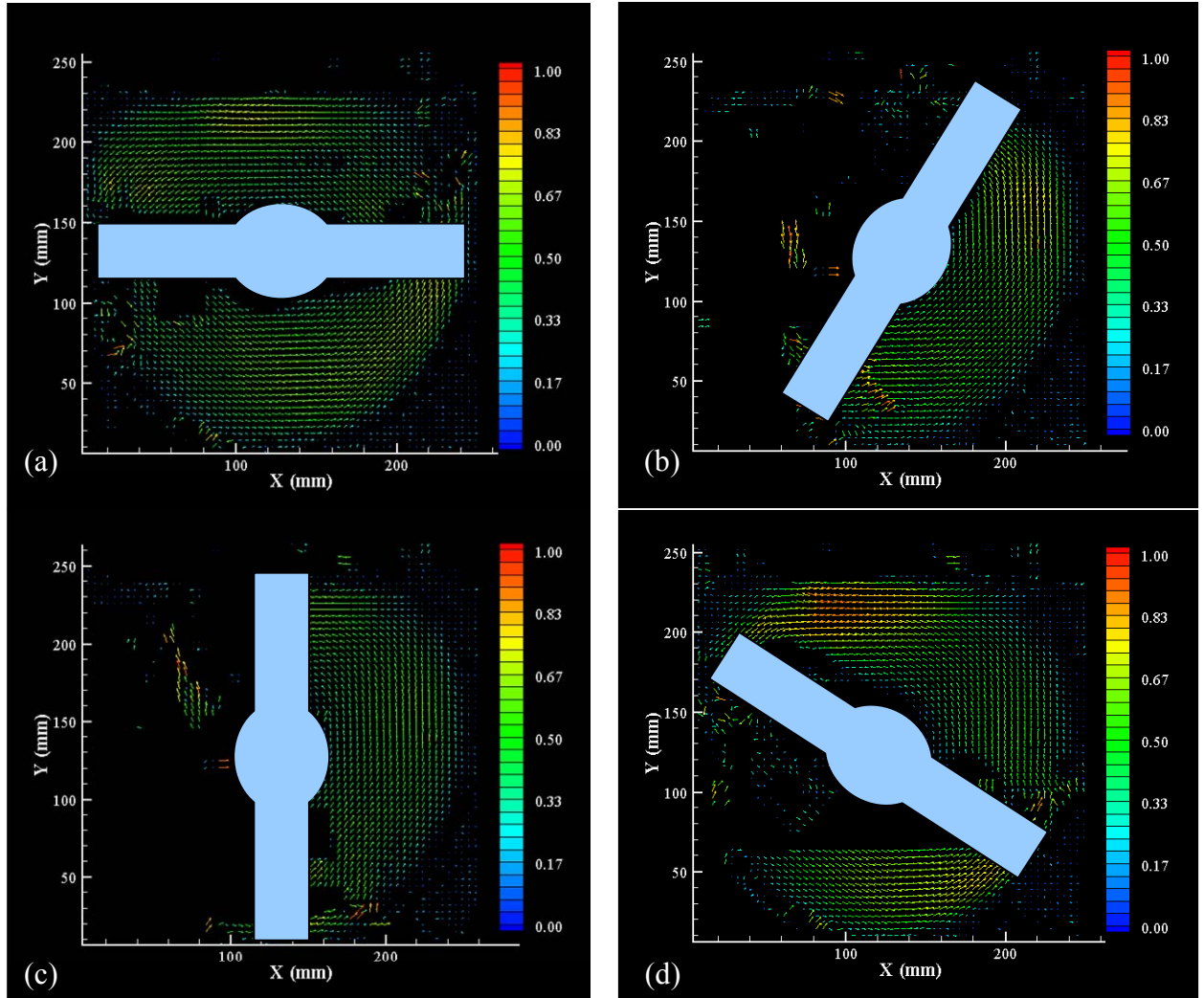


Figure 5-16. Normalised velocity for the experiment performed with an agitation speed of 11 rpm with 0.5% CMC (a) impeller position 1 (b) impeller position 2 (c) impeller position 3 (d) impeller position 4. The blue shape in the middle represents the impeller.

When the speed increases (Figure 5-17), the overall velocity magnitude increases in the bulk region ($U^* \sim 0.55$) and in the regions of local maxima ($U^* \sim 0.9$). The velocity fields recorded here are similar to those recorded for the experiments performed with water. High speed agitation causes more disturbances on the free-surface than low speed agitation, which explains the increase of the velocity magnitude in regions near the free-surface.

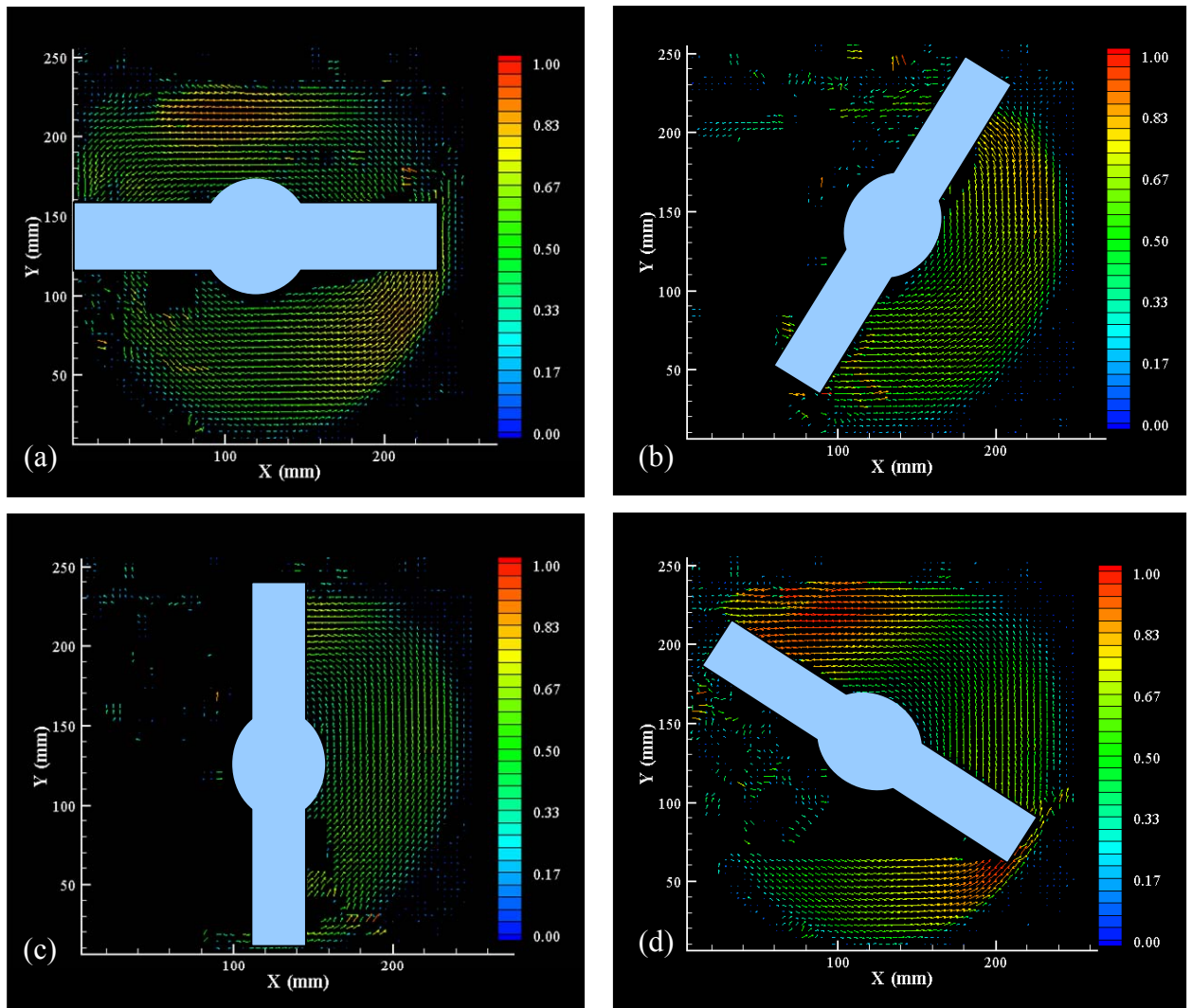


Figure 5-17. Normalised velocity for the experiment performed with an agitation speed of 22 rpm with 0.5% CMC (a) impeller position 1 (b) impeller position 2 (c) impeller position 3 (d) impeller position 4. The blue shape in the middle represents the impeller.

Overfilled experiments were performed at 22 rpm agitation speed and for 3 different fluids (water, 0.25% CMC solution and 0.5% CMC solution). Movies showing the agitation of a solution of CMC at 0.5% at an overfilled level can be seen in the CD included with this work at the back of the thesis (Mushroom_Overfilled vessel.wmv and Visualisation_overfilled vessel.wmv).

Figure 5-18 displays the normalised velocities recorded for the experiment performed with water at the 4 different impeller positions ((a), (b), (c) and (d)).

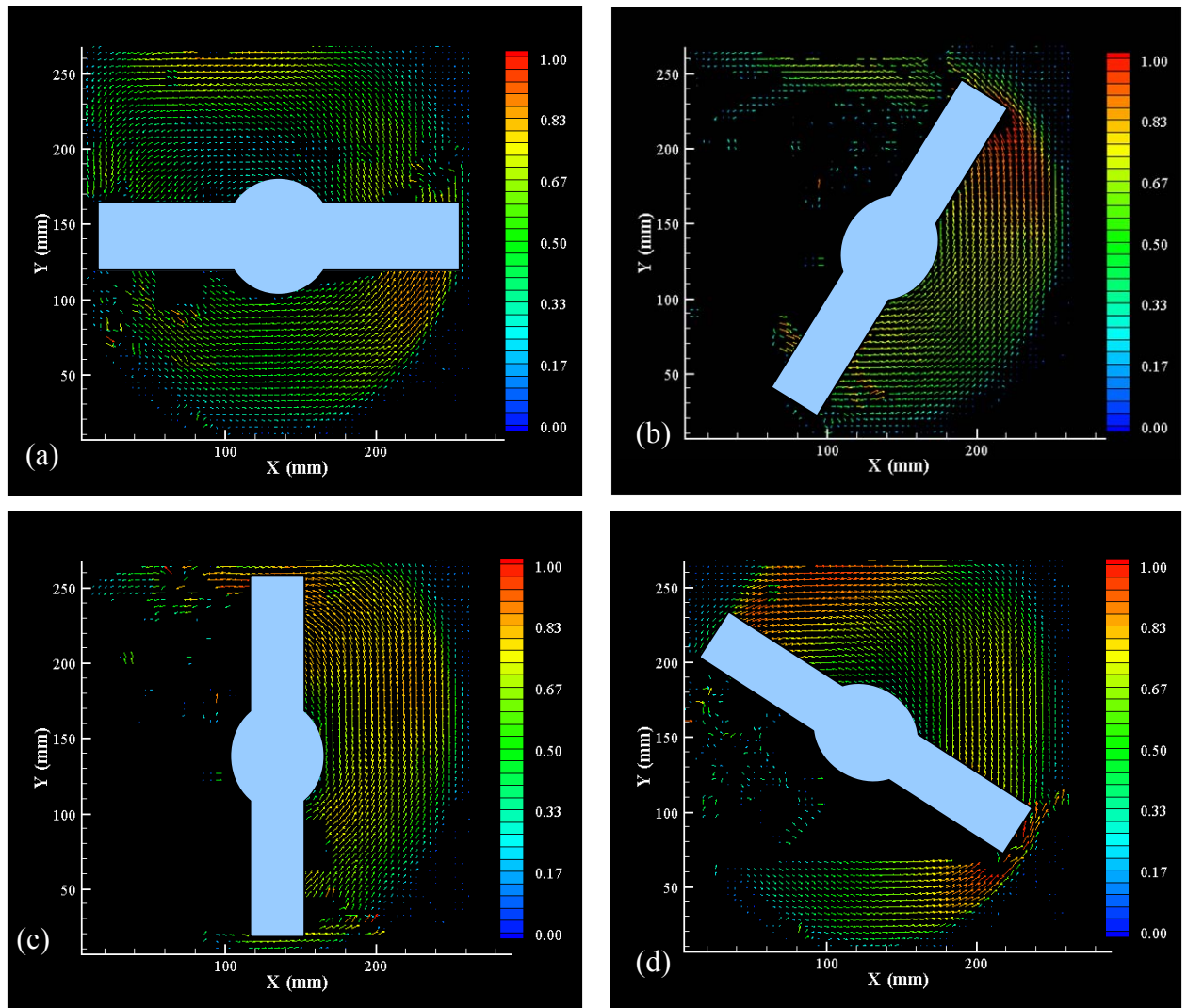


Figure 5-18. Normalised velocity for the overfilled experiment performed with an agitation speed of 22 rpm with water (a) impeller position 1 (b) impeller position 2 (c) impeller position 2 (d) impeller position 4. The blue shape in the middle represents the impeller.

Increasing the filling level (overfilling) causes changes in the fluid flow pattern. In position 1, the velocity magnitude of the bulk is of order $U^* \sim 0.5$ (same as with normal filling level) and local maxima at the free-surface is low ($U^* \sim 0.7$). When the vessel is overfilled, the tip of the impeller in vertical position is approximately at the same level as the surface of the fluid, causing fewer disturbances on the free-surface. In addition, a local minimum in velocity (which was not observed for the experiments performed at the normal filling level) was identified ($U^* \sim 0.15$) just above the impeller axis. At position 2 a new local maximum

($U^* \sim 0.9$) is observed at the trailing edge of the impeller in the top corner of the vessel. At positions 3 and 4, the velocities recorded in the bulk region are high ($U^* \sim 0.7$) when compared with the experiments performed at the normal filling level. Regions of local maxima are recorded at the free-surface.

5.4.2. Velocity profiles

To examine the flow in more detail, the normalised velocities profiles were measured along the X and Y axes. The three different locations (A, B, C) of the calculated velocity profiles are shown in Figure 5-19 (a). Figure 5-19 (b) gives the respective impeller positions during the measurements.

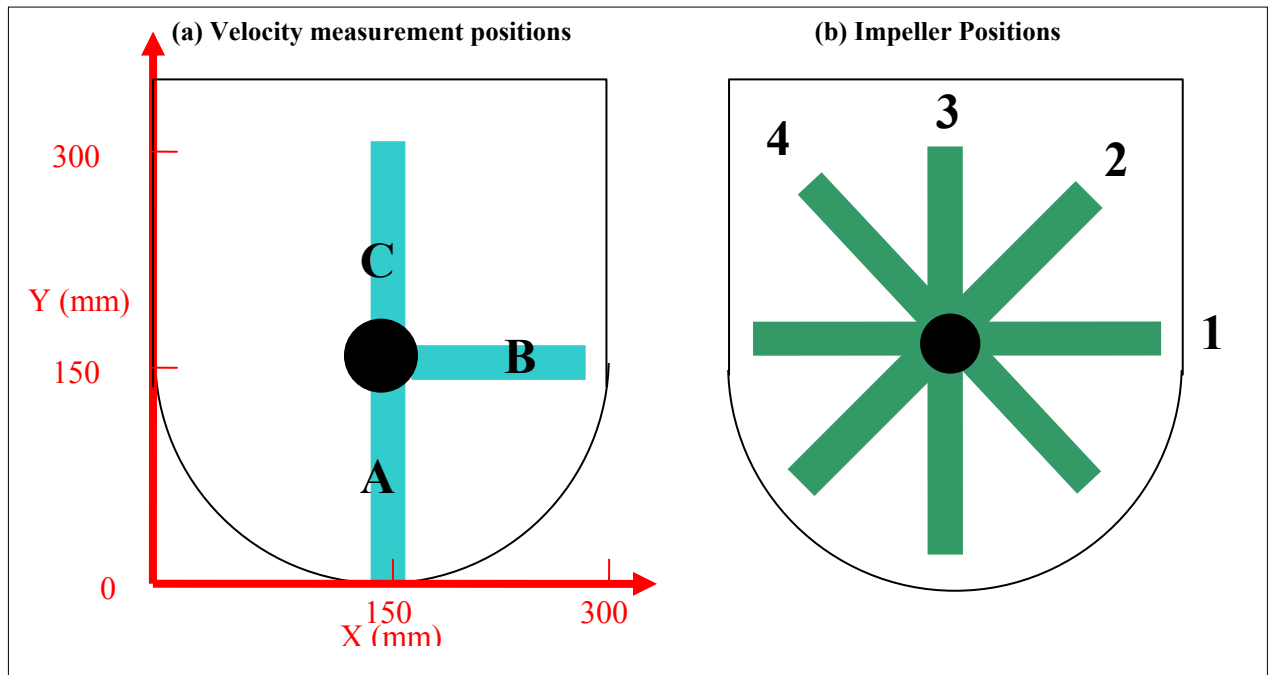


Figure 5-19. Measurement positions: (a) Velocity measurement positions (b) Impeller position

Figure 5-20 and Figure 5-22 show the normalised velocity magnitudes along the Y axis obtained for positions A and C with the impeller in various locations (see Figure 5-19b). On

these graphs, the bottom of the vessel is at $Y = 0$ mm and the centre of the vessel is at $Y = 150$ mm.

Figure 5-21 shows the normalised velocity magnitudes looking along the X axis for position B. On this graph, the left side of the vessel is at $X = 0$ mm and the centre of the vessel is at $X = 150$ mm. Each Figure sub-plot represents a different experiment: (a) is the experiment performed at low agitation speed (11 rpm), (b) is performed at medium agitation speed (22 rpm), (c) is performed at high agitation speed (33 rpm) and (d) is performed with an overfilled vessel for medium agitation speed (22 rpm). Each graph plots the data from three different fluids.

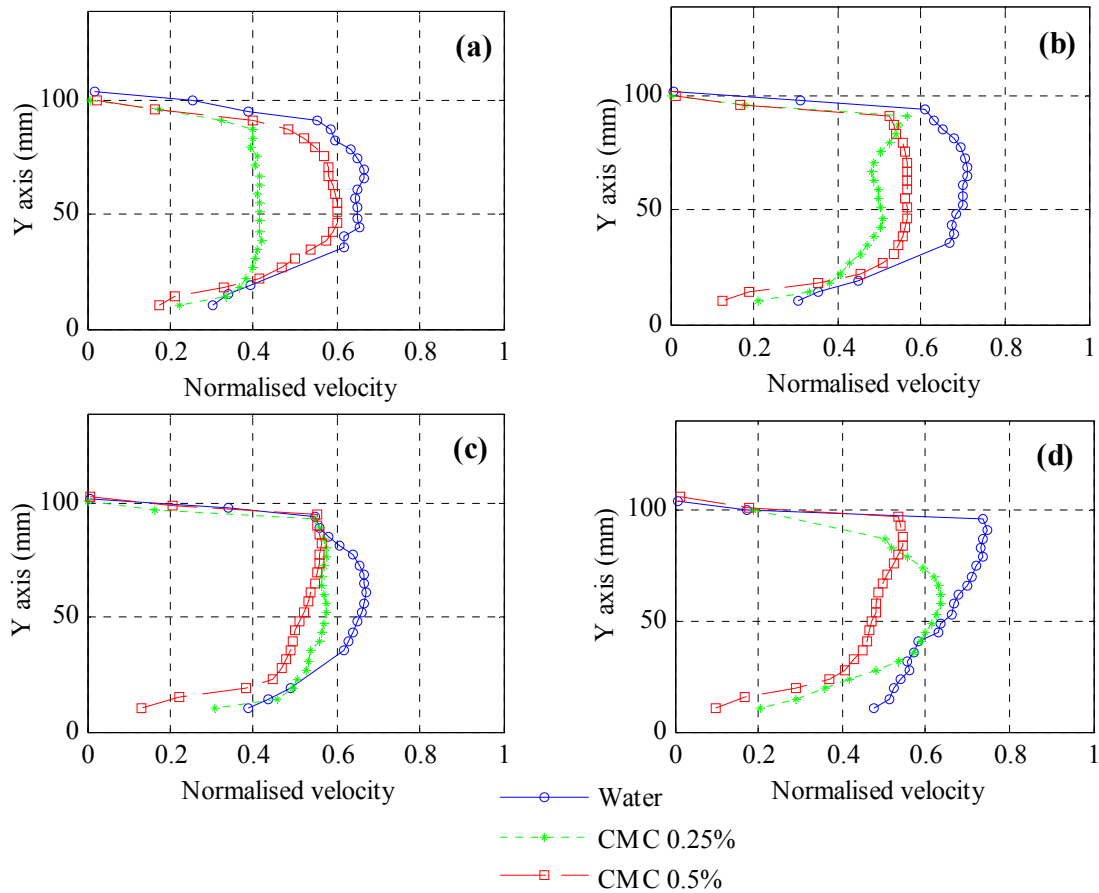


Figure 5-20. Impeller position 1, velocity measurement position (A): (a) Low speed (b) Medium speed (c) High speed (d) Overfilled medium speed

Figure 5-20(a) shows that the general shape of the velocity profile between the centre and the bottom of the vessel assumes a bullet shape. Surprisingly, the lowest and highest viscosities used (water and 0.5%CMC) give similar magnitudes, whilst the velocity magnitude for the 0.25% CMC is much smaller. As the impeller speed is increased, the profiles move closer together and the normalised magnitude increases slightly. Hence, the flow is not generally self similar as would be expected for turbulent flows. The shape of the profile for the overfilled case changes and becomes much sharper close to the impeller shaft. This may be due to the formation of the local minimum above the shaft observed in Figure 5-18 (a), which suggests the centre of the rotation of the fluid has shifted to above the impeller axis. This change in flow pattern may be expected to alter the thermal processing of the fluid, which confirms what was observed by the TTI study in §4.3.2 showing that the thermal treatment received by the TTIs was different when the vessel was overfilled.

A similar bullet shape velocity profile can be observed between the centre and the side wall of the vessel in Figure 5-21(a). The velocity profiles have the same magnitude and are much more self-similar. The magnitude of the normalised velocity increases with the increase of the agitation speed. In addition, the overfilled experiment (d) presents the highest magnitude ($U^* \sim 0.61-0.78$).

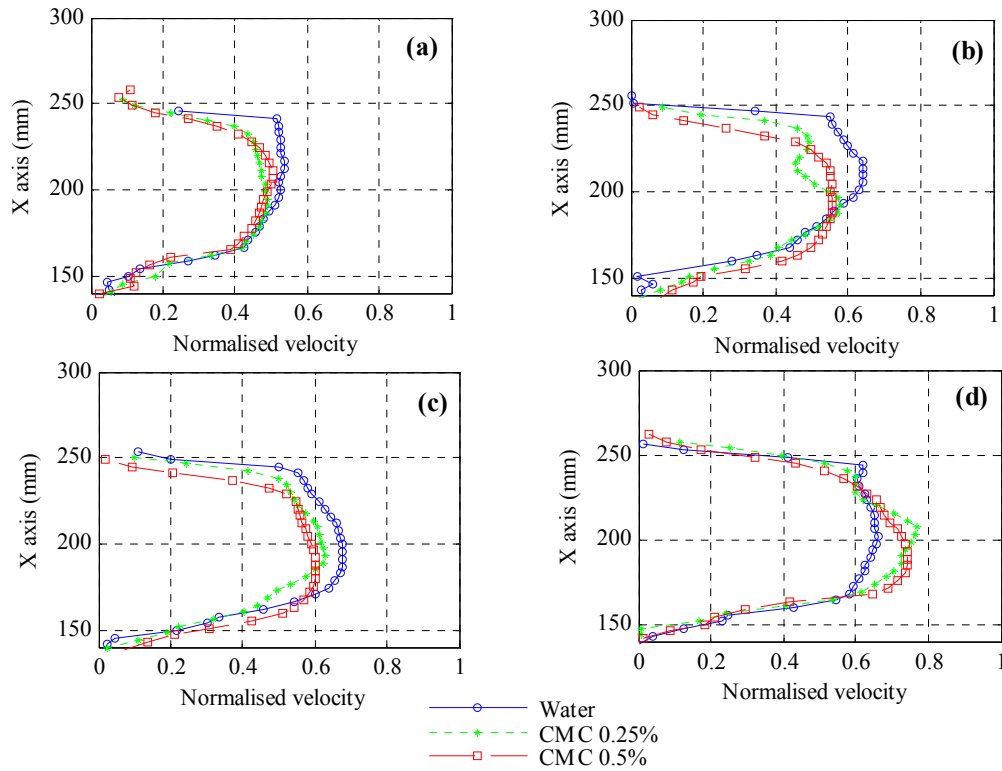


Figure 5-21. Impeller position 3, velocity measurement position (B): (a) Low speed (b) Medium speed (c) High speed (d) Overfilled medium speed

Figure 5-22 shows the velocity profiles obtained between the centre and the free surface. The general shape of the velocity profile has a peaked shape. At the free surface, velocities have no reason to go back to zero since the surface is unconfined. Again, it can be observed that the profiles are self similar and a change in agitation speed does not modify the magnitude of the velocity profiles. From bottom to top, the profiles are close to being linear for the experiment performed at the normal filling level. In the case of the overfilled experiment, some non-linearity at Y (150-200) can be observed.

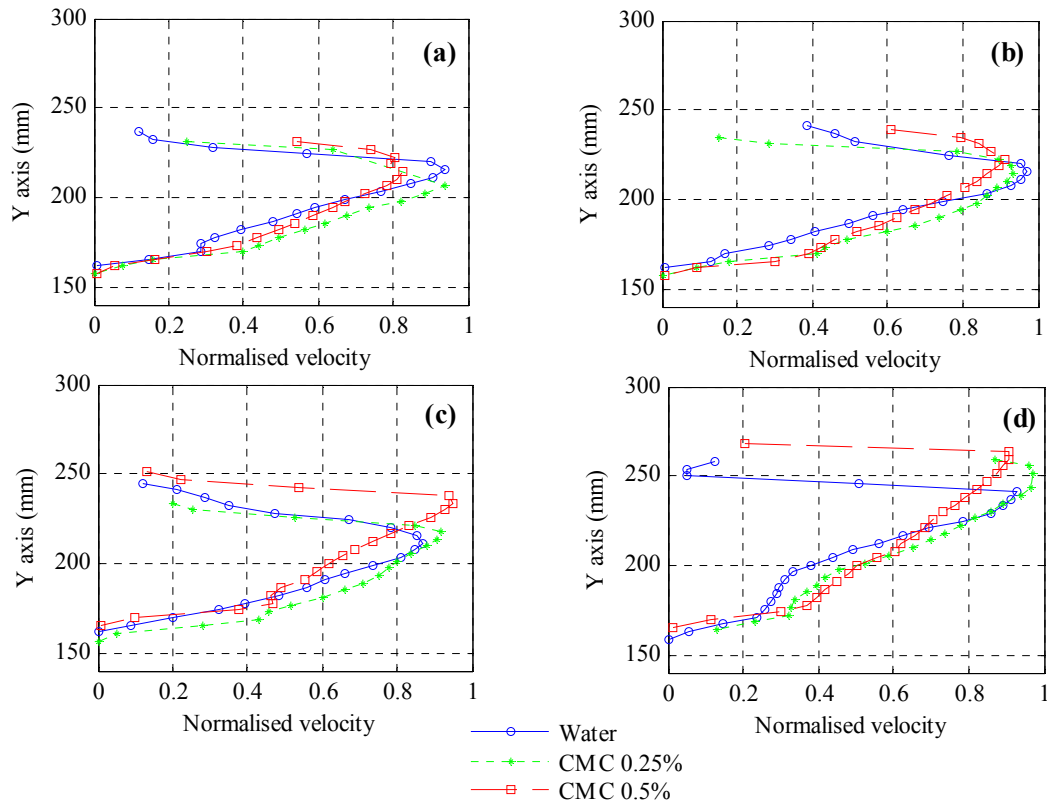


Figure 5-22. Impeller position 4, velocity measure position (C); Water —○—, CMC 0.25% —+—, CMC 0.5% —□— ; (a) Low speed (b) Medium speed (c) High speed (d) Overfilled medium speed

5.5. Conclusions

The flow inside the model vessel was investigated using the PIV technique. This study showed that the flow is laminar/transitional through the bulk of the vessel. The only regions where significant flow instabilities were generated are located at the free surface and at the trailing edge of the impeller. Mixing throughout the bulk can therefore be expected to occur by laminar mechanisms with some mixing by eddy diffusion present at the free surface.

The velocity profiles in the vessel are generally unaffected by the viscosity and the agitation speed. However, notable differences are present for the overfilling case. Indeed, the profile shape changes at location (A) and (C), this is indicative of a potentially subtle flow pattern change. The location of a local minimum above the impeller axis on overfilling would seem

to indicate a shift in the centre of rotation of the fluid – leading to a change in flow pattern. In §4.3.2, it was demonstrated that this change in flow pattern had some influence on the thermal processing within the vessel.

Chapter 6

Investigations of the flow behaviour of TTIs and the fluid in a model ‘Vesuvio’ vessel using Positron Emission Particle Tracking (PEPT)

6.1. Introduction

In this Chapter, PEPT is used to determine the velocities of both the fluid (using a free tracer particle) and the TTIs (using a tracer encapsulated within a TTI tube) using the scaled down ‘Vesuvio’ vessel described in §5.2. As shown in Chapter 5, the motion of the fluid is predominantly laminar; hence the mechanism of mixing is expected to be mostly due to shear and elongation with some mixing due to eddy diffusion caused by local instabilities near the free-surface. Therefore, the quality of mixing can be assessed by examination of the occupancy and velocity distribution of the tracer within the entire vessel, clearly if there is a difference between the behaviour of the TTI tracer and the free tracer, this could lead to a discrepancy between the thermal P values recorded by the TTI compared with thermal processing delivered to the fluid. The experiments were designed to focus on the applicability of the TTIs for low and high viscosity fluids over a range of impeller speeds which give similar power per unit mass to the fluid as on the industrial scale (§4.3). The effect of overfilling of the vessel, which can occur within industry, is also considered.

6.2. Model vessel and fluids used for the PEPT experiments

The fluids used for the experiments were water, aqueous solutions of starch at different concentrations and a CMC solution. The starch solutions used for these experiments have been previously described in §4.2.1. Concentrations of 4% and 5% by mass were used. The

CMC solution was used at a concentration of 0.5% by mass. The properties of the fluid were determined in §5.2.1.

The scaled down version of the ‘Vesuvio’ vessel was the same as described in §5.2 and was designed to fit within the cavity of the PEPT camera which was of limited size. The scaling down method at constant power per unit mass is the same as for the PIV experiments.

The Reynolds numbers were calculated (the same way as it was described in §4.2.2.) for 3 different agitation speeds (11 rpm, 22 rpm and 33 rpm) for the model vessel and given in Table 6-1 below.

Table 6-1. Reynolds numbers for the model vessel

		11 rpm	22 rpm	33 rpm
Reynolds number	Water	1220	2450	3680
	Starch 4%	210	550	945
	Starch 5%	30	65	95
	CMC 0.5%	180	495	900

Table 6-1 shows that the fluid flow can be considered as transitional for all experiments. The properties of the fluid is as described in §5.2.3.

6.3. Positron Emission Particle Tracking (PEPT)

6.3.1. Positron camera

The positron camera used for this study was the Forte camera manufactured by ADAC laboratories (California), purchased by the University of Birmingham in June 1999. Two gamma camera heads are fixed face to face on a motorised gantry enabling the size of the gap between the detectors to be altered and to rotate the cameras on a horizontal axis. Each head

(camera) consist of a 16 mm thick single sodium iodide crystal covering a surface area of $590 \times 470 \text{ mm}^2$ which is optically connected to an array of 55 photomultipliers. The size of the camera field of view is $80 \times 50 \times 40 \text{ cm}^3$. The location of a tracer with a speed of 1 ms^{-1} can be detected within 0.5 mm 250 times per second while a slow moving tracer can be detected within 100 μm 50 times per second.

The PEPT algorithm determines the ‘minimum distant point’ by identifying the closest point where all the trajectories of the event emitted by a single radioactive tracer pass. The events detected far from this point are removed. From the remaining points, the ‘minimum distant point’ is once more calculated. This is done until a fraction, f , of the events are left which depends on the material geometry and scattering that it produces. Therefore, f is a set parameter, and from this value, the accuracy of the location can be calculated. This accuracy depends on the spatial resolution of the camera and the size of the sample of events measured at one location.

6.3.2. Radioactive tracer preparation

The radioactive tracers were made from the radioactive water produced by the cyclotron as described in § 2.2.3.2. Purified water was bombarded with a 33MeV ^3He beam inside the cyclotron for 30 min at a current of 10 μA . ^{18}F produced was present in ionic state and therefore it was possible to adsorb it onto a particle made from strong-base anion exchange resin. Once the tracer was produced, it was coated with a layer of lacquer and paint to avoid the leaching of the radioactivity into the water in the tank and to control the density (the tracer has to be isokinetic with the fluid). The tracer could not be used immediately after painting to allow the paint to dry and the total production time of the tracer is \sim two hours from the

production of the radioactive water. Considering that the half time of the ^{18}F is relatively short, the time taken to produce the tracer is critical since the number of experiments that can be performed depends on the level of radioactivity. The final tracer composition can be seen in Figure 6-1. The tracer used was of 600 μm diameter with a density of 1100 - 1200 kg m^{-3} .

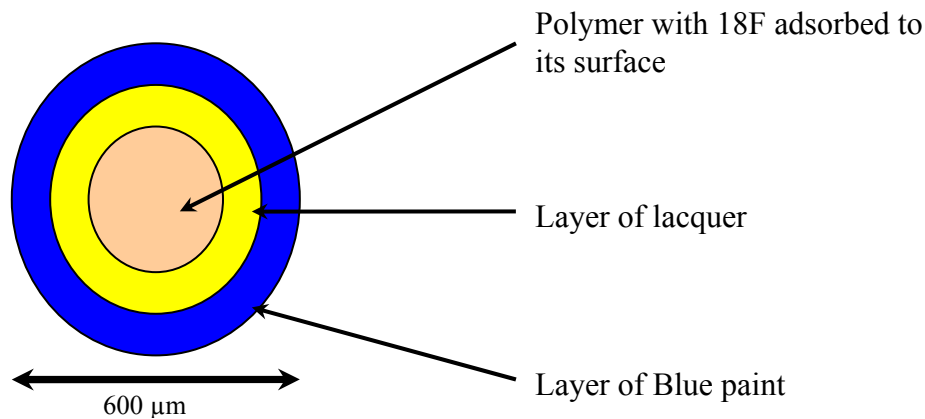


Figure 6-1. Radioactive tracer composition

The tracers were used in two different ways:

- The tracer was added to the fluid and used to track the fluid motion. This tracer will be called free tracer hereafter.
- The tracer was fixed onto a TTI (Figure 6-2) and this was added to the fluid. The TTI motion was therefore recorded in this experiment. This tracer will be called TTI tracer hereafter.

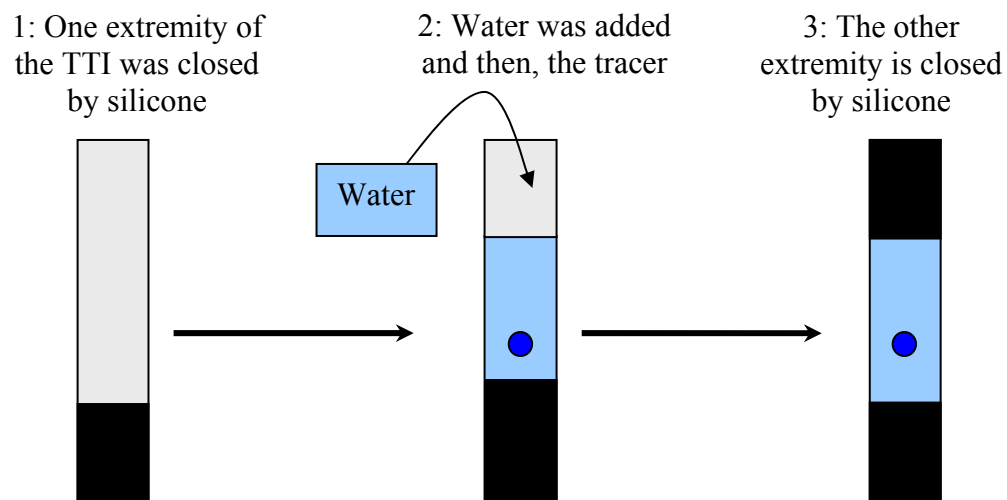


Figure 6-2. Addition of the radioactive tracer to the TTI

6.3.3. Experimental design

The model vessel was placed between the detectors of the PEPT camera leaving a gap of 0.55 m. The set up is shown in Figure 6-3 below, together with the Cartesian axial coordinates used (b).

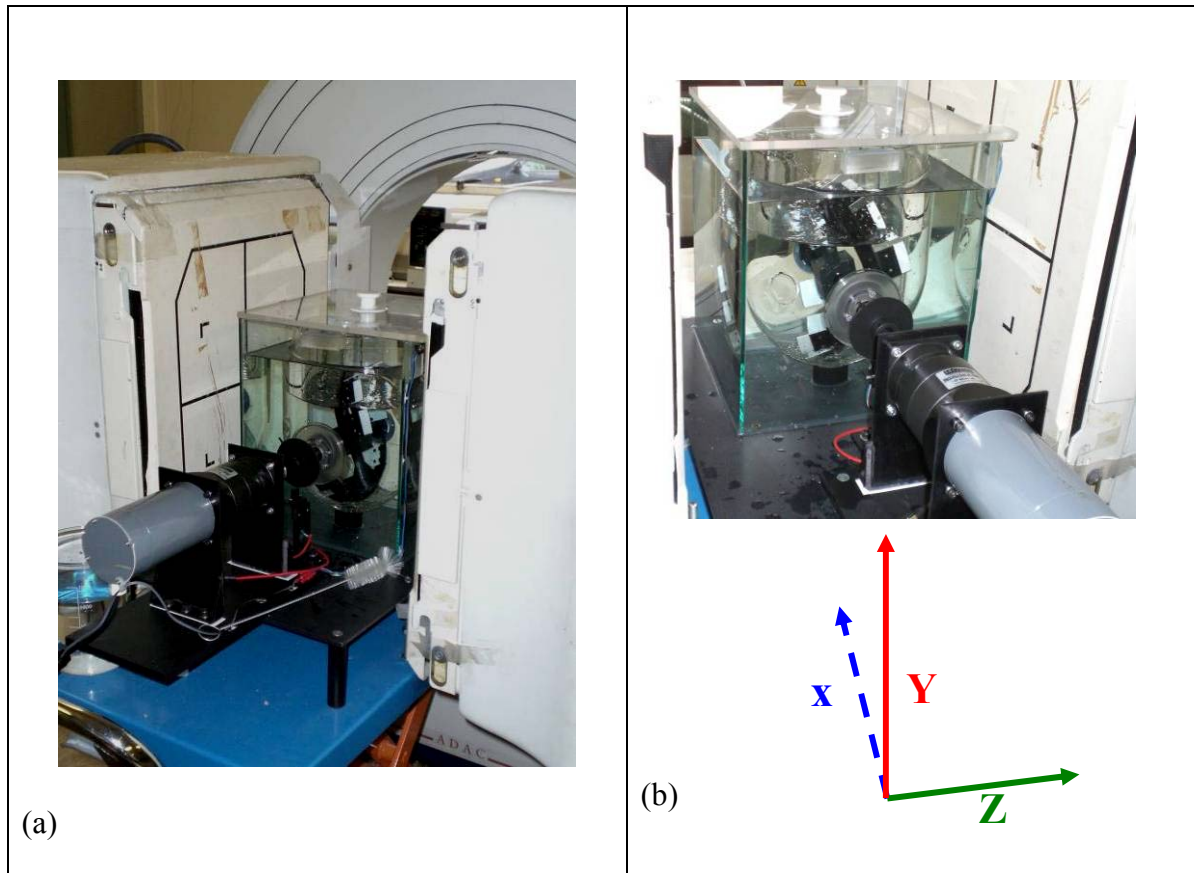


Figure 6-3. The reduced scale vessel used with the PEPT camera

A total of 18 experiments were performed on the model vessel. Factor such as fluid viscosity, agitation speed, filling level and tracer type on the mixing efficiency were studied. As in Chapter 5, the recommended filling level of the model vessel was 7.5 litres and the overfilling level was 9 litres. The same three different agitation speeds were used: 11 rpm, 22 rpm and 33 rpm (which were calculated from scaling down at constant power per unit mass). The tracers used were: the free tracer (which is expected to be isokinetic with the fluid) and the TTI tracer. Each experiment was performed for 30 minutes in order to ensure sufficient sampling time. A summary of the experiments that were carried out is given in Table 6-2 below.

Table 6-2. Summary of the experiments performed with the PEPT camera

#	Fluid used	Agitation speed	Filling level	Tracer used
1	Water	22 rpm	Recommended level	Free tracer
2	Water	22 rpm	Recommended level	TTI tracer
3	Water	22 rpm	Overfilled level	Free tracer
4	Water	22 rpm	Overfilled level	TTI tracer
5	CMC 0.5%	22 rpm	Recommended level	Free tracer
6	CMC 0.5%	22 rpm	Recommended level	TTI tracer
7	Starch Medium viscosity (4%)	22 rpm	Recommended level	Free tracer
8	Starch Medium viscosity (4%)	22 rpm	Recommended level	TTI tracer
9	Starch Medium viscosity (4%)	22 rpm	Overfilled level	Free tracer
10	Starch Medium viscosity (4%)	22 rpm	Overfilled level	TTI tracer
11	Starch Medium viscosity (4%)	33 rpm	Recommended level	Free tracer
12	Starch Medium viscosity (4%)	33 rpm	Recommended level	TTI tracer
13	Starch High viscosity (5%)	22 rpm	Recommended level	Free tracer
14	Starch High viscosity (5%)	22 rpm	Recommended level	TTI tracer
15	Starch High viscosity (5%)	22 rpm	Overfilled level	Free tracer
16	Starch High viscosity (5%)	22 rpm	Overfilled level	TTI tracer
17	Starch High viscosity (5%)	11 rpm	Recommended level	Free tracer
18	Starch High viscosity (5%)	11 rpm	Recommended level	TTI tracer

From the PEPT experiments, 3-D data of the position of the tracer versus time were obtained. The data obtained from the PEPT experiments were further processed using Matlab 7 and Tecplot 9. These two software packages were described previously. The data were processed in two different ways:

(1) All the 3-D data obtained from the whole vessel were processed and projected into a 2-D plane. Various parameters were calculated with these software packages, including:

- Occupancy, which is the percentage of time in which an area within the vessel is occupied by the tracer. Occupancy was determined on the Z and Y axis in 2-D (axes definitions given in Figure 6-3b).

- Normalised velocity was determined on the Z and Y axis in 2-D.
- The path that the tracer takes inside the vessel in 2-D was determined on the X and Y axis.

(2) The second way was done by processing the data by 'zones'. The 3-D data obtained for vessel were divided into three separate parts along the X axis. The data from each part were processed separately. By dividing the data into 'zones', it was easier to understand the behaviour of the fluid in 3-D. For each zone, the velocity on the X axis was calculated. The calculation of this parameter allowed understanding of the behaviour of the fluid on the X axis. Ultimately, this gave a more clear idea of the fluid flow pattern in 3-D. The zones are given in Figure 6-4.

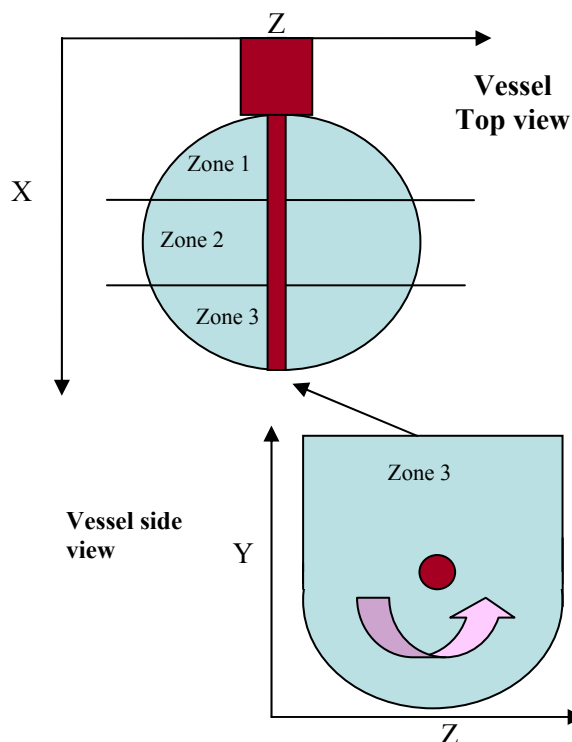


Figure 6-4. The model vessel zones

The Matlab codes used for the calculation of these parameters can be seen in Appendix C.

6.4. Results

6.4.1. Error in PEPT measurements

Before carrying out the data analysis, the error related to the location of the tracer was investigated. The location of the tracer is determined by detection of the gamma ray events emitted by the radioactive tracer as described in § 2.2.3.2. The PEPT algorithm then determines the location of the tracer by identifying the closest point to all the trajectories of the events as illustrated in Figure 6-5 below.

The error in PEPT measurement varies according to the fluid, the material of the equipment and the speed and radioactivity of the tracer. This error in determining the location of the tracer can be calculated from equation 6.1.

$$\text{Tracer location error} = \frac{\sigma_d}{\sqrt{n}} \quad (6.1)$$

Where σ_d is the standard deviation of the perpendicular distances (d in Figure 6-5) of the location from all trajectories and n is the number of events. This error is determined for one standard deviation, therefore the results are confidence at 66%. In order to increase this confidence to 95%, the error should be multiplied by 1.96 in order to have 2 standard deviations.

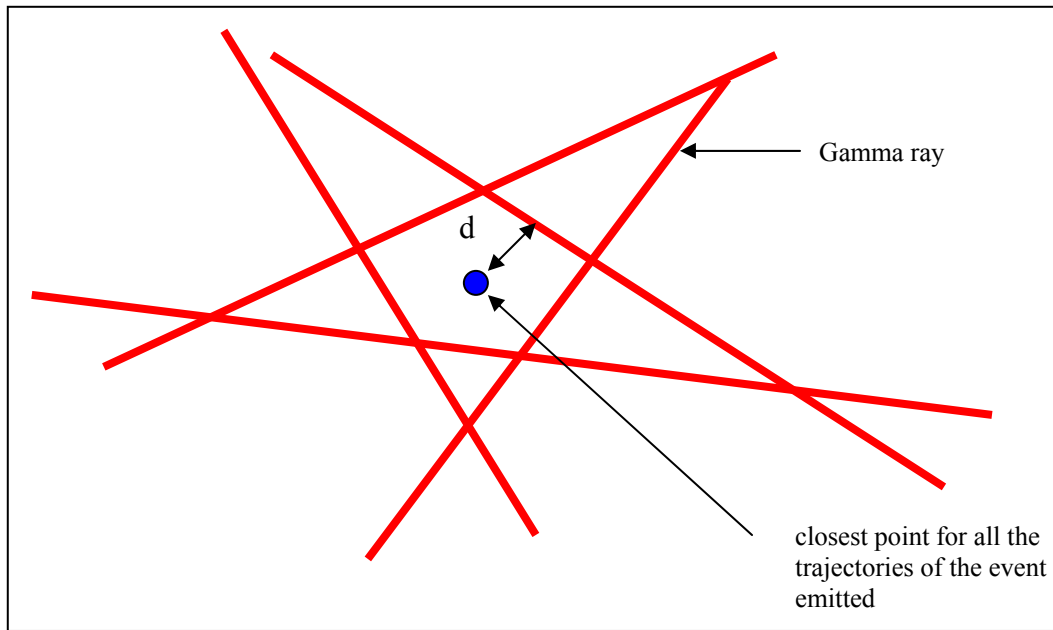


Figure 6-5. Identification of the tracer location

Therefore, the location of the tracer can be determined within a sphere of radius: $1.96\sigma/\sqrt{n}$.

For example, for an agitation speed of 0.28 ms^{-1} , the location of the tracer is within a sphere of diameter 3.4 mm.

6.4.2. Comparison between PIV and PEPT

Chapter 5 described the use of the PIV technique to investigate the fluid flow. This section compares the results obtained from the investigations carried out with both techniques. However, it should be noted the PIV technique is impeller resolved and the PEPT technique is not. This will bring a bias during the comparison of the results.

The comparison of the two techniques was performed on the normalised velocity profile recorded along the Z and Y axis (Figure 6-6) of the vessel. The parameters used during the

experiments with PIV had to be similar to those used for PEPT in order to be able to do this comparison.

Only three experiments were comparable:

- Experiment performed with water (22 rpm, normal filling level)
- Overfilled experiment performed with water (22 rpm)
- Experiment performed with a solution of 0.5% CMC (22 rpm, normal filling level)

For the experiments performed with PEPT, since it is a 3-D measurement technique, the normalised velocities were taken from a 2-D section in the centre of the vessel (see Figure 6-6 (a)).

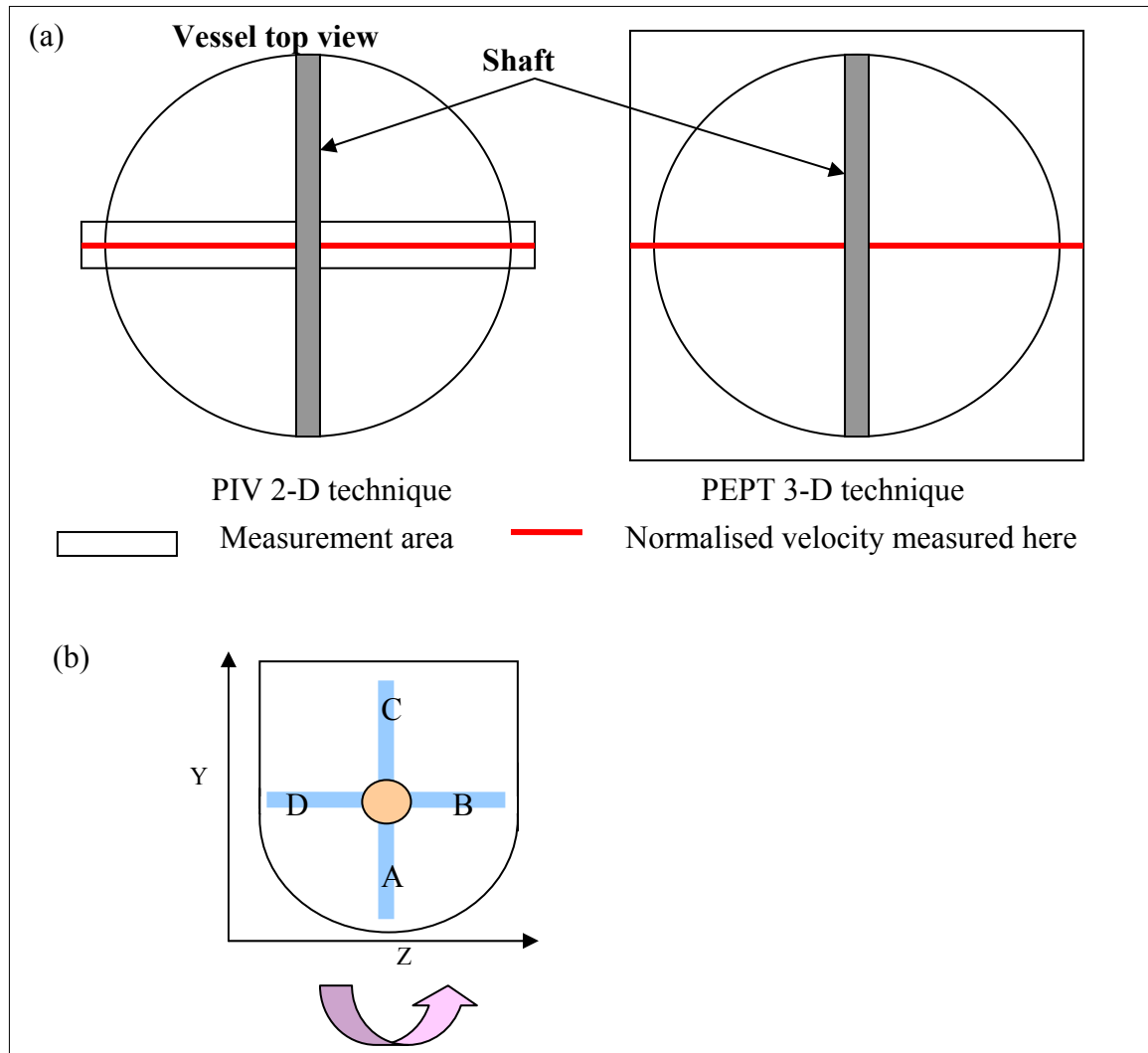


Figure 6-6. (a) Area of measurement for PIV and PEPT (b) Velocity measurement position

Figures 6-7 to 6-9 plot the velocity profiles of the three experiments described previously for measurements in positions A, B and C (Figure 6-6 (b)). For Positions A and C, the normalised velocity magnitudes are plotted along the Y axis and for Position B, the normalised velocity magnitudes are plotted along the Z axis. Figure 6-7(a) shows that the velocity profile obtained from the PEPT between the bottom and the centre of the vessel is a bullet shape, as observed by using the PIV. Figure 6-7 (b) and (c) also shows that the two techniques recorded similar velocity profiles. The velocity profile recorded by PIV and PEPT between the centre and the free surface is peak shaped. Figure 6-8 shows the experiments performed using water with an overfilled vessel and again similar profiles are recorded by

both techniques. In addition, the non linearity of the velocity profiles observed with PIV in position C is shorter and of higher magnitude for the PEPT data.

Figure 6.9 shows the agreement between the PIV and PEPT velocity profile graphs for the experiments performed with 0.5% CMC. Therefore, in general, there is good agreement between the PIV and PEPT data, the small deviations are likely due to fact that the PIV data are resolved by impeller position, whilst the PEPT data are not.

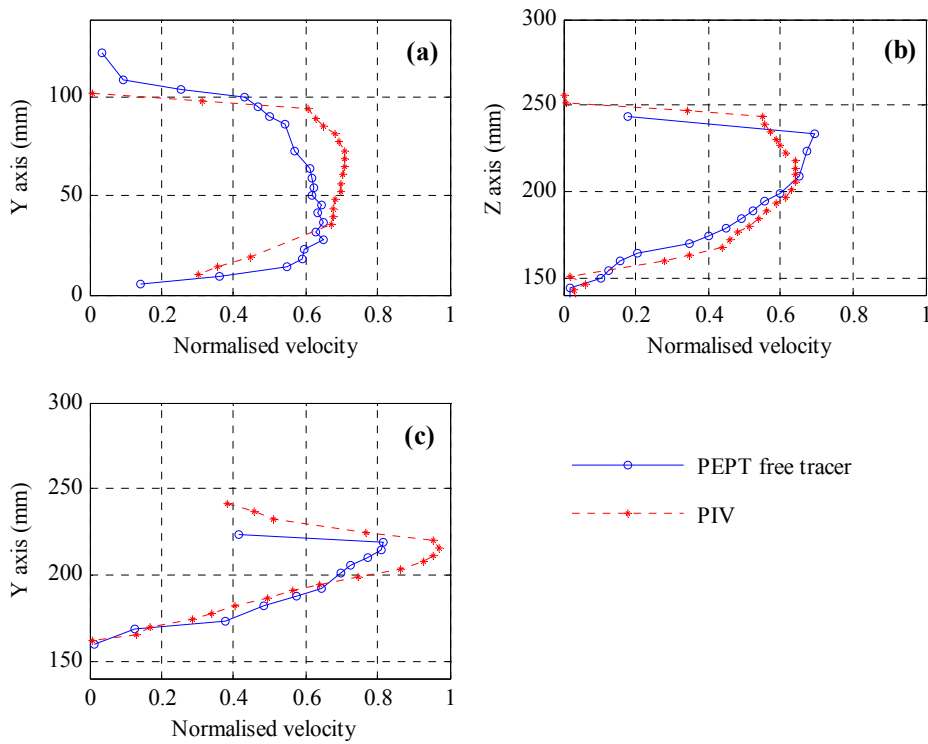


Figure 6-7. Experiment performed with water (normal filling level) PEPT and PIV velocity profile (a) Position A, (b) Position B and (c) Position C

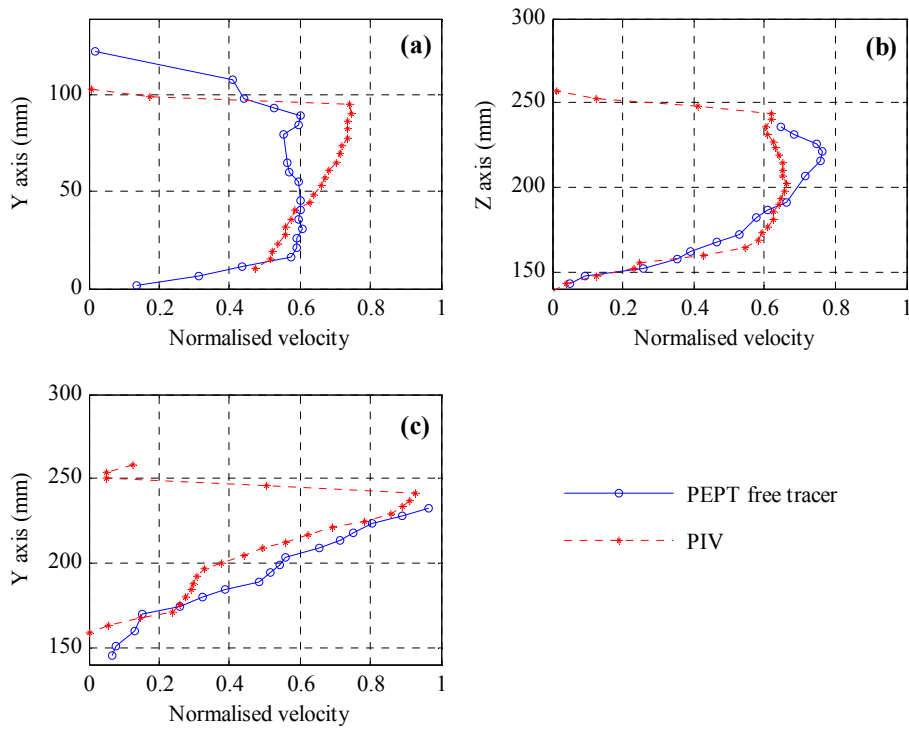


Figure 6-8. Experiment performed with water (overfilled level) PEPT and PIV velocity profile (a) Position A, (b) Position B and (c) Position C

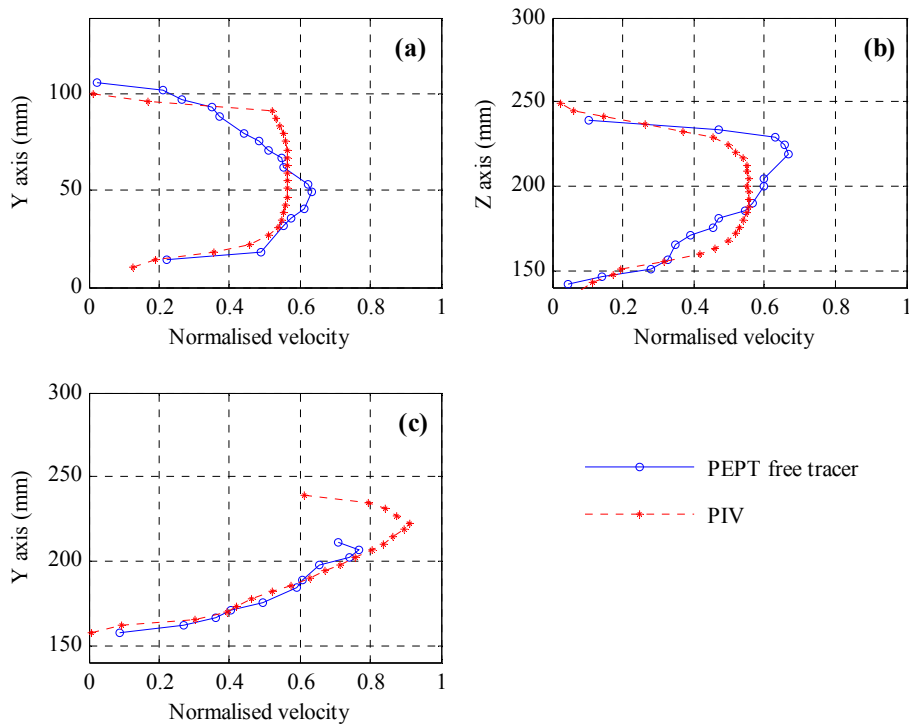


Figure 6-9. Experiment performed with a solution of 0.5% CMC (normal filling level), PEPT and PIV velocity profile (a) Position A, (b) Position B and (c) Position C

Overall, it can be noted that the highest velocities are recorded at measurement position C which corresponds to the position located just below the surface of the vessel. This is to be expected since some turbulence is generated at the surface of the vessel and this results in the normalised velocities in this area to be higher than other areas in the vessel.

6.4.3. Comparison of flow behaviour of free and TTI tracers

The focus of this section is to evaluate the suitability of the TTI to determine thermal treatment efficiency within the vessel since they are used as a thermal process validation tool in a wide range of equipment. When TTIs are used in a large agitated vessel such as the one used by Giusti Ltd, it is difficult to know if the thermal treatment received by the TTIs is representative of the thermal treatment that the food product receives and whether the TTIs are isokinetic with the fluid. In addition, TTIs should not interfere with the flow path of the fluid inside the vessel.

In Figure 6-10, the occupancy, the normalised velocity and the tracer path plots for the experiment performed with water at 22 rpm are shown. For each parameter, (occupancy, normalised velocity and tracer path), the data obtained from the free tracer and the TTI are plotted next to each other in order to facilitate the comparison.

Figure 6-10 (a) shows the occupancy plot of the free tracer. This plot indicates that the tracer passes through all locations and zones inside the vessel. In addition it should be noticed that the tracer stays a significant amount of time at the surface of the vessel to the left and also below the impeller shaft. It is probable that the tracer got stuck at these locations for a period of time. Figure 6-10 (b) shows the occupancy plot for the TTI tracer and the results are very different. This plot indicates that the tracer does not pass through all locations inside the

vessel. The tracer seems to move in circles around the impeller and does not pass through the surface of the fluid.

Figure 6-10 plot (c) shows the normalised velocity plot for the free tracer. The graph shows that generally the velocities within the vessel vary between 20% and 50% of U_{tip} . The highest speeds are recorded at the free-surface of the vessel ($U^* \sim 0.84$). The fact that the velocities recorded at the surface of the vessel to the left and also below the impeller shaft are low confirms that the tracer got stuck at these locations for a period of time. Figure 6-10 plot (d) shows the normalised velocity plot for the TTI tracer which shows the velocity of the TTI also varied between 20% and 50% of U_{tip} . The highest speeds are recorded at the surface of the fluid in the vessel and at the side of the vessel when the impeller brings the fluid down ($U^* \sim 0.84$). This indicates that the TTI goes down towards the bottom of the vessel faster than it goes up towards the surface. The TTI tracer in water is not neutrally buoyant, and has a significant sedimentation velocity of 12 s (for 10 cm). The high normalised velocity recorded here is caused by the combination of the gravitational force and the impeller acting on the tracer. In addition, it can be noticed that a vortex is formed near the impeller. This vortex was not observed when the experiments were performed with the free tracer.

Figure 6-10 (e) shows the path taken by the free tracer along the X axis. This plot confirms that the tracer passes through all locations inside the vessel. Figure 6-6 plot (c) shows the path that the TTI tracer takes. This plot shows that the tracer seems to have stayed a longer time in one side of the vessel.

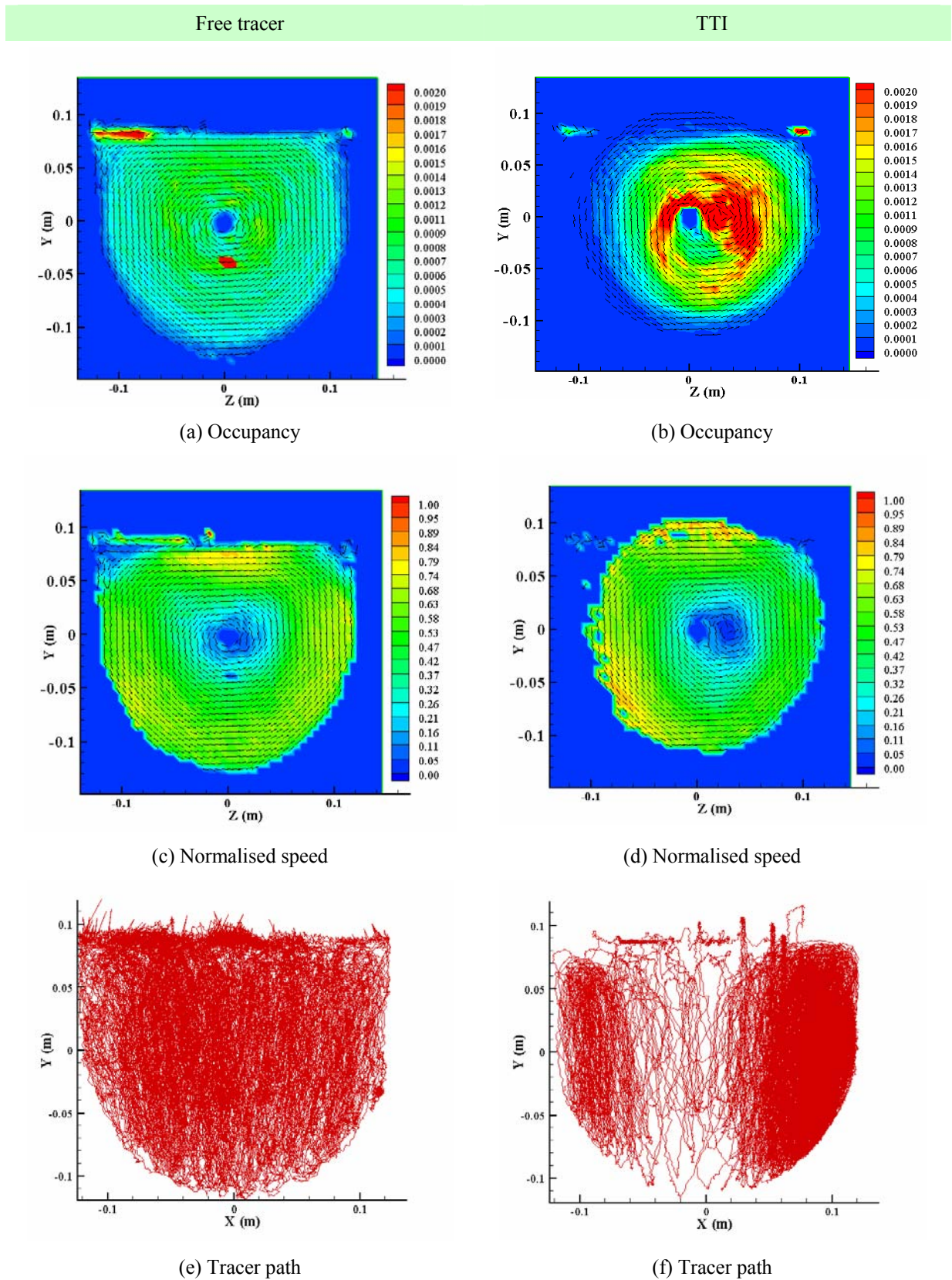


Figure 6-10. Experiments performed with water and at 22 rpm (a) Occupancy plot for the free tracer (b) Occupancy plot for the TTI tracer (c) Normalised speed plot for the free tracer (d) Normalised speed plot for the TTI tracer (e) Free tracer path (f) TTI tracer path

The comparison of the two tracers was performed on the normalised velocity profile recorded along the Z and Y axis (Figure 6-6) of the vessel. The normalised velocity profiles were calculated from the 2-D projection (on the Z and Y axis) of the 3-D data. In § 6.4.2, only a 2-D section of the 3-D data was taken for the calculation of the velocity profile since it was done to compare the results obtained from PEPT and PIV (which is 2-D measurement technique). Figures 6-11 plots the velocity profiles obtained by both tracer for measurement positions A, B, C and D (Figure 6-6 (b)). For Positions A and C, the normalised velocity magnitudes are looked along the Y axis and for Positions B and D, the normalised velocity magnitudes are looked along the Z axis.

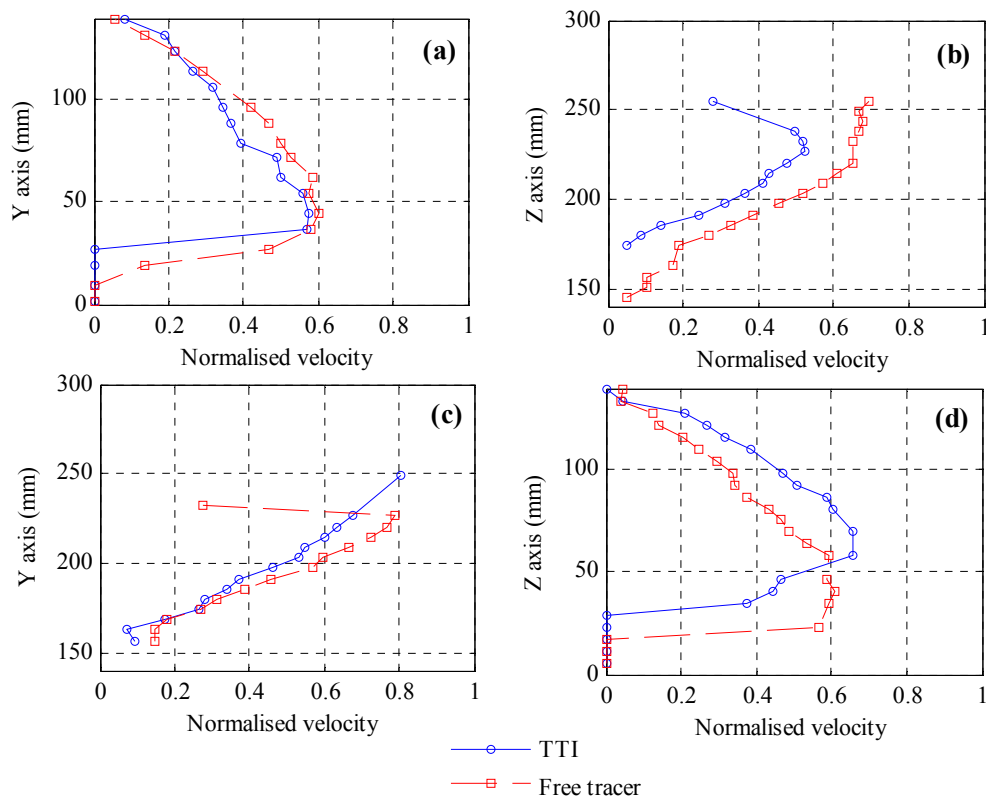


Figure 6-11. Comparison of the velocity fields of the free tracer and the TTI tracer for the experiment performed with water at 22 rpm. Each subfigure show the various positions of the velocity measurement (a) Position A, (b) Position B, (c) Position (C) and (d) Position D

Figure 6-11 (a) shows that between the bottom and the centre of the vessel, the shape of the velocity profiles obtained by the two tracers are reasonably similar although the TTI tracer velocities are slightly smaller in magnitude. A similar observation can be made for the velocity profiles recorded between the centre and the free-surface (Figure 6-11 (c)). At the horizontal positions (B and D), the velocity profiles of the two tracers show greater discrepancy. In position (B) where the impeller is scooping up the product (Figure 6-11(b)), the magnitude of the velocity profile of the TTI ($U^* \sim 0.5$) is considerably lower than the free tracer ($U^* \sim 0.7$) due to the sinking of the TTI against the bulk motion. When it is scooped down (Figure 6-11(d)), the maximum velocity recorded by the TTI ($U^* \sim 0.68$) is higher than the one recorded by the free tracer ($U^* \sim 0.61$), since the fluid motion and the sedimentation now act in the same direction. These significant differences between the velocities of the TTI and the free tracer suggest the use of the TTI as a tracer is not appropriate for low viscosity fluids.

As the viscosity increases, the occupancy plots of the free and the TTI tracer become much more similar (Figure 6-12 (a) and (b)). Both types of tracer now pass through all locations in the vessel, as confirmed by the tracer path plots (Figure 6-12 (e) and (f)). In the case of the free tracer, it appears to get stuck for a certain time at the surface of the fluid. The normalised velocity plots (Figure 6-12 (c) and (d)) give very similar results and, apart from close to the free surface, the velocity magnitudes in the bulk of the vessel are $\sim 0.4 - 0.6$. The maxima recorded with both tracers is located at the free surface ($U^* \sim 0.79$).

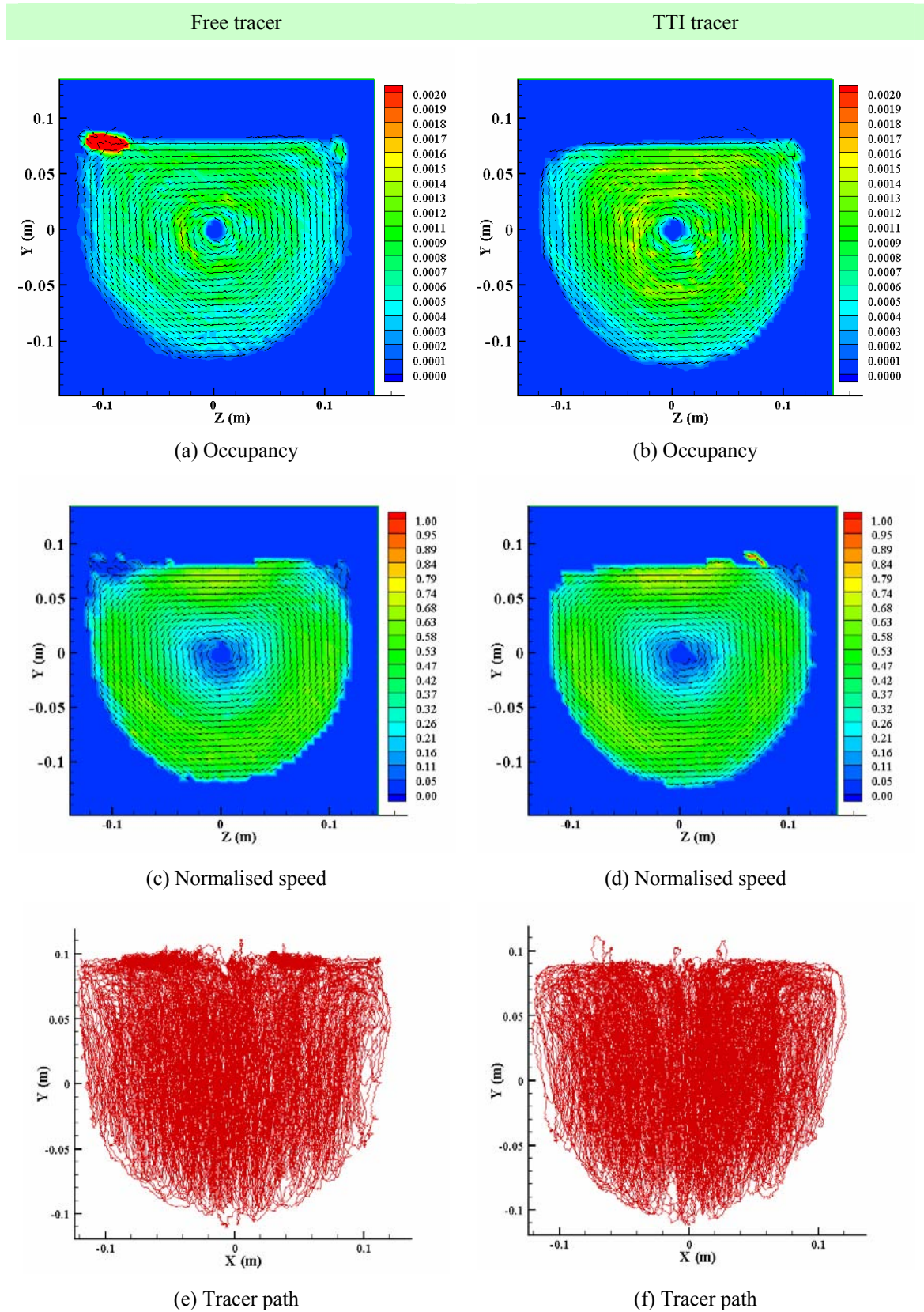


Figure 6-12. Experiments performed with 0.5% CMC and at 22 rpm (a) Occupancy plot for the free tracer (b) Occupancy plot for the TTI tracer (c) Normalised speed plot for the free tracer (d) Normalised speed plot for the TTI tracer (e) Free tracer path (f) TTI tracer path.

Figure 6-13 shows that the shape and the magnitude of velocity profiles recorded by the TTI and the free tracer are almost similar (for the four positions). However, for the two horizontal positions, a slight difference between the two tracers can still be observed, although the differences are now much smaller as the sedimentation velocity of the TTI in the more viscous fluid is close to zero (see §4.2.3.1). In the scooping up part (b), the TTI tracer (peak value of $U^* \sim 0.52$) goes slower than the free tracer (peak value of $U^* \sim 0.6$) and in the scooping down part, the TTI tracer (peak value of $U^* \sim 0.6$) goes faster than the free tracer (peak value of $U^* \sim 0.5$). Despite this small difference, the TTI can still be used reliably as a fluid flow tracer.

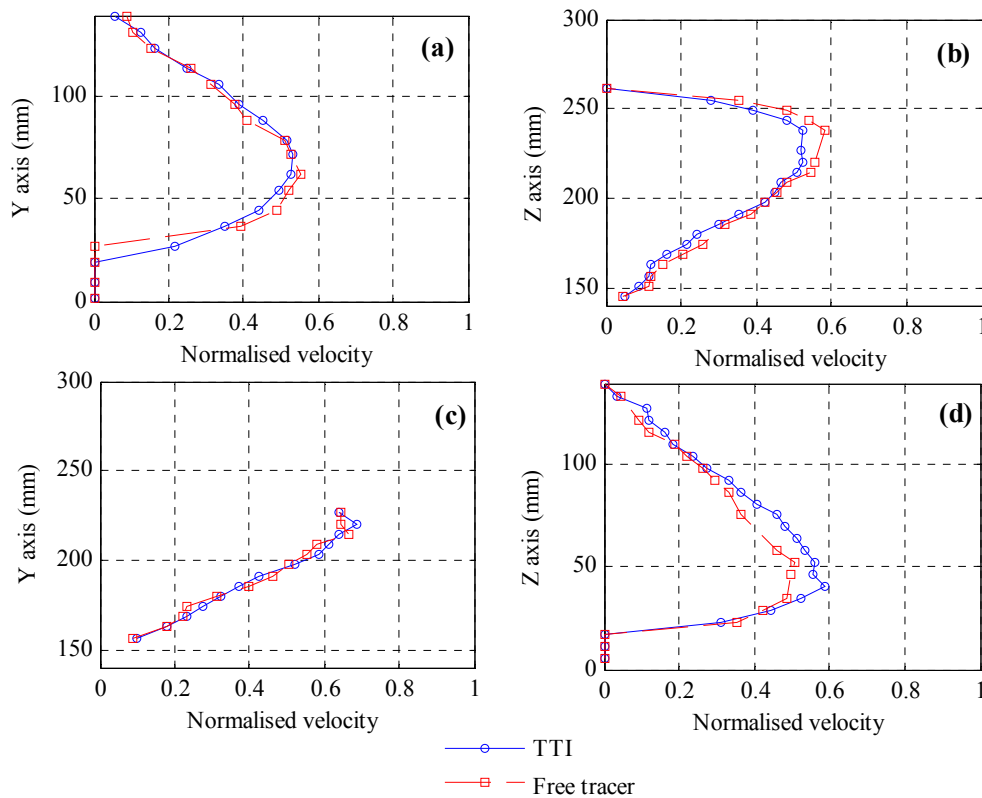


Figure 6-13. Comparison of the velocity fields of the free tracer and the TTI tracer for the experiment performed with 0.5% CMC at 22 rpm. Each subfigure show the various positions of the velocity measurement (a) Position A, (b) Position B, (c) Position C and (d) Position D

Using a similar approach as used for the PIV data, it was decided to investigate the data obtained from the PEPT for the two extreme cases in terms of expected mixing performance.

The two extremes were:

- the ‘best mixing’ scenario: high speed agitation (33 rpm) and low fluid viscosity (4% starch)
- the ‘worst mixing’ scenario: low speed agitation (11 rpm) and high fluid viscosity (5% starch)

Figure 6-14 shows the data from the best case scenario. Figures 6-14 (a) and (b) show that the tracers pass through all locations in the vessel. Red spots close to the impeller shaft can be observed which means that the tracers might have been stuck at this location for a period of time. Figures 6-14 (c) and (d) show that the normalised velocity plots give similar results and, apart from close to the free surface, the velocity magnitudes in the bulk of the vessel are $\sim 0.4 - 0.6$. The maximum velocities recorded are again located at the free surface ($U^* \sim 0.79$). Figures 6-14 (e) and (f) confirms that both tracers pass through all locations in the vessel.

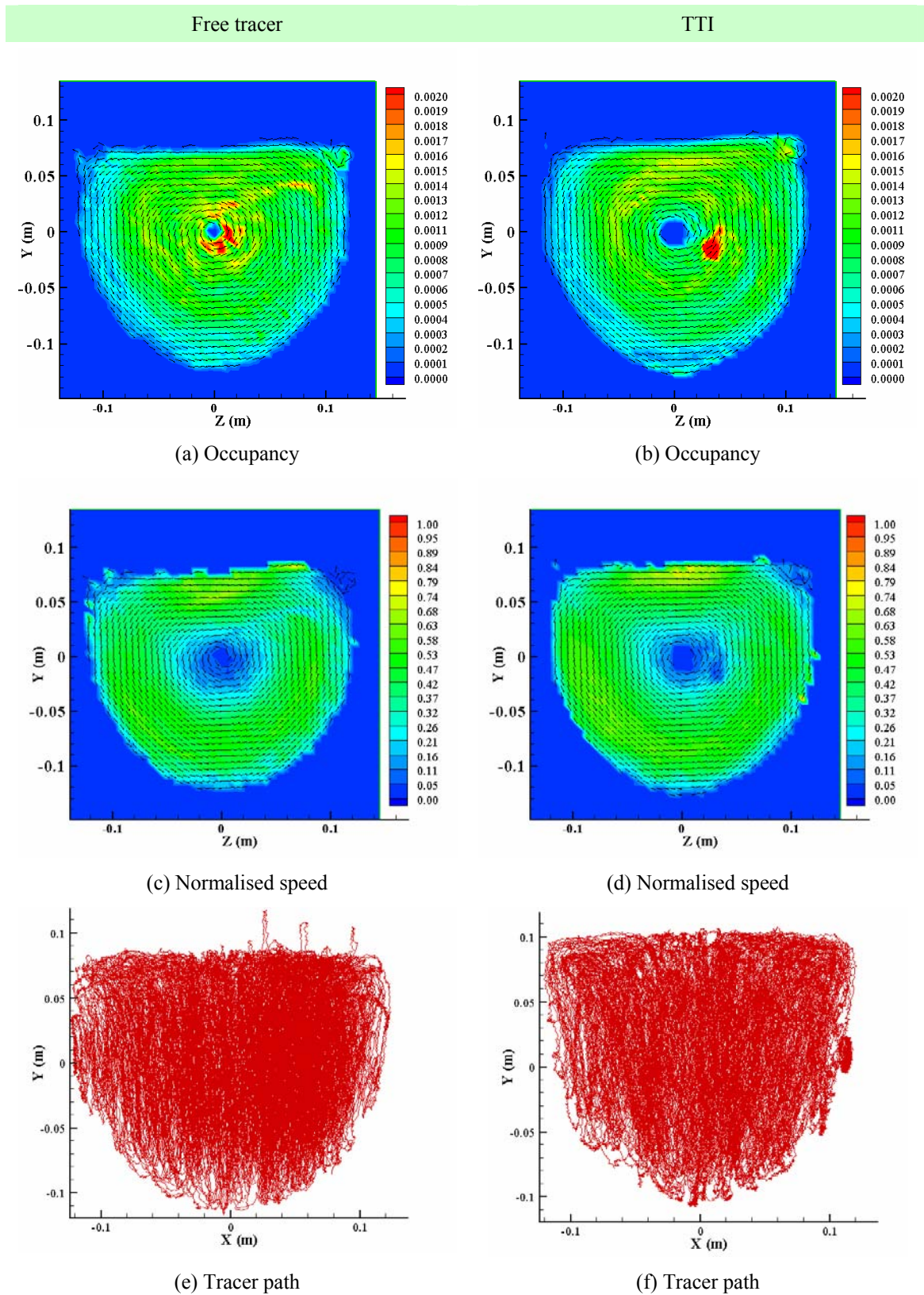


Figure 6-14. Experiments performed with 4% starch and at 33 rpm (a) Occupancy plot for the free tracer (b) Occupancy plot for the TTI tracer (c) Normalised speed plot for the free tracer (d) Normalised speed plot for the TTI tracer (e) Free tracer path (f) TTI tracer path

As the impeller speed and the viscosity increase, the velocity profiles of the TTI and the free tracer remain similar for the four positions. However, for the two horizontal positions, the slight difference between the two tracers that was observed for the experiments performed with CMC is still present.

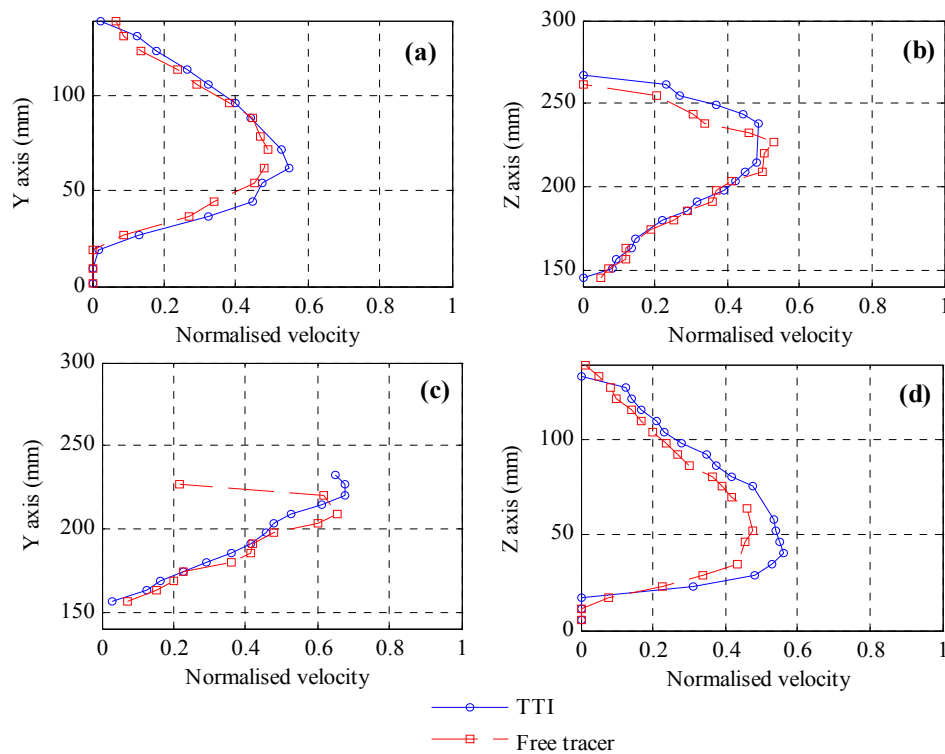


Figure 6-15. Comparison of the velocity fields of the free tracer and the TTI tracer for the experiment performed with 4% starch at 33 rpm. Each subfigure show the various positions of the velocity measurement (a) Position A, (b) Position B, (c) Position (C) and (d) Position D

As the speed decreases and the viscosity of the fluid further increases, the mixing within the vessel is less uniform (Figure 6-16). Indeed, the tracer does not pass through all locations throughout the vessel (Figure 6-16 (a), (b), (e) and (f)) and some parts of the vessel are not covered by both tracers. This is due to low agitation speed which caused the tracers not to be able to move through the entire vessel. The normalised velocity plots (Figure 6-16 (c) and (d)) give similar results and the velocity magnitudes in the bulk of the vessel are $\sim 0.3 - 0.6$. Decreasing the speed to 11 rpm and increasing the viscosity cause the velocity magnitude at the free-surface to decrease ($U^* \sim 0.74$). The same observation can be made for both tracers.

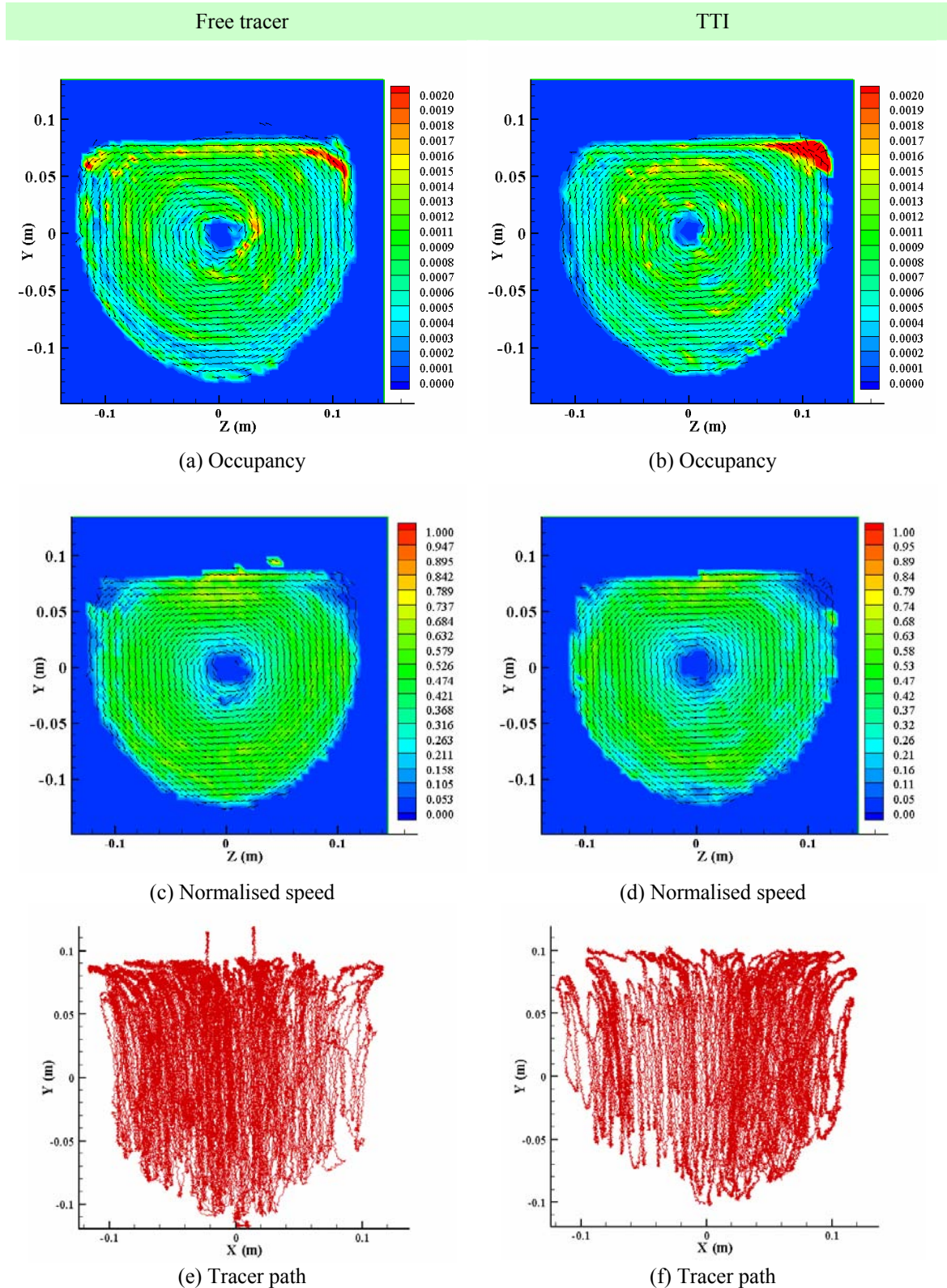


Figure 6-16. Experiments performed with 5% starch and at 11 rpm (a) Occupancy plot for the free tracer (b) Occupancy plot for the TTI tracer (c) Normalised speed plot for the free tracer (d) Normalised speed plot for the TTI tracer (e) Free tracer path (f) TTI tracer path.

The velocity profiles for both tracers are similar in shape and magnitude (Figure 6-17). This shows again that TTIs can be used whatever the speed of the agitation as long as they are isokinetic with the fluid.

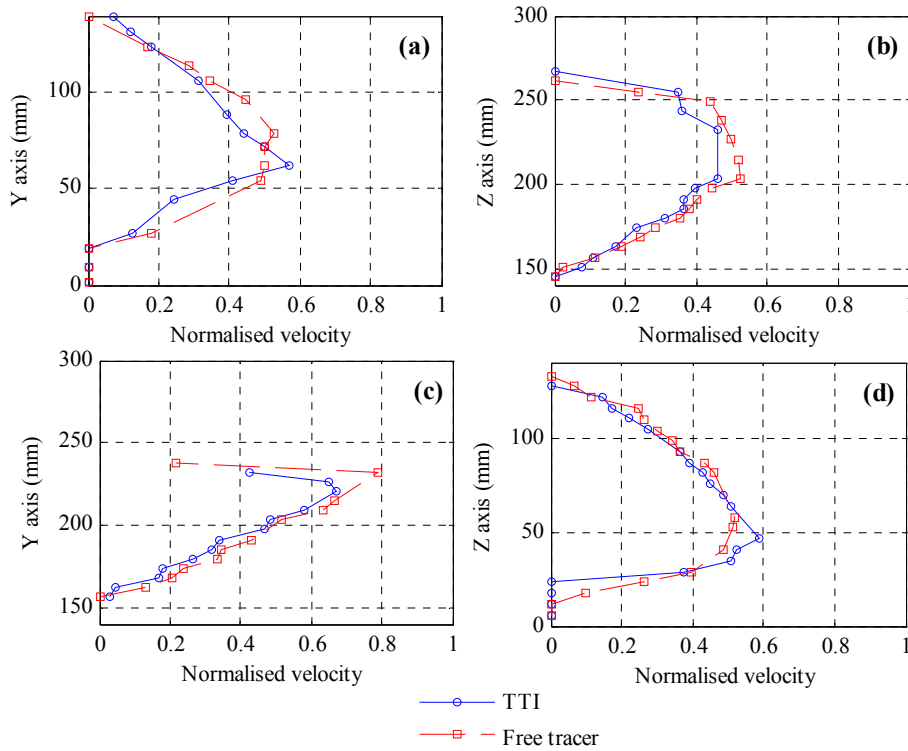


Figure 6-17. Comparison of the velocity fields of the free tracer and the TTI tracer for the experiment performed with 5% starch at 11 rpm. Each subfigure show the various positions of the velocity measurement (a) Position A, (b) Position B, (c) Position (C) and (d) Position D

Figure 6-18 shows the effect of changing the filling level to overfilled using 4% starch at 22 rpm. Both tracers still give similar information. Figure 6-18 (a) and (b) shows that the tracers went through most of the areas inside the vessel. In addition, the presence of a vortex located above the impeller can be observed (this vortex was not observed for the experiments performed at the required filling level). This vortex was observed as a region of low velocity above the impeller shaft in the PIV experiments (§ 5.4.1) and corroborates the assumption that the centre of the rotation has shifted to above the impeller axis. In addition for both fluids, just above the impeller, where the vortex is located, the velocity is very low ($U^* \sim 0.16$). The tracer path shows that the tracer spends significant amount of time in the left zone of the vessel ($X = -0.1$ to 0).

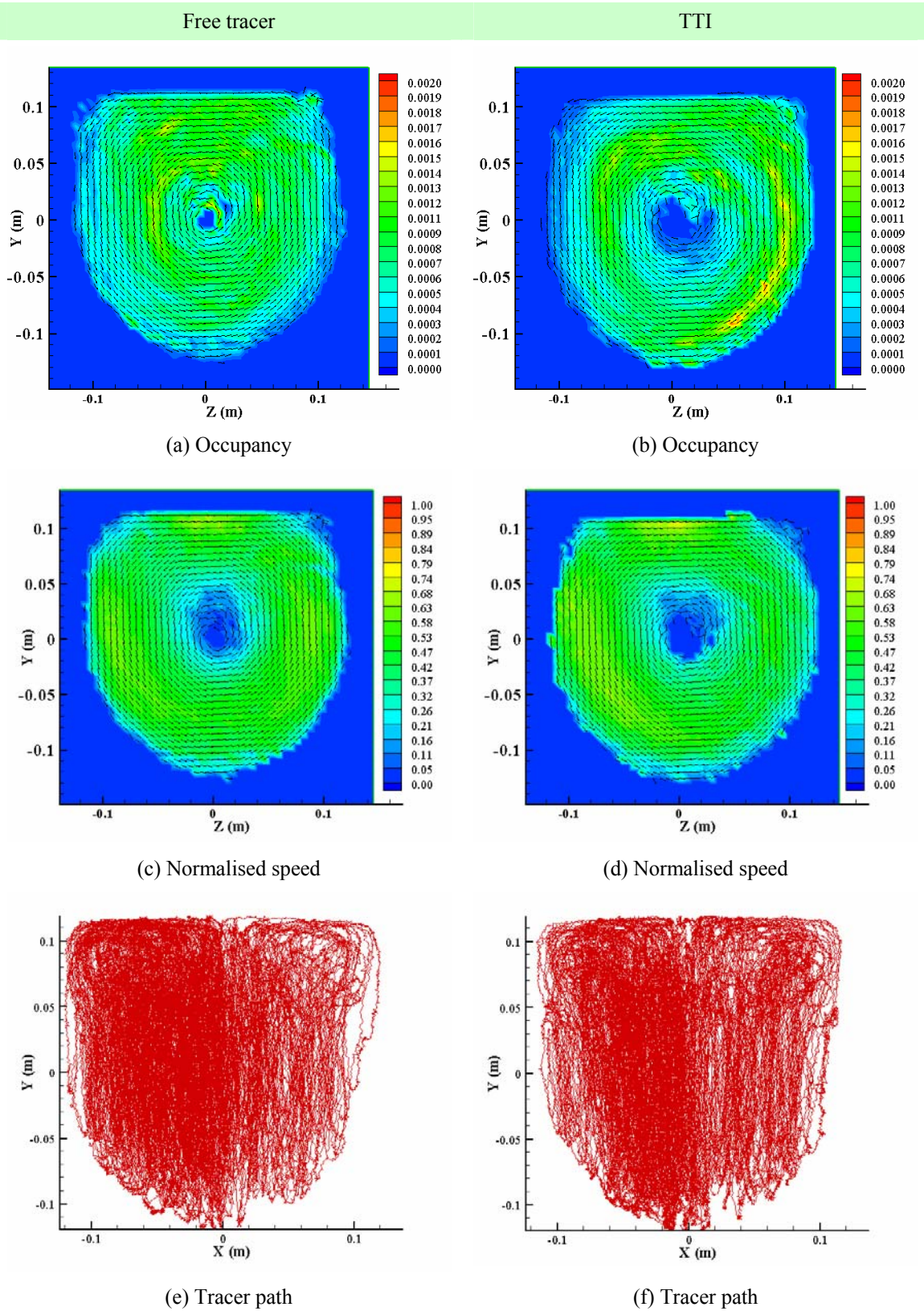


Figure 6-18. Experiments performed with an overfilled vessel, 4% starch and at 22 rpm (a) Occupancy plot for the free tracer (b) Occupancy plot for the TTI tracer (c) Normalised speed plot for the free tracer (d) Normalised speed plot for the TTI tracer (e) Free tracer path (f) TTI tracer path

The velocity profiles for both tracers are similar in shape (Figure 6-19). However, for the two horizontal positions, the magnitudes are very different between the two tracers. Surprisingly, the TTI tracer ($U^* \sim 0.7$) goes faster than the free tracer ($U^* \sim 0.5$) for both positions (up and down).

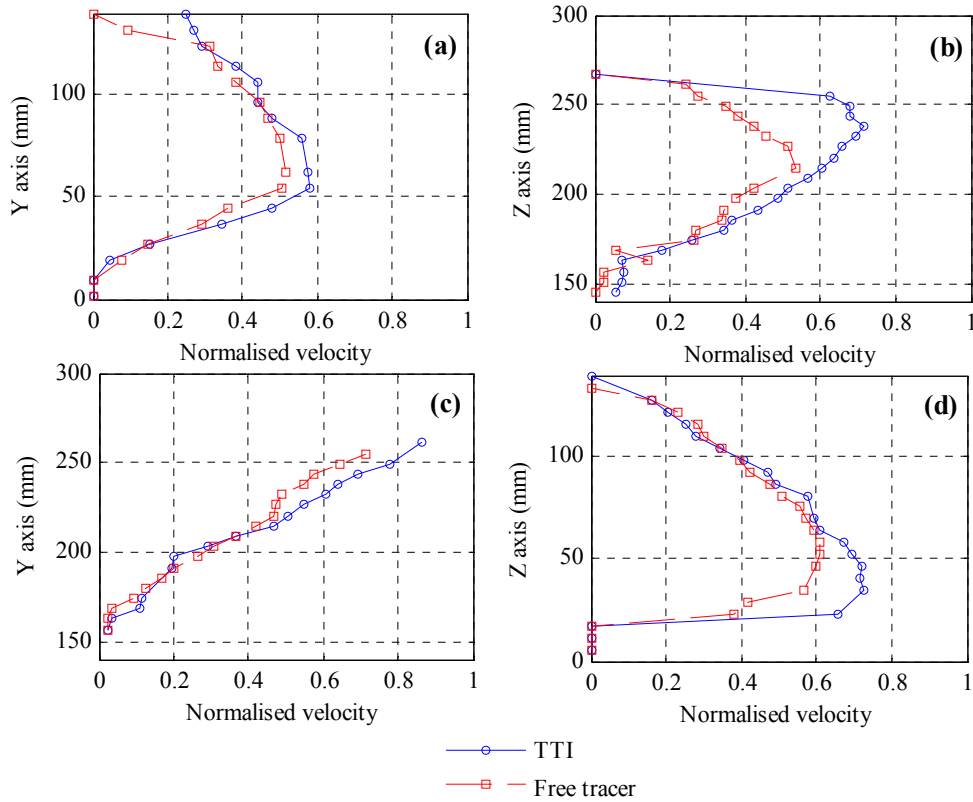


Figure 6-19. Comparison of the velocity fields of the free tracer and the TTI tracer for the experiment performed with and overfilled vessel and 4% starch at 22 rpm. Each subfigure show the various positions of the velocity measurement (a) Position A, (b) Position B, (c) Position (C) and (d) Position D

6.4.4. Transverse movement inside the vessel

The transverse movement across the vessel was studied by plotting for each of the zones (1, 2 and 3) described in § 6.3.3 the velocity on the X axis. During mixing, the displacement of the fluid along the X axis is essential since it validate that the fluid went through all location in the vessel.

Figure 6-20 gives the velocity plots (the u velocity) on the X axis of the vessel for the zones 1, 2 and 3. Plot (a) is the velocity contour of the zone 1, plot (b) is the velocity contour of the zone 2 and plot (c) is the velocity contour of the zone 3 for the experiment performed with 4% starch and at 22 rpm. This figure gives a better understanding of the path that the tracer follows along the X axis of the vessel. When the impeller scoops the fluid and is above the fluid level, the fluid moves in opposite directions away from the centre of the vessel towards the wall of the vessel. Following this when the impeller goes back to the surface of the water, this time the fluid moves towards the centre of the vessel. See the attached CD where a movie showing the movement of the impeller can be seen [Visualisation_Normal filling level.wmv]. Figure 6-21 is a schematic drawing of the movement of the tracer within the vessel. In addition, it should be noted that when the viscosity of the fluid and the impeller speed change, the mixing pattern is not modified (the Figures are given in the CD at the back of this thesis).

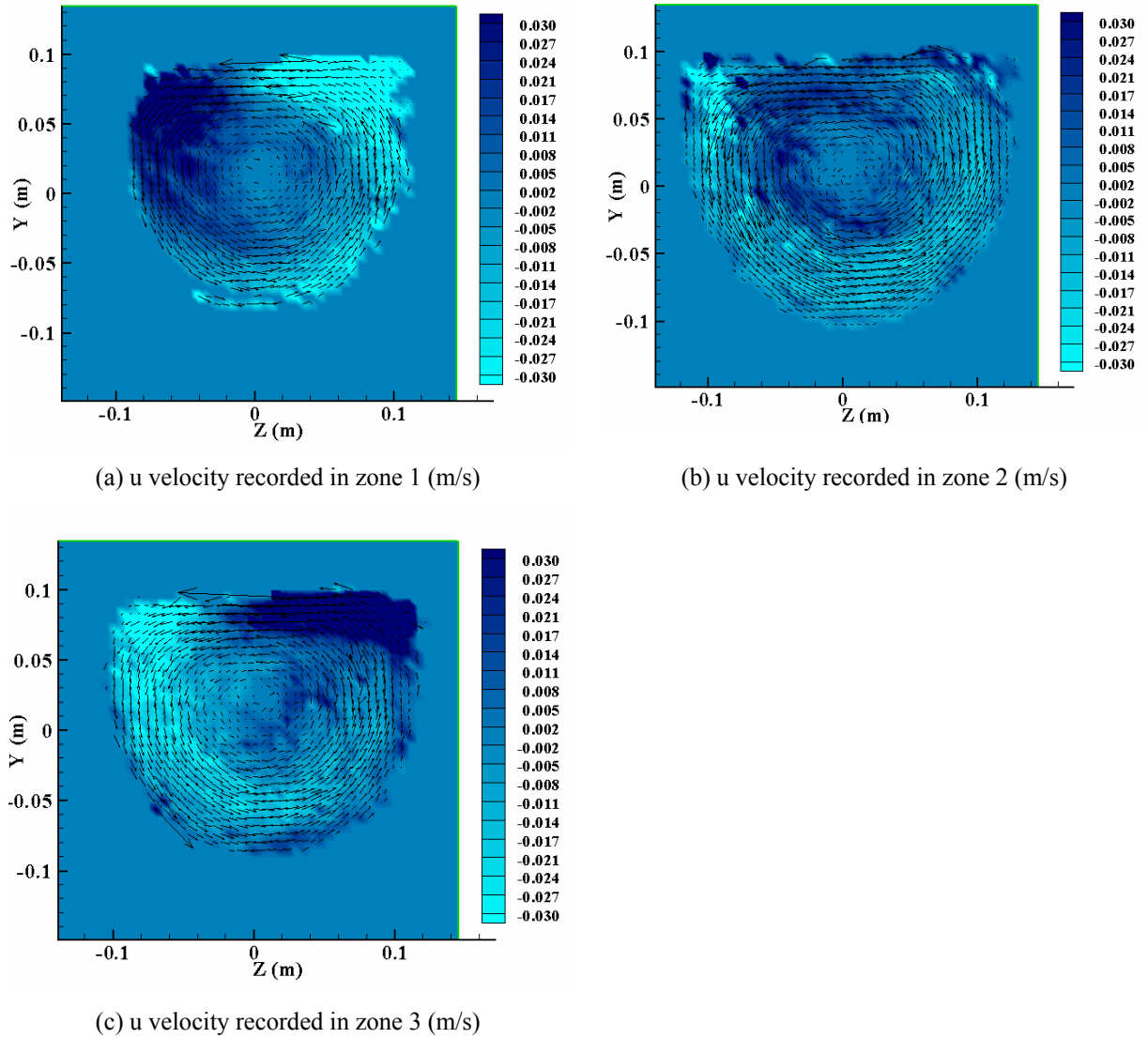


Figure 6-20. Experiments performed with 4% starch at 22 rpm with the free tracer (a) Velocity on the x axis zone 1 (b) Velocity on the x axis zone 2 (c) Velocity on the x axis zone 3

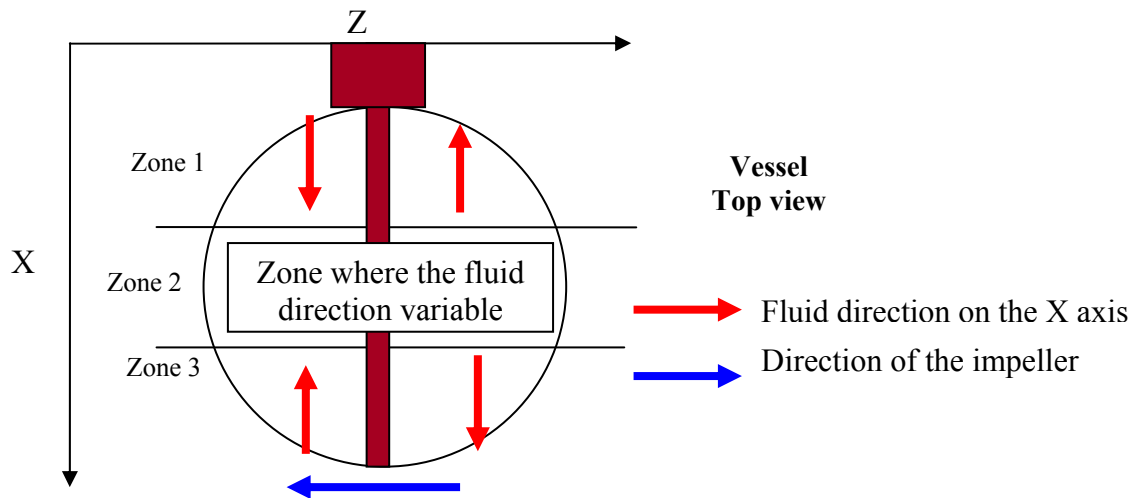
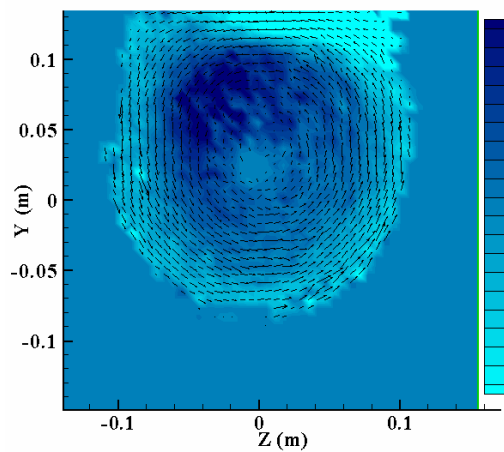
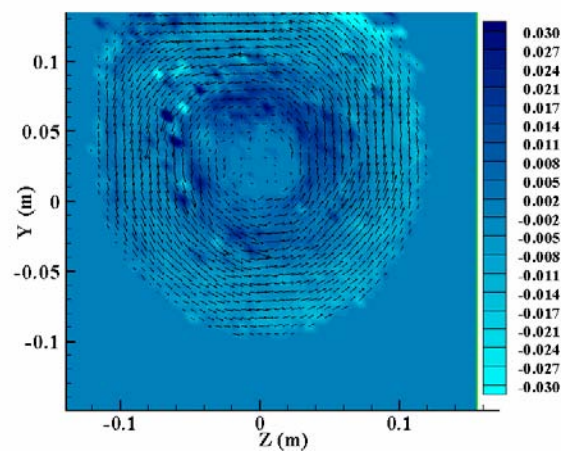


Figure 6-21. The velocity direction on the X axis seen from the top of the vessel

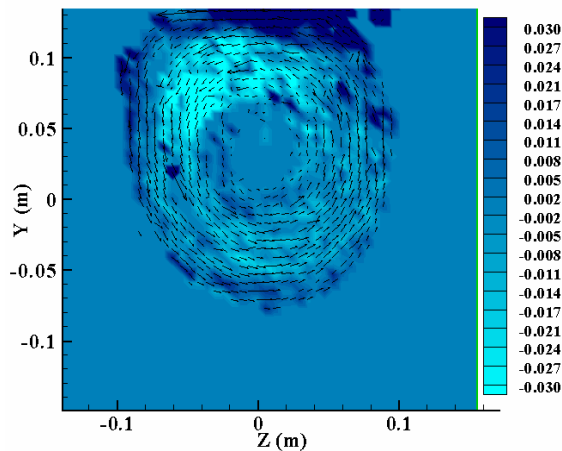
As the fluid level increases inside the vessel, the zones approach gives more evidence for the modification in the mixing pattern. Figure 6-22 gives the velocity plots (the u velocity) on the X axis for zones 1, 2 and 3. On the X direction, the mixing direction recorded here in zone 2 is similar to that described for the experiment performed with the normal filling level. However, the velocities recorded on the X axis for zone 1 and 3 vary more. In the area around the impeller of zone 1 and 3, the fluid moves towards the centre of the vessel. Outside this area, the fluid moves in opposite directions away from the centre of the vessel towards the wall of the vessel.



(a) u velocity recorded in zone 1 (m/s)



(b) u velocity recorded in zone 2 (m/s)



(c) u velocity recorded in zone 3 (m/s)

Figure 6-22. Experiments performed with an overfilled vessel, with water at 22 rpm (a) Velocity on the x axis zone 1 (m/s) (b) Velocity on the x axis zone 2 (m/s) (c) Velocity on the x axis zone 3 (m/s)

The overfilled experiments performed with the water and 5% starch confirm the findings of this experiment. However, when the viscosity increases the size of the vortex decreases and for 5% starch the vortex cannot be observed (see attached CD, file: PEPT_data_figure_thesis.doc).

Understanding the transverse movement inside the vessel is essential since it can potentially help to determine the mixing efficiency inside the vessel. The central part of the vessel is the transitional area (zone 2). Indeed, during the mixing, the tracer moves from one side of the vessel (zone 1 or 3) to the other side (zone 3 or 1). During this movement, the tracer will pass through zone 2. Therefore, the higher the number of times that the tracer moves from one side to the other, the better the mixing. Table 6-3 shows various parameters which were calculated for zone 2 in order to have a better understanding of this transverse movement:

- The average number of rotations around the vessel shaft that the tracer does when it moves from zone 1 (or zone 3) to zone 3 (or zone 1)
- The standard deviation of the number of rotations around the vessel shaft that the tracer does when it moves from zone 1 (or zone 3) to zone 3 (or zone 1)
- The number of times that the tracer moves from zone 1 (or zone 3) to zone 3 (or zone 1) during the 30 minute experiment
- The average time (s) it takes for the tracer to move from zone 1 (or zone 3) to zone 3 (or zone 1)
- The standard deviation of the time (s) it takes for the tracer to move from zone 1 (or zone 3) to zone 3 (or zone 1).

In the table, the values of the TTI and the free tracer are given together in order to evaluate the efficiency of the TTI in determining the thermal treatment efficiency.

Table 6-3. Investigation of zone 2

Experiment number	1		2		3		4		5		6		7		8		9	
Fluid used	Water		0.5% CMC		4% Starch		5% starch		Water		4% starch		5% starch		4% starch		5% starch	
Agitation speed (rpm)	22		22		22		22		22		22		22		33		11	
Filling level	Normal		Normal		Normal		Normal		Overfilled		Overfilled		Overfilled		Normal		Normal	
Nature of the tracer	TTI	Free	TTI	Free	TTI	Free	TTI	Free	TTI	Free	TTI	Free	TTI	Free	TTI	Free	TTI	Free
Average number of rotations around the vessel shaft	1.7	1.6	2.5	1.8	2.7	3.5	9.5	18.8	1.6	1.5	1.3	2.5	9.4	15.6	2.3	3.1	19.7	8.3
Standard deviation of the number of rotations around the vessel shaft	1.3	1.5	1.8	1.1	1.4	1.9	3.8	2.5	1.7	1.4	1	2.5	5	5.6	1.9	18	7.4	5.6
Number of times the tracer moves from zone 1 to zone 3 (or zone 3 to zone 1)	11	58	33	23	22	20	7	5	65	70	23	19	6	5	52	16	3	3
Average time (s) for the tracer to move from zone 1 to zone 3 (or zone 3 to zone 1)	5.63	4.69	7.6	6.36	10.2	12.25	35.6	27.9	4.87	4.9	6.33	6.39	40.9	55.34	5	6.6	98	54
Standard deviation of the time (s) for the tracer to move from zone 1 to zone 3 (or zone 3 to zone 1)	3.45	2.23	4.04	3.24	4.7	5.2	14.67	6.2	3.3	3.1	2.95	3.6	9.2	12.1	3.1	3.98	38.7	14

The first experiment described in Table 6-3 is the experiment performed with water with the normal filling level. The results from this experiments show that the number of rotations by the two tracers through zone 2 are very similar, as are the average time and standard deviation values. However, it should be noted that the number of times the tracer moves through zone 2 is different. The TTI tracer only moves 11 times while the free tracer moves 58 times. This shows clearly that the TTI circulates less than the free tracer and therefore the TTI does not represent the fluid flow as accurately as the free tracer when the processed fluid is water.

The second experiment shows the results obtained for the processing of solution made from 0.5% CMC. The number of rotations around the impeller shaft increased for both the TTI and the free tracer (2.5 – 1.8) when compared with the experiments performed with water. The number of times the two tracers move through zone 2 is similar (33-23). The time taken for the two tracers to move from zone 1 to zone 3 (or zone 3 to zone 1) is higher than for the experiments performed with water. When the viscosity of the fluid increases, (i) the number of rotations around the shaft through zone 2 increases (ii) the number of times the tracer moves from one zone to the other decreases (iii) the average time (and its standard deviation) it takes for the tracer to move through zone 2 increases. This was also observed for the experiments performed with the two solutions of starch. For the experiment performed with 5% starch, the tracer moves only 7 times (for the TTI) and 5 times (for the free tracer) through zone 2.

As the filling level increases, the transverse movement inside the vessel is not modified. When the two experiments performed with 4% starch are compared, the tracer from the overfilled experiments takes less time to move through zone 2. For the free tracer, it takes

12.25 s when the filling level of the vessel is normal and it takes 6.39 s when the vessel is overfilled.

As the agitation speed changes, the time it takes to move through zone 2 varies accordingly. It takes 54 seconds for the free tracer to move from one zone to the other for the experiment performed at low speed and it takes 6.6 seconds when the speed is increased.

The results of this table help to demonstrate several important points:

- Increasing the viscosity of the fluid reduces the transverse mixing
- Overfilling the vessel alters the flow pattern but the transverse mixing characteristics are similar
- Increasing the agitation speed reduces the time for the tracer to move between zones thus improving the transverse mixing

6.5. Conclusion

In this Chapter, the applicability of the TTIs to determine the thermal treatment efficiency of the vessel was investigated by using the PEPT technique to determine whether the flow behaviour of the TTIs is similar to the fluid motion. In addition, the effect of overfilling the vessel was studied. The velocity profile of the liquid phase recorded by PIV (Chapter 5) and the free PEPT tracer were compared with good correlation between the two techniques.

In general, TTIs can be used to evaluate thermal treatment of fluids only if the TTIs are isokinetic with the fluid. TTIs can not be reliably used to determine thermal treatment of

fluids such as water since the TTIs are not isokinetic with water and do not follow the fluid path due to settling effects.

Overall, it was seen that changes in fluid viscosity or changes in agitation speed does not affect the mixing pattern inside the vessel. However, overfilling the vessel changes the mixing pattern (formation of a vortex for low viscosity fluid) inside the vessel. This was previously observed by the TTI study (Chapter 4) and the PIV work (Chapter 5).

Chapter 7

Conclusions and Future Work

This thesis describes an experimental study of the thermal and mixing performance of a bespoke low shear food mixer, the 250 litre Giusti ‘Vesuvio’ vessel, used for thermal treatment. The work has been focussed on the following objectives

- validation of the statistical reliability of TTIs;
- application of the TTI technique to an industrial-scale ‘Vesuvio’ vessel;
- determination of flow regime for fluids of different rheology and at different fill heights and rotational speeds using PIV;
- use of PEPT to determine the trajectories of the fluid and the TTIs separately to enable justification of the TTI technique when the TTIs follow the fluid streamlines and are isokinetic with the fluid.

7.1. Validation of the statistical reliability of TTIs

The ability of TTIs to evaluate the efficiency of thermal treatment was investigated using a Peltier stage and a PCR device to generate a range of temperature-time profiles. The study shows that there is a good correlation between the responses of TTIs and thermocouples for a range of non isothermal processes. It was found that the variability of the responses of TTIs and thermocouples increases when the holding time of the time temperature profile increases. However, it was observed that the increase of the error from the thermocouples is lower than

the increase of the error of the TTIs. The error was found to be around $\pm 20\%$ over a wide range of temperature- profiles.

In practice, the accuracy of the TTIs will be constrained by (i) a lower limit of P, where there is sufficient thermal lag between the TTIs and the process, so that the TTI value is not correct, and (ii) a higher limit of P, where the value of the enzyme activity is so low that it is not sensitive to the change in P. In between, is the operational window in which measurements can be taken with accurately which is approximately 2 to 8 minutes at 85°C for BAA and 5 to 30 minutes at 85°C for BLA.

This study shows that TTIs can be used as a tool for process validation when thermocouples can not be used. However, to ensure safety, it is suggested that TTIs should not be used alone for on-line thermal process monitoring, but should be used in combination with other methods.

7.2. Application of the TTI technique to an industrial-scale ‘Vesuvio’ vessel

The TTIs were used together with thermocouples to investigate the thermal efficiency of the ‘Vesuvio’ vessel. Parameters such as fluid viscosity, different heating options and filling level were investigated. The results from the TTIs showed that

- the thermal process efficiency is lowered when the apparent viscosity of the fluid increases, which can be overcome by the extra mixing induced by steam injection.;
- overfilling the vessel modifies the heating efficiency of the vessel. This might be caused by a change in the fluid mixing pattern, as discussed Chapters 5 and 6.

In addition, this work showed that the product does not get most of its cooking during the initial heating up time, most in fact occurs during the holding time.

7.3. Use of PIV technique to investigate the fluid flow inside the vessel

The fluid flow inside the vessel was investigated using PIV technique. Regions of high and low velocity were identified within the vessel. This study showed that the flow is laminar/transitional through bulk of vessel and it was found that the only regions where significant flow instabilities were generated are located at the free surface and at the trailing edge of the impeller. Mixing throughout the bulk can therefore be expected to occur by laminar flow mechanisms with some mixing by eddy diffusion present at the free surface.

The parameters investigated were fluid viscosity, agitation speed and filling level. It was found that the velocity profiles inside the vessel were not modified when the viscosity or the agitation speed was changed; however, notable differences were present when the vessel was overfilled.

7.4. Investigations of the flow behaviour of TTIs and the fluid in a model ‘Vesuvio’ vessel using Positron Emission Particle Tracking (PEPT)

TTIs can only be used reliably to determine the thermal treatment efficiency of the vessel if their motion is isokinetic with the fluid and follows the fluid streamlines. This was investigated by using the PEPT technique. Significant differences in the path taken by the TTI and the fluid were observed when the TTI had a significant settling velocity in the fluid. Hence TTIs cannot be assumed to give reliable results in low viscosity fluids (e.g. water) or at very low agitation speeds.

The overfilling of the vessel was investigated with the PEPT technique. The results confirm that the mixing pattern within the vessel is modified when compared to the normal filling level. Overfilling the vessel causes the apparition of a small vortex above the impeller which causes local drop of velocity. This was shown to affect the thermal treatment efficiency when measured with TTIs.

7.5. Future work

Based on the findings from this work, some further work could be undertaken in the following areas:

- In this work, the TTIs were used at pasteurisation temperature. Similar validation work could be repeated for the newly developed sterilisation TTIs used to assess thermal treatment performed at sterilisation temperatures, and then apply these to the ‘Vesuvio’ vessel which can also be used under these conditions. Validation work is essential in order to ensure the reliability of the technique: the experiments performed in this study to validate the pasteurisation TTI could be repeated for the sterilisation TTI. However, since the existing Peltier plate has a maximum temperature of 118°C, an alternative heat source which has the ability to reproduce the complex time temperature profiles required is needed. The sterilisation TTI could be used on the ‘Vesuvio’ vessel which is designed for temperatures up to about 125°C. In this case, in addition to the jacket heating and the steam injection, the vessel is pressurised in order to reach these temperatures.
- When the ‘Vesuvio’ vessel is used at sterilisation temperatures, it would be interesting to study the effect of increased pressure upon the TTIs. The use of high pressures might

modify the response of the TTIs and therefore cause a misinterpretation of the thermal processing.

- The variability of the TTI itself was investigated in this work under controlled conditions by the author. In industry, it is most probable that the analysis of TTIs would be performed by several people, which introduces uncertainty. It would be interesting to understand the variability in the results obtained from the analysis performed by different individuals. This variability was observed when comparing the results obtained by the University of Birmingham and the CCFRA for the calculation of the D_T and z values. This showed that more work is needed on the investigation of the TTI variability.
- Only one type of impeller was used in this study. Other types of impellers could be fitted inside the vessel and their performances could be investigated and compared with the impeller used in this work. In addition, more fluids with differing rheologies or with the addition of solids could be investigated and for each fluid, an impeller could be specially designed. This would help to improve the design and applicability of the equipment and improve understanding further of the effect of the impeller design on the mixing pattern.
- The PEPT work was performed on the scale down version of the ‘Vesuvio’ vessel, however PEPT could be performed directly on the ‘Vesuvio’ vessel by using the newly developed mobile PEPT. Results obtained from the model vessel and the ‘Vesuvio’ vessel could be compared in order to gain a better understanding of the vessel design. The use of the mobile PEPT on the ‘Vesuvio’ vessel could help to investigate the effect of the steam injection and the jacket heating on the mixing performance. By putting the radioactive

tracer on a TTI, it could at the same time be used to monitor the thermal treatment and the mixing efficiency.

- In this work, the vessel was made of glass, it therefore could not be heated using a jacket nor could steam be injected toward its centre. However, this might affect the mixing within the vessel. A new vessel could be designed made from stainless steel and steam injection and jacket heating could be fitted into it. This would result in the possibility to study heating and flow regime simultaneously using PEPT.

References

- Adameczyk, A. A. and Rimai, L. (1988) 2-Dimensional particle tracking velocimetry (PTV): Technique and image processing algorithms. *Experiments in Fluids* 6, 373-380.
- Adams, M.R. and Moss, M.O. (2000) *Food microbiology* 2nd Ed, The Royal Society of Chemistry: Cambridge
- Adams, J. B. and Langley, F. M. (1998) Nitrophenyl glucoside hydrolysis as a potential time temperature integrator reaction. *Food Chemistry* 62, 65-68.
- Adrian, R. J. (2005) Twenty years of particle image velocimetry. *Experiments in Fluids* 39, 159-169.
- Adrian, R. J. (1991) Particle-imaging techniques for experimental fluid mechanics. *Ann Rev Fluid Mech* 23, 261-304.
- Aubin, J., Le Sauze, N., Bertrand, J., Fletcher, D. F., and Xuereb, C. (2004) PIV measurements of flow in an aerated tank stirred by a down- and an up-pumping axial flow impeller. *Experimental Thermal and Fluid Science* 28, 447-456.
- Bakalis, S., Cox, P. W., Wang-Nolan, W., Parker, D., and Fryer, P. J. (2003) Use of positron emission particle tracking (PEPT) technique for velocity measurements in model food fluids. *Journal of Food Science* 68, 2684-2692.
- Bakalis, S., Fryer, P. J., and Parker, D. J. (2004) Measuring velocity distributions of viscous fluids using positron emission particle tracking (PEPT). *AIChE Journal* 50, 1606-1613.
- Bakalis, S., Cox, P. W., Russell, A. B., Parker, D. J., and Fryer, P. J. (2006) Development and use of positron emitting particle tracking (PEPT) for velocity measurements in viscous fluids in pilot scale equipment. *Chemical Engineering Science* 61, 1864-1877.
- Ball, C. and Olson, F. (1957) *Sterilization in food technology*. Mc Graw Hill: New York.
- Barigou, M. (2004) Particle tracking in opaque mixing systems: An overview of the capabilities of PET and PEPT. *Chemical Engineering Research and Design* 82, 1258-1267.

Barker, D. B. and Fourney, M. E. (1977) Measuring fluid velocities with speckle patterns. *Optics Letters* 1, 135-137.

Bhowmik, S. R. and Tandon, S. (1987). A method for thermal process evaluation of conduction heated foods in retortable pouches. *Journal of Food Science* 52, 202-209.

Bigelow, W. D. (1921). The logarithmic nature of thermal death time curves. *Journal of Infectious Diseases* 29, 528-536.

Bridgwater, J., Forrest, S., and Parker, D. J. (2004) PEPT for agglomeration? *Powder Technology* 140, 187-193.

Chung, K. H. K., Barigou, M., and Simmons, M. J. H. (2007) Reconstitution of 3-D flow field inside miniature stirred vessels using a 2-D PIV technique. *Chem Eng Res Des* 85, 1-8.

Claeys, W. L., Van Loey, A. M., and Hendrickx, M. E. (2002). Intrinsic time temperature integrators for heat treatment of milk. *Trends in Food Science & Technology* 13, 293-311.

Cornish-Bowden, A., & Wharton, C. W. (1988). Simple enzyme kinetics. *Enzyme Kinetics* (pp. 73). IRL Press Ltd: Oxford.

Cox, P. W., Bakalis, S., Ismail, H., Forster, R., Parker, D. J., and Fryer, P. J. (2003) Visualisation of three-dimensional flows in rotating cans using positron emission particle tracking (PEPT). *J Food Eng* 60, 229-240.

De Haan, S. W. H., Roodenburg, B., Morren, J., and Prins, H. Technology for preservation of food with pulsed electric fields (PEF). IEEE AFRICON Conference 2, 791-796. (2002).

Deliza, R., Rosenthal, A., Abadio, F. B. D., Silva, C. H. O., and Castillo, C. (2005) Application of high pressure technology in the fruit juice processing: Benefits perceived by consumers. *J Food Eng* 67, 241-246.

Devlieghere, F., Vermeiren, L., and Debevere, J. New preservation technologies: Possibilities and limitations (2004) *International Dairy Journal* 14, 273-285

Durango, A. M., Soares, N. F. F., Benevides, S., Teixeira, J., Carvalho, M., Wobeto, C., and Andrade, N. J. (2006) Development and evaluation of an edible antimicrobial film based on yam starch and chitosan. *Pack Technol Sci* 19, 55-59.

Durst, F., Melling, A., and Willert, C. (1981) *Principles and Practice of Laser-Doppler Anemometry*. Academic Press: London.

Fan, X., Parker, D. J., and Smith, M. D. (2006a) Enhancing ¹⁸F uptake in a single particle for positron emission particle tracking through modification of solid surface chemistry. *Nuclear Instruments and Methods in Physics Research Section A: Accelerators, Spectrometers, Detectors and Associated Equipment* 558, 542-546.

Fan, X., Parker, D. J., and Smith, M. D. (2006b) Labelling a single particle for positron emission particle tracking using direct activation and ion-exchange techniques. *Nuclear Instruments and Methods in Physics Research Section A: Accelerators, Spectrometers, Detectors and Associated Equipment* 562, 345-350.

Fangary, Y. S., Barigou, M., Seville, J. P. K., and Parker, D. J. (2000) Fluid trajectories in a stirred vessel of non-Newtonian liquid using positron emission particle tracking. *Chemical Engineering Science* 55, 5969-5979.

Fangary, Y. S., Seville, J. P. K., and Barigou, M. (1999) Flow studies in stirred tanks by positron emission particle tracking (PEPT). *Institution of Chemical Engineers Symposium Series* 23-34.

Fellows, P. J. (2000) Heat sterilisation. In: *Food processing technology, Principles & Practice*, pp. 250-277. Ed Wood head publishing.

Fitzpatrick, S., Ding, Y., Seiler, C., Lovegrove, C., Booth, S., Forster, R., Parker, D., and Seville, J. P. K. Positron Emission Particle Tracking studies of a wurster process for coating applications. *Pharmaceutical Technology*. (2003).

Fonberg-Broczek, M., Windyga, B., Ski, J., Ska, M., Pietrzak, D., and Prestamo, G. (2005) High pressure processing for food safety. *Acta Biochimica Polonica* 52, 721-724.

Franzetti, L., Martinoli, S., Piergiovanni, L., and Galli, A. (2001) Influence of active packaging on the shelf-life of minimally processed fish products in a modified atmosphere. *Pack Technol Sci* 14, 267-274.

Frisch, U. (1995) *Turbulence*, Cambridge University Press: Cambridge

Frazier, W. C. and Westhoff, D. C. (1978) *Food microbiology*. McGraw-Hill: New York.

Fryer, P. J., Pyle, D. L., and Rielly, C. D. (1997) *Chemical engineering for the food industry*. Blackie Academic & Professional: London.

Fryer, P.J., Robbins, P.T., (2005) Heat transfer in food processing: ensuring product quality and safety, *Applied Thermal Engineering* 25, 2499-2510

Fryer, P.J., Simmons, M.J.H., Mehauden, K., Bakalis, S., 2008. Validation of thermal processing using time temperature indicators as process probes. *Japan J. Food Eng.*, 9 (1), 33-42.

Giannakourou, M. C., Koutsoumanis, K., Nychas, G. J. E., and Taoukis, P. S. (2005) Field evaluation of the application of time temperature integrators for monitoring fish quality in the chill chain. *International Journal of Food Microbiology* 102, 323-336.

Goff, H. G. (1999) Food Preservation. In: *Wiley Encyclopaedia of Food Science and Technology*, pp. 953-959. Ed F. J. Francis. John Wiley & Sons: New York.

Grant, I. and Smith, G. H. (1988) Modern developments in Particle Image Velocimetry. *Optics and Lasers in Engineering* 9, 245-264.

Guiavarc'h, Y. P., Deli, V., Van Loey, A. M., and Hendrickx, M. E. (2002a) Development of an enzyme Time Temperature Integrator for sterilization processes based on *Bacillus licheniformis* α -amylase at reduced water content. *Journal of Food Science* 67, 285-291.

Guiavarc'h, Y. P., Dintwa E., Van Loey, A. M., Zuber F.T., and Hendrickx, M. E. (2002b) Validation and use of an enzymatic Time Temperature Integrator to monitor thermal impacts inside a solid/liquid model food. *Biotechnology* 18, 1087-1094.

Guiavarc'h, Y., Sila, D., Duvetter, T., Van Loey, A., and Hendrickx, M. (2003) Influence of sugars and polyols on the thermal stability of purified tomato and cucumber pectinmethylesterases: a basis for TTI development. *Enzyme and Microbial Technology* 33, 544-555.

Guiavarc'h, Y. P., Van Loey, A. M., Zuber F.T., and Hendrickx, M. E. (2004a) *Bacillus licheniformis* α -amylase immobilized on glass beads and equilibrated at low moisture content: potentials as a time temperature integrators for sterilisation processes. *Innov. Food Sci. Emerg. Tech* 5, 317-325.

Guiavarc'h, Y. P., Van Loey, A. M., Zuber F.T., and Hendrickx, M. E. (2004b) Development Characterization and use of a high-performance enzymatic time temperature integrator for control of sterilization process impacts. *Biotechnology and Bioengineering* 88, 15-25.

Guiavarc'h, Y. P., Van Loey, A. M., and Hendrickx, M. E. (2005a) Extended study on the influence of z-value(s) of single and multicomponent Time Temperature Integrators on the accuracy of quantitative thermal process assessment. *Journal of Food Protection* 68, 384-395.

Guiavarc'h, Y. P., Zuber F.T., Van Loey, A. M., and Hendrickx, M. E. (2005b) Combined use of two single-component enzymatic Time Temperature Integrators: Application to industrial continuous rotary processing of canned Ravioli. *Journal of Food Protection* 68, 375-383.

Haentjens, T., Van Loey, A. M., Hendrickx, M. E., and Tobback, P. (1998) The use of α -Amylase at reduced water content to develop time temperature integrators for sterilization processes. *lebensm -Wiss u -Techno* 31, 467-472.

Hall, J. F., Barigou, M., Simmons, M. J. H., and Stitt, E. H., 2005, Comparative study of different mixing strategies in small high throughput experimentation reactors. *Chemical Engineering Science* 25-10-2004.

Harnby, N., Edwards, M. F., and Nienow, A. W. (1992) *Mixing in the process industries*. Butterworth Heinemann: Oxford.

Hendrickx, M. E., Weng, Z., Maesmans, G., and Tobback, P. (1992) Validation of time temperature integrator for thermal processing of food under pasteurisation conditions. *International of Food Science and Technology* 27, 21-31.

Hendrickx, M. E., Maesmans, G., De Cordt, S., Noronha, J., Van Loey, A. M., and Tobback, P. (1995) Evaluation of the integrated time temperature effect in thermal processing of foods. *Critical reviews in Food Science and Nutrition* 35, 231-262.

Hewitt, C. J. The synthesis of alpha-amylase (E.C.3.2.1.1.) by *Bacillus amyloliquefaciens* B20. 1993. University of Birmingham, School of Chemical Engineering.

Holdsworth, S. D. (1985) Optimisation of thermal processing -- A review. *J Food Eng* 4, 89-116.

Holdsworth, S. D. (1993). Rheological models used for the prediction of the flow properties of food products. *Food Bioproducts Processing*, 71, 139-179.

Kerry, J. P., O'Grady, M. N., and Hogan, S. A. (2006) Past, current and potential utilisation of active and intelligent packaging systems for meat and muscle-based products: A review. *Meat Sci* 74, 113-130.

Khan, F. R. Investigation of Turbulent Flows and Instabilities in a Stirred Vessel using Particle Imaging Velocimetry. PhD thesis, Loughborough 1-230. (2005).

La Fontaine, R. F. and Shepherd, I. C. (1996) Particle image velocimetry applied to a stirred vessel. *Experimental Thermal and Fluid Science* 12, 256-264.

Lado, B. H. and Yousef, A. E. (2002) Alternative food-preservation technologies: Efficacy and mechanisms. *Microbes and Infection* 4, 433-440.

Lambourne, T., & Tucker, G.S. (2001). Time temperature Integrators for validation of thermal processes. R&D report (pp. 132). Campden & Chorleywood Food Research Association.

Lauterborn, W. and Vogel, A. (1984) Modern optical techniques in fluid mechanics. *Ann Rev Fluid Mech* 16, 223-244.

Law, A. W. K. and Wang, H. (2000) Measurement of mixing processes with combined digital particle image velocimetry and planar laser induced fluorescence. *Experimental Thermal and Fluid Science* 22, 213-229.

Lewis, M., & Heppell, N. (2000). Kinetics for microorganism death and changes in biochemical components. *Continuous thermal processing of foods* (pp. 1-465). Aspen publication: New York

Lloyd, E., Cronje, M., and Tucker, G. Time temperature integrator: Guidelines on their preparation, processing and analysis. (1999). Campden & Chorleywood Food Research Association.

Lopez, A. A complete course in canning and related processes. 12th. (1987). Baltimore. The canning trade.

Maesmans, G., Hendrickx, M. E., De Cordt, S., and Tobback, P. (1993) Theoretical considerations on design of multicomponent time temperature integrators in evaluation of thermal processes. *Journal of Food processing and Preservation* 369-389.

Maesmans, G., Hendrickx, M. E., De Cordt, S., Van Loey, A. M., Noronha, J., and Tobback, P. (1994a) Combined use of the equivalent point method and a multi-component time temperature integrator in thermal process evaluation: Influence of kinetic characteristics and reference temperature. *Food Control* 5, 249-256.

Maesmans, G., Hendrickx, M. E., De Cordt, S., Van Loey, A. M., Noronha, J., and Tobback, P. (1994b) Evaluation of process value distribution with time temperature integrators. *Food Research International* 27, 413-423.

Maesmans, G., Hendrickx, M. E., De Cordt, S., and Tobback, P. (1995) Theoretical consideration of the general validity of the equivalent point method in thermal process evaluation. *Journal of Food Engineering* 24, 225-248.

Maesmans, G., Hendrickx, M. E., De Cordt, S., and Tobback, P. (2005) Feasibility of the use of a time temperature integrator and a mathematical model to determine fluid to particle heat transfer coefficients. *Food Research International* 27, 39-51.

Manas, P. and Pagan, R. (2005) Microbial inactivation by new technologies of food preservation. *Journal of Applied Microbiology* 98, 1387-1399.

Marra, F. and Romano, V. (2003) A mathematical model to study the influence of wireless temperature sensor during assessment of canned food sterilization. *J Food Eng* 59, 245-252.

Mavros, P. and Baudou, C. (1997) Quantification of the performance of agitators in stirred vessels: Definition and use of an agitation index. *Chem. Eng. Res. Des.* 75, 737-745.

Mavros, P., Naude, I., Xuereb, C., and Bertrand, J. (1997) Laser Doppler velocimetry in agitated vessels: Effect of continuous liquid stream on flow patterns. *Chem. Eng. Res. Des.* 75, 763-776.

Mavros, P., Xuereb, C., and Bertrand, J. (2005) Determination of 3-D Flows fields in agitated vessels by laser-Doppler velocimetry: Effect of impeller type and liquid viscosity on liquid flow patterns. *Trans I ChemE* 74, 658-667.

Mehauden, K., Cox, P.W., Bakalis, S., Simmons, M.J.H., Tucker, G.S., Fryer, P.J., 2007. A novel method to evaluate the applicability of Time Temperature Integrators to different temperature profiles. *Innov. Food Sci. Emerg. Tech.* 8 (4), 507-514, doi:10.1016/j.ifset.2007.03.001.

Mehauden, K., Cox, P.W., Bakalis, S., Cox, P.W., Fryer, P.J., Simmons, M.J.H., 2008. Use of time temperature integrators for determining thermal processing efficiency in agitated vessels. *Innov. Food Sci. Emerg. Tech.* 9 (3), 385-395, doi:10.1016/j.ifset.2007.10.006

Metzer, A.B. and Otto, R.E. (1957), Agitation of non-Newtonian fluids, *AIChE* 3, 3-10

Meynart, R. (1983) Speckle velocimetry: An application of image analysis techniques to the measurement of instantaneous velocity fields in unsteady flow. *International Congress on Instrumentation in Aerospace Simulation Facilities* 30-36.

Mortimer, S. and Wallace, C. (1998) *HACCP - A practical approach*. Aspen Publisher Inc: Gaithersburg.

Nerin, C., Tovar, L., Djenane, D., Camo, J., Salafranca, J., Beltran, J. A., and Roncales, P. (2006) Stabilization of beef meat by a new active packaging containing natural antioxidants. *J Agric Food Chem* 54, 7840-7846.

Noll, S. J. Peltier Device Information Directory www.peltier-info.com/info.htm. (1999). 2005.

O'Reilly, C. E., Kelly, A. L., Murphy, P. M., and Beresford, T. P. (2001) High pressure treatment: Applications in cheese manufacture and ripening. *Trends in Food Science and Technology* 12, 51-59.

Ohlsson, T. (1980) Optimal sterilization temperatures for flat containers. *Journal of Food Science* 45, 848-852.

Parker, D. J., Forster, R. N., Fowles, P., and Takhar, P. S. (2002) Positron emission particle tracking using the new Birmingham positron camera. *Nuclear Instruments and Methods in Physics Research, Section A: Accelerators, Spectrometers, Detectors and Associated Equipment* 477, 540-545.

Parker, D., Fan, X., Forster, R., Fowles, P., Ding, Y., and Seville, J. P. K. (2005a) Positron imaging studies of rotating drums. *Canadian Journal of Chemical Engineering*.

Parker, D. J., Sadrmomtaz, A., Fan, X., and Ingram, A. (2005b) Developments in PEPT for process applications. 4th world congress on industrial process tomography. Industrial Process Tomography. Japan 5-8 septembre 2005

Paul, E.L, Atiemo-Obeng, V., Kresta, S.M. (2003) *Handbook of Industrial Mixing: Science and practice*, Wiley-IEEE: New York

Raffel, M., Willert, C., and Kompenhans, J. (1998) *Particle Image Velocimetry, A practical guide*. Springer-Verlag: New York.

Randox (2006). Amylase ethylidene blocked-p-NPG7 manual. [AY1582].

- Reyes-De-Corcuera, J. I., Cavalieri, R. P., Powers, J. R., Tang, J., and Kang, D. H. (2005) Enzyme-electropolymer-based amperometric biosensors: An innovative platform for time-temperature integrators. *J Agric Food Chem* 53, 8866-8873.
- Richardson, P. (2001) *Thermal technologies in food processing*. Woodhead publishing limited: Cambridge.
- Richardson, P. (2004) *Improving the thermal processing of food* Woodhead publishing limited: Cambridge.
- Riva, M., Piergiovanni, L., and Schiraldi, A. (2001) Performances of time-temperature indicators in the study of temperature exposure of packaged fresh foods. *Pack Technol Sci* 14, 1-9.
- Robb, F. T., Maeder, D. L., Brown, J. R., Di Ruggiero, J., Stump, M. D., Yeh, R. K., Weiss, R. B., and Dunn, D. M. (2001) Genomic Sequence of Hyperthermophile, *Pyrococcus furiosus*: Implications for physiology and enzymology. *Methods in enzymology* 330, 134-157.
- Roychoudhury, S., Parulekar, S. J., and Weigand, W. A. (1988) Cell growth and -amylase production characteristics of *Bacillus amyloliquefaciens*. *Biotechnology and Bioengineering* 33, 197-206.
- Sacharow, S. Shelf life extension using packaging techniques. 709, 125-126. (2006).
- Schutyser, M. A. I., Briels, W. J., Rinzema, A., and Boom, R. M. (2003) Numerical simulation and PEPT measurements of a 3-D conical helical-blade mixer: A high potential solids mixer for solid-state fermentation. *Biotechnology and Bioengineering* 84, 29-39.
- Sharp, K.V. and Adrian, R.J., (2001) PIV study of small-scale flow structure around a Rushton turbine, *AIChE Journal* 47, 766-778
- Shimoni, E., Anderson, E. M., and Labuza, T. P. (2001) Reliability of time temperature indicators under temperature abuse. *Journal of Food Science* 66, 1337-1340.
- Simmons, M. J. H., Zhu, H., Bujalski, W., Hewitt, C. J., and Nienow, A. W. (2007) Mixing in a model bioreactor using agitators with a high solidity ratio and deep blades. *Chem. Eng. Res. Des.* 85, 1-9.
- Spielger, M. R. (1988). *Schaum's outline series theory and problems of statistics*. McGraw-Hill: New York

- Stanislas, M., Kompenhans, J., and Westerweel, J. (2000) *Particle Image Velocimetry, Progress towards industrial application*. Kluwer Academic Publisher: Dordrecht.
- Stellema, C. S., Vlek, J., Mudde, R. F., de Goeij, J. J. M., and van den Bleek, C. M. (1998) Development of an improved positron emission particle tracking system. *Nuclear Instruments and Methods in Physics Research Section A: Accelerators, Spectrometers, Detectors and Associated Equipment* 404, 334-348.
- Stewart, E. M. (2004) Food preservation: New alternatives to old technologies. *Food Science and Technology* 18, 30-32.
- Stoforos, N. G., & Taoukis, P. S. (1998). A theoretical procedure for using multiple response time-temperature integrators for the design and evaluation of thermal processes. *Food Control*, 9, 279–287.
- Taoukis, P. S. and Labuza, T. P. (1989) Reliability of time temperature indicators as food quality monitors under non isothermal conditions. *Journal of Food Science* 54, 789-792.
- TSI Inc. Innovations in Flow and Particle Diagnostics. 2002.
- Tucker, G.S. and Holdsworth, S. D. (1991) Mathematical modelling of sterilisation and cooking processes for heat preserved foods, applications of a new heat transfer model. *Food Bioprocesses Processing* 69, 5-12.
- Tucker, G.S. Application of Time Temperature Integrators for validation of Pasteurisation Processes. 77. (1999). Campden & Chorleywood Food Research Association Group. R & D report.
- Tucker, G.S., Lambourne, T., Adams, J. B., and Lach, A. (2002) Application of a biochemical time temperature integrator to estimate pasteurisation values in continuous food processes. *Innov. Food Sci. Emerg. Tech* 3, 165-174.
- Tucker, G.S., Cronje, M., and Lloyd, E. Evaluation of a time temperature integrator for mild pasteurisation processes. 215. (2005a). Camden & Chorleywood Food Research Association.
- Tucker, G.S., Brown, H. M., Fryer, P. J., Cox, P. W., Poole, F. L., Lee, H. S., and Adams, M. W. W. A sterilisation time temperature integrator based on amylase from the hyperthermophilic organism *Pyrococcus furiosus*. 222, 1-40. (2005b). Chipping Campden, CCFRA.

Tucker, G.S., Brown, H. M., Fryer, P. J., Cox, P. W., Poole, II, Lee, H. S., et al. (2007). A sterilisation Time–Temperature Integrator based on amylase from the hyperthermophilic organism *Pyrococcus furiosus*. *Innov. Food Sci. Emerg. Tech* 8, 63–72.

Valentas, K. J., Rotstein, E., and Singh, R. P. (1997) *Handbook of Food Engineering Practice*. CRC Press LLC: Boca Raton.

Van Loey, A. M., Ludikhuyze, L., Hendrickx, M. E., De Cordt, S., and Tobback, P. (1995) Theoretical consideration on the influence of the Z-value of a single component time/temperature integrator on thermal process impact evaluation. *Journal of Food Protection* 58, 39-48.

Van Loey, A. M., Hendrickx, M. E., De Cordt, S., Haentjens, T., and Tobback, P. (1996a) Quantitative evaluation of thermal processes using time temperature integrators. *Trends in Food Science & Technology* 7, 16-26.

Van Loey, A. M., Hendrickx, M. E., Smout, C., Haentjens, T., and Tobback, P. (1996b) Recent advances in process assessment and optimisation. *Meat Sci* 43, 81-98.

Van Loey, A. M., Arthawn, A., Hendrickx, M. E., Haentjens, T., and Tobback, P. (1997) The development and use of an α -amylase based time temperature integrators to evaluate in -pack pasteurisation processes. *lebensm -Wiss u -Techno* 30, 94-100.

Wells, J. H. and Singh, R. P. (1988) Application of time-temperature indicators in monitoring changes in quality attributes of perishable and semi perishable foods. *Journal of Food Science* 53, 148-152.

Welt, B. A., Sage, D. S., and Berger, K. L. (2003) Performance Specification of Time-temperature Integrators Designed to Protect Against Botulism in Refrigerated Fresh Foods. *Journal of Food Science* 68, 2-9.

Weng, Z., Hendrickx, M. E., Maesmans, G., and Tobback, P. (1991) Immobilized peroxidase: A potential bioindicateur for evaluation of thermal processes. *Journal of Food Science* 56, 567-570.

Willert, C., Raffel, M., Kompenhans, J., Stasicki, B., and La'hler, C. (1996) Recent applications of particle image velocimetry in aerodynamic research. *Flow Meas Instrum* 7, 247-256.

Wu,H. and Patterson,G.K. (1989) Laser-Doppler measurements of turbulent-flow parameters in a stirred mixer, *Chemical Engineering Science* 44, 2207-2221

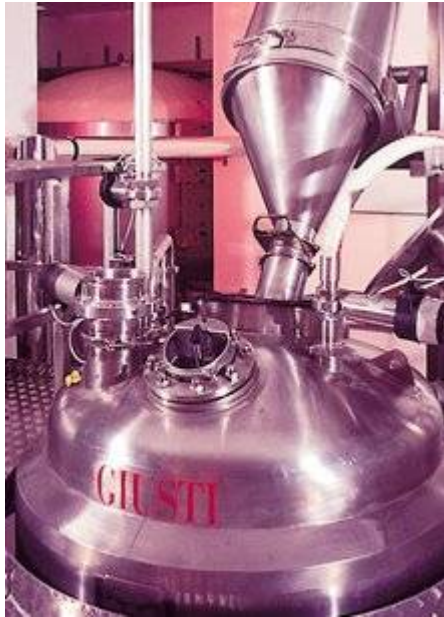
Yang, Z., Parker, D. J., Fryer, P. J., Bakalis, S., and Fan, X. (2006) Multiple-particle tracking-an improvement for positron particle tracking. *Nuclear Instruments and Methods in Physics Research Section A: Accelerators, Spectrometers, Detectors and Associated Equipment* 564, 332-338.

Yu, B., Zheng, B., Lin, C. X., Pena, O. J., and Ebadian, M. A. (2003) Laser Doppler anemometry measurements of laminar flow in helical pipes. *Experimental Thermal and Fluid Science* 27, 855-865.

Appendix A: http://www.briggsplc.co.uk/about_tg.htm

PROCESSING SYSTEMS THAT **KNOW NO BOUNDARIES**

About Us - T Giusti



T Giusti is a market leader in wet processing in the food, health & beauty and pharmaceutical markets and is a long standing member of the Briggs Group. Briggs acquired Giusti in 1994, allowing the Group to use its capabilities in a wider range of markets. Giusti have been providing cooking, cooling, mixing, and blending technology since 1918. The name is synonymous with excellence and equipment that provides solid return on investment year after year. Giusti equipment has a reputation for outstanding longevity.

Giusti has a reputation not only for excellent fabrication quality, but also cost-effective and imaginative process solutions. Leading companies Worldwide benefit from Giusti's approach. The company is fully backed by the resources of the Briggs Group, and the experience gained in major projects across the globe.

The Briggs Group offers a full package of in-house automation and control solutions, working with all of the main system providers, including Siemens, Rockwell (Allen Bradley), Omron, Mitsubishi, Schneider, Wonderware and Intellution.

Project management, consultancy and design services define the group's impressive capabilities. Links with key industry R&D facilities and academic institutions ensure the company leads the way in developing new solutions.

Appendix B: <http://www.briggspc.co.uk/food/vesuvio.htm>

Vesuvio



Vesuvio is a new concept in cook/cool systems for the Food Processing industry. The system comprises two separate skidded packages. The first includes the main cooking and cooling vessel, MCC cabinet and controls package. The other is the vacuum cooling plant.

Vesuvio is particularly aimed at cooked products with water content, where cooling times on all of the standard systems are typically 40 minutes from 98°C to 4°C. Heating times are equally impressive and benefit greatly from the use of Giusti's patented Vapinject steam injection unit - and burn-on is also much reduced.

All Vesuvio systems feature the GiustiMix scraped surface agitator for gentle but effective agitation of shear sensitive products and excellent temperature homogeneity.

Control comes via a fully featured GiustiMax modular control package which allows either manual or semi automatic operation via a touch screen control panel and a suite of simple but effective control screens.

A 250 litre trial system is available for product trials at the Campden and Chorleywood Food Research Association Group (CCFRA) in Chipping Campden, UK.

GIUSTI VESUVIO - Standard Vessel Sizing					
Litres	250L	500L	1000L	1500L	2000L
US Gallons	65	130	265	400	530
Agitator Drive	2.2KW	3.0KW	4.0KW	7.5KW	7.5KW
No. of Cleaning Heads	1	1	2	2	2
No. of Vapinjects	1	2	2	3	3
Giusti Flush Seat Valve	75mm/3"	75mm/3"	75mm/3"	75mm/3"	75mm/3"

SWINGARM MOUNTED CONTROL INTERFACE

Touch screen control panel (A) is mounted on an adjustable swingarm mount for easy, flexible control. Panel is IP65, NEMA 12 rating, fully integrated MCC control cabinet (B) to IP55, NEMA 12 standard.

GIUSTIMAX CONTROL PROGRAMME

Vesuvio includes as standard a fully featured GiustiMax modular control system. The system is capable of manual or semi-automatic operation (see inset opposite).

LID

Lid (C) is hydraulically counterbalanced for ease of opening – one person operation. Lid can be locked in position via quick release swing bolts (D) – one of which is a 'safety bolt' to prevent inadvertent opening of lid under pressure – also interlocked via the GiustiMax control system.

SAFETY GRID AND INTERLOCKS

Vesuvio is fitted with a standard removable safety grid to allow additions via the top of vessel with agitator running. Safety grid (E) is interlocked to prevent agitator from running when grid is removed.

CP CAPABILITY

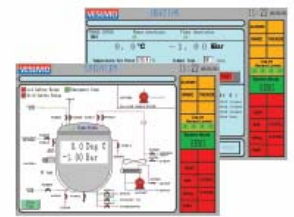
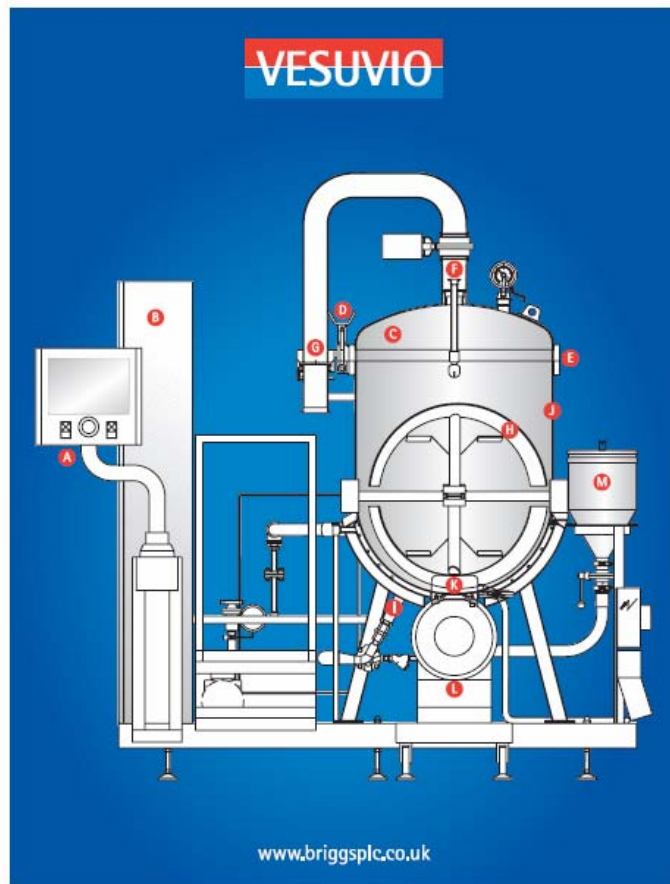
Full CP capability is offered via 40 mm (1 1/2") tri-clamp (F) connection. Giusti can option a separate stand alone CP skid or in-plant CP system can be connected in. Standard specification relies on Tofigong Semi Magnum® rotary spray heads – 1 unit on 250L and 500L vessel sizes, 2 units on 1000L and above. An option for Tofigong T20G heads can be offered for difficult applications.

VACUUM COOLING FACILITY

A separate but included vacuum cooling plant is connected via a 150mm/6" or 200mm/8" vacuum connection with make or break unit (G) to allow lid (C) to be opened. Vacuum cooling provides the most rapid cooling medium for products with a water content. Typical cooling from 80°C to 2°C in 40 minutes. This cooling time is typical but applies equally across the range of standard vessel sizes. Product foaming is controlled via a lid mounted conductivity probe. System is fitted with 'autovac' valves.

GIUSTIMAX AGITATOR

Giusti patented spoon style agitator (H) for handling shear sensitive particulates, gives thorough distribution of product without damage. Thoroughly field tested and tested over many years. Floating PTFE scrapers (not sprung) fitted as standard (see below).



VAPINJECT

Giusti patented direct steam injector unit (I) for rapid heating times and elimination of burn-on. Rapidly heats products not sensitive to the addition of water to 95°C. Above 95°C temperature can be raised by conventional jacket heating. The Vapinject technique involves the injection of outside steam and air – hundreds of proven systems in operation.

VESSEL

Pressure vacuum vessel (J) to PED 5500 standards for ASME as required. All contact parts stainless steel 316L. Jacket rated at 5.5 Bar pressure and vessel rated at 1 Bar pressure and full vacuum. Polished to (4) rs internally and satin dull externally. Fully hooded jacket to hemisphere as standard.

GIUSTI FLUSH SEAT OUTLET VALVE

Pneumatically actuated 75mm/3" Giustivalve (K) – purpose built and designed by Giusti for full vessel compatibility, hygiene and CP capability.

OPTIONAL EXTRAS

- This list is not exhaustive:
- T20G CP head upgrade
- Load cells integrated to control system
- Recirculation via high-wear in-line Impactor emulsifier (L)
- Product feed hoppers to suit vacuum loading (M)
- Stand alone CP skid
- Data transfer to PC
- Additional jacket heating zones
- 100mm/4" Giustivalve upgrade



Appendix C

Matlab codes

A. Calculation velocity for PIV data

```
%A=load('C:\Documents and Settings\Karin\My Documents\PIV Matlab
codes\low-speedpos1water\low-speedpos1waterAvg.vec')
fname1 = input('Folder directory? e.g. (C:) >> ','s')
fname2 = input('Folder name? (e.g. TRIAL) >> ','s')
ms=input('Maximum speed:')
maxframe=input('error frame:')
fname3 = [fname1,'\',fname2,'\',fname2,'Avg.vec']
A=csvread([fname3],1,0);
xt=find(A(:,5)<maxframe);
A(xt,3:4)=0;
C=sqrt(A(:,3).^2+A(:,4).^2);
xt2=find(C>ms);
A(xt2,3:4)=0;
data=A;

save('exname.vec', 'A', '-ASCII')

clear A C fname1 fname2 fname3 maxframe ms xt xt2
```

B. Calculation rms for PIV data

```
fname1 = input('Folder directory? e.g. (C:) >> ','s')
fname2 = input('Folder name? (e.g. TRIAL) >> ','s')
nfiles = input('Last Frame? (e.g. 499) >> ')
ms=input('Maximum speed:')
maxframe=input('error frame:')
fname3 = [fname1,'\',fname2,'\Vector\',fname2,'00000.vec']
fname4 = [fname1,'\',fname2,'\',fname2,'Avg.vec']

s=csvread([fname3],1,0);
xt=find(s(:,5)<1);
s(xt,3:4)=NaN;
s(:,5)=[];
format short e;
s(:,1:2)=s(:,1:2)/1000;
x = s(:,1);
y = s(:,2);
z = s(:,3);
b = find (y == s (1,2));
b1 = max (size (b));
a = find (x == s (1,1));
a1 = max (size (a));
U =reshape(z,b1,a1);
U = U;
z = s(:,4);
V =reshape(z,b1,a1);
V = V;
```

```
X=reshape(x,b1,a1);
Y=reshape(y,b1,a1);

for i = 1 : nfiles;

if i < 10
fname3 = [fname1,'\',fname2,'\Vector\',fname2,'0000',int2str(i),'.vec']
elseif 100 > i & i > 9
fname3 = [fname1,'\',fname2,'\Vector\',fname2,'000',int2str(i),'.vec']
elseif 1000 > i & i > 99
fname3 = [fname1,'\',fname2,'\Vector\',fname2,'00',int2str(i),'.vec']
else
fname3 = [fname1,'\',fname2,'\Vector\',fname2,'0',int2str(i),'.vec']
end

if exist (fname3)>0

s=csvread([fname3],1,0);
xt=find(s(:,5)<1);
s(xt,3:4)=NaN;
s(:,5)=[];
z = s(:,3);
U2 =reshape(z,b1,a1);
z = s(:,4);
V2 =reshape(z,b1,a1);
U=cat(3,U,U2);
V=cat(3,V,V2);
end
end
clear U2 V2;

ss=csvread(fname4,1,0);
xxt=find(ss(:,5)<maxframe);
ss(xxt,3:4)=NaN;
ss(:,5)=[];
format short e;
ss(:,1:2)=ss(:,1:2)/1000;
xx = ss(:,1);
yy = ss(:,2);
zz = ss(:,3);
b = find (yy == ss (1,2));
b1 = max (size (b));
a = find (xx == ss (1,1));
a1 = max (size (a));
UU =reshape(zz,b1,a1);
UU = UU;
zz = ss(:,4);
VV =reshape(zz,b1,a1);
VV = VV;
c1=sz(1,2);
for i=1:b1
    for j=1:a1
        clear ru rv
        ru=find (~isnan(UU(i,j)));
        rv=find (~isnan(VV(i,j)));
        UA(i,j) = UU(i,j);
        VA(i,j) = VV(i,j);
        if sqrt(UA(i,j).^2+VA(i,j).^2)>ms
```

```
    VA(i,j)=NaN;
    UA(i,j)=NaN;
end
    end
end
MAu=zeros(b1,a1,nfiles+1);
MAv=zeros(b1,a1,nfiles+1);
MAu=U;
MAv=V;

for i=1:b1
    for j=1:a1
        for k = 1 : nfiles+1;

            if MAu(i,j,k) < 1e+10
                MAu(i,j,k)=U(i,j,k);

            else
                MAu(i,j,k)=UA(i,j);
            end
        end
    end
end
for i=1:b1
    for j=1:a1
        for k = 1 : nfiles+1;

            if MAv(i,j,k) < 1e+10
                MAv(i,j,k)=V(i,j,k);

            else
                MAv(i,j,k)=VA(i,j);
            end
        end
    end
end
Nu=zeros(b1,a1);
Nv=zeros(b1,a1);
for i=1:b1
    for j=1:a1
        douilleu=find (~isnan(U(i,j,:)));
        douillev=find (~isnan(V(i,j,:)));
        aa=0;
        av=0;
        aa=length (douilleu);
        av=length (douillev);
        Nu(i,j)=aa;
        Nv(i,j)=av;
    end
end
for i=1:b1
    for j=1:a1
        for k = 1 : nfiles+1;
            rmstempu(i,j,k)=((UA(i,j)-MAu(i,j,k)).^2);
            rmstempv(i,j,k)=((VA(i,j)-MAv(i,j,k)).^2);
            disp(k);
        end
        rmsusum=sum(rmstempu,3);
```

```
rmsvsum=sum(rmstempv,3);
rmsu(i,j)=sqrt(rmsusum(i,j)./(Nu(i,j)-1));
rmsv(i,j)=sqrt(rmsvsum(i,j)./(Nv(i,j)-1));
end
end
figure,
%contourf(flipud(X'),flipud(Y'),flipud(sqrt(UA.^2+VA.^2)))
%hold on
contourf(X,Y,(rmsu.^2+rmsv.^2).^1/2);
set(gca,'DataAspectRatio',[1 1 1])
A=(rmsu.^2+rmsv.^2).^1/2;
z=reshape(A,3782,1);
T=[x y z];
T(:,1:2)=T(:,1:2)*1000;
d=find (isnan(T(:,3)));
T(d,3)=0;
header=['x ,y ,Standard deviation '];
dlmwrite('overfilledmediumspeedpos4CMC0.25%.txt',header,'delimiter',' ');
dlmwrite('overfilledmediumspeedpos4CMC0.25%.txt',T,'delimiter',' ','-append')
```

C. Calculation of occupancy, velocity, normalised velocity, rms...for PEPT

Use function Totalvel

```
function [cyl Occ]=totalvel(fdata);
fdata=filtra(data,'ON');
fdata(:,2)=fdata(:,2)-mean(fdata(:,2));
fdata(:,3)=fdata(:,3)-mean(fdata(:,3));
fdata(:,4)=fdata(:,4)-mean(fdata(:,4));
t=fdata(:,1);
x=fdata(:,2);y=fdata(:,3);z=fdata(:,4);
cyl=velest(t,x,y,z,5,5,5);
cylf=cyl;
Occ=Oaxis_sc(cyl);
header=['y ,z ,u ,v ,w ,occ,passes,stdu,stdv,stdw,veltot,dnormtot,stdtot'];
dlmwrite('exp1.watermediumspeedttiibis.txt',header,'delimiter',' ')
dlmwrite('exp1.watermediumspeedttiibis.txt',occ,'delimiter',' ','-append')
```

Function Oaxis_sc

```
function Occ = Oaxis_sc(A)
n_el=size(A,1);
n_y=50; n_z=50;
% correction values
flag=input('flag: '); %correction On flag=1
%correction Off flag=0
if flag==1
    corr_y=input('insert displacement in y direction: ');
    corr_z=input('insert displacement in z direction: ');
    A(:,2)=A(:,2)-corr_y;
    A(:,3)=A(:,3)-corr_z;
    y_m=-0.155;
    z_m=-0.145;
    dy=(0.29)/n_y;
    dz=0.29/n_z;
else
    y_m=min(A(:,2));
    z_m=min(A(:,3));
    dy=(max(A(:,2))-min(A(:,2)))/n_y
```

```

    dz=(max(A(:,3))-min(A(:,3)))/n_z
end
i=1;
H=zeros(n_y+1,n_z+1,8);
total_T=A(end,7);
yy=1;zz=1;
for i=2:n_el-1,
    y=floor((A(i,2)-y_m)/dy)+1;
    z=floor((A(i,3)-z_m)/dz)+1;
    dt=(A(i+1,7)-A(i-1,7))/2;
    if dt<600/1000
        H(y,z,1)=H(y,z,1)+A(i,4)*dt;           %u
        H(y,z,2)=H(y,z,2)+A(i,5)*dt;           %v
        H(y,z,3)=H(y,z,3)+A(i,6)*dt;           %w
        %H(y,z,4)=H(y,z,4)+1;                   %locations
        if (y==yy & z==zz)                       %I'm in the same cell
            H(y,z,5)=H(y,z,5)+dt;
        else                                       %I'm in a new cell
            H(yy,zz,5)=H(yy,zz,5)+dt;
            H(y,z,4)=H(y,z,4)+1; %passes
        end
        yy=y; zz=z; %ad majora
    end
end
%loop to find standard deviation for each velocity component
for i=2:n_el-1,
    y=floor((A(i,2)-y_m)/dy)+1;
    z=floor((A(i,3)-z_m)/dz)+1;
    dt=(A(i+1,7)-A(i-1,7))/2;
    H(y,z,6)=(H(y,z,1)/H(y,z,5)-A(i,4))^2;      %su
    H(y,z,7)=(H(y,z,2)/H(y,z,5)-A(i,5))^2;      %sv
    H(y,z,8)=(H(y,z,3)/H(y,z,5)-A(i,6))^2;      %sw
end
j=1;
Occ=zeros(n_y*n_z,13);
for i1=1:n_y,
    for i3=1:n_z,
        Occ(j,1)=i1*dy+y_m;
        Occ(j,2)=i3*dz+z_m;
        if(H(i1,i3,4)>2)
            Occ(j,3)=Occ(j,3)+(H(i1,i3,1)/H(i1,i3,5));%mean velocities
            Occ(j,4)=Occ(j,4)+(H(i1,i3,2)/H(i1,i3,5));
            Occ(j,5)=Occ(j,5)+(H(i1,i3,3)/H(i1,i3,5));
            Occ(j,8)=Occ(j,8)+H(i1,i3,6)/H(i1,i3,4); %std
            Occ(j,9)=Occ(j,9)+H(i1,i3,7)/H(i1,i3,4);
            Occ(j,10)=Occ(j,10)+H(i1,i3,8)/H(i1,i3,4);
        end
        Occ(j,6)=Occ(j,6)+H(i1,i3,5)/total_T;    %Occupancy
        Occ(j,7)=Occ(j,7)+H(i1,i3,4);
        j=j+1;
    end
end
il
Occ(:,8)=sqrt(Occ(:,8));Occ(:,9)=sqrt(Occ(:,9));Occ(:,10)=sqrt(Occ(:,10));
Occ(:,11)=(Occ(:,3).^2+Occ(:,4).^2+Occ(:,5).^2).^5;
Occ(:,12)=((Occ(:,3).^2+Occ(:,4).^2+Occ(:,5).^2).^5)/0.28;
Occ(:,13)=(Occ(:,8).^2+Occ(:,9).^2+Occ(:,10).^2).^5;
End

```

Hazardous Substances Policy - Assessment CHEMICAL HAZARD AND RISK ASSESSMENT

School/Dept Chemical Engineering Assessment Number

Assessor Karin Mehauden Date of Assessment January 2005

Notes Guidance on making an assessment is given in *Chemical Hazard and Risk Assessment (GUIDANCE/22/CHRA/03)*.
Guidance is also available from the attached *Guidance on Completing the Chemical Hazard and Risk Assessment Form*.
Substance data is available in HAZDAT. Use a continuation sheet or word processor to expand any section of this form.
An MS Word file for this form is available from <http://www.hsu.bham.ac.uk/univ/hspolicy/hs15/HS2ASSFM.DOC>.

1 **LOCATION OF THE WORK ACTIVITY** G29 Chemical Engineering Building

2 **PERSONS WHO MAY BE AT RISK**

List names where possible All personnel working in the above locations

3 **ACTIVITY ASSESSED** Spectrophotometer analysis

4 **MATERIALS INVOLVED** Attach copies of data sheet(s)

NAME and CAS NUMBER	AMOUNT	HAZARD	RISK PHRASES	REPORTABLE?
α -Amylase Bacillus sp. Type II-A Lyophilized powder	250g	Harmful	May cause sensitization by inhalation	No
Trizma base $C_4H_{11}NO_3$ used to prepare the tris buffer	6,057g/l (tris buffer concentration)	Irritant	Irritating to the eyes/the respiratory system/ The skin	No
Hydrochloric acid (to prepare the tris buffer)	Few drops to obtain a pH between 8,5-8,6	Toxic	Toxic by inhalation, cause burns, irritating to respiratory system, toxic if inhaled	No
Ethylidene Blocked pNPG ₇ (Randox kit)= Amylase reagent	1.0 mmol/l		Avoid ingestion or contact with skin or mucous membranes	No

If substance is reportable, have you reported it to the Health and Safety Unit? YES/NO (see Note 4)

5 **INTENDED USE**

Give brief details and attach protocol/instructions
Quantitative determination of Amylase in solution
250 g of amylase is dissolved in the tris buffer. 20 μ l of this solution is put inside some pieces of pipe coated with silicone. These pipes are put in the water bath at 85°C for different durations. After that, 10 μ l of the amylase is extracted from the pipes and mixed with 290 μ l of tris buffer. 20 μ l of this solution is analysed by spectrophotometer. 1ml of Amylase reagent (Randox kit) is added to the cuvette to start the reaction. The reaction is followed against time

6 **RISKS to HEALTH and SAFETY from INTENDED USE**

From personal exposure or hazardous reactions. Refer to OELs, flash points, etc., as appropriate. Are pregnant women, breast-feeding mothers especially at risk?

N/A

7 **CONCLUSIONS ABOUT RISKS**

Is level of risk acceptable? Can risk be prevented or reduced by change of substance/procedure? Are control measures necessary?

Level of risk acceptable, all chemicals have been COSSH assessed

8	CONTROL MEASURES		
Additional to <i>Good Chemical Practice</i> , e.g., fume cupboard, etc. Any special requirements, e.g., glove type, etc.			
Specific control measures not required			
9	INSTRUCTION/TRAINING		
Specify course(s) and/or special arrangements.			
Attended laboratory Chemical Safety and Safety Training courses			
10	MONITORING		
Performance of control measures,			
None required			
Personal exposure		Health Surveillance, specify measures agreed with Health and Safety Unit	
11	WASTE DISPOSAL PROCEDURE		
None required			
12	REVIEW		
Enter the date or circumstances for review of assessment (maximum review interval 5 years)			
Annual			
13	EMERGENCY ACTION		
TO CONTROL HAZARDS		To stabilize situation eg spread absorbent on liquid spill; eliminate sources of ignition, etc.	
In case of spillage on the floor, glass pieces are swept up with a brush and a pan and disposed into the glass bin. The liquid spillage must be cleaned with paper towel and disposed into the adequate bin			
TO PROTECT PERSONNEL		Evacuation, protection for personnel involved in clean-up, Special First Aid	
The adequate protective clothing, including goggles and Gloves must be worn			
In the case of contact with any chemicals, flush affected area with copious amounts of water			
TO RENDER SITE OF EMERGENCY SAFE		Clean-up/decontamination	
Clean up in case of chemicals spillages: Mopped up the floor thoroughly with water.			
14	EMERGENCY CONTACT	NAME	PHONE
		Peter Fryer	4545 1

Assessment Number

Hazard and Risk Assessment Summary

School/Dept Chemical Engineering	Location of Activity G29 Chemical engineering building	Date of Assessment January 2005
Assessor Karin Mehauden	Activity Assessed (Attach protocols) Quantitative determination of Amylase in solution with a spectrophotometer	

Assessment of Hazard and Risk									Control Measures Required		
HAZARD (List only hazards from which there is a significant risk of serious harm under foreseeable conditions)	PERSONS AT RISK (See key, Indicate number)	PERSONA L HARM?			LIKELIHOOD of HARM?						
		F	Mj	Mn	Y	Pr	Po	R			
• Spillage of chemicals during transport	Pg S Ug			X			X		Use of Bottle carriers, the adequate protective clothing to be worn.		
• During the preparation of solutions (tris buffer) hazard associated with the use of harmful agents	Pg S Ug			X		X			Wear adequate protective clothing, goggles, and gloves. Use a fume cupboard. Label any container used and dipose them in the correct bin.		
• Performing the experiment: Hazard associated with the use of the spectrophotometer, machinery or equipment.	Pg S Ug			X			X		Before any utilization, spectrophotometer surrounding should be checked. Wear adequate protective clothing, goggles and gloves.		

Key	PERSONS AT RISK Ug Undergraduate Pg Postgraduate S Staff C Contractor V Visitor Pa Patient Pu General Public Yp Young Person Nm New/Expectant Mother	PERSONAL F Fatality Mj Major Injury Mn Minor Injury	LIKELIHOOD Y Yes/ Very High Pr Probable Po Possible R Remote	Risk Significance <table style="width: 100%; border-collapse: collapse;"> <tr> <td></td> <td>Y</td> <td>Pr</td> <td>Po</td> <td>R</td> <td></td> </tr> <tr> <td>F</td> <td>✓</td> <td>✓</td> <td>✓</td> <td>✓</td> <td rowspan="3">✓ = Significant risk</td> </tr> <tr> <td>Mj</td> <td>✓</td> <td>✓</td> <td>✓</td> <td>✓</td> </tr> <tr> <td>Mn</td> <td>✓</td> <td>✓</td> <td>X</td> <td>X</td> <td>X = Insignificant risk</td> </tr> </table>		Y	Pr	Po	R		F	✓	✓	✓	✓	✓ = Significant risk	Mj	✓	✓	✓	✓	Mn	✓	✓	X	X	X = Insignificant risk	Date for Review January 2006
	Y	Pr	Po	R																								
F	✓	✓	✓	✓	✓ = Significant risk																							
Mj	✓	✓	✓	✓																								
Mn	✓	✓	X	X		X = Insignificant risk																						

Major Injury: Loss of or broken limb
 Loss of or damaged eye
 Loss of consciousness
 Acute illness needing medical treatment
 Permanent ill health or disability

g:\aww7text\guidance\17ra.doc
19.12.00

Assessment Number

Hazard and Risk Assessment Summary

School/Dept	Chemical Engineering	Location of Activity	Room 207	Date of Assessment	26/05/2007
Assessor	Karin Mehauden	Activity Assessed (Attach protocols)	Investigation of flow in inside the Giusti's model vessel using laser based optical techniques (PIV)		

Assessment of Hazard and Risk									Control Measures Required	
HAZARD <small>(List only hazards from which there is a significant risk of serious harm under foreseeable conditions)</small>	PERSONS AT RISK <small>(See key, Indicate number)</small>	PERSONAL HARM?			LIKELIHOOD of HARM?					
		F	Mj	Mn	Y	Pr	Po	R		
Eye damage from exposure to laser radiation (Nd:YAG Class IV laser source)	Pg 1 (user)		X				X		Use laser interlock whenever in front of laser output and assembling light arm. Never look into path of laser beam. Remove watch and any jewellery that could cause the laser beam to be reflected. Set laser Q-switch to lowest suitable power. Wear suitable laser goggles. Follow start-up and shutdown procedure and turn off laser after use. Avoid large reflections/ scattering of laser beam. Use blackout curtains to completely enclose equipment. Received training on PIV equipment from K. Chung and A Tsoligkas Use laser interlock whenever in front of laser output and assembling light arm. Keep exposed skin out of path of laser beam. Take care when operating around traverse or trailing cables. Do not obstruct traverse whilst moving.	
Eye damage from exposure to Class IV laser radiation.	S 2, Pg 4 (others in lab)		X					X		
Skin damage from exposure to Class IV laser radiation.	Pg 1 (user)			X			X			
Tripping over automated traverse unit/ trailing cables (Pedestrian Access Hazard HPW 1)	Pg 1 (user)			X			X			

Key	PERSONS AT RISK		PERSONAL		LIKELIHOOD		Risk Significance					Date for Review	N/A
	Ug	Undergraduate	F	Fatality	Y	Yes/ Very High		Y	Pr	Po	R		
	Pg	Postgraduate	Mj	Major Injury	Pr	Probable	F	✓	✓	✓	✓	✓ = Significant risk	
	S	Staff	Mn	Minor Injury	Po	Possible	Mj	✓	✓	✓	✓	X = Insignificant risk	
	C	Contractor			R	Remote	Mn	✓	✓	X	X		
	V	Visitor											
	Pa	Patient											
	Pu	General Public											
	Yp	Young Person											
	Nm	New/Expectant Mother											

Major Injury: Loss of or broken limb
Loss of or damaged eye
Loss of consciousness
Acute illness needing medical treatment
Permanent ill health or disability

Hazard and Risk Assessment Summary

School/Dept

School of Physics

Assessor

Karin Mehauden

Location of Activity

PEPT room

Date of Assessment

26/05/2007

Activity Assessed
(Attach protocols)

Investigation of flow in inside the Giusti's model vessel
using laser Positron Emission Particle Tracking

Assessment of Hazard and Risk								Control Measures Required			
HAZARD <small>(List only hazards from which there is a significant risk of serious harm under foreseeable conditions)</small>	PERSONS AT RISK <small>(See key, Indicate number)</small>	PERSONAL HARM?			LIKELIHOOD of HARM?						
		F	Mj	Mn	Y	Pr	Po	R			
Contact with the radioactive tracer	Pg 1 (user)		X				X		Received training on PEPT equipment from Dr. X Fan Avoid contact with the tracer Always wear gloves Carry on the work with trained staff		

Key

PERSONS AT RISK

Ug Undergraduate
Pg Postgraduate
S Staff
C Contractor
V Visitor
Pa Patient
Pu General Public
Yp Young Person
Nm New/Expectant Mother

PERSONAL

F Fatality
Mj Major Injury
Mn Minor Injury

LIKELIHOOD

Y Yes/ Very High
Pr Probable
Po Possible
R Remote

Risk Significance

F

✓

Y

✓

Pr

✓

Po

✓

R

✓

✓ = Significant risk

Mj

✓

✓

✓

✓

✓

✓

✓

X = Insignificant risk

Mn

✓

✓

✓

X

X

Date for Review

N/A

Major Injury:

Loss of or broken limb
Loss of or damaged eye
Loss of consciousness
Acute illness needing medical treatment
Permanent ill health or disability